Photophysics of Fluorescent Molecules in Micellar Systems

THESIS

Submitted in partial fulfilment
of the requirements for the degree of

DOCTOR OF PHILOSOPHY

by

SUNITA JOSHI

Under the supervision of
Dr. D. D. Pant

BITS Pilani
Pilani | Dubai | Goa | Hyderabad

BIRLA INSTITUTE OF TECHNOLOGY & SCIENCE
PILANI – 333 031 (RAJASTHAN) INDIA

2015

BIRLA INSTITUTE OF TECHNOLOGY & SCIENCE

PILANI - 333 031 (RAJASTHAN)

CERTIFICATE

This is to certify that the thesis entitled "**Photophysics of Fluorescent Molecules in Micellar Systems"** and submitted by **Sunita Joshi** ID.No. **2010PHXF410P,** for award of Ph.D. Degree of the Institute, embodies original work done by her under my supervision.

_____

Signature the Supervisor

Name in capital block letters : D. D. PANT (Ph.D.)

Designation : Associate Professor, Department of Physics
BITS-Pilani, Pilani Campus

Date: _____

Dedicated to……

My parents and brothers……
…….for their love and care

My mentor……
…….for his invaluable advices

My friends……
…….for everything

Acknowledgements

This thesis, as I see it, is not the end but just the beginning of my research journey. However, at the juncture of this milestone achievement and before continuing the journey further, I would like to express my sincere gratitude to number of people to whom I am really indebted to for their help, support and motivation in all my endeavors. I am grateful to numerous local and global "peers" who have contributed towards shaping this thesis.

I would like to express my deep and sincere gratitude to my guide, **Dr. D. D. Pant** for his invaluable guidance, constant encouragement, unstinted inspiration, keen interest and good wishes. His wide knowledge and his logical way of thinking on critical scientific problems have been of great value for me. I am also grateful to him for being patient while critically reviewing this thesis.

I am immensely thankful to the Vice-Chancellor, Directors, Deputy Directors and Deans of Birla Institute of Technology & Science (BITS), Pilani for providing me the opportunity to pursue my doctoral studies by providing necessary facilities and financial support.

My whole-hearted gratitude to Prof. Sanjay Kumar Verma, Dean, Academic Research Division (ARD), BITS Pilani, and to Dr. Rakesh Choubisa Convenor, Departmental Research Committee (DRC), Department of Physics, BITS Pilani, Pilani Campus for his official support and encouragement. I own my sincere thanks to Dr. Hemant Jadhav Associate Dean ARD, Dr. Navin Singh, nucleus members of ARD. I overwhelmingly acknowledge the office staff of ARD, whose secretarial assistance helped me in submitting the various evaluation documents in time.

It gives me immense pleasure to thank Dr. D. D. Pant, Head, department of physics and my Doctoral Advisory Committee (DAC) members, Prof. Debashis Bandyopadhyay and Dr. Rakesh Choubisa for their support, critical review and suggestions during the progress review and to review my draft thesis. Also, I wish to express my gratitude to all the faculty members of physics department for their kind support time-to time.

I would like to thank all my dear friends and co-scholars, in particular Mr. Parvej Alam, Mrs. Rituparna, Mrs. Santosh Kumari, Mr. Amrit Sarmah, Mr. Jitendra Kumar, Mrs. Monika Poonia, Mrs. Keerti, Mr. Ravi, Mrs. Suman Kumari and all others for moral support, diversified help, good wishes and several funs which will always be remembered. A Special thanks to my group members- Mr. Tej and Ms. Ritika. I would also like to thank to Dr. Amit Kumar Tiwari and Mr. Sonu from chemistry department BITS Pilani for their valuable help in learning lifetime measurements. I thank all research scholars of physics and chemistry department. I fell short in words to thank Mrs. Uma Pant for her blessings.

I deeply acknowledge BITS Pilani, UGC and CSIR for the financial assistance provided during my PhD tenure.

Finally, I owe my heartfelt gratitude and indebtness to my grandparents, my mummy, my papa, my elder brother Narendra, my bhabhi Deepika and younger brother Anoop who have always encouraged me to follow my heart and inspired my inquisitive mind throughout my childhood and study career. It is their inspiration, encouragement, blessings and support that helped me to achieve what I am today. Lastly, I wish to apologize if I forgot the names of persons who had helped me in any way.

Date: _____ **Sunita Joshi**

Abstract

It is well known that photoexcitation of a molecule generally induces changes in its electronic and geometrical structures, which in turn lead to the changes in its interactions with the nearby molecules and its environment. In many cases, the molecular interactions are greatly augmented in the excited electronic state where the energy of excitation is used partly as the driving force for the reaction dynamics, leading to various photophysical and photochemical processes, which include electronic charge redistribution, electron and proton transfer, large amplitude intramolecular torsional motions, trans-cis isomerization, intramolecular vibrational redistribution, intermolecular vibrational relaxation (vibrational cooling), internal conversion, solvation etc.

Last two decades have witnessed the increasing significance of various organized assemblies on biological processes. Reactants embedded in molecular assemblies like micelles, reverse micelles, cyclodextrins, vesicles, etc., achieve a greater degree of organization compared to their geometries in homogeneous solution and can mimic many reactions in biosystems. They can also have potential applications in nanoparticle synthesis, pharmaceuticals and many other uses. The local viscosity/rigidity within the organized assemblies are appreciably different from that in the bulk liquid medium and as a result, these systems can alter the photoprocess of the entrapped molecule quite drastically.

This thesis describes the characterization and modulation of photophysical properties of fluorescent molecules in micellar systems. In the introduction part of the thesis, detailed information about different photophysical and photochemical processes of molecules and the structure of micelles is provided. The scope of the present study is briefed by stating the research gap and the work done in this thesis. The materials, methods and instruments used in the present study are also explained.

One of the important photophysical properties studied here in this thesis is the estimation of ground and excited state dipole moments of the fluorescent molecules. This study is of interest because knowledge of dipole moments is useful in extracting parameters like polarizability in non-linear optical materials, understanding nature of the emitting state and determining the tunability of the emission energy as a function of

the medium. There are various techniques available for estimation of ground state and excited state dipole moments of organic molecules. Here, in this study, the solvatochromic method and quantum chemical calculations are employed for estimating the ground and excited state dipole moments of different Quinine Sulfate (QS) and Quinidine (QD) species. These molecules are very sensitive to surrounding solvent, we have estimated dipole moments of these molecules in different forms using solvatochromic shift method and found higher dipole moment in the excited state compared to the ground state.

The highly sensitive fluorescence properties of QS towards the changes in polarity and viscosity of the environment around it has been chosen initially to study the probe molecule in different micellar systems. Steady state and time-resolved measurements of Quinine Sulfate dication (QS^{2+}) in ionic and neutral micelles have been carried out at concentrations above the Critical Micelle Concentrations (CMC) in aqueous phase. It has been observed that fluorescence properties of QS^{2+} are remarkably modulated in micelles compared with the bulk phase. The location of the probe molecule in micellar systems is ascertained by a variety of spectral parameters such as Edge Excitation Red Shift (EERS), average fluorescence decay time, radiative and non radiative rate constants, and rotational relaxation time. These results are relevant to understand the role of surface charge of membranes in the interaction of membranes with the membranes. Influenced by the high sensitivity of QS, it is further used to study interaction of QS^{2+} with anionic, Sodium dodecylsulfate (SDS) surfactant at different premicellar, micellar and postmicellar concentrations in aqueous phase using steady state, time-resolved fluorescence and fluorescence anisotropy techniques. It has been demonstrated that QS^{2+} could sense the change in microenvironment around it during the premicellar, micellar and postmicellar concentrations of SDS.

We observed that there is fluorescent complex formation between QS^{2+} molecules and surfactant monomers at lower concentrations of SDS. At post micellar concentrations the red shift in fluorescence spectrum, increase in quantum yield and increase in fluorescence lifetimes are attributed to incorporation of solute molecules to micelles. The micropolarity and microviscosity of environment around QS^{2+} in SDS micelles are also studied. Fluorescence intensity of water soluble QS^{2+} changes with the

change in concentration of SDS and this observation is used to determine CMC of SDS. In order to obtain the location and mobility of QS^{2+} molecules in micellar systems, rotational relaxation of a probe molecule in micellar assembly is determined using time resolved anisotropy measurements. All the different techniques used in this study reveal that the photophysics of QS^{2+} is very sensitive to the microenvironment of SDS micelles and QS^{2+} molecules reside at the water-micelle interface.

Further, the photophysical behaviour and rotational relaxation dynamics of QS in aqueous solutions of SDS at different pH have been studied using steady state and time resolved fluorescence spectroscopy. It has been observed that the cationic form of QS (at pH 2) forms a fluorescent ion pair complex with the surfactant molecules at lower concentrations of surfactant, however, for higher concentrations of SDS, the probe molecule binds strongly with the micelles and resides at the water-micelle interface. At pH 7, QS is singly protonated in bulk aqueous solution and at lower concentrations of SDS, aggregation between probe and surfactant molecules has been observed. Whereas, at higher concentrations of SDS at pH 7, an additional fluorescence peak corresponding to dicationic form of QS appears and this has been attributed to double protonation of the QS molecule due to change in local pH. At pH 12, an increase in fluorescence intensity and fluorescence lifetimes have been observed and these observations are attributed to an increase in radiative rate due to the incorporation of QS at the micelle-water interface. The local pH at micellar surface has been found different from the pH of bulk solution.

List of abbreviations and symbols

Symbol	Abbreviation
QS	Quinine Sulfate
QD	Quinidine
QS^{2+}	Quinine Sulfate dication
QS^{+}	Quinine Sulfate monocation
QD^{2+}	Quinidine dication
QD^{+}	Quinidine monocation
CMC	Critical Micellar Concentration
EERS	Edge Excitation Red Shift
SDS	Sodium dodecylsulfate
λ_{ex}	Excitation Wavelength
λ_{em}	Emission Wavelength
Φ	Quantum yield
η	Viscosity
TCSPC	Time Correlated Single Photon Counting
T	Lifetime
k_r	Radiative rate constant
k_{nr}	Non-radiative rate constant
α	Pre-exponential factor
$\langle\bar{\tau}\rangle$	Average lifetime
S-V	Stern- Volmer
K_{sv}	Stern -Volmer quenching constant
K_q	Quenching rate constant
Q	Quencher
r_h	Hydrodynamic radius
DSE	Debye-Stokes-Einstein
θ_0	Cone angle
D_w	Wobbling diffusion coefficient

Symbol	Abbreviation
S	Order parameter
FCE	Frank-Condon Excited State
FCG	Frank-Condon Ground State
IC	Internal Conversion
ISC	Intersystem Crossing
ET	Electron Transfer
ESPT	Excited State Proton Transfer
FRET	Fluorscence Resonance Energy Transfer
E_T	Energy transfer efficiency
ESIPT	Excited State Intramolecular Proton Transfer
CT	Charge Transfer
D-A	Donar-Acceptor
LE	Locally Excited
ICT	Internal Charge Transfer
D	Donar
A	Acceptor
$(\bar{\nu}_a - \bar{\nu}_f)$	Stokes shift
CTAB	Cetyltrimethyl ammonium bromide
TX-100	4-(1,1,3,3-Tetramethylbutyl)phenyl-polyethylene glycol
K_B	Binding constant
K_A	Association constant
Γ	Emissive rate of fluorophore
PMT	Photomultiplier Tube
CFD	Constant Fraction Discriminator
TAC	Time to Amplitude Convertor
MCA	Multichannel Analyzer
LED	Light Emitting Diode
FWHM	Full Width Half Maximum
μ_e	Excited state dipole moment
μ_g	Ground state dipole moment

Symbol	Abbreviation
E	Dielectric constant
n	Refractive index
DFT	Density Functional Theory
a_0	Onsager radius
Å	Angstrom
SWE	Shorter Wavelength Excitation
χ^2	Chi-square
CAC	Critical Aggregation Concentration

CONTENTS

List of Figures

List of Tables

Chapter 1

Introduction

1.1 Fluorescence spectroscopy

Fluorescence occurs when a fluorescent material (a fluorophore) is excited into a higher electronic state by absorbing an incident photon and cannot return to the ground state except by emitting a photon. The emission usually occurs from the lowest vibrational level of the excited electronic state and goes to an excited vibrational state of the ground electronic state. Thus fluorescence signals occur at longer wavelengths than absorption wavelengths. The energies and relative intensities of the fluorescence signals give information about structure and environments of the fluorophores.

Absorption of UV radiation by a molecule excites it from a vibrational level in the electronic ground state to one of the many vibrational levels in the electronic excited state. This excited state is usually the first excited singlet state. A molecule in a high vibrational level of the excited state will quickly fall to the lowest vibrational level of this state by losing energy to other molecules through collision. The molecule will also distribute the excess energy to other possible modes of vibration and rotation.

Molecules in the excited singlet state can undergo spin conversion to form a triplet electronic energy state. The emission from triplet state is termed as phosphorescence and is generally shifted to longer wavelengths (lower energy) relative to fluorescence, which arises when unpaired electrons are present in the system. If all the electrons are paired, the multiplicity is one, governed by the Equation 1.1:

$$M = 2S + 1 \tag{1.1}$$

where, M is the multiplicity and S is the spin of the electrons, which is either +1/2 or -1/2. Thus, if all the electrons are paired, the spin value is equal to zero and the multiplicity is equal to one, which defines the singlet electronic state. In the case of the triplet state, where the electrons are unpaired, solving for Equation 1.1 gives a multiplicity of 3 and hence the triplet electronic state. The total electron spin angular momentum S must be conserved in a radiative transition. Thus in most molecules strong

absorption and emission are singlet-singlet in character, the triplet transition being prohibited. The introduction of a heavy atom into the skeleton of an absorbing molecule or the solvent may cause a breakdown of the spin conservation rule for molecules, facilitating a change in multiplicity and allows the triplet transition. Other than fluorescence and phosphorescence, there are many different decay pathways by which a molecule in the excited state can relax to the ground electronic state and these processes will be discussed in more detail later.

Among the various analytical techniques, fluorescence spectroscopy is one of the most fashionable techniques due to high sensitivity and selectivity, together with the advantage of spatial and temporal resolution and the possibility of remote sensing using optical fibers.[1] Fluorescence is an important investigational tool in many areas of analytical science, due to its high sensitivity and selectivity. It is the basic reporting technique in many chemical sensors and biosensors with a broad range of applications in clinical diagnostics, environment monitoring, agriculture and in various industrial technologies.[2] It has become a very potential technique in DNA sequencing, immunoassays, flow cytometry and genetic analysis.[1,3]

Fluorescence competes successfully with other detection methods that are based on electrochemical response or on the change in mass, heat, or refractive index on target binding because of the following reasons:

- With proper dye selection and proper experimental conditions, the absolute sensitivity may reach the limit of single molecules. So the fluorescence detection from a single molecule is possible.
- It has a high speed of response.[4] This response is in the scale of fluorescence lifetime of photophysical or photochemical events which can be as short as 10^{-8}- 10^{-10} s.
- It allows sensing at a distance from analyzed object in a non-invasive manner and allows formation of images.[5]
- Apart from all these advantages, one of the significant features of the fluorescence technique is its versatility. Fluorescence sensing can be done in solid, liquid and gas media, and at all kinds of interfaces between these phases. Fluorescence detection can be equally well-suited for remote industrial control and for sensing different targets within the living cells.[2]

There are generally two kinds of detection approaches in the area of fluorescence spectroscopy.[1] First approach is that when a molecule itself is fluorescent, then direct fluorometric detection is possible by means of a spectrofluorometer operating at appropriate excitation and observation wavelength. Based on this approach several fields of application have been reported such as analysis of air and water organic pollutants, oils, foods such as cow milk that has amino acids of intrinsic fluorescence, drugs such as morphines, monitoring of industrial processes, monitoring of species of clinical relevance such as proteins in blood serum, criminology, in crude oils.[6]

The second approach is indirect approach which is useful for detection of the metal ions and the molecules which are non fluorescent. Detecting the metal ions and these molecules may be conducted by means of indirect approaches (1) reaction of a non-fluorescent molecule of interest with a reagent to generate fluorescent products (or fluorophore) that can be monitored using fluorescence; (2) complex between the non-fluorescent compound and fluorophore to generate fluorescence complex that can be monitored using fluorescence; (3) collision of fluorescent analyte with an ion or molecule to generate fluorescence decrease that can be monitored. Such fluorescence decrease is dependent on the specific ions or molecules and their concentrations.

1.1.1 Theory of fluorescence

Fluorescence spectroscopy dates back to 1852, when Sir G. G. Stokes described the mechanism of the absorption and emission process.[7] Thus, the observation and development of fluorescence spectroscopy has a history that dates far back in time. The technique relies on the interaction between light and matter, which can be described by the Equation1.2:[7]

$$E = h\nu = \frac{hc}{\lambda} \tag{1.2}$$

where, E is the energy, h is Planck's constant, ν is the frequency and c is the speed of light, respectively. Equation shows that there is a relationship between energy and frequency.

Moreover, the frequency is related to the wavelength of light by the Equation 1.3:[7]

$$\nu = \frac{c}{\lambda} \tag{1.3}$$

where, λ is the wavelength (expressed in nm). Figure 1.1 shows the relationship between the energy levels within a molecule. As shown, molecules contain a series of closely spaced energy levels. Furthermore, molecules can be excited from the ground state to higher excited states by absorbing a discrete quantum of light that is equal to the energy difference between the states. Moreover, the electronic states contain vibrational and rotational energy levels (Figure 1.1), which leads to one of the key features of fluorescence. Once a molecule absorbs a specific energy of light it can relax via different radiative and nonradiative decay pathways.

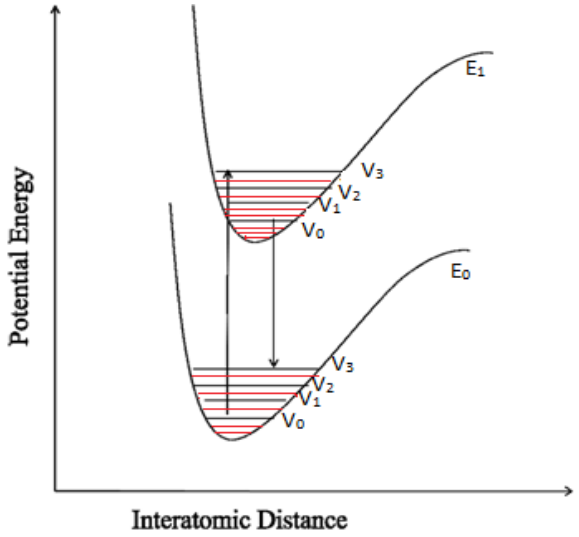

Figure 1.1 Potential energy diagram of a diatomic molecule showing the different electronic energy states and their associated vibrational and rotational energy levels. Figure adopted from Lakowicz, J.R., *Principles of Fluorescence Spectroscopy*. ed.; Kluwer Academic/Plenum: New York, 1999

1.1.2 Stoke's shift

Figure 1.2 shows the normalized absorption and fluorescence emission spectrum of the Quinidine monocation (QD^+) in cyclohexane.[8] This Figure clearly shows that the fluorescence is shifted to longer wavelengths (lower energy) from the absorption. Absorption of light typically occurs from the lowest vibrational level of the ground state to a higher vibrational level but the fluorescence takes place from the lowest vibrational level of the first excited state. Thus, absorption occurs at a higher energy than the subsequent fluorescence. This phenomenon is known as the Stokes shift and is defined by the Equation 1.4:

$$\text{Stokes shift} = 10^7\left(\frac{1}{\lambda_{ex}} - \frac{1}{\lambda_{em}}\right)(\text{cm})^{-1} \quad (1.4)$$

where, λ_{ex} and λ_{em} are the maximum wavelengths for the excitation and emission, respectively. These values are expressed in units of nm.

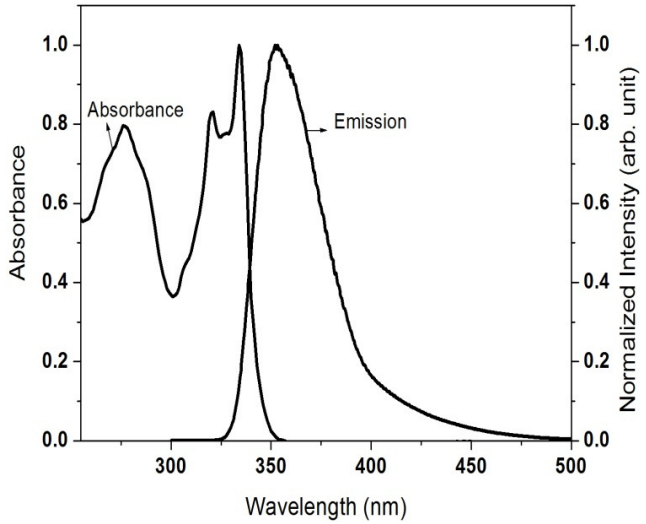

Figure 1.2 Normalized absorption and fluorescence emission spectrum of Quinidine monocation (QD^+) in Cyclohexane. The concentration of Quinidine monocation is of the order of mM. Figure taken from Estimation of ground and excited state dipole moments of Quinidine monocation and Quinidine dication: Experimental and numerical methods. *Journal of Molecular liquids* **2013,** *179*, 88

1.1.3 Quantum yield

Every molecule has a characteristic property that quantitatively describes the molecules ability to fluoresce, which is known as the Quantum yield (or quantum efficiency). The Quantum yield (ϕ) is defined by the Equation 1.5:

$$\phi = \text{no. of photons emitted / no. of photons absorbed} \quad (1.5)$$

where, ϕ is the Quantum yield. Thus, the higher the Quantum yield, the greater the fluorescence intensity. On the other hand, molecules that possess a Quantum yield close to zero are basically non-fluorescent. These molecules still absorb light but have efficient non-radiative decay pathways to dissipate the energy (i.e. collisions). The precise determination of absolute Quantum yields of fluorescence is much difficult than the relative determination of Quantum yield. The Quantum yield of a molecule can be determined experimentally using a known standard and the Equation 1.6:[3]

$$\phi_{\text{sample}} = \frac{A_{\text{reference}}}{F_{\text{reference}}} \times \frac{F_{\text{sample}}}{A_{\text{sample}}} \times \frac{\eta^{2}{}_{\text{sample}}}{\eta^{2}{}_{\text{reference}}} \times \phi_{\text{reference}} \qquad (1.6)$$

where, $A_{\text{reference}}$ and A_{sample} are the absorbances at the excitation wavelength, $F_{\text{reference}}$ and F_{sample} are the integrated fluorescence intensities; and $\eta_{\text{reference}}$ and η_{sample} are the refractive indices for the reference and the sample solutions, respectively. Thus, the Quantum yield is an important property for fluorescence applications and can be determined experimentally.

The relaxation processes in excited electronic state are mainly divided in two broad categories: photophysical and photochemical processes. A brief description about these processes is given in the following sections.

1.1.4 Photophysical processes in excited electronic states

Photophysics concerns processes induced by electromagnetic radiation that do not produce an irreversible change in the covalent structure of the system. Photophysical processes include the light-induced generation of excited states, transitions between excited states, and relaxations that return the system to its initial ground state.

Once a molecule absorbs suitable quanta of light, it goes to one of the vibrational levels of one of its electronically excited states, called Frank-Condon Excited (FCE) state. This transition occurs in 10^{-15}s, a time too short for significant displacement of nuclei. This is the Franck-Condon principle. The number of possible ways by which molecule losses its energy and returns to the ground state can be depicted by Jablonski diagram (Figure 1.3).

Molecule present in higher vibrational level of the higher excited electronic state (say S_2) dissipates its excess vibrational energy as thermal energy and goes to zero vibrational level (v = 0) of the S_2 state. The energy gap between the higher electronic states is generally smaller than the energy gap between S_1 state and S_0 state. For this reason molecule arrives at S_1 state quickly by Internal Conversion (IC) or Quantum mechanical tunnelling, followed by vibrational relaxation to v = 0 level of S_1 state. Now, if there is an overlap between the zero vibrational level of S_1 state and higher vibrational level of S_0 state, molecule comes back to the S_0 state by Internal Conversion. The molecule can also release its excitation energy as photon. This radiative deactivation

process of molecule from S_1 state to S_0 state is called fluorescence. Sometimes the zero vibrational level of S_1 state couples with the higher vibrational levels of the lowest triplet state i.e., T_1. In such cases, the molecule in the S_1 state can also undergo a spin-conversion to the first triplet state T_1. This process is called Intersystem Crossing (ISC).

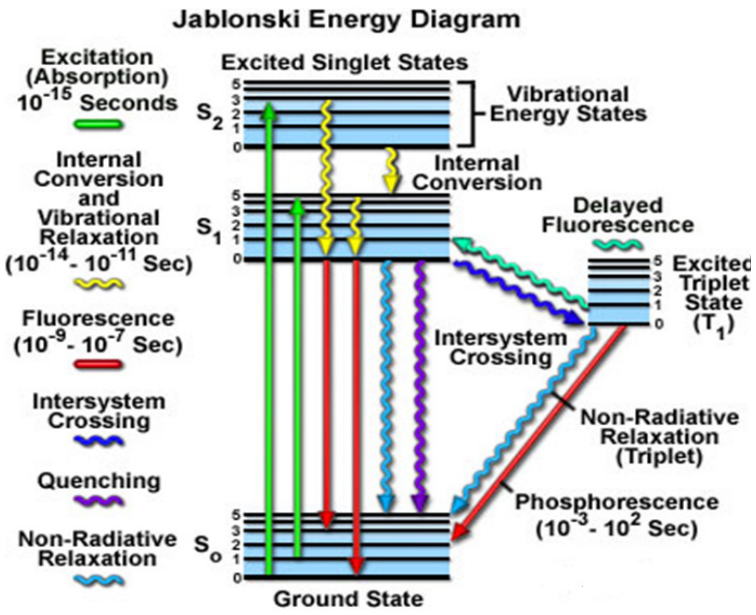

Figure 1.3 Jablonski diagram showing fates of polyatomic molecules upon photoexcitation[3]

The molecule at higher vibrational level of T_1 state quickly losses its vibrational energy and arrives at v = 0 level of T_1 state. From T_1 state also molecule can return to S_0 state either by non-radiative process, i.e. Intersystem Crossing or by radiative process i.e. phosphorescence. Transition from T_1 to the singlet ground state (S_0) is forbidden and as a result the rate constants for triplet emission are several orders of magnitude smaller than those of fluorescence. Both radiative processes leave the molecule to the Frank-Condon Ground (FCG) state, from where molecule goes to zero vibrational level of S_0 state by collisional deactivation process. However, an electronic spectrum is affected by various factors such as substituents, pH, nature of solvents etc.

The various deactivation routes of an excited molecule may be broadly classified into two categories, one is the radiative transitions and the other is non-radiative transitions. Radiative transitions routes are fluorescence, phosphorescence and radiative energy transfer (trivial process). On the other hand, possible routes open to non-radiative transitions are: (i) Internal Conversion (IC), (ii) Intersystem Crossing (ISC), (iii) Non-

radiative energy transfer, (iv) Photoinduced Electron Transfer (ET) and (v) Excited State Proton Transfer (ESPT).

Radiationless transition between two electronic states may be represented as the presence of the point of intersection of potential energy surfaces. A crossing point is the point of equal energy for both the curves. The irreversible radiationless transfer of energy involves two steps: (a) the horizontal transfer of energy at the isoenergetic point from the zero-point level of higher electronic energy state to the high vibrational level of the lower electronic state and (b) the rapid loss of excess vibrational energy after transfer. The radiationless transitions are governed by three factors. They are

(1) Density of state ρ_E which is defined as the number of vibrational levels per unit energy interval at the energy of the initial value.

(2) Energy gap ΔE between the interacting electronic states.

(3) Vibronic overlap or Franck-Condon factor.

The major nonradiative deactivation routes from excited molecules are (i) Internal Conversion and (ii) Intersystem Crossing (iii) Fluorescence Resonance Energy Transfer.

(i) Internal Conversion (IC): It is a radiationless passage between the electronic energy states of same spin multiplicity or between the different vibrational levels of the same electronic state.[9,10] The internal conversion rate constant for $S_1 \rightarrow S_0$ is small ($10^9 - 10^7$ sec^{-1}) compared to the rate constant for higher states like $S_2 \rightarrow S_1$ etc. ($10^{14} - 10^{11}$ sec^{-1}). However it has been observed that with the increase of energy gap between S_1 and S_0, the internal conversion efficiency decreases.[11,12] Internal conversion between $T_2 \rightarrow T_1$ has also been observed for some molecules.[13]

(ii) Intersystem Crossing (ISC): It describes the radiationless transition process between states of different spin multiplicity and depends on spin orbit coupling.[9] Due to large energy gaps; transition from S_1 to S_0 is not always probable by radiationless transition mechanism. Under these circumstances the molecule has two alternatives: (i) to return to the ground state by fluorescence emission or (ii) to cross over to the lowest triplet state non-radiatively.

Since $T_1 - S_0$ energy differences are normally of the order of 20,000 cm^{-1} and $S_1 - T_1$ energy differences are commonly of the order of 3000-9000 cm^{-1}, the intersystem crossing probability ($S_1 \rightarrow T_1$) is considerably greater than the probability of direct transition from the ground state to the triplet state. The intersystem crossing rate[14] for $S_1 \rightarrow T_1$ transition is $10^{11} - 10^{8}$ sec^{-1} and that for $T_1 \rightarrow S_0$ transition is $10^{3} - 10^{2}$ sec^{-1} i.e. it depends on the energy gap between singlet and triplet states.

(iii) Fluorescence Resonance Energy Transfer (FRET): Is a distance-dependent interaction between the electronic excited states of two chromophoric molecules in which excitation is transferred from a donor molecule to an acceptor molecule without emission of a photon. A donor chromophore, initially in its electronic excited state, may transfer energy to an acceptor chromophore through nonradiative dipole–dipole coupling. This mechanism is termed "Förster Resonance Energy Transfer" or "Fluorescence Resonance Energy Transfer".

According to Forster's theory, the efficiency of FET depends mainly on the following factors: (i) The extent of overlap between the donor emission and the acceptor absorption, (ii) the orientation of the transition dipole of donor and acceptor and (iii) the distance between the donor and the acceptor.[15,16]

Efficiency of energy transfer for a single donar-acceptor pair at a fixed distance depends on the donor-to-acceptor separation distance *r* with an inverse 6th power law due to the dipole-dipole coupling mechanism: [15,16]

$$E_T = \frac{1}{1+\left(\frac{r}{R_0}\right)^6} \tag{1.7}$$

with R_0 being the Förster distance of this pair of donor and acceptor, i.e. the distance at which the energy transfer efficiency is 50%. The Förster distance depends on the overlap integral of the donor emission spectrum with the acceptor absorption spectrum and their mutual molecular orientation as expressed by the following Equation1.8: [15,16]

$$R_0^6 = \frac{9Q_0(\ln 10)k^2 j}{128\pi^2 n^4 N_A} \tag{1.8}$$

where, Q_0 is the fluorescence Quantum yield of the donor in the absence of the acceptor, κ^2 is the dipole orientation factor, n is the refractive index of the medium, N_A is Avogadro's number, and J is the spectral overlap integral calculated as[15,16]

$$J = \int f_D(\lambda)\varepsilon_A(\lambda)\lambda^4 d\lambda \tag{1.9}$$

where, f_D is the normalized donor emission spectrum and ε_A is the acceptor molar extinction coefficient. κ^2 =2/3 is often assumed. This value is obtained when both dyes are freely rotating and can be considered to be isotropically oriented during the excited state lifetime. If either dye is fixed or not free to rotate, then κ^2 =2/3 will not be a valid assumption. In most cases, however, even modest reorientation of the dyes results in enough orientational averaging that κ^2 = 2/3 does not result in a large error in the estimated energy transfer distance due to the sixth power dependence of R_0 on κ^2. Even when κ^2 is quite different from 2/3 the error can be associated with a shift in R_0 and thus determinations of changes in relative distance for a particular system are still valid. Fluorescent proteins do not reorient on a timescale that is faster than their fluorescence lifetime. In this case κ^2 remains in the limit $0 \leq \kappa^2 \leq 4$.

1.1.5 Photochemical processes in excited state

1.1.5.1 Excited state proton transfer

The transfer of a proton from one atom to another is one of the most extensively studied phenomena in photochemistry of molecules and proteins.[17,18] This elementary reaction plays an immense role in several essential physical, chemical, and biological processes including acid–base neutralization, electrophilic addition and enzymatic reactions.[19] Excited State Proton Transfer (ESPT) process is the main non-radiative pathway in the excited state of many biological probe molecules. In almost of the cases ESPT results in dual emission. One of these emission bands arises from the neutral excited state and hold a mirror image relationship with the absorption spectrum. The other emission band arises from the deprotonated (anion) or protonated (cation) species produced in the photoexcited state with a large Stokes shift.[20] The existence of hydrogen bonding prior to dislocation has classified the proton transfer reactions into two types: (i) Excited State Intermolecular Proton Transfer (ESPT) and (ii) Excited State Intramolecular Proton Transfer (ESIPT).

(i) In Excited State Intermolecular Proton Transfer (ESPT) process, the proton is transferred from one molecule (proton donor) to another (proton acceptor). This type of reaction finds applications in the study of proton hydration dynamics[21,22] and as probes to study the microenvironment of the fluorophore in protein,[23-25] micelle,[26-28] reversed micelle[29-31] and cyclodextrin[32-34] media.

(ii) Excited State Intramolecular Proton Transfer (ESIPT) occurs within the molecule itself and generally proceeds along the preformed hydrogen bonds within picosecond time scale, with a very low or inappreciable barrier.[35-39] The phototautomers are usually formed in the excited state and relax quickly to the corresponding ground state and fluoresce with a large Stokes' shift. Generally, ESIPT reactions are followed by rise and decay of the strong Stokes shifted fluorescence of the tautomer produced through the ESIPT process. Majority of the applications of the ESIPT chromophores are based on the photophysical properties, such as design of fluorescent chemosensors by perturbation of the ESIPT process on interaction of chromophore with the analytes.

1.1.5.2 Charge transfer

Among various photophysical and photochemical processes, Charge Transfer (CT) is an important and fundamental interaction, underlying most problems in photophysical, photochemical as well as photobiological processes.[40-44] It is the basis of numerous present and possible future developments including organic conductors and superconductors, Light Emitting Diodes (LEDs) as well as production and storage of electricity. The concept of CT refers to excitation into a state that involves a complete transference of an electron from a donor to an acceptor or between them in the excited state of either of the species. This phenomenon imparts an effect on the emission spectra by developing a new structureless band at a longer wavelength region.

There are two phenomenologically different ideas concerning the CT. The first one, through space interaction, is applicable when the two chromophoric parts are within van der Waals distance[45] and the other one, through bond interaction, deals with rigid systems when the distance is much larger.[46] In the ground state the Donor–Acceptor (D–A) complex possesses no stabilization energy apart from the very small resonance energy due to the ionic structure $D^{+}A^{-}$.

In spectroscopy, we generally see two fluorescence band, a 'normal' fluorescence band or the Locally Excited (LE) band and a second, strongly red-shifted Charge Transfer (CT) band. Locally Excited state of the exciplex, DA* is the origin of LE band, A* being the lowest singlet excited state of A. The ideal systems for the study of the charge transfer processes are electron donor–acceptor molecules.[47,48] These molecules not only provide a testing ground for the contemporary theories of CT process, but they are also useful for the study of solvation dynamics[49] and nonlinear optical properties,[50] etc.

The CT reactions may be classified as (i) Intermolecular Charge Transfer and (ii) Intramolecular Charge Transfer.

(i) In an intermolecular charge transfer process, an electron from a molecule with high charge density (donor) is transferred to another molecule with low charge density (acceptor) leading to the formation of a new complex called Charge Transfer (CT) complex. In this case the transition occurs from the highest filled molecular orbital of the donor to the lowest empty molecular orbital of the acceptor. Additional charge transfer is also possible on promotion of an electron to higher unoccupied orbitals of the acceptor. The CT complexes are regarded as important materials due to their ample applications.[51-54] The CT complexes have been reported as important reaction intermediates in many chemical reactions.[55,56] The question of participation of CT complexes in organic synthesis, and in understanding reaction mechanisms has been debated since the classical work interaction of iodine with aromatic hydrocarbons of Benesi and Hildebrand.[57] The review work of Mataga et. al. has focused elaborately on the fundamental aspects of charge transfer process and CT complex chemistry.[58]

(ii) Intramolecular Charge Transfer is a fundamental process and has always been attracting considerable attention as a topic of central importance in photochemistry and photobiology.[59-64] A charge separation may result from the transfer of an electronic charge upon excitation from a Donor (D) site to an Acceptor (A) site within a suitable molecule. In such Internal Charge Transfer (ICT) process, positive and negative charges are localized in two different separated functional parts of the same molecule. This new charge

distribution generally leads to a large increase of the dipole moment, and hence causes a marked solvatochromic effect and a large Stokes shift.

The solvent polarity sensitive organic Donor–Acceptor (D–A) compounds have been claiming increasing interest and are being used as the fluorescent probes to study different microenvironments.[65-70] Among various fluorophores showing ICT properties, coumarins and aminonaphthalimides are the prominent ones.[66,48,71-73] Through their extensive studies Berces, Kossanyi, and co-workers discussed the influence of geometry of the molecule or intramolecular geometrical relaxation process on the emitting properties of various ICT probes.[74-76] Yuan and Brown studied the photophysical properties of aminonaphthalimides in various media.[77]

1.1.6 Factors affecting fluorescence

There are many factors that can affect the fluorescence of a molecule. Typically, these factors can be broken into two sub-groups, those which are of a structural nature and those that have to do with the environment surrounding the molecule. Since the work presented in later chapters deals more with the effect of the environment on the fluorescence, this section will focus more on environmental factors that affect the fluorescence of a molecule. Structurally, it is worth noting that most unsubstituted aromatics exhibit an intense fluorescence in the UV-Visible range of the electromagnetic spectrum. Moreover, as the conjugation increases, the fluorescence shifts to longer wavelengths (lower energy).

Environmental effects encompass factors such as; solvent environment, the presence of "heavy" atoms, temperature, concentration and the rigidity of the environment (e.g. thin films). An example of solvent effects is the observed red shift in the fluorescence of polar molecules as the dielectric constant of the solvent increases. It is thought that the observed red shift is due to the fact that the excited electronic state of a polar molecule is more polar than its ground state. Thus, as the solvent environment becomes more polar, it more effectively stabilizes the excited state. Thus, a shift to lower energy is observed.

Another significant environmental effect is the "heavy" atom effect, which promotes intersystem crossing. As a result, in these cases, phosphorescence is the predominante form of emission (Figure 1.3). This effect results from the presence of

heavy atoms, either as a substituent within the molecule or contained in the solvent. For example, the ratio of the phosphorescence to fluorescence in naphthalene is 48 times larger in an alcohol containing bromide than in the alcohol without bromide.[7] Furthermore, the presence of other heavy atoms, such as the halogens or oxygen, is thought to increase the rate of intersystem crossing. The effect of temperature on the fluorescence emission of molecules has been studied extensively and it has been shown that the fluorescence decreases (as well as the Quantum yield) with increasing temperature. One reason for this is the degradation of the fluorescence species at high temperatures. Furthermore, increase in fluorescence due to decreasing temperature can be rationalized by the fact that cooling down a solution increases the viscosity of the medium, thereby decreasing the rate of collisions. Thus, as the rate of collisions decreases, the propensity for energy to be dissipated via collisional deactivation is reduced. Moreover, other processes involving the excited singlet state, such as intermolecular bonding, tend to occur more slowly as the temperature decreases.[7] The rigidness of the media that a molecule is in, can have a dramatic effect on the fluorescence emission. As the environment becomes more rigid, the viscosity increases, thereby causing a decrease in the rate of bimolecular collisions. As a result, a viable non-radiative pathway becomes less significant and the molecule is more likely to fluoresce than to undergo collisional deactivation. Furthermore, some aromatic molecules have conjugation that gives rise to two different isomers, a trans- and a cis-isomer. For example, the dye molecule Cyanine 3 has a fluorescent trans and a non-fluorescent cis form.[78,79] In a rigid environment, the dye is less likely to isomerize to its non-fluorescent cis form and decay non-radiatively. Thus, the rigid environment leads to an increase in the fluorescence intensity of the molecule. The concentration of fluorescent molecules has a significant effect on their fluorescence properties. The fluorescence emission is dependent on the power of the excitation beam, given by the Equation 1.10:[80]

$$F = K'(P_0 - P) \tag{1.10}$$

where, F is the fluorescence, P_0 is the power of the incident beam, P is the power of the beam after it has transversed through the sample and K' is a constant that depends on the Quantum yield of the system. The fluorescence intensity is related to the power of the beam by Beer's Law[80]

$$\frac{P}{P_0} = 10^{-\varepsilon bc} \tag{1.11}$$

where, ε is the molar absorptivity, b is the pathlength and c is the concentration. Note that the absorbance is given:[80]

$$A = \varepsilon bc \tag{1.12}$$

Substituting Equation 1.11 into Equation 1.10 yields:[80]

$$F = K' P_0 (1 - 10^{-\varepsilon bc}) \tag{1.13}$$

Moreover, Equation 1.13 can be expanded to a Maclaurin series to give the Equation 1.14:[80]

$$F = K' P_0 \left[2.3\varepsilon bc - \frac{(2.3\varepsilon bc)^2}{2!} + \frac{(2.3\varepsilon bc)^3}{3!} ..... \right] \tag{1.14}$$

If the exponential factor $2.3\varepsilon bc$ is small, the subsequent terms in the series are small relative to the first. Thus, the Equation can be approximated to:[80]

$$F = 2.3 K' \varepsilon bc P_0 \tag{1.15}$$

and at constant power, Equation 1.15 simplifies to the Equation 1.16:[80]

$$F = Kc \tag{1.16}$$

Thus, at low concentrations, the fluorescence emission as a function of concentration is linear. At higher concentrations, when the absorbance increases, the exponential terms in Equation 1.14 starts to dominate. Therefore, the fluorescence emission as a function of concentration deviates from a linear trend. At higher concentrations, the fluorescence typically begins to decrease. It is worth noting that self-quenching caused by increased collisions between molecules, thus increasing the rate of collisional deactivation, could explain the observed deviation from the linear trend. Furthermore, the increase in the concentration of the molecules can induce the molecule to form aggregates, which alters their spectroscopic properties.

1.1.6.1 Substituent effect

Substituents can bring about substantial changes in the absorption and fluorescence spectra of the parent molecules. With increasing the extension of conjugation in the direction of linear annelation both the absorption and fluorescence band maxima and intensities of transition increase e.g. benzene, naphthalene and anthracene. According to Kasha's rule fluorescence is possible if the $\pi \rightarrow \pi^*$ is the lowest energy transition, and phosphorescence if $n \rightarrow \pi^*$ is the lowest energy transition.[81] Fluorescence Quantum yield thus depends upon the rate of non-radiative processes with respect to the rate of radiative process. Substitution of alkyl group on the aromatic ring has little effect which results in the small red shifts in the absorption and fluorescence spectra. Substitution of alkyl side chain increases, the vibrational degrees of freedom and thereby increases internal conversion, so the fluorescence Quantum yield decreases. Substitution of electron donating group, e.g. –OH, $-NH_2$, $-N(CH_3)_2$, $-OCH_3$ on benzene ring results in large red shift, whereas the presence of halogen atoms on aromatic molecule decreases the fluorescence Quantum yield with increase in atomic number of the halogen atom, due to the heavy atom effect.[82] These heavy atoms actually increase the spin-orbit coupling and thus the rate of intersystem crossing. The introduction of hetero atom sometimes increases the rate of non-radiative process which results in the decrease in fluorescence Quantum yield.[83,84]

1.1.6.2 Effect of solvent

The electronic spectra are generally affected by the environment around the molecules. The position and intensity of absorption and fluorescence spectra are thus altered by the environment. To characterize different biological system or biomimicking system using a certain probe, photophysical characterization of a probe molecule in different types of solvents is important. Generally, an absorption and emission spectrum of a probe in a variety of solvents (nonpolar, polar - aprotic and protic) is recorded at reasonable probe concentration. This will involve both solute-solute and solute-solvent interactions. Thus the spectral characteristics of the molecules depend on the nature of the solvent as well as on the solute. In this section, the effect of solvents on the spectral properties of the solute molecules is only discussed which can be broadly classified into two classes: general solvent interactions and specific interactions.

1.1.6.2.1 Dispersive or general solvent interactions

These interactions basically involve the electrostatic forces, and the spectral shifts can be correlated with the refractive index (n) and dielectric constant (ε) of the solvents. General interactions can be further divided into following types:-

i **Dipole-Dipole interaction:** Here both solute and solvent molecules have permanent dipole moment.

ii **Dipole-Induced Dipole interaction:** Here either solvent or solute is having permanent dipole moment which induces a dipole in the other.

iii **Induced Dipole-Induced Dipole interaction (London Dispersion forces):** Here both solute and solvent molecules do not have permanent dipole moment.

The magnitude of these interactions follow the order I > II > III.

1.1.6.2.2 Specific interactions

Specific interactions include hydrogen bonding, complex formation between solute and solvent. These interactions which are stronger than non-specific interaction between solute and solvent can result changes in absorption and fluorescence spectra of molecules.

The electronic transitions can be divided into three different kinds, (i) $\pi \rightarrow \pi^*$, (ii) Charge Transfer and, (iii) $n \rightarrow \pi^*$. In all these transitions, the dipole moment of the molecule is altered and thus interactions with the solvent molecules depend upon the change in the dipole moment. The hydrogen bond interaction changes the spectral characteristics of molecules to a great extent. The hydrogen bonding properties between solvent and solute in the ground state are often different from that in the first singlet excited state.

According to Frank –Condon principle, absorption of light occurs within 10^{-15} s, is too short compared with the period of nuclear motion. At the instant of its formation of FCE (Figure 1.4) state, the excited solute molecule is momentarily surrounded by a solvent cage whose size and orientation is similar to those that are present in the ground state.

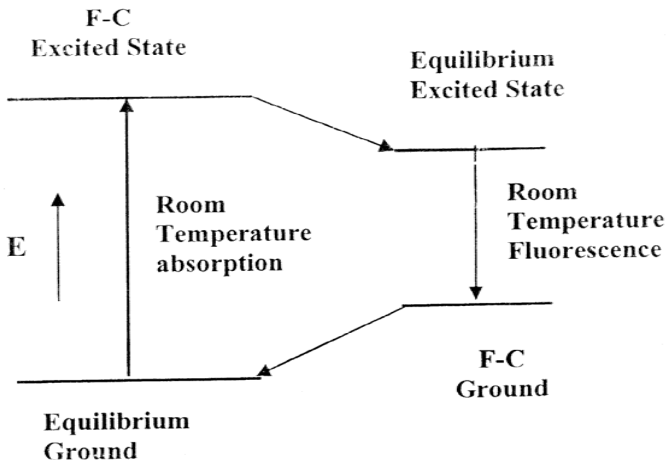

Figure 1.4 Schematic representation of equilibrium and Frank-Condon (F-C) electronic states[3]

The molecule in the FCE state relaxes vibrationally to the lowest vibrational level of the first excited singlet state within the time scale of 10^{-13}s. Subsequent to excitation and vibrational relaxation, the solvent cage reorganizes accordingly in the new environment, due to the change in charge distribution and thus the dipole moment upon excitation, within the time scale of 10^{-11} and 10^{-12}s. This solvent reorganization or reorientation is commonly called as "solvent relaxation". The combined effect of vibrational, solvent and geometry relaxations is termed as thermal relaxation. By these processes, an equilibrium excited state is formed in which solvent configuration is optimal for the geometry and electron distribution of the excited molecule. Emission occurs from the equilibrium excited state to the metastable FCG state. Because of the rapid transition, the molecule in the FCG state is still in the environments which are similar to that in the excited state. Vibrational and solvent relaxation further brings it to equilibrium ground state. Since the thermally relaxed excited state is lower in energy than FCE state and FCG state is higher in energy than thermally relaxed ground state, fluorescence occurs at longer wavelength than absorption. This loss in energy between absorption and fluorescence is called the Stoke's-shift and is denoted by $(\bar{v}_a - \bar{v}_f)$, where $\bar{v}_a$ and $\bar{v}_f$ are the reciprocal of wavelength of absorption and fluorescence spectral respectively.

The distinction between these kinds of transitions can be made on the basis of molar extinction coefficient, effect of solvents on spectral characteristics and emission

properties. In general n→ π^* transitions are very weak and get blue shifted in the presence of protic solvents and phosphorescence is the major pathway for the deactivation of excited state energy. On the other hand, both π→ π^* and Charge Transfer (CT) bands are strong and band maxima get red shifted with the increase in polarity or proton donar capacity of solvent and fluorescence is generally observed as compared to phosphorescence. The solvatochromic shift is more in case of CT transition than π→ π^* transition.

The specific or non-specific interactions between the fluorophore and solvent drew the attention of many researchers. It is widely reported that, the solvatochromic plots satisfactorily correlated with the emission maxima as approximately linearly dependent on the solvent polarity functions of various forms.[85,86] In some cases, exceptions from the correlation appear in strongly hydrogen-bonding protic solvents, e.g., alcohols or water.[87,88] The first systematic study of the effects of solvents on fluorescence spectra of aromatic molecule has been done by Pringsheim[89] and Forster.[90] Pimental,[91] Mataga and Tsumo[92] have reported on the significance of the hydrogen bonding in the solvent effect.

Lippert,[93,94] McRae[95] and Suppan[96] have carried out the quantitative treatment of the effect of solvents on the absorption and fluorescence spectra. Oshika,[97] Lippert[93,94] and Mataga et. al.[98] were the first to derive equations relating changes in the dipole moments on excitation with spectral changes. These equations were modified by Liptay,[99] Bilot and Kawski[100] and Bakhshiev[101] by including polarizability of the fluorophores and dispersive interactions. Later, Lippert and Mataga et. al.[93,94,98] modified the equation by neglecting the polarizability effects of the fluorophore.

Most theories[99-107] of the solvent effect on the location of the absorption, $\bar{\nu}_a$, and fluorescence bands, $\bar{\nu}_f$, lead, in spite of different assumptions, to similar expressions for the difference $\bar{\nu}_a - \bar{\nu}_f$:

$$\bar{\nu}_a - \bar{\nu}_f = S_1 f(\varepsilon, \eta) + \text{const.} \tag{1.17}$$

and the sum $\bar{\nu}_a + \bar{\nu}_f$:

$$\bar{\nu}_a + \bar{\nu}_f = -S_2 \phi(\varepsilon, \eta) + \text{const.} \tag{1.18}$$

where

$$\phi(\varepsilon, n) = f(\varepsilon, n) + 2g(n) \tag{1.19}$$

and
$$S_1 = \frac{2(\mu_e - \mu_g)^2}{hca_0^3} \tag{1.20}$$

$$S_2 = \frac{2(\mu_e^2 - \mu_g^2)}{hca_0^3} \tag{1.21}$$

μ_e and μ_g denotes the excited and ground state dipole moments, respectively; α is the mean static polarizability and a_0 is the Onsager cavity radius of the solute; ε and n are the electric permittivity and refraction index of the solvent, respectively; c denotes the speed of light in vacuum and h is the Planck constant. However, the applied solvent parameters *f(ε, n)* and □*(ε, n)* differ significantly in the individual theories. The solvent parameters *f(ε, n)* and □*(ε, n)* which result from the theory of Bilot and Kawski[100,105] by employing the simplest quantum-mechanical second-order perturbation theory and taking into account the Onsager reaction field for a spherical cavity radius a_0 and a polarizability α are:

$$f(\varepsilon,n) = \frac{\dfrac{\varepsilon-1}{2\varepsilon+1} - \dfrac{n^2-1}{2n^2+1}}{\left(1-\dfrac{2\alpha}{a_0^3}\cdot\dfrac{\varepsilon-1}{2\varepsilon+1}\right)\left(1-\dfrac{2\alpha}{a_0^3}\cdot\dfrac{n^2-1}{2n^2+1}\right)^2} \tag{1.22}$$

$$g(n) = \frac{\dfrac{n^2-1}{2n^2+1}\left(1-\dfrac{\alpha}{a_0^3}\cdot\dfrac{n^2-1}{2n^2+1}\right)}{\left(1-\dfrac{2\alpha}{a_0^3}\cdot\dfrac{n^2-1}{2n^2+1}\right)^2} \tag{1.23}$$

For an isotropic polarizability of the solute the condition $\alpha / a_0^3 = 1/2$ is frequently fulfilled and Equations (1.22) and (1.23) are considerably simplified:[108,109]

$$f(\varepsilon,n) = \frac{2n^2+1}{n^2+2}\left(\frac{\varepsilon-1}{\varepsilon+2} - \frac{n^2-1}{n^2+2}\right) \tag{1.24}$$

$$g(n) = \frac{3}{2}\frac{n^4-1}{(n^2+2)^2} \tag{1.25}$$

Generally, when dipole moments μ_e and μ_g are not parallel but form an angle β, the use of (1.20) and (1.21) leads to: [105]

$$\mu_e = \left(\mu_g^2 + \frac{1}{2}S_2 hca_0^3\right)^{\frac{1}{2}} \tag{1.26}$$

$$\cos\beta = \frac{1}{2\mu_g\mu_e}\left[(\mu_e^2 + \mu_g^2) - \frac{S_1}{S_2}(\mu_e^2 + \mu_g^2)\right] \tag{1.27}$$

Assuming that the symmetry of the investigated solute molecule remains unchanged upon electronic transition, and the ground and excited state dipole moments are parallel, based on (1.20) and (1.21) one obtains: [105,110]

$$\mu_g = \frac{1}{2}(S_2 - S_1)\left(\frac{1}{2}\frac{hca_0^3}{m_1}\right)^{\frac{1}{2}} \tag{1.28}$$

$$\mu_e = \frac{1}{2}(S_1 + S_2)\left(\frac{1}{2}\frac{hca_0^3}{m_1}\right)^{\frac{1}{2}} \tag{1.29}$$

by dividing (1.29) by (1.28):

$$\mu_e = \mu_g \frac{|S_1 + S_2|}{|S_2 - S_1|} \tag{1.30}$$

The parameters S_1 and S_2 occurring in (1.17) and (1.18) for the difference $\bar{\nu}_a - \bar{\nu}_f$ and the sum $\bar{\nu}_a + \bar{\nu}_f$ of the wavenumbers, which are linear functions of the solvent polarity parameters $f(\varepsilon, n)$ and $\phi(\varepsilon, n)$, can be determined from the slopes of the straight lines. With this method we use the extrapolation technique of the linear fit to the experimental data corresponding to the gaseous phase. In this way we obtain dipole moments of an isolated molecule, free from solvents. Only such a value of the dipole moment is characteristic for a given molecule.

Similar to the equations derived by different researchers, Lippert-Mataga equation also considers only the non-specific interactions between the fluorophore and solvent and not the specific interactions. Hence, it can be applicable only for the fluorophore in non-polar and polar aprotic solvents. But the term polarity is loosely used to describe both non-specific and specific interactions. Hence different polarity scales were also reported for fluorescent probes where all types of interactions are considered. The number of dyes designed and studied for different polarity scales are available in the literature.

To infer the charge separation of the probe molecule in the presence of polar solvents, in the excited state, the excited state dipole moments can be calculated

experimentally as well as theoretically. The experimental calculations can be done by measuring the solvatochromism either from the solvent polarity effect on the Stokes-shift or from the fluorescence shift alone, which is advisable if the absorption and emission transitions have different orbital origins. This can be calculated theoretically by performing quantum chemical calculations. Among the various methods used for experimental determination of dipole moment include microwave conductivity,[111] Stark splitting[112] and thermochromic shift method.[113] These methods are generally considered to be accurate, but their use is limited because they are equipment sensitive and the studies have been restricted to very simple molecules. However, the experimental determination of dipole moment based on analysis of the solvatochromism of absorption and fluorescence maxima (discussed above in detail) is quite popular. Recently Joshi et. al.[114,115,8] reported the excited state dipole moment of Quinine Sulfate and Quinidine species by performing solvatochromic study.

1.1.7 Time-resolved fluorescence studies

1.1.7.1 Fluorescence intensity decay and lifetime

Time-resolved fluorescence spectroscopic methods give the information regarding the kinetics of the various processes involved in the deactivation of the excited state.[3] The fluorescence intensity decay is a plot of fluorescence intensity as a function of time. Fluorescence intensity decay, $I(t)$, for a system having single fluorophore is a single exponential and is given as Equation 1.31:[3]

$$I(t) = I_0 e_{\tau}^{-t} \tag{1.31}$$

where, I is the fluorescence intensity at time t, I_0 is the maximum fluorescence intensity during excitation and τ is the average time spent by the fluorophore in the excited state before coming to ground state. Measurement of this property can give information as to what molecule is present, how the solvent environment affects the molecule, as well as the presence of dye aggregates. The fluorescence lifetime is a useful parameter to get ideas about local environment around a fluorophore because of its sensitivity to excited state interactions. Thus, this property of molecules is useful in the field of fluorescence and can be measured using Time Correlated Single Photon Counting (TCSPC) technique, which will be described more fully in next chapter.

The fluorescence lifetime is related to the radiative and the nonradiative rates. The relation between the fluorescence Quantum yield (ϕ) and fluorescence lifetime (τ) is given as Equation1.32:[3]

$$\tau = \frac{1}{k_r + k_{nr}} = \frac{\phi}{k_r} \tag{1.32}$$

where, k_r and k_{nr} are the rate constants for radiative and non-radiative processes, respectively.

Some systems may have more than one fluorescent species and hence the fluorescence intensity decay has to be fitted with multiexponential function instead of single exponential function. For multiexponential function the fluorescence intensity decay Equation will be such as:[3]

$$I(t) = \sum_{i=0}^{n} a_i e^{\frac{-t}{\tau_i}} \tag{1.33}$$

where, α_i and τ_i are ith preexponential factor (amplitude) and the lifetime in the multiexponential decay, respectively. The average lifetime $\langle\bar{\tau}\rangle$ of the multiexponential decays is defined as in Equation 1.34:[3]

$$\langle\bar{\tau}\rangle = \frac{\sum_i \alpha_i \tau_i^2}{\sum_i \alpha_i \tau_i} \tag{1.34}$$

1.1.7.2 Fluorescence quenching

The process in which fluorescence intensity of the fluorophore decreases is known as fluorescence quenching.[3] The variety of process e.g. excited state reactions, energy transfer, complex formation, collisions with similar and different molecules can lead to decrease in fluorescence intensity.

In general, fluorescence quenching is referred to a process where the electronic energy of the excited molecule is transferred to the translational energy of the quencher molecule. The fluorescence quenching can take place by two mechanisms:

1.1.7.2.1 Dynamic quenching

In dynamic quenching the quencher must diffuse to the fluorophore during its excited state lifetime. Upon contact, the fluorophore returns to the ground state, without emission of photon. It is described by the Stern-Volmer[116] (S-V) expression as given in Equation 1.35:

$$\frac{I_0}{I} = \frac{\tau_0}{\tau} = 1 + K_{SV}[Q] \tag{1.35}$$

$$K_q = \frac{K_{SV}}{\tau_0} \tag{1.36}$$

where, I_0 and I are the intensity, τ_0 and τ are decay time in the absence and presence of quencher, respectively, K_{SV} is the Stern-Volmer quenching constant and [Q] is the concentration of quencher. A plot of $\frac{I_0}{I}$ or $\frac{\tau_0}{\tau}$ verses [Q] yields a straight line passing through 1. From slope, one can calculate Stern-Volmer quenching constant (K_{SV}) and quenching rate constant (K_q) of the system can be calculated using Equation 1.36. Dynamic quenching is also called collisional quenching.

1.1.7.2.2 Static quenching

In case of static quenching a non-fluorescent complex is formed between the fluorophore and the quencher in the ground state. Because of this the concentration of the free emitting fluorophore decreases and thereby decreasing the fluorescence intensity. In this case[3, 116] the Stern-Volmer Equation is:

$$\frac{I_0}{I} = 1 + K_S[Q] \tag{1.37}$$

where, K_S is the association constant of complex formation in the ground state. From the plot of $\frac{I_0}{I}$ versus [Q], the slope gives the value of K_S. In either event the primary requirement is that the quencher and the fluorophore must be in contact with each other.

Static and dynamic quenching can be distinguished (Figure 1.5). In the case of dynamic quenching, the excited state lifetime decreases with the increase of quencher concentration and $\frac{I_0}{I} = \frac{\tau_0}{\tau}$ whereas in the case of static quenching lifetime does not

depend on quencher concentration and $\frac{\tau_0}{\tau} = 1$. Moreover, dynamic quenching is diffusion controlled. With the increase of temperature the value of diffusion coefficient increases, thereby increasing the biomolecular quenching rate constant. On the other hand, increased temperature is likely to result in decreased stability of complexes, and thus decreasing the rate of static quenching.

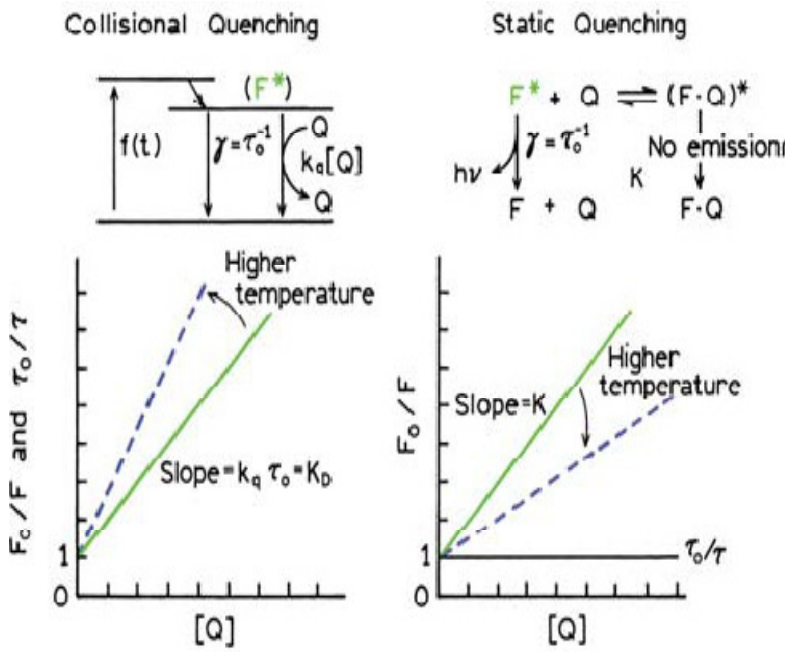

Figure 1.5 Comparison of dynamic and static quenching[3]

1.1.7.3 Fluorescence anisotropy

The fluorescence emission, emitted from the samples excited with polarized light is also polarized. This polarization is due to photoselection of the fluorophores according to their orientation relative to the direction of the polarized excitation. This photoselection is proportional to the square of the cosine of the angle between the absorption dipole of the fluorophore and the axis of polarization of the excitation light. The orientational anisotropic distribution of the excited fluorophore population relaxes by rotational diffusion of the fluorophores and excitation energy transfer to the surrounding acceptor molecules. The polarized fluorescence emission becomes depolarized by such processes. The fluorescence anisotropy measurements reveal the average angular displacement of the fluorophore which occurs between absorption and subsequent emission of a photon.

Fluorescence anisotropy measurement reflects the extent of restriction imposed by the microenvironment on the dynamic properties of the fluorophore. Fluorescence anisotropy helps to find out the probable location of the probe in the microheterogeneous environment.[3,117]

1.1.7.3.1 Steady state fluorescence anisotropy

The steady state fluorescence anisotropy, r can be represented as[3]

$$r = \frac{I_{VV} - GI_{VH}}{I_{VV} + 2GI_{VH}} \tag{1.38}$$

where, I_{VH} and I_{VV} are the intensities obtained from the excitation polarizer oriented vertically and emission polarizer oriented in horizontal and vertical directions, respectively. The factor G is defined as $G = I_{HV}/I_{HH}$, where I_{HV} and I_{HH} are the intensities obtained from the excitation polarizer oriented in horizontal position and emission polarizer oriented in vertical and horizontal position, respectively.

1.1.7.3.2 Time-resolved fluorescence anisotropy

The fluorescence anisotropy decay of the organic probe molecule is directly related to the reorientation dynamics of excited molecule and hence it is the best method to investigate the molecular dynamics near the location of the probe molecule.[118-120]

The time-resolved fluorescence anisotropy, r (t) is defined as in Equation 1.39:[3]

$$r(t) = \left[I_{\text{II}}(t) - GI_{\perp}(t)\right] / \left[I_{\text{II}}(t) + 2GI_{\perp}(t)\right] \tag{1.39}$$

where, G represents the correction factor for the detector sensitivity to the polarization detection of emission, $I_{\text{II}}(t)$ and $I_{\perp}(t)$ are fluorescence decays polarized parallel and perpendicular to the polarization of the excitation light, respectively.

Generally, the fluorescence anisotropy decay of the fluorescence probe molecule residing in micelles, mixed micelles or reverse micelles is having two components, fast and slow components. This biexponential fluorescence anisotropy decay is generally not because of its different locations, but due to its various kinds of rotational motions.[121] For detailed explanation of the biexponential behaviour of anisotropy decay as a result of different types of rotational motions, the theoretical models often used are the two-step and wobbling -in-a cone model.[122] These models are applicable for spherical micelles.

Two-step model

According to the two-step model the fast and slow motions are assumed to be seperable. If two motions are independent, the total rotational anisotropy function will be biexponential as:[122]

$$r(t) = r_0\left[\alpha_1 \exp^{\left(\frac{-t}{\tau_{1r}}\right)} + \alpha_2 \exp^{\left(\frac{-t}{\tau_{2r}}\right)}\right] \tag{1.40}$$

where, r_0 is the limiting anisotropy to represent the inherent depolarization of the probe molecule, τ_{1r} and τ_{2r} are the fast and slow rotational relaxation components of the probe molecule in various media i.e. in the present case micellar media, respectively, α_1 and α_2 are the relative amplitudes of two components, respectively. Based on the two step model, both lateral diffusion of the fluorophore (τ_D) and the rotational motion of the micelle as a whole (τ_m) contribute to the slow rotational relaxation time (τ_{2r}). τ_{2r} is related to the relaxation time corresponding to the τ_m and the relaxation time corresponding to the τ_D as follows (Equation 1.41): [122]

$$\frac{1}{\tau_{2r}} = \frac{1}{\tau_D} + \frac{1}{\tau_M} \tag{1.41}$$

To compute the τ_M, Debye-Stokes-Einstein (DSE) equation is used assuming that the spherical micelle is rotating in the solvent (in our case water) with sticking boundary conditions[123] as follows:

$$M = \frac{4\pi\eta r_h^3}{3kT} \tag{1.42}$$

where, r_h is the hydrodynamic radius of the micelle, η is the shear viscosity of water, k is the Boltzmann constant and T is the temperature in Kelvin scale.

Wobbling in a cone model

The restricted motion of a rodlike rotor with the transition moment parallel to the long axis is described by the wobbling-in-a-cone model.[121] This model describes the internal motion of the probe (τ_e) in terms of a cone angle (θ_0) and wobbling diffusion coefficient (D_w). The schematic representation of wobbling–in-a-cone model is shown in Figure 1.6. To measure the spatial restrictions of the motion of the probe molecule in its

surrounding, the order parameter, S is often computed. The value of the order parameter ranges from 0 to 1, where a value of 0 indicates no restriction and 1 means complete restriction of the rotational motion of the probe molecule. The order parameter is related to recovery decay of anisotropy by:

$$r(t) = r_0\left[S^2 \exp^{\left(\frac{-t}{\tau 2r}\right)} + (1-S^2)\exp^{\left(\frac{-t}{\tau 1r}\right)}\right] \tag{1.43}$$

after comparing equations one can calculate S as, $S^2 = \alpha_{2r.}$

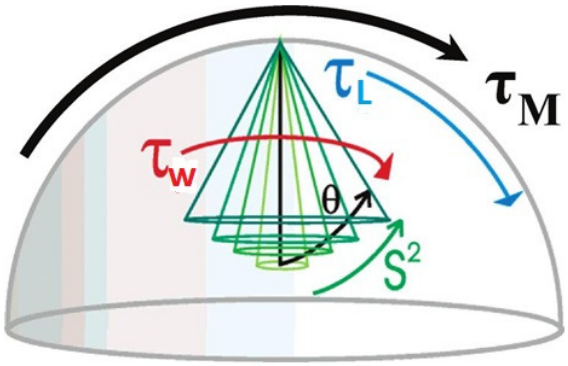

Figure 1.6 Schematic representation of wobbling-in-a-cone model of rotational dynamics

The order parameter is a measure of the equilibrium orientational distribution of the fluorophore. The order parameter is zero if the fluorophore tumbles freely and the equilibrium orientational distribution is completely random. For the micellar solution the value of order parameter generally lies in the range of 0.55-0.88, indicating that the equilibrium orientational distribution is highly constrained because of the aqueous or non-aqueous interface in the micelles or reverse micelles. If the order parameter value is less than 0.5 in micelles then it can be explained on the basis of spinning-in-equatorial-band model.[124] The order parameter does not contain any information about dynamical properties of the fluorophore. The dynamics are instead reflected in the faster rotational correlation time, which can be described by the wobbling motion of the fluorophore. According to the wobbling-in-a-cone model, the order parameter is related to the cone angle, θ_0 as in Equation 1.44, and according to the spinning-in-equatorial-band, the order parameter is related to the cone angle, θ_0 as in Equation 1.45:

$$\theta_0 = \cos^{-1}\left[\frac{1}{2}\left((1+8S)\frac{1}{2}-1\right)\right] \tag{1.44}$$

$$s^2 = \left[\frac{1}{2}(1-\cos^2\theta_0\right]^2 \tag{1.45}$$

An effective relaxation time (τ_e) corresponding to the restricted rotational diffusion is related to the fast relaxation (τ_{1r}) and slow relaxation time (τ_{2r}) as in Equation 1.46:

$$\frac{1}{\tau_{1r}} = \frac{1}{\tau_e} + \frac{1}{\tau_{2r}} \tag{1.46}$$

The wobbling diffusion coefficient, D_w is calculated using Equation 1.47:

$$D_W = \frac{7\theta_0^2}{24\tau_e} \tag{1.47}$$

1.2 Microheterogeneous environments

The last two decades have witnessed the importance of the organized assemblies on biological and photophysical processes. Reactants accommodated in molecular assemblies like micelles, reverse micelles, cyclodextrins, vesicles, etc., often achieve a greater degree of organization compared to their geometries in homogeneous solution, can mimic reactions in biosystems and also have potential for energy storage.[125] The interiors of these assemblies are quite different from the bulk solution phase. For aqueous solutions of micelles, cyclodextrins, proteins, the inner core is relatively less polar than the bulk aqueous phase. A reverse picture is found when one deals with reverse micelles. Not only the polarity but also the local viscosity/rigidity within the organized assemblies are appreciably different from the bulk liquid medium; as a result, these can alter a photoprocess drastically. In this section, we will discuss the architecture of a few organized assemblies and see how they can modify the photoprocesses like ICT.

1.2.1 Micelles

Surfactants can self-organize under specific environmental conditions in solution to form micelles. The micelle-forming amphiphiles or surfactants essentially fall in two categories, 'ionic' and 'non-ionic'. They basically contain non-polar hydrocarbon or polyoxyethylenic chain (called tail) and an ionic or polar group (called the head). When self-interactions of both surfactants and solvent molecules cannot be compensated by their mutual interactions, the surfactant molecules tend to associate in a regular pattern forming 'association colloids' or 'micelles'.[126] Reactions in micellar aggregates are

simple model systems for chemical processes occurring at the interfaces in the living cell. The most important properties of the micellar systems are their ability to solubilise a variety of molecules insoluble in bulk (aqueous) solution and their substantial catalytic effect on many reactions. The knowledge of the structure of the micelles, the local environment, the local concentration and the relative orientation of the solubilised molecules is of fundamental importance in understanding the nature of the solubilisation and the physical and chemical behaviour of the solubilised species. Micelles which are used as membrane biomimetic agents, gain importance by virtue of their capacity to provide a matrix for arranging the reaction sequentially for efficient interaction, i.e., they help in compartmentalization of the reactants dynamically. Water molecules which are tightly bound to the surfactant head groups of micelles resemble the hydrophilic pockets of enzymes and have high viscosities, low mobilities and polarities. The ability of micellar solution to incorporate solubilised material is an important property of micelles and provides the basis for the widespread use of surfactants and micellar solutions in industrial, biological, and synthetic chemical/catalytic applications. Micelle catalyzed reactions in biological systems provide information regarding the mechanism of tuning of reactions occurring on biological surfaces because micelles are simpler and can be easily modified. The micelles are well explored as drug carriers for water-insoluble drugs,[127] nanocarriers for efficient drug delivery,[128] and found to have applications in cultural heritage conversation,[129] oil fields and thickneners for personal and home made products.[130]

Depending on nature of hydrophilic head group, surfactants are classified as (i) ionic, (ii) non-ionic. Ionic are the ones having either positive, negative or both charges on the surface active part of molecule. They have further three sub classes depending upon charge (a) Anionic surfactants (b) Cationic surfactants (c) Zwitterionic surfactants:

(i) Ionic surfactants

(a) Cationic surfactants: The head group of this class of surfactants possesses positive charge. The general formula of cationic surfactant is $R_nX^+Y^-$, where R represents one or more hydrophobic chains, X is head group and Y is counterion, For example, Cetyltrimethyl ammonium bromide (CTAB) [$C_{16}H_{33}N^+(CH_3)_3Br^-$], Cetylpyridinium chloride (CPyCl) [$C_6H_5N^+C_{16}H_{33}Cl$], will fall under this category.

(b) Anionic surfactants: These types of surfactants contain negatively charged head group. They are by far the largest surfactant class. Carboxylate, sulfate, sulfonate and phosphate are the polar groups found in anionic surfactants. The counterions most commonly used are sodium, potassium, calcium and various protonated alkyl amines. Sodium and potassium impart water solubility, whereas calcium and magnesium promote oil solubility of surfactants. Examples include Sodium dodecylsulfate (SDS) [$C_{12}H_{25}SO_4^-Na^+$], Alfa-olefinic Sulfonate (AOS) [$CH_3(CH_2)_9C_2H_4SO_3^-Na^+$].

(c) Zwitterionic surfactants: These types of surfactants possess both anionic and cationic groups on the hydrophobic moiety. Depending on the pH of the solution and the structure of the surfactants it can be either an anionic, cationic or neutral species. The more common zwitterionic surfactants include N-alkyl and C-alkyl betains as well as phosphatidyl amino alcohols and acids, e.g. 3-(Dimethyldodecylamino)- propane1sulphonate [$CH_3(CH_2)_{11}N^+(CH_3)_2CH_2CH_2CH_2SO_3$], [(dodecyldimethylammonio)alkyl] phenyl phosphinates [$C_{12}H_{25}N^+(CH_3)_2(CH_2)_nC_6H_5PO_2^-$].

(ii) Non-ionic surfactants: The head group of this class of surfactants does not possess any charge. They have either polyether or a polyhydroxyl unit as a polar group. They are second largest surfactant class. Most nonionic surfactants are polyoxyethylene and polyoxypropylene derivatives of compounds such as alkyl phenols and alcohols, fatty acid esters, alkylamides, amides and mercaptants or polyalcohols, carbohydrate esters, fatty alkanol amides and fatty amine oxides. Examples: Triton X-100, Tweens, Brijs, etc.

In addition to these different types of surfactants, gemini surfactants are special class of surfactants which have two hydrophobic tail and two polar head groups covalently linked through a spacer. The spacer chain can be hydrophilic or hydrophobic, rigid or flexible in nature. The polar head groups can be neutral, positively or negatively charged. These noval surfactants attract considerable attention because of their unique properties which are superior to monomeric surfactants.[131]

Apart from these synthetic surfactants, there are some surfactants which are naturally occurring such as simple lipids (carboxylic acid esters), complex lipids (fatty acid esters containing phosphorous, nitrogen bases, and/or sugars), bile acids such as cholic and deoxycholic acid.

1.2.1.1 Formation of micelles

Surfactant molecules consist of hydrophilic (head group) and hydrophobic (hydrocarbon tail) parts. The effect of adding surfactant molecules into the water is shown in Figure 1.7. Starting with low concentration of surfactant (Figure 1.7a), the surfactant partitions between the surface and solution, as on the surface it can get its tails out of water. Increasing the amount of surfactant in solution, and as the surface becomes crowded (Figure 1.7b), at a certain concentration the surfactant will start to self assemble again try to keep the hydrophobic tails out of contact with water. The concentration above which surfactant start aggregating or micelles start forming is known as the Critical Micellar Concentration (CMC) (Figure 1.7d). CMC is an important physicochemical parameter of self-assembling surfactant systems. There are various methods reported for the determination of the CMC, viz. surface tension,[132] fluorescence,[133] conductance,[134] viscosity,[135,136] dynamic light scattering,[137]sound velocity,[138,139] calorimetry,[140] dye solubilisation etc. The most frequently used methods are surface tension, conductivity and fluorescence method. The conductance method is applicable only to ionic surfactants. These properties when measured as a function of concentration of the surfactant show curves with sharp inflections at the CMC.

The formation of micelles is not always a single step process as discussed above i.e. micelles are not suddenly forming from free individual surfactant molecule, but some cases, formation of micelles preceded by the formation of different comparatively smaller aggregates known as premicellar aggregates (Figure 1.7c). It means some of the surfactant molecules are aggregated below the CMC range and the concentration at which premicelles are formed is known as premicellar concentration.

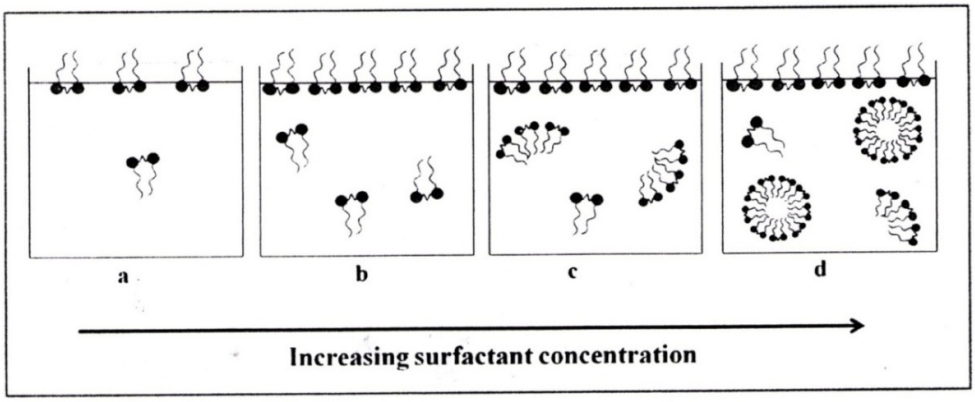

Figure 1.7 Various steps involved in the formation of micelles

1.2.1.2 Micellar size, shape and character

'Micellization' is typically characterized by a rather well-defined Critical Micelle Concentration (CMC) where certain physical properties show abrupt changes. The CMC is an important parameter to characterize micelle formation, both for small surfactant molecules and for amphiphilic block copolymers. The determination of the CMC involves the measurement of a physical quantity that changes upon micellization, such as surface tension, solution enthalpy, or light scattering intensity. The determination of CMC is generally based on the localization of the position of a breaking point in the concentration dependencies of selected physical or chemical properties of surfactant solutions. Because of the surface activity of these substances, measurements of the surface tension of surfactant solutions represent the principal method of CMCs determination. However, it is rather tedious and time consuming procedure. The conductometric method is based on the finding breaking point on the curves, which describes the concentration dependence of conductivity. It is well-known, that the conductivity of any solution is directly proportional to the concentration of its ions. The point, where the micelle formation starts, is indicated on the concentration dependence of specific conductivity, as a breaking point. A very useful method to determine the CMC is based upon fluorescent probes added to the solution or covalently linked to the hydrophobic moiety of the amphiphlic molecule. In this case, the CMC can be determined from a change in the intensity or shape of fluorescence spectra, a solvatochromic shift, a change in fluorescence lifetime or in the polarization occurring upon micellization. CMC generally depends on the chemical structure of the surfactant, added electrolytes, presence of organic additives and temperature. The details regarding the same are provided below:

1.2.1.2.1 Structure of the surfactant

CMC of the surfactants depends on the hydrophobic tails, headgroups as discussed below:

1.2.1.2.1.1 Effect of hydrophobic chain length

The increase in number of carbon atoms in unbranched hydrocarbon chain length of surfactants leads to decrease in CMC. However for the chain greater than 16, this rule is no longer holds possibly due to coiling of chains in solutions.[141] The value of CMC

usually becomes one half on addition of each methylne group to straight hydrohphobic chain attached to single terminal hydrophilic group. However, in nonionic surfactants each methylene group reduces CMC to one-tenth of its original value. A phenyl group, being part of hydrophobic group, is considered equivalent to about three and half methylene group. If the hydrocarbon chain is branched, the carbon atom on which branching occurs appears to exhibit one half of effect than on staright chain. The presence of sp^2 hybridized carbon (in case of C=C bond) causes CMC to increase.[132,141]

1.2.1.2.1.2 Effect of headgroup

The surfactants having same hydrophobic but different headgroups have pronounced difference between their CMC values.[141] The aqueous solution of nonionic surfactants has much lower CMC than that of ionics with same number of carbon atoms. The effect of the variation of the headgroups on the CMC is more significant in case of Gemini surfactant due to presence of two headgroups. Gemini surfactants with cationic, anionic, zwitterionic or nonionic headgroups have been reported. Okhara et. al.[142-144] synthesized a very large number of anionic Gemini surfactants with sodium sulfate, sulfonate, phosphate or carboxylate headgroups. They observed that these surfactants are highly soluble in water. Engbert's et. al.[145] synthesized bisphophate gemini surfactants and they observed very low CMC values.

1.2.1.2.2 Effect of added Electrolytes

In aqueous solution the presence of electrolyte causes a change in the CMC, the effect being more pronounced for anionic and cationic than for zwitterionic surfactants and more pronounced for zwitterionics than for nonionics. The change in the CMC of nonionics and zwitterionics on the addition of electrolyte has been attributed mainly to the "salting out" or "salting in" of the hydrophobic groups in the aqueous solvent by the electrolyte, rather than the effect of the latter on the hydrophilic groups of the surfactant.[146,147] Salting in or salting out by an ion depends upon whether the ion is a water structure breaker or a water structure maker. Ions with a large ionic charge/radius ratio, such as F^-, are highly hydrated and are water structure makers. They salt out the hydrophobic groups of the monomeric form of the surfactant and decrease the CMC. Ions with a small ionic charge/ radius ratio, such as CNS^-(Thiocyanate), are water structure breakers; they salt in the hydrophobic groups of the monomeric form of the surfactant and increase the CMC.[148]

1.2.1.2.3 Effect of organic additives

The presence of organic materials in surfactants can be due to the impurities or byproducts during manufacturing process of commercial surfactants and may produce marked changes in the CMC in aqueous media.[149] These materials markebly decrease the CMC of the surfactants either by being incorporated into the micelle[149] or increase the CMC by modifying solvent-micelle or solvent-surfactant interactions.

1.2.1.2.4 Temperature

The effect of temperature on the CMC of surfactants in aqueous medium is complex, the value appearing first to decrease with temperature to some minimum and then to increase with further increase in temperature. Temperature increase causes decreased hydration of the hydrophilic group, which favours micellization.[150] However, temperature increase also causes disruption of the structured water surrounding the hydrophobic group, an effect that disfavours micellization. The relative magnitude of these two opposing effects, therefore, determines whether the CMC increases or decreases over a particular temperature range.[148]

For a given surfactant, at a given temperature, only a certain amount of monomer can be accommodated in the water cavities proposed by "flickering cluster model" of water structure and any further addition of surfactant will result in formation of micelles.[151] Further addition of surfactant provides a driving force to minimize contact of the monomer hydrocarbon chains with water. Therefore, according to Langmuir's principle of differential solubility, the hydrocarbon chains cluster to form a core (micellar core), while the polar groups interact with the water.[151]

The first model proposed to explain the micellar structure is Hartley model.[152] According to this model micelles are considered as globular structures having a hydrocarbon core surrounded by a highly hydrophilic region formed by the surfactant head groups, counterions and water molecules (Figure 1.8). It follows spherical aggregate containing 50-200 monomer units. The radius of the sphere is approximately equal to the extended length of the hydrocarbon chain of the surfactant. The ionic head groups of the surfactants and a portion of the counterions from a compact "stern" layer at the micellar surface, in which bout 60-75% of the micellar charge is believed to be neutralized.[153] The remaining counterions form a diffused Gouy-Chapman layer where

they are dissociated from the micellar region and are free to exchange with ions distributed in the bulk aqueous phase. On the macroscopic scale, a micellar medium could be described as a mixed aqueous-organic solvent.[151] The hydrocarbon portion of the micelle cannot have an open space at the center and consequently, micelle size does not exceed the maximum (stretched out) length of the hydrocarbon chain.[154]

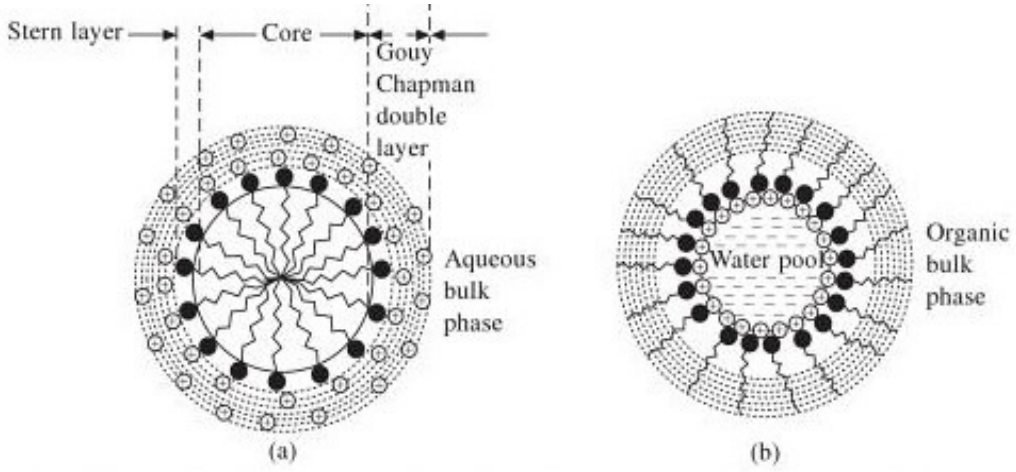

Figure 1.8 Spherical cross section of an idealized anionic (a) normal micelle, (b) reverse micelle, (●) polar head group, (⊕) the counterion, (~) the hydrocarbon chain

Experimental evidence has been produced supporting the view that water cannot rigorously be excluded from the micellar core. Further, it is also supported by ^{1}H NMR, ^{13}C NMR and by other spectroscopic studies.[151] Menger's model[155] proposed that micelles are open structures containing a series of microchannels allowing deeper water penetration.

According to the "reef" model water does not penetrate beyond the ionic group whereas "Fjord" model states that, water percolates nearly to the center of the micelle. Menger et. al.[156] proposed that water cannot reach the very centre of the micellar core but can penetrate as far as seven carbon atoms away from head group. They also proposed the "porous cluster" model using ^{13}C NMR, Optical Rotator Dispersion (ORD) and molecular models.[157]

Micellar structures are dynamic in nature and in equilibrium with monomers and other forms of aggregates in solution. Depending on the temperature, concentration, and other experimental variables, the micelles may be roughly spherical, ellipsoidal, disk like or rod-shaped and bilayers. Depending on the head group structure, ionic micelles have

been found to be either (a) spherical at all concentrations, (b) rod shaped at all concentrations, (c) spherical at low concentrations and rod shaped at high concentrations (Figure1.9).[158]

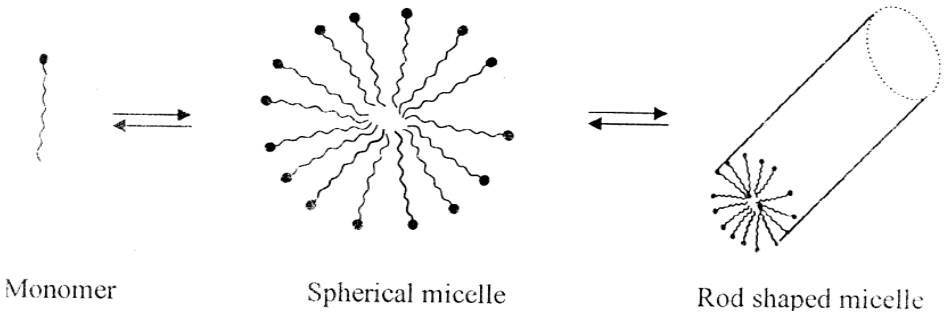

Figure 1.9 Dynamic equilibrium between monomers and various structural organization of surfactant molecules

Micelles are formed by the completion of two forces: (1) the hydrophobic interaction between the tails provides the driving force for aggregation and (2) the electrostatic or steric repulsion between the head groups limits the size that a micelle can attain. Hence, depending on the structure of the surfactant and charge on the head group the micelle shape can vary. Micellar shape depends on the relative values of tail length (*l*), head group area (*a*) and the molecular volume (*v*) of the molecule.[159] Israelachvili et. al.[160] reported that depending on the value of packing parameter p (= *v*/*al*), the surfactant aggregates could acquire different shapes (Figure 1.10).

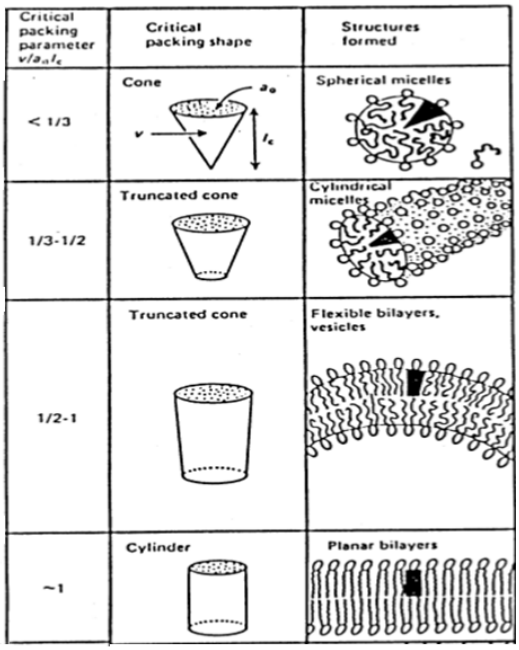

Figure 1.10 Different shapes of micelle based on critical packing parameter

They showed that, micelles are spherical for p<1/3 and ellipsoidal and cylindrical for 1/3<p <1/2. The surfactant aggregates tend to be bilayers for p>1/2 and in suitable cases this results in formation of vesicles.[159]

Micelles can be further classified into two types, depending upon the kind of solvent used:

1. **Normal or aqueous micelles:**
   Surfactants are molecules containing a hydrophobic long chain with a polar head group. The head group may be ionic or neutral. If these molecules are dissolved in water, they have a tendency to form aggregates spontaneously, that is, surfactant molecules will arrange themselves into organized molecular assemblies, also called normal micelles. In the normal micelle the surfactant is oriented in such a way that the hydrophobic hydrocarbon chains are towards the interior of the micelle, leaving the hydrophilic groups in contact with the aqueous medium.

2. **Inverted or reverse micelles:**
   Reverse micelles are nanometer-sized droplets of water, or polar solvent, that are surrounded by a layer of surfactant molecules (such as AerosolOT) and immersed in a nonpolar solvent. In this case, the molecular association occurs in nonpolar solvents like hexane, heptanes, octane etc. The polar headgroups of the surfactant molecules point inward, toward the polar solvent pool, and the alkyl chains point outward, toward the bulk organic solvent (Figure 1.8 b). The structure and dynamic properties[161] of the reverse micelles have been reviewed by many authors.[162,163] Lisiecki et. al.[164] used reverse micelle as microreactor[165] to synthesize in situ nanometallic copper particles. Recently, reverse micelles were used as noval drug carriers for sustained drug release.[166]

Eventhough, the formation of micelles can be monitored by different techniques, dye-surfactant interaction is substantially used for this purpose. Moreover, in most of the reported cases surface tensions of surfactant solutions have been measured for the determination of CMCs. However, it has been reported in the literature[167] that the surface tension method can be erroneous for commercial grade surfactants under common conditions, because this method is very sensitive to the presence of impurities and much lower CMC values are obtained with the surface tension method than with the dye micellization method. Since Hartley[168] demonstrated

the use of sulphonaphthalein indicators to monitor the detergent aggregate, there are significant numbers of reports with different types in this context.

It has been observed in many cases of surfactants that the occurrence of the micellar phase is preceded by the formation of different comparatively smaller aggregates known as premicellar aggregates.[169-174] Hadgiivanova et. al.[175,176] developed a thermodynamic model to study the aggregation mechanism. The study on photophysical properties, such as absorbance, fluorescence excitation, emission and their shifts, the relative intensity of vibronic bands, anisotropy, Quantum yields and excited state lifetimes of the dyes has provided significant information on the micellar structure at the molecular level.[177-181] Premicellar aggregation, CMC, post-micellar aggregation, association constant, micropolarity and microviscosity of the micellar environment around the probe can also be determined by choosing the appropriate probe molecule.[182]

1.2.1.3 Location of probe in micelle

Depending on the nature, charge, size and type of interaction between surfactant and probe decides exact location of solublization. Solublization is believed to take place at number of different sites in micelle as mentioned below and made clear in Figure 1.11(a) on the surface of micelle (b) between the hydrophilic headgroups (in case of polyoxyethylenated surfactant) (c) in the outer core of micellar interior (between hydrophilic headgroups and first few carbon atoms in the hydrophobic portion (d) in the core of the micelles.

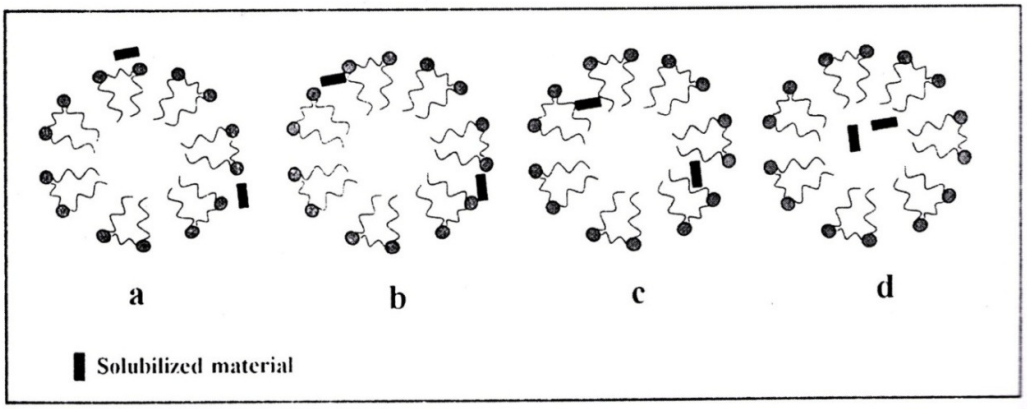

Figure 1.11 Various possible locations of solubilised materials

For example pyrene, hydrophobic probe is weakly soluble in water and solubilised preferentially in the interior hydrophobic regions of these aggregates.[183,184] But in case of ionic styrl dye, the position of the probe in the micelle vary with the charge of the head group of surfactant.[172] In the case of probe exhibiting charge transfer character in polar environment, the mode of binding of probe with the micelle depends on the dipolar nature of the probe and chemical structure of the surfactant.[182]

1.2.1.4 Fluorophore-micelle binding

The dye–surfactant interactions have also been the subject of many studies in view of the fact that they mimic many biological processes taking place between the large organic molecules and biomembrane and can act as a model redox system.[185-188] Further, such interactions between ionic dye and charged surfaces is of interest in numerous applications ranging from the design of electronic devices to the characterization of drug-delivery systems. Therefore the binding constants and association constants of the fluorophore in micellar environments have been determined to understand the degree of interaction between dye and the micellar units. Different equations are used for calculating binding constant, by making use of spectroscopic data.

According to the method described by Almgren et. al.[189] using fluorescence intensity data, the binding constant of the probe molecule to the micelles can be determined by the use of Equation 1.48:

$$\left[(I_\alpha - I_0)/(I_C - I_0)\right] = 1 + \left(K[M]\right)^{-1} \tag{1.48}$$

where, I_0, I_c and I_α are the fluorescence intensities of probe in the absence of surfactant, at an intermediate surfactant concentration, and under conditions of complete probe-micelle interaction respectively; K is the binding constant and [M] is the micellar concentration, given by

$$[M] = \frac{(S - CMC)}{N} \tag{1.49}$$

where, S represents the surfactant concentration and N is the aggregation number of a micelle concerned. The binding constant (K) values have been determined from the slopes of the plots of $\left[(I_\alpha - I_0)/(I_C - I_0)\right]$ against $[M]^{-1}$.

According to the model proposed by Sepulveda and co-workers,[190] the binding constant of the probe molecule to micelles can be determined by the use of the Equation 1.50:

$$\frac{F - F_0}{[Det] - CMC} = K_S F_m - K_S F \tag{1.50}$$

where, F, F_0, and F_m are fluorescence intensities of probes at intermediate concentrations of surfactant, in water and when it is completely bound to the micelle. [*Det*] is concentration of surfactant, CMC is critical micelle concentration and K_S is binding constant. From the slope of the plot $(F - F_0)/([Det] - CMC)$ vs fluorescence intensity, F, the binding constant K_S can be calculated.

According to Gawandi et. al.,[191,192] discussed in detail later in chapter 5. We calculated the equilibrium association constant using absorption data in the region of low surfactant concentration

$$\left\{\varepsilon_{aq} - A/[C]_T l\right\}^{-1} = (\varepsilon_{aq} - \varepsilon_c)^{-1} + \left\{(\varepsilon_{aq} - \varepsilon_c) K_A \left([S]_T - f_C [C]_T\right)\right\}^{-1} \tag{1.51}$$

where, absorbance (A), molar absorption coefficients of the free and complex dye at a given wavelength are ε_{aq} and ε_c, l is the optical path length, f_c is the fraction of the probe present as the complex, $[C]_T$ and $[S]_T$ are the total probe and surfactant concentrations.

A plot of $\{\varepsilon_{aq} - A/[C]_T l\}^{-1}$ vs $\{([S]_T - f_c[C]_T)\}^{-1}$ should be linear with the association constant (K_A) = intercept/slope.

The binding constant, K_B can be shown related[191] to the measured absorbance of the probe as

$$\left\{A/[C]_T l - \varepsilon_c\right\}^{-1} = \left(\varepsilon_m - \varepsilon_c\right)^{-1} + \left\{(\varepsilon_m - \varepsilon_c) K_B \left([M]_T - f_m [C]_T\right)\right\}^{-1} \tag{1.52}$$

where, f_m is the fraction of the probe in the micellar form and $[M]_T$ is the total micelle concentration given by

$$[M]_T = \frac{\left([S]_T - CMC\right)}{N} \tag{1.53}$$

N is the average number of surfactant molecules in the micellar aggregate.

A plot of $\{(A/[C]_T l) - \varepsilon_c\}^{-1}$ vs $([M]_T - f_m[C]_T)\}^{-1}$ should be linear with binding constant (K_B) = intercept/slope.

1.3 Scope of present work

Measurement of the fluorescence properties (fluorescence spectrum, excitation spectrum, quantum yield, dipole moment and fluorescence lifetimes) of molecules is critical to the development of an understanding of photophysics of the molecules. Study of dynamical processes at the surfaces and interfaces is a fascinating subject with practical applications in many important areas such as in nanotechnology, biotechnology, separation chemistry and electrochemistry. Particularly, fluorescent molecules in the presence of surfactants-micelles-reverse micelles and nanoparticles have been a subject of intense investigations in recent years. The nano-micro and macro structural organization of micelles have profound effects on the spectral properties of molecules.

Micelles are multicomponent systems, where a given solvent is isolated from a continuous phase solvent by surfactant or surfactant and co-surfactant pair. The water near the micellar interface possesses some characteristics of water at the biological membranes. Consequently, these micellar solutions are excellent model systems for the use in studying biologically relevant processes and have been utilized to investigate processes in restricted environments. Understanding the dynamics of confined fluorescent molecules has received considerable attention, because the dynamical characteristics of confined molecules differ considerably from its bulk molecules.

To clarify and to understand the microstructure of the surfaces and interfaces, we studied the photophysical and dynamical processes of spectroscopically important probe molecules using the most suitable and versatile technique steady state and time resolved fluorescence spectroscopy. The effects of the change in micropolarity, microviscosity and ionic strength on to the solvent motion of different liquids have been studied at different interfaces using fluorescent probe molecule. Excited state dynamics in conjugation with the photophysics, photochemistry and rotational dynamics of molecules at the interfaces is expected to provide detailed information about the microstructure of micelles, location and dynamics of probe molecules in these microheterogeneous systems.

Electron transfer is an important primary chemical reaction in many biological processes, such as respiration and photosynthesis. This work will increase in our understanding of how biological membranes influence these elementary reactions. Specific questions to be addressed include: what role does water play in electron transfer processes at the micellar interface? What affects the structure of the micellar interface does have on electron transfer processes? How does the restrictive environment affect these processes? In addition, does the micellar interface facilitate or hinder electron transfer across the micellar wall?

Characterization of micellar systems in terms of determination of micropolarity and microviscosity of the environment around drug or probe molecules, binding with substrate, folding and denaturation behaviour of proteins and their interactions with different surfactants deserve obvious importance. Many cellular functions are related to the viscosity of the environment, and the alteration in cell membrane viscosity is well known to be responsible for several diseases, e.g. cell malignancy, hypercholesterolemia, atherosclerosis and heart diseases. The precise measurements of viscosity in biological systems, and in particular real-time measurements of viscosity changes on a microscopic scale, require the development of methods that are applicable at molecular level. Therefore, determination of viscosity changes on a microscopic scale is a challenge. Although, some fluorescent probe molecules have been used for this purpose, their fluorescence properties are not that much sensitive to the microviscosity and sometimes they are insensitive to the polarity change of the environment. Therefore, it is imperative to find out probe molecules, whose fluorescence properties will be dependent on both viscosity and polarity of medium.

Our interest on the photophysics of Quinine Sulfate (QS) and related compounds in biomimicking microheterogeneous systems originates principally from several important aspects of these molecules. First, this molecule (QS) is highly fluorescent, have unique photophysical properties and very sensitive to the surrounding environment in bulk solutions. Second the photophysical process in QS and its related molecules have been explored for designing of optical sensors for halides. QS is used in medical applications and also used as fluorescence Quantum yield standard.

The contents of the different chapters in the present thesis are briefly given below.

Chapter 1: This chapter of the thesis presents the basic aspects of photophysical and photochemical processes involving excited chromophoric molecules. This chapter also describes the general aspects of micelles used as the confined medium in the present study. The systems that have been chosen for the investigation in the present study are described in this chapter.

Chapter 2: It deals with the methods used in the present research work. Different instrumental techniques used in the present study to carry out different photophysical and photochemical measurements have been described briefly in this chapter. Working principle of the Time Correlated Single Photon Counting (TCSPC) spectrometer has been discussed in this chapter with some greater detail. Basic principles of the other instrumental techniques used in the present study, e.g. absorption spectrophotometry, steady-state spectrofluorimetry have also been described briefly in this chapter.

Chapter 3: This chapter discusses about the estimation of dipole moment in ground and excited states of fluorescent molecules such as Quinine Sulfate monocation (QS^+), Quinine Sulfate dication (QS^{2+}), Quinidine monocation (QD^+) and Quinidine dication (QD^{2+}), using solvatochromic shift method and quantum mechanical calculations. The spectroscopic techniques utilized in this chapter are UV-Visible absorption spectroscopy and fluorescence emission spectroscopy.

Chapter 4: This chapter presents the results that show the effects of micellar surface charge on the photophysics of a well known fluorescent molecule Quinine Sulfate dication (QS^{2+}) in cationic, Cetyltrimethylammonium bromide (CTAB), anionic, Sodium dodecylsulfate (SDS) and neutral, Triton X-100 (TX-100) surfactants at concentrations above the Critical Micelle Concentrations (CMC) in aqueous phase. Results have been explained on the basis of electrostatic interaction between positively charged probe (QS^{2+}) and charge that different surfactants headgroups contain. We have observed that QS^{2+} molecule has the extraordinary capability to sense the surrounding environment which make it very efficient for surface and interface studies and can also be used as a probe to investigate the mobility of solvent molecules around the excited molecules.

Chapter 5: Photophysical characterization of QS^{2+} in normal micelles formed by anionic surfactants Sodium dodecylsulphate (SDS) has been studied at different premicellar,

micellar and postmicellar concentrations in aqueous phase using steady state, time-resolved fluorescence and fluorescence anisotropy techniques. The QS^{2+}- SDS binding constant and association constants were determined by monitoring the changes in the absorption and steady-state fluorescence. We observed here that at lower concentrations of SDS in aqueous solution of QS^{2+}, there is fluorescent complex formation between monomers of surfactant and QS^{2+} molecules. The complex formed in present system studied was highly fluorescent which in general are non fluorescent. The time-resolved fluorescence and anisotropy measurements were also carried out to support the steady-state measurements.

Chapter 6: Photophysics and rotational relaxation dynamics of Quinine Sulfate (QS) have been investigated inside anionic micellar medium at different pH, using steady state and time-resolved fluorescence spectroscopic techniques. It has been observed that the cationic form of Quinine Sulfate (at pH 2) forms a fluorescent ion pair complex with the surfactant molecules at lower concentrations of surfactant, however, at higher concentrations of SDS, the probe molecule binds strongly with the micelles and resides at the water-micelle interface. At pH 7, QS is singly protonated in bulk aqueous solution and at lower concentrations of SDS aggregation between probe and surfactant molecules has been observed. However, at higher concentrations of SDS, at pH 7, an additional fluorescence peak corresponding to dicationic form of QS appears and this has been attributed to double protonation of the QS molecule. Different photophysical properties of QS studied at pH 7 show substantial changes in the presence of SDS micelles compared to that in the bulk water solution. At pH 12, an increase in fluorescence intensity and fluorescence lifetimes have been observed and these observations are attributed to an increase in radiative rate due to the incorporation of QS at the micelle-water interface. The local pH at micellar surface has been found different from the pH of bulk solution.

References:

(1) B. Valeur, *Molecular Fluorescence: Principles and Applications*, Wiley-VCH Verlag GmbH, 2001.

(2) A. P. Demchenko, *Introduction to fluorescence sensing*, Springer, Dordrecht, London, 2009.

(3) J. R. Lakowicz, *Principles of Fluorescence Spectroscopy*, Springer, New York, 2006.

(4) J. Jett, R. Keller, J. Martin, B. Marrone, R. Moyzis, R. Ratliff, N. Seitzinger, E. Shera, C. Stewart, *J. Biomol. Struct. Dyn.* **1989**, *7*, 301.

(5) R. H. Pottier, Y. F. A. Chow, J. P. LaPlante, T. G. Truscott, J. C. Kennedy, L. A. Beiner, *Photochem. Photobiol.* **1986**, *44*, 679.

(6) A. Ryder, *Appl. Spectrosc.* **2002**, *56*, 107.

(7) G. G. Guilbault, *Practical Fluorescence; Theory, Methods and Techniques*. ed.; M. Dekker, New York, 1973.

(8) S. Joshi, R. Bhattacharjee, T. Varma Y, D. D. Pant, *J. Mol. Liq*. **2013**, *179*, 88.

(9) K. L. Litvinenko, N. M. Webber, S. R. Meech, *J. Phys. Chem. A* **2003**, *107*, 2616

(10) G. W. Robinson, R. P. Frosch, *J. Chem. Phys.* **1963**, *38*, 1187.

(11) H. Yamaguchi, M. Higashi, K. Fujimori, *Spec. Chim. Act. A.* **1990**, *46*, 7106.

(12) L. S. Föster, Dadby, *J. Phys. Chem.* **1962**, *66*, 838.

(13) K. Hamanoue, T. Nakayama, M. Ito, *Chem. Soc. Faraday Trans.* **1991**, *87*, 3487.

(14) J. F. Rabek, *Experimental Methods in Photochemistry and Photophysics,* John Wiley and Sons, New York, 1982.

(15) N. J. Turro, *Modern Molecular Photochemistry*, The Benzamin Publishing Company Inc., 1978.

(16) N. Mataga, T. Kubota, *Molecular Interactions and Electronic Spectra*, Marcel Dekker, New York, 1970.

(17) L. G. Arnaut, S. J. Formosinho, *J. Photochem. Photobiol. A: Chem.* **1993**, *75*, 1.

(18) S. J. Formosinho, L. G. Arnaut, *J. Photochem. Photobiol. A: Chem.* **1993**, *75*, 21.

(19) L. Stryer, *Biochemistry*, Freeman, San Francisco, 1981.

(20) N. Chattopadhyay, *J. Photochem. Photobiol. A: Chem.* **1995**, *88*, 1.

(21) D. Huppert, E. Kolodney, *Chem. Phys*. **1981**, *63*, 401.

(22) G. W. Robinson, P. J. Thistlethwaite, J. Lee, *J. Phys. Chem.* **1986**, *90*, 4224.

(23) A. Mallick, N. Chattopadhyay, *Photochem. Photobiol.* **2005**, *81*, 419.

(24) B. Sengupta, P. K. Sengupta, *Biopolymer* **2003**, *72*, 427.

(25) G. Guharay, B. Sengupta, P. K. Sengupta, *Proteins Struct. Funct. Genet.* **2001**, *43*, 75.

(26) X. Wang, J. Wang, Y. Wang, H. Yan, P. Li, R. K. Thomas, *Langmuir* **2004**, *20*, 53.

(27) A. Mallick, N. Chattopadhyay, *Biophys. Chem.* **2004**, *109*, 261.

(28) N. Chattopadhyay, R. Dutta, M. Chowdhury, *J. Photochem. Photobiol. A: Chem.* **1989**, *47*, 249.

(29) S. Panja, S. Chakravorti, *Chem. Phys. Lett.* **2003**, *367*, 330.

(30) D. A. Kelker, A. Chattopadhyay, *J. Phys. Chem. B* **2004**, *108*, 12151.

(31) A. P. Varela, M. G. Miguel, A. L. Macanita, R. S. Becker, H. D. Burrows, *J. Phys. Chem.* **1995**, *99*, 16093.

(32) A. Mallick, B. Haldar, N. Chattopadhyay, *J. Photochem. Photobiol. B: Biol.* **2005**, *78*, 215.

(33) N. Chattopadhyay, *J. Photochem. Photobiol. A: Chem.* **1991**, *58*, 31.

(34) J. E. Hansen, E. Pines, G. R. Fleming, *J. Am. Chem. Soc.* **1992**, *96*, 6904.

(35) M. Barroso, L. G. Arnaut, S. J. Formosinho, *J. Phys. Chem. A* **2007**, *111*,591.

(36) M. H. Van Benthem, G. D. Gillespie, *J. Phys. Chem.* **1984**, *88*, 2954.

(37) N. P. Earnsting, A. Mordzinski, B. Dick, *J. Phys. Chem*. **1987**, *91*, 1404.

(38) B. Dick, N. P. Earnsting, *J. Phys. Chem*. **1987**, *91*, 4261.

(39) K. Das, D. S. English, J. W. Petrich, *J. Phys. Chem. A* **1997**, *101*, 3241.

(40) N. Mataga, *Pure Appl. Chem.* **1984**, *56*, 1255.

(41) F. Barbara, W. Jarzeba, *Adv. Photochem.* **1990**, *15*, 1.

(42) J. W. Verhoeven, *Pure Appl. Chem.* **1990**, *62*, 1585.

(43) T. Kakitani, N. Matsuda, A. Yoshimori, N. Mataga, *Prog. React. Kinet.* **1995**, *20*, 347.

(44) N. Mataga, H. Miyasaka, *Adv. Chem. Phys.***1999**, *107*, 431.

(45) N. Mataga, S. Nishikawa, T. Asahi, T. Okada, *J. Phys. Chem.* **1990**, *94*, 1443.

(46) R. M. Hermant, N. A. C. Bakker, T. Scherer, B. Kirjnen, J.W. Verhoven, *J. Am. Chem. Soc.***1990**, *112*, 1214.

(47) M. R. Wasieleaski, *Chem. Rev.* **1992**, *92*, 435.

(48) A. Mallick, B. Haldar, P. Purkayastha, S. Maiti, N. Chattopadhyay, *Chem. Phys. Lett.* **2003**, *368*, 688.

(49) N. Nandi, K. Bhattacharyya, B. Bagchi, *Chem. Rev.* **2000**, *100*, 2013.

(50) D. S. Chemla, J. Zyss, *Nonlinear optical Properties of Organic Molecular and Crystals*, Academic Press, New York, 1987.

(51) R. S. Mulliken, *J. Am. Chem. Soc.* **1952**, *74*, 811.

(52) S. D. Bella, I. L. Fragla, M. Rather, *J. Am. Chem. Soc.* **1993**, *115*, 682.

(53) S. M. Andrade, S. M. B. Costa, R. Pansu, *J. Am. Chem. Soc.* **2000**, *226*, 260.

(54) P. Pal, A. Saha, A. K. Mukherjee, D. C. Mukherjee, *Spectrochim. Acta. A* **2004**, *60*, 2013.

(55) T. Roy, K. Dutta, M. K. Nayek, A. K. Mukherjee, M. Banerjee, B.K. Seal, *J. Chem. Soc., Perkin Trans II* **2000**, 531.

(56) F. P. Fla, J. Palou, R. Valero, C. D. Hall, P. Peers, *J. Chem. Soc., Perkin Trans II* **2000**, 1925.

(57) H. A. Benesei, J. H. Hildebrand, *J. Am. Chem. Soc.* **1949**, *71*, 1703.

(58) N. Mataga, H. Chosrowjan, S. Taniguchi, *J. Photochem. Photobiol. C* **2005**, *6*, 37.

(59) M. E. Michel-Beyerle, *The Reaction Center of Photosynthetic Bacteria, Springer-Verlag*, Berlin, 1995.

(60) A. B. Diner, G. T. Babock, in: A.B. Diner, G.T. Babock (Eds.), *In Structure Dynamics And Energy Conversion Efficiency in Photosystem II*, Kluwer, Dordrecht, 1996, pp. 213.

(61) Z. R. Grabowski, K. Rotkiewicz, *Chem. Rev*. **2003**, *103*, 3899.

(62) S. L. Wang, T. I. Ho, *J. Photochem. Photobiol. A: Chem.* **2000**, *135*, 119.

(63) A. Onkelinx, F.C. De Schryver, L. Viance, M. Van der Auweraer, K. Iwai,M. Yamamoto, M. Ichikawa, H. Masuhara, M. Maus, W. Retting, *J. Am. Chem. Soc.* **1996**, *118*, 2892.

(64) M. El-Kemary, M. Elkhouly, M. Fujitsuka, O. Ito, *J. Phys. Chem. A* **2000**, *104*, 1196.

(65) X. Wang, J. Wang, Y. Wang, H. Yan, P. Li, R.K. Thomas, *Langmuir* **2004**, *20*, 53.

(66) A. Mallick, N. Chattopadhyay, *Biophys. Chem.* **2004**, *109*, 261.

(67) R. B. Macgregor, G. Weber, Nature **1986**, *319*, 70.

(68) S. Panja, S. Chakravorti, *Chem. Phys. Lett.* **2001**, *336*, 57.

(69) S. K. Ghosh, S. C. Bhattacharya, *Chem. Phys. Lipid* **2004**, *131*, 151.

(70) S. M. Dennison, J. Guharay, P. K. Sengupta, *Spectrochim. Acta. A* **1999**, 55, 1127.

(71) S. Mukherjee, K. Sahu, D. Mandal, S. K. Mandal, K. Bhattacharyya, *Chem. Phys. Lett.* **2004**, *384*, 128.

(72) P. Hazra, N. Sarkar, *Chem. Phys. Lett.* **2001**, *342*, 303.

(73) M. Oelgemoller, A.G. Griesbeck, *J. Photochem. Photobiol. C: Rev*. **2002**, *3* 109.

(74) P. Nemes, A. Deneler, L. Biczok, T. Berces, V. Wintgens, P. Valat, J. Kossanyi, *J.Photochem. Photobiol. A* **1998**, *113*, 225.

(75) V. Wintgens, P. Valat, J. Kossanyi, A. Demeter, L. Biczok, T. Beras, *N. J. Chem.* **1996**, *20*, 1149.

(76) A. Demeter, T. Berces, L. Biczok, V. Wintgens, P. Valat, J. Kossanyi, *J. Phys. Chem.* **1996**, *100*, 2001.

(77) D. Yuan, G.R. Brown, *J. Phys. Chem. A* **1997**, *101*, 3052.

(78) K. Jia, Y. Wan, A. D. Xia, S. Y. Li, F. B. Gong, G. Q. Yang, *J. Phys. Chem. A* **2007,** *111*, 1593.

(79) J. Widengren, P. Schwille, *J. Phys. Chem. A* **2000,** *104*, 6416.

(80) D. A. Skoog, F. J. Holler, *Principles of Instrumental Analysis*. 5th ed.; Saunders College Pub.: Philadelphia, 1998.

(81) M. Kasha, *Disc. Faraday Soc.* **1950**, *9*, 14.

(82) S.G. Schulman, *Fluorescence and phosphorescence spectroscopy: Physicochemical principles and practice*, Pergamon Press, Oxford, 1977.

(83) N. Mataga, T. Okada, N. Yamamoto, *Chem. Phys. Lett.* **1967**, *1*, 119.

(84) N. Mataga, S. Tsumo, *Bull. Chem. Soc. Jpn.* **1957**, *30*, 367.

(85) W. Rettig, *J. Mol. Struct.* **1982**, *84*, 303.

(86) P. Suppan, *Chem. Phys. Lett.* **1986**, *128*, 160.

(87) D. Pilloud, P. Suppan, L. Van Haelst, *Chem. Phys. Lett*., **1987**, *137*,130.

(88) W. Baumann, H. Bischof, J. C. Frohling, C. Brittinger, W. Rettig, K. Rotkiewicz, *J. Photochem. Photobiol. A: Chem.* **1992***, 64,* 49.

(89) P. Pringsheim, *Fluorescence and phosphorescence*, Inter-Science, New York, 1949.

(90) T. Forster, *Fluorescencz organisher verbindungen*, Vanderhock and Rupreht, Gottingen, 1951.

(91) G. C. Pimentel, *J. Am. Chem. Soc.* **1957**, *79*, 3323.

(92) N. Mataga, S. Tsumo, *Bull. Chem. Soc. Jpn.* **1957**, *30*, 368.

(93) E. Lippert, Z. Naturforsch, **1955**, *10a*, 541.

(94) E. Lippert, Z. Naturforsch, Teil A **1962**, *17*, 621.

(95) E. G. McRae, *J. Phys. Chem.* **1957**, *61*, 562.

(96) P. Suppan, *J. Chem. Soc. A* **1968**, 3125.

(97) Y. Oshika, *J. Phys. Soc. Japan* **1954**, *9*, 594.

(98) N. Mataga, Y. Kaifu, M. Koizumi, *Bull. Chem. Soc. Jpn*. **1955**, *28*, 690.

(99) W. Liptay, *Z. Naturforsch* **1965**, *20a*, 1441.

(100) L. Bilot, A. Kawski, Z. Naturforsch. **1962**, *17a*, 621.

(101) N. G. Bakhshiev, *Opt. Spektrosk.* **1961**, *10*, 717.

(102) Y. Ooshika, *J. Phys. Soc. Jpn.* **1954**, *9*, 594.

(103) E. G. McRae, J. Phys. Chem.**1957**, *61*, 562.

(104) E. Lippert, *Ber. Bunsenges. Phys. Chem.* **1957**, *61*, 962.

(105) L. Bilot, A. Kawski, *Z. Naturforsch.* **1963**, *18a*, 256.

(106) N. G. Bakhshiev, *Opt. Spektrosk.* **1964**, *16*, 821.

(107) A. Kawski, *Acta Phys. Pol*. **1966**, *29*, 507.

(108) A. Kawski, I. Uzarewicz, *Bull. Acad. Pol. Sci. Ser. Sci. Math. Astron. Phys.* **1963**, *11*, 625.

(109) A. Kawski, *Acta Phys. Pol.* **1964**, *25*, 625.

(110) A. Kawski, *Naturwissenshaften* **1964**, *51*, 82.

(111) J. Czekella, *Z. Elektrochem*. **1960**, *64*, 1221.

(112) J. Czekella, *Chimica* **1961**, *15*, 26.

(113) A. Kawski, B. Kukli´nski, P. Bojarski, *Z. Naturforsch.* **2002**, *57a*, 716.

(114) S. Joshi, D. D. Pant, *J. Mol. Liq*. **2012**, *166*, 49.

(115) S. Joshi, D. D. Pant, *J. Mol. Liq.* **2012**, *172*, 125.

(116) V. O. Stern, M. Volmer, *Z. Phys.* **1919**, *20*, 183.

(117) A. Mallick, B. Haldar, S. Maiti, N. Chattopadhyay, *J. Colloid interface Sci.* **2004**, *278*, 215.

(118) J. Yang, R. S. Roller, M. A. Winnik, *J. Phys. Chem. B* **2006**, *110*, 11739.

(119) Y. D. Paila, M. Kombrabail, G. Krishnamoorthy, A. Chattopadhyay, *J. Phys. Chem. B* **2011**, *115*, 11439.

(120) G. Jia, Z. Feng, C. Wei, J. Zhou, X.Wang, C. Li, *J. Phys. Chem. B* **2009**,*113*,16237.

(121) J. Kinoshita, S. Kawato, A. Ikegami, *J. Biophys.* **1977**, *20*, 289.

(122) N.C. Maiti, M. M. G. Krishna, P. J. Britto, N. Periasamy, *J. Phys. Chem. B.* **1997**, *101*, 11051.

(123) E. L. Quitevis, A. H. Marcus, M. D. Fayer, *J. Phys. Chem.* **1993**, *97*, 5762.

(124) L. B. A. Johansson, A. Niemi, *J. Phys. Chem.* **1987**, *91*, 3020.

(125) S. Hashimoto, J. K. Thomas, *J. Am. Chem. Soc.* **1985**, *107*, 4655.

(126) J. H. Client, *Surfactant Aggregation*, Blackie/Chapman & Hall, London/ NewYork, 1991.

(127) V. Torchilin, *Pharm. Res.* **2007**, *24*,1.

(128) J. Zeng, X. Xu, X. Chen, Q. Liang, X. Bian, L. Yang, X. Jing, *J. Controlled Release* **2003**, *92*, 227.

(129) E. Carretti, L. Dei, P. Baglioni, *Langmuir* **2003**, *19*, 7867.

(130) J. Yang, Curr. Opin. Colloid Interface Sci. **2002**, *7*, 276.

(131) R. Zana, *Chem. Tech.* **1993**, *23*, 30.

(132) M. J. Rosen, *Surfactants and Interfacial Phenomenon*, Wiley Interscience, New York, 1978.

(133) K. P. Ananthapadmanabhan, E. D. Goddard, N. J. Turro, P. L. Kuo, *Langmuir* **1985**, *1*, 352.

(134) D. F. Evans, M. Allen, B. W. Ninham, A. Fouda, *J. Solution Chem.* **1984**, *13*, 87.

(135) M. Bielawska, A. Chodzinska, B. Janczuk, A. Zdziennicka, *Colloids Surf. A: Physicochem. Eng. Aspects* **2013**, *424*, 81.

(136) A. Goldszal, A. M. Jamienson, J. A. Mann, J. Polak, C. Rosenblatt, *J. Colloid Interface Sci.***1998**, *180*, 261.

(137) E. Kudryashov, T. Kapustina, S. Morrrissey, V. Buckin, K. Dawson, *J. Colloid Interface Sci.***1998**, *203*, 59.

(138) R. Zielinski, *J. Colloid Interface Sci.***2001**, *235*, 201.

(139) M. Bergston, J. S. Pedersen, *Phys. Chem. Chem. Phys*. **1999**, *1*, 4437.

(140) A. L. Thompson, B. J. Love, *J. Colloid Interface Sci.* **2013**, *398*,270.

(141) D. Attwood, A. T. Florence, *Surfactant systems*, Chapman and Hall, London, 1985.

(142) Y. P. Zhu, A. Masuyama, M. Okahara, *J. Am. Oil Chem. Soc.* **1990**, *67*, 459.

(143) Y. P. Zhu, A. Masuyama, Y. I. Kirito, M. Okahara, *J. Am. Oil Chem. Soc.* **1991**, *68*,539.

(144) Y. P. Zhu, A. Masuyama, Y. I. Kirito, M. Okahara, M. J. Rosen, *J. Am. Oil Chem. Soc.* **1992**, *69*, 626.

(145) F. L. Duivenvoorde, M. C. Feiters, S. J. V. Gaast, J. B. F. N. Engberts, *Langmuir* **1997**, *13*, 3737.

(146) P. Mukerjee, *Adv. Colloid Interface Sci.* **1967**, *1*, 241.

(147) A. Ray, Nature **1971**, *231*, 313.

(148) M. J. Rosen, Surfactants and interfacial phenomena, Third ed., Wiley, New Jersey, 2004.

(149) M. J. Schick, F. M. Fowkes, *J. Phys. Chem.* **1957**, *61*, 1062.

(150) R. Zielinski, S. Ikeda, H. Nomura, S. Kato, *J. Colloid Interface Sci.* **1989**, *129*, 175.

(151) M. E. D. Garcia, A. Sanz-Medel, *Talanta* **1986**, *33*, 255.

(152) G. S. Hartley, *Aqueous solution of paraffin chain salts*, Herman, Paris, 1936.

(153) K. Kalyanasundaram, *Photochemistry in microheterogeneous systems*, Academic Press, Orlando, FI, 1987.

(154) H. V. Tartar, *J. Phys. Chem.* **1955**, *59*, 1195.

(155) F. M. Menger, *Acc. Chem. Res*. **1979**, *12*, 111.

(156) F. M. Menger, H. Yoshinaga, K. S. Venkatasubban, A. R. Das, *J. Org. Chem.* **1981**, *46*, 415.

(157) F. M. Menger, B. J. Boyer, *J. Am. Chem. Soc.* **1980**, *102*, 5936.

(158) P. P Lussi, *Biological and technical relevance of reversed micelles,* Plenum Press, New York, 1983.

(159) P. S. Goyal, V. K. Aswal, *Curr. Sci.* **2001**, *80*, 972.

(160) J.N. Israelachvili, D. J. Mitchell, B. W. Ninham, *J. Chem. Soc.,Faraday Trans. 2* **1976**, *72*, 1525.

(161) J. Faeder, B. M. Ladanyi, *J. Phys. Chem. B* **2000**, *104*, 1033.

(162) N. E. Levinger, *Curr. Opin. Colloid Interface Sci*. **2000**, *104*, 1033.

(163) M. P. Pileni, *Chem. Phys. Lett.* **1985**, *118*, 414.

(164) I. Lisiecki, M. P. Pileni, *J. Am. Chem. Soc.* **1993**, *115*, 3887.

(165) M. P. Pileni, *J. Phys. Chem.* **1993**, *97*, 6961.

(166) S. Vrignaud, N. Anton, P. Gayet, J. P. Benoit, P. Saulnier, *Eur. J. Pharm. Biopharm.* **2011**, *79*, 197.

(167) A. Patist, S. Bhagwat, K. Penfield, P. Aikens, D. Shah, *J. Surfactants Deterg.* **2000**, *3*, 53.

(168) G. S. Hartley, *Trans. Faraday Soc.* **1934**, *30*, 44.

(169) P. K. Behera, S. Mohapatra, S. Patel, B. K. Mishra, *J. Photochem. Photobiol. A: Chem* **2005**, *169*, 253.

(170) P. Das, A. Chakrabarty, A. Mallick, N. Chattopadhyay, *J. Phys. Chem. B* **2007**, *111*, 11169.

(171) S. S. Jaffer, S. K. Saha, G. Eranna, A. K. Sharma, P. Purkayastha, *J. Phys. Chem. C* **2008**, *112*, 11199.

(172) J. H. Mathias, M. J. Rosen, L. Davenport, *Langmuir* **2001**, *17*, 6148.

(173) R. Sabate, M. Gallardo, J. Estelrich, *J. Colloid Interface Sci.* **2001**, *233*, 205.

(174) R. Zana, *Noval surfactants*, in: K. Holmberg (Ed.), Dekker, New York, 1998.

(175) R. Hadgiivanova, H. Diamant, *J. Phys. Chem. B* **2007**, *111*, 8854.

(176) R. Hadgiivanova, H. Diamant, *J. Chem. Phys.* **2009**, *130*, 114901.

(177) D. Sahoo, S. Chakravorti, *Photochem. Photobiol.* **2009**, *85*, 1103.

(178) J. Qian, Y. Xu, X. Qian, J. Wang, S. Zhang, *J. Photochem. Photobiol. A: Chem.* **2008**, *200*, 402.

(179) A. Mishra, G. B. Behera, M. M. G. Krishna, N. Periasamy, *J. Lumin.* **2001**, *92*, 175.

(180) P. K. Mishra, S. Panigrahi, U. Dash, A. B. Mandal, *J. Colloid Interface Sci.* **2010**, *345*, 392.

(181) P. K. Mishra, H. P. Mishra, U. Dash, A. B. Mandal, *J. Colloid Interface Sci.* **2009**, *333*, 590.

(182) S. S. Jaffer, M. Sowmiya, S. K. Saha, P. Purkayastha, *J. Colloid Interface Sci.* **2008**, *325*, 236.

(183) K. Kalyanasundaram, J. K. Thomas, *J. Am. Chem. Soc.* **1977**, *99*, 2039.

(184) R. C. Dorrance, T. F. Hunter, *J. Chem. Soc. Faraday Trans. 1* **1972**, *68*, 1312.

(185) R. K. Dutta, S. N. Bhat, *Bull. Chem. Soc. Jpn.* **1992**, *65*, 1089.

(186) R. K. Dutta, S. N. Bhat, *Colloids Surf. A* **1996**, *106*, 127.

(187) S. S. Shah, R. Ahmad, S. W. H. Shah, K. M. Asif, K. Naeem, *Colloids Surf. A* **1998**, *137***,** 301.

(188) A. K. Chibisov, V. I. Prokhorenko, H. Gomer, *Chem. Phys.* **1999**, *250*, 47.

(189) M. Almgren, F. Grieser, J. K. Thomas, *J. Am. Chem. Soc.* **1979**, *101*, 279.

(190) C. Hirose, L. Sepulveda, *J. Phys. Chem.* **1981**, *85*, 3689.

(191) S. N. Guha., P. N. Moorthy , K. N. Rao., *Proc Indain Acad. Sci (Chem. Sci.)* **1982**, *91*,73.

(192) V. B. Gawandi, S. N.Guha, K. I. Piyadarsini, H. Mohan*, J. Colloid Interface Sci.* **2001**, *242*, 220

Chapter 2

Methods and Instrumentation

2.1 Methods

2.1.1 Preparation of solutions

All the samples of Quinine Sulfate (QS) and related molecules studied in this thesis were prepared by dissolving the appropriate concentrations of molecules in Milli Q water. To prepare the aqueous solutions of different concentrations of SDS, CTAB and TX-100, with constant concentration of QS (10^{-4} M), required amount of QS and different surfactant concentrations of SDS, CTAB and TX-100 were added to form micellar solution of different concentrations i.e premicellar, micellar and postmicellar. The pHs of the solutions were adjusted to different pH values by adding a small amount of $NaOH/H_2SO_4$ to the solution. To ensure the equilibrium of the micelles in the solutions, measurements were conducted only after 24 h of sample prepared.

2.1.2 Fluorescence Quantum yield Calculation

Quantum yield of fluorescence ($\phi_{\text{fluorescence}}$) is defined as the ratio of the number of fluorescence photons emitted from the sample to the number of light photons absorbed by the sample. Thus $\phi_{\text{fluorescence}}$ is expressed by the following equation.

$$\phi_{\text{fluorescence}} = \text{no. of photons emitted / no. of photons absorbed} \qquad (2.1)$$

Since the determination of the absolute number of photons absorbed and emitted by the sample is very difficult, the fluorescence Quantum yield of a unknown sample is normally determined by using a comparative method, where the integrated emission intensity of the sample is compared with that of an optically matched (very close absorbance at the excitation wavelength) reference sample whose Quantum yield is already known. Thus, keeping the excitation wavelength same for both the sample and the reference, the fluorescence Quantum yield of the sample (ϕ_{sample}) can be expressed with respect to the Quantum yield of the reference ($\phi_{\text{reference}}$) by using the equation[1]

$$\phi_{\text{sample}} = \frac{A_{\text{reference}}}{F_{\text{reference}}} \times \frac{F_{\text{sample}}}{A_{\text{sample}}} \times \frac{n^{2}{}_{\text{sample}}}{n^{2}{}_{\text{reference}}} \times \phi_{\text{reference}} \qquad (2.2)$$

where, $A_{\text{reference}}$ and A_{sample} are the absorbances at the excitation wavelength, $F_{\text{reference}}$ and F_{sample} are the integrated fluorescence intensities and $\eta_{\text{reference}}$ and η_{sample} are the refractive indices for the reference and the sample solutions, respectively.

2.1.3 Edge excitation red shift (EERS)

The shift in emission spectrum on excitation at the red edge of the first absorption spectrum is known as Edge Excitation Red Shift (EERS). EERS is expressed as the difference in the wavenumber (cm^{-1}) between the emission maximum obtained at different excitation wavelength for different sample solutions. These red-edge effects were related to the existence of excited-state distribution of fluorophores on their interaction energy with the environment and the slow rate of dielectric relaxation of this environment.

2.1.4 Solvatochromic shift method

Solvatochromic effect also called solvatochromic shift, refers to the correlation of absorption and emission spectra with the polarity of the solvent. This is caused by the presence of differing polarities of the ground and excited state of a chromophore. Therefore, a change in the solvent polarity will lead to a change in stabilization energy for each of the ground and excited states. This will in turn change the energy gap between these two states. This can be greatly influenced by various polar interactions including: hydrogen bonding, dipole-dipole, cation-dipole, etc. and has been discussed in detail in chapter 1.

2.1.5 Determination of micropolarity of environment around the fluorophore

Determination of the polarity in the immediate vicinity of the fluorophore provides valuable information about the location of the probe in micellar environments. Fluorescent probes serve important roles in determining the microscopic polarity, viscosity and refractive index of the biological and biomimicking environments.[1,2] These parameters around a probe in biomimetic environments can be estimated by comparison of spectral properties of fluorophore in the environment with those of probe in pure solvents of known polarities.[1-7] The polarity of homogeneous and microheterogeneous

media cannot be exactly same, however a relative estimate of such environment is made through such measurements. Khumbhakar et. al.[8] determined the micropolarity around coumarin 153 in TX-100 and they suggested that the fluorophore resides in the core region of micelle. From the absorption and fluorescence spectra of probe in different solvents, we calculated the corresponding Stoke's shifts. The Stoke's shift was ploted as a function of viscosity, polarity and dielectric constant of the solution and the relevant data and plots are given in respective chapters.

2.1.6 Determination of microviscosity of environment around the fluorophore

The steady-state fluorescence anisotropy measurement is important in biophysical and biochemical research in the sense that any factor which is responsible for change in size, shape, or segmental flexibility of a molecule will also change the observed anisotropy. The extent of restrictions imposed by the microenvironment on the dynamic properties of the molecule is directly manifested through the values of fluorescence anisotropy. Fluorescence anisotropy of a fluorescent probe molecule is intimately connected with the viscosity of the microenvironment around it. Hence, microviscosity is estimated from a comparison of the fluorescence anisotropy of a fluorescent probe in an environment with those of the probe in different environments of known viscosities. To know the microviscosity around QS, which is present in a microheterogeneous environment, the steady state and time-resolved fluorescence anisotropy is measured.

2.2 Instrumentation

2.2.1 Ground state absorption measurements

To understand the effect of light on chromophoric molecules, it is very important to know the detailed absorption and fluorescence emission characteristics of the systems under investigation. Optical absorption (ultraviolet-visible; UV-vis) spectroscopy is a widely used technique to obtain information about the ground state absorption characteristics of the chemical systems in terms of the wavelengths of the absorption bands and the extinction coefficients at different wavelengths. UV-vis absorption spectroscopy, being dependent on the electronic structure and the environment of the absorbing chromophore, allows the characterization or the identification of various chromophoric systems and their microenvironments. Changes in the solvent polarity,

polarizability and hydrogen bonding characteristics often induce significant shift in the absorption spectra.[9-12] Hence, this simple photochemical technique can provide many useful information regarding the nature of interactions between the ground-state of a chromophoric molecule and its surrounding environment. Measurements of the optical absorption spectra and thus to get knowledge about the absorbances of the experimental solutions in the ground-state are always very essential to adjust the concentration of the absorbing species in the solution for the purpose of their investigations using different other photochemical techniques.

The absorbance (A) of an absorbing species in a solution is directly proportional to the concentration (C) of the species and its molar extinction coefficient (ε_λ) at the measuring wavelength λ and is given by the equation

$$A = \log\left(\frac{I_0}{I}\right) = \varepsilon_\lambda cl \tag{2.3}$$

where, I_0 and I are the intensities of the incident and transmitted light, respectively, and l is the path length for the light beam passing through the sample. For absorbance measurements, the sample is usually kept in a quartz cuvette of 1 cm path length.

Figure 2.1 Photograph of spectrophotometer (a) JASCO V-570 (b) Thermo Evolution 201

Ground-state optical absorption spectra for the chemical systems to be investigated in the present study were carried out using either of the two double beam UV-vis spectrophotometers one from Jasco, kyoto, Japan (model V530), available in the central analytical laboratory of the institute, and the other from Thermo Evolution 201 available in the newly developed spectroscopy laboratory of our department. Photographs of the

instrument are shown in Figure 2.1. The wavelength range covered in both the spectrophotometers is 200-1100 nm. As the light sources, both the spectrophotometers use tungsten (W-lamp) for the 1100 to 350 nm region and a deuterium (D_2 lamp) for the 350-200 nm region. In both the spectrophotometers Si-photodiodes are used as the light detectors. The minimum wavelength resolution for the two spectrophotometers is 0.2 nm and lowest absorbance measurable is ~0.005. The schematic of a typical double beam UV-vis spectrophotometer is shown in Figure 2.2.

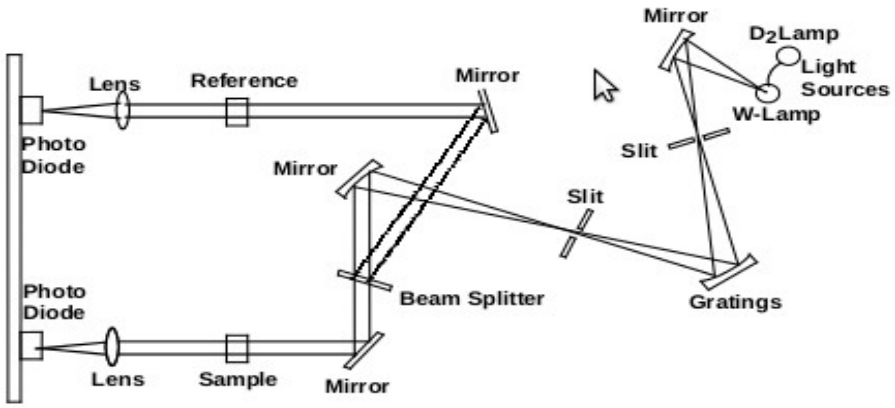

Figure 2.2 Schematic of a double beam UV-vis spectrophotometer

A beam of light from a visible and/or UV light source is separated into its component wavelengths by a prism or diffraction grating. Each monochromatic (single wavelength) beam in turn is split into two equal intensity beams by a half-mirrored device. One beam, the sample beam passes through a small transparent container (cuvette) containing a solution of the compound being studied in a transparent solvent. The other beam, the reference beam passes through an identical cuvette containing only the solvent. The intensities of these light beams are then measured by electronic detectors and compared. The intensity of the reference beam, which should have suffered little or no light absorption, is defined as I_0. The intensity of the sample beam is defined as I.

2.2.2 Steady state fluorescence measurements

Fluorescence measurements were performed using a Shimadzu RF-5301PC scanning spectrofluorimeter. Photograph of instrument is shown in Figure 2.3. The spectrofluorophotometer irradiates a sample with excitation light and measures the fluorescence from the irradiated sample to perform a qualitative and quantitative

analysis. The block diagram of the instrument is shown in Figure 2.4. The brief description of its components is given below.

This instrument is equipped with the light source of 150W Xenon lamp. The lamp housing is provided with ozone self-decomposition. The excitation monochromator isolates a band of a particular wavelength from the light from the Xenon lamp to obtain excitation light. Since brighter excitation light will contribute to higher sensitivity of the spectrofluorophotometer, the excitation monochromator incorporates a diffraction grating with a large aperture to collect the largest possible amount of light. The monochromator is of blazed holographic concave diffraction grating (F/2.5 for both excitation and emission sides) with the measurable scan range of 220-750 nm. The schematic of a typical steady-state spectrofluorimeter is shown in Figure 2.5.

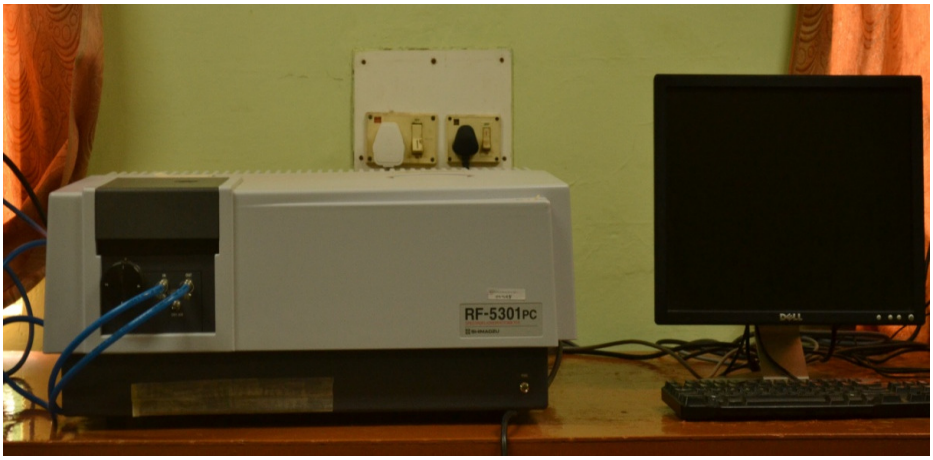

Figure 2.3 Photograph of the steady state spectrofluorimeter

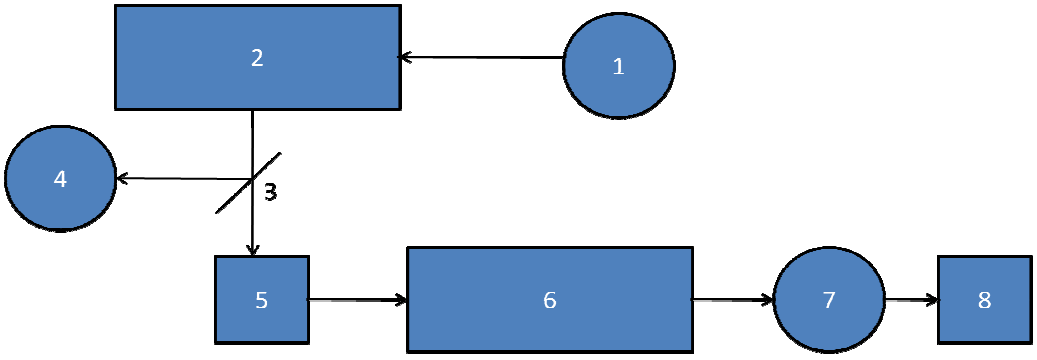

(1) 150 W Xenon Lamp (2) excitation monochromator (3) Beam splitter
(4) Monitor side photomultiplier tube (5) Cell holder (6) emission monochromator (7) Fluorescence side photomultiplier tube (8) Recorder

Figure 2.4 Block diagram of steady- state spectrofluorimeter

The cell holder holds a cell fitted with sample.

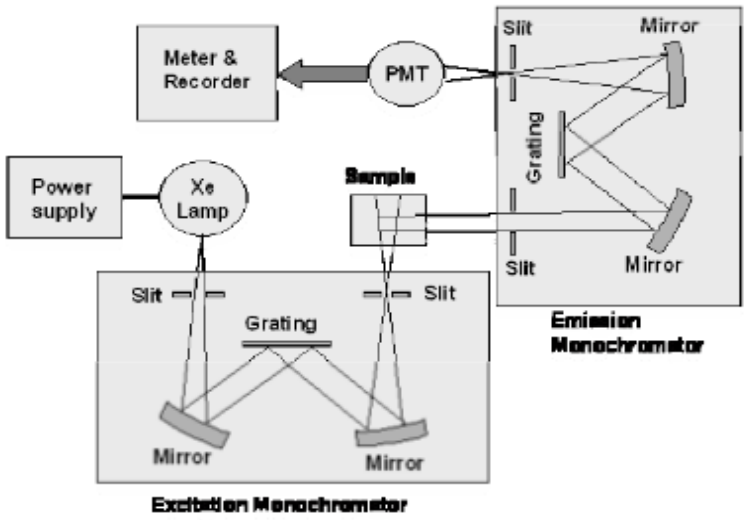

Figure 2.5 Schematic of a steady-state fluorescence spectrometer

The emission monochromator selectively receives fluorescence emitted from the sample and the photomultiplier tube measures the intensity of the fluorescence. The monochromator has a diffraction grating whose size is the same as that of the excitation monochromator to collect the greatest possible amount of light.

A light beam from the xenon lamp is incident upon the excitation monochromator. From the excitation monochromator, part of the beam is directed to the monitor detector through the beam splitter. All the drive components including the wavelength motor and slit control motor are operated according to signals from the internal computer. On the other hand, output signals from the monitor detector and fluorescence measurement detector (photomultiplier) are fed to the A/D converter and the internal computer for processing, and then output data is sent to the personal computer.

The detector in this system consists of photomultiplier tube for both photometry (R3788-02) and monitor (R212-14) sides. Generally, the Xenon lamps used on spectrofluorophotometers are characterized by very high emission intensity and an uninterrupted radiation spectrum. However, their tendency to unstable light emission will result in greater signal noise if no countermeasure is incorporated. In addition, the non-uniformity in the radiation spectrum of the Xenon lamp and in the spectral sensitivity characteristics of the photomultiplier tube (these criteria are generally called instrument

functions) causes distortion in the spectrum. To overcome these factors, the photomultiplier tube monitors a portion of excitation light and feeds the resultant signal back to photomultiplier tube for fluorescence scanning. This scheme is called the light-source compensation system. It also has variable slit width facility (1.5/3/5/10/15/20 nm) with the wavelength accuracy of $\pm$ 1.5 nm.

The steady-state fluorescence anisotropy measurements were performed with the same steady-state spectrofluorimeter fitted with a polarizer attachment (105UV polarizers), manufactured by POLACOAT Co., USA. The measurement was obtained by placing one polarizer on each of excitation and emission sides.

2.2.3 Fluorescence lifetime measurements

Time-resolved fluorescence measurements are very essential to obtain information regarding the kinetics and dynamics of various photochemical and photophysical processes involved in the deactivation of the excited molecules. Excitation of a sample containing fluorophoric molecules with a very short pulse of light results in an initial population (n_0) of fluorophores in the excited state. Since emission from the individual excited molecules is a random process, for a given time window following photoexcition with an ultrashort light pulse each of the excited fluorophores should have the same probability to emit a fluorescence photon. This condition effectively results the excited state population to decay following a first order rate Equation as, [9-16]

$$\frac{dn(t)}{dt} = -(k_r + k_{nr})n(t) \tag{2.4}$$

where, $n(t)$ is the number of excited molecules at time t following the very short pulse excitation of the sample, k_r is the radiative decay rate constant and k_{nr} is the nonradiative decay rate constant of the excited fluorophores. In an actual experiment, it is often difficult to know the exact number of the excited molecules present in the sample. However, knowing the fact that the fluorescence intensity is directly proportional to the number of excited molecules present in the solution, then Equation 2.4 can be simply expressed in terms of the time-dependent intensity $I(t)$ and the integration of the resulting equation gives us the expression for the fluorescence decay $I(t)$ as,

$$I(t) = I_0 \exp^{\left(\frac{-t}{\tau_f}\right)} \tag{2.5}$$

where, I_0 is the intensity at time zero and τ_f is the fluorescence lifetime of the sample and the latter is related to the radiative and nonradiative decay rate constants as,

$$\tau_f = \frac{1}{k_r + k_{nr}} \tag{2.6}$$

If the width of the excitation pulse is unusually short (δ-pulse) and the response time of the detection system is very fast compared to the fluorescence lifetime of the sample, the fluorescence lifetime can be obtained from the observed fluorescence decay by using the following two procedures. In the first method, the τ_f can be obtained simply by noting the time at which the fluorescence intensity decreases to 1/*e* of its initial value. In the other method, the lifetime can be determined from the slope of the plot of log $I(t)$ versus t.[9-14] In the cases where the fluorescence lifetime of the sample is quite short such that the excitation pulse width and/or the response time of the detection system distorts the observed decay, it is not possible to apply the above two simple analysis procedures to obtain the fluorescence lifetime of the sample. In such cases, the observed fluorescence decays are analysed following a deconvolution procedure, which will be described in the latter part of this section. Regarding the fluorescence decay, however, it is important to mention here that since the excited fluorophores emit randomly, different molecules spend different length of times in the excited states. Thus, for an ensemble of excited molecules in the system, some may emit at very short times following the excitation but others may emit at times much longer than the measured fluorescence lifetime of the sample. Accordingly, the time distribution of these emitted photons actually represents the measured fluorescence decay curve of the experimental sample. It is thus evident that, the estimated lifetime from the observed fluorescence decay is actually the statistical average of the times that the excited molecules spend in the excited state.

The lifetime of the fluorophore in the absence of nonradiative processes is called the intrinsic or natural lifetime and is given by

$$\tau_n = \frac{1}{\Gamma} \tag{2.7}$$

where, Γ is emissive rate of fluorophore.

In principle, the natural lifetime τ_n can be calculated from the absorption spectra, extinction coefficient, and emission spectra of the fluorophore. We can theoretically estimate radiative rate using Strickler Berg Equation from the absorption and emission spectra of the fluorophore using[2]

$$\Gamma \approx 2.88\times10^{-9} n^2 \frac{\int F(\overline{\upsilon})d\overline{\upsilon}}{\frac{\int F(\overline{\upsilon})d\upsilon}{\overline{\upsilon}^3}} \int \frac{\varepsilon(\overline{\upsilon})d\overline{\upsilon}}{\overline{\upsilon}} \tag{2.8}$$

$$= 2.88\times10^{-9} n^2 \left\langle \overline{\upsilon}^{-3} \right\rangle^{-1} \int \frac{\varepsilon(\overline{\upsilon})d\overline{\upsilon}}{\overline{\upsilon}} \tag{2.9}$$

where, $F(\overline{\upsilon})$ is the emission spectrum plotted on the wavenumber (cm^{-1}) scale , $\varepsilon(\overline{\upsilon})$ is the absorption spectrum, and n is the refractive index of the medium. The integrals are calculated over the $S_0 \leftrightarrow S_1$ absorption and emission spectra.

As already mentioned, the time-dependent fluorescence measurement is very important to investigate the dynamics and mechanism of the photoinduced processes in the excited singlet (S_1) state of the molecules. Two methods of measuring time-resolved fluorescence are in widespread use, the time-domain and frequency-domain methods.[1]

In time-domain or pulse fluorometry, the sample is excited with a pulse of light (Figure 2.6). The width of pulse is made as short as possible and is preferably much shorter than the decay time τ of the sample. The time-dependent intensity is measured following the excitation pulse, and the decay time τ is calculated from the slope of a plot of log *I(t)* verses t, or from the time at which intensity decreases to 1/e of the value at $t = 0$. The intensity decays are often measured through a polarizer oriented at 54.7° from the vertical z-axis. This condition is used to avoid the effects of rotational diffusion and/or anisotropy on the intensity decay.

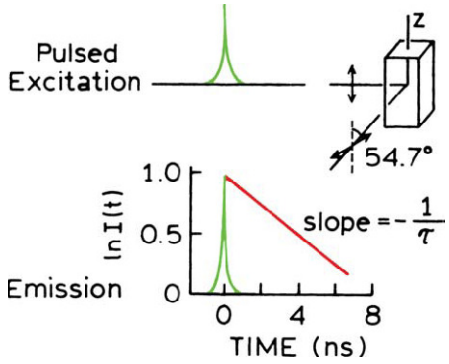

Figure 2.6 Pulse or time-domain lifetime measurements

The alternative method of measuring the decay time is the frequency-domain or phase-modulation method. In this case the sample is excited with intensity modulated light; typically, sine wave modulation is employed (Figure 2.7). The amplitude–modulated excitation should not be confused with the electrical component of an electromagnetic wave. The intensity of the incident light is varied at a high frequency ($\omega = 2\pi$ times the frequency in hertz) comparable to the reciprocal of the decay time τ. When a fluorescent sample is excited in this manner, the emission is forced to respond at the same modulation frequency. Owing to the lifetime of the sample, the emission is delayed in time relative to excitation. This delay is measured as a phase shift (ϕ) which can be used to calculate the decay time. Magic-angle polarizer conditions are also used in frequency domain measurements.

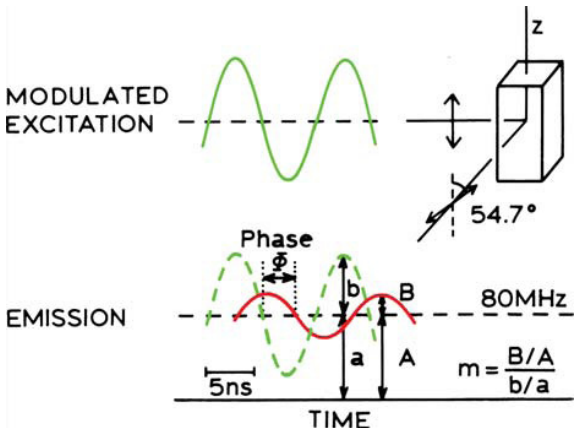

Figure 2.7 Phase-modulation or frequency-domain lifetime measurements. The ratios B/A and b/a represent the modulation of the emission and of the excitation, respectively

Time-Correlated Single Photon Counting (TCSPC) technique is the most widely used experimental method to measure the time-dependent fluorescence of a sample in the nanosecond to picosecond time scales. In the present study a TCSPC spectrometer from Horiba Jobin Yvon IBH, UK (model Data Station Hub) was used to measure the fluorescence lifetimes of the samples under investigation. The important aspects related to the present TCSPC spectrometer are described in the following sections.

The pulse method is frequently used in combination with Time Correlated Single Photon Counting (TCSPC). The sample is excited with a short pulse of light, and the time between the pulse and detection of the first emitted photon is measured. The course of fluorescence intensity with time (Figure 2.8) is recorded by multiple repetition of this procedure.

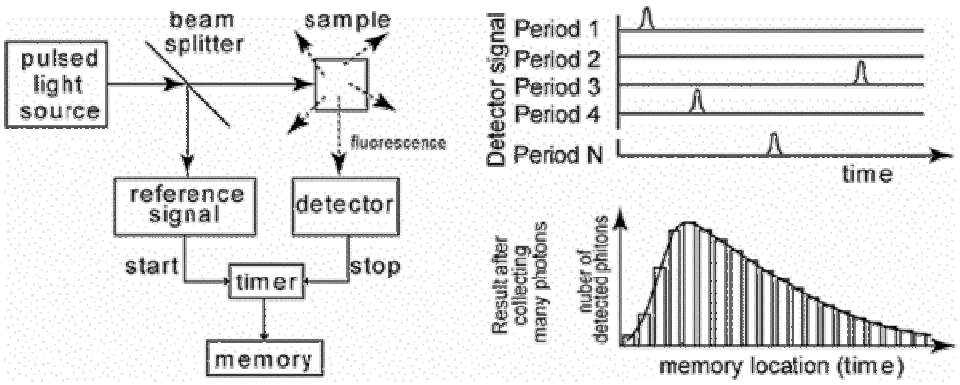

Figure 2.8 Schematics of Time Correlated Single Photon Counting. The arrival time of the first photon after an excitation pulse is measured and stored in memory. The histogram of many arrival times of photons represents the "fluorescence intensity versus time" curve

2.2.3.1 Basic principles of TCSPC technique

The instrument used in the present study for time-resolved fluorescence measurement works on the principle of Time Correlated Single Photon Counting (TCSPC) technique, where each single photon emitted by the sample is detected following its excitation by a short light pulse.[13-16] Photograph of instrument is shown in Figure 2.9. The principle of TCSPC measurement relies on the fact that the time-dependent probability distribution of the single photon emission from an excited molecule following its excitation is equivalent to the time-dependent changes in the fluorescence intensity of the sample following its δ-pulse excitation.[13-16] The schematic diagram of a typical TCSPC set up is shown in Figure 2.10.

According to Figure 2.10, an excitation pulse (optical pulse) from the pulsed excitation source is split into two parts, one part is used to excite the sample kept in the sample chamber and the other part of the light pulse is directed to a start Photomultiplier Tube (PMT). The optical signal at the start PMT generates an electrical START pulse, which is then routed through a Constant Fraction Discriminator (CFD) to the START input of the Time to Amplitude Converter (TAC) unit to initiate its charging operation. On receiving the start pulse, the TAC continues to undergo charging linearly with time. The part of the optical pulse, which excites the sample, effectively gives rise to the emission photons. These photons are then detected one by one by the stop PMT (at the right angle to the direction of excitation) to generate

electrical STOP pulses for each of the individual photons received. The STOP pulses thus generated in the stop PMT are also routed through a CFD and a variable delay line to the STOP input of the same TAC unit.

On receiving the first STOP pulse, the TAC unit stops its charging operation and subsequently generates an electrical output pulse (TAC-output), having amplitude proportional to the time difference (Δt) between the START and the STOP pulses reaching the TAC unit. The TAC output pulse is then fed to the input of a Multichannel Analyzer (MCA) through an Analog-to-Digital Converter (ADC). The ADC generates a numerical value proportional to the height of the TAC output pulse and thus selects the corresponding memory address (channel) in the MCA, where a single count is added up.

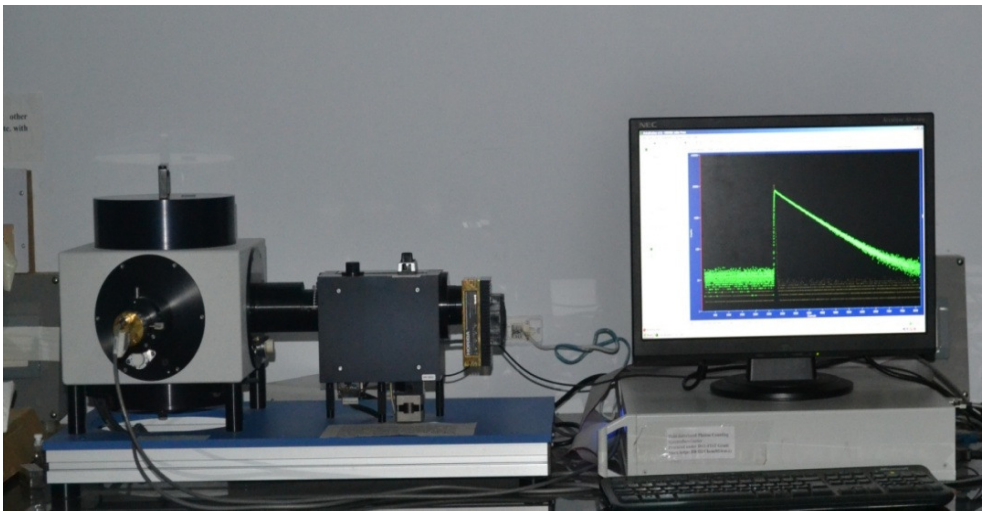

Figure 2.9 Photograph of the time-resolved spectrofluorimeter

The above cycle (from the triggering of the pulsed excitation light source to the data storage in the MCA) is repeated for a large number of times and thus a histogram of counts is collected in the MCA channels. The distribution of the counts against the channel number in the MCA then represents the fluorescence decay curve of the sample, provided the collection rate of the emission photons by the stop PMT is kept very low, only about 2% or less, compared to the repetition rate of the excitation pulses.[13-16] This experimental condition effectively means that following an excitation pulse, in no circumstances more than one emission photon can be detected by the stop PMT. Thus, in the TCSPC measurement, for about 98% cases of the excitation pulses, though the

sample is excited, there is effectively no emission photon that is directed to the stop PMT. Only about 2% cases of the sample excitations by the pulsed light source there is an effective emission of photon that is directed to the stop PMT and detected by the TCSPC setup. Such a low count rate is essential to maintain the time-dependent probability distribution of the photon emission from a single molecule following its excitation process. From the measured fluorescence decay curves, the fluorescence lifetimes of the samples are estimated following a suitable analysis procedure and introducing a proper time calibration for the MCA channels.[13-17]

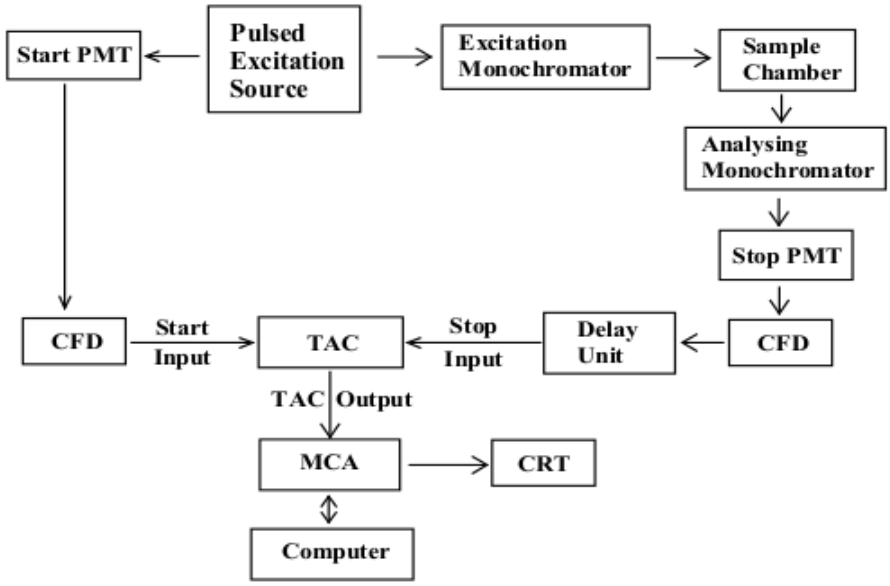

Figure 2.10 Schematic diagram of a Time Correlated Single Photon Counting Spectrometer

2.2.3.2 Important components of a TCSPC spectrometer

The TCSPC instrument used in the present study is from Horiba Jobin Yvon IBH, UK, Model Datastation Hub. The important components of the present TCSPC instrument are as given below.

(a) Pulsed excitation source*:* Different light emitting diodes (LED's) and diode lasers, having different emission wavelengths are used as the excitation sources in the IBH machine. With 375 nm diode laser excitation, the instrument response function for the spectrometer is about 165 ps (FWHM). With the LED excitation sources, the instrument response function is about 70 ps (FWHM). The repetition rate for excitation pulses is usually kept at 1 MHz and 500 KHz.

(b) Constant Fraction Discriminator (CFD): In a typical TCSPC instrument, the signals from the two PMTs (START and STOP PMTs) are routed through two independent CFDs to achieve the following two goals: (1) To improve the signal to noise ratio (S/N) by discarding the signals below a threshold height such that the counts recorded by the instrument are genuinely due to the photons detected by the PMTs and not due to spurious electrical noises. (2) To provide the correct timing information for the START and STOP inputs to the TAC unit such that the timing jitter in the detection is minimized. As the simple leading edge discriminators are always associated with significant timing errors, the CFDs are recognized to be the best suited discriminators for the TCSPC measurements to obtain accurate timing information for the START and STOP events.

(c) Variable Delay Line: A variable delay line is incorporated in the path of the STOP signal, between the CFD and the TAC, to intentionally delay the STOP pulse such that it reaches the TAC unit only after the START pulse and thus fruitfully counted by the TCSPC instrument. Moreover, by adjusting the variable delay line it is possible to trigger the TAC-MCA combination effectively such that the measured fluorescence decay curve is placed and stored within the suitable range of the MCA channels.

(d) Time-to-Amplitude Converter (TAC): In TCSPC instrument the time-correlation between the START and STOP event is carried out by using the TAC unit. In fact, this unit is considered as the heart of the TCSPC instrument.[13,15,18-20] On receiving the START pulse, following a preset delay (set in the TAC itself), a timing capacitor in the TAC start charging linearly with time from a constant current source. The charging is discontinued upon receiving a STOP pulse. Once the charging process is stopped, the TAC unit generates an output pulse (VTAC) for which the amplitude is proportional to the charge accumulated on the TAC capacitor and consequently is a measure of the time-difference (Δt) between the arrivals of the START and STOP pulses to the TAC, because the charging process of the capacitor in the TAC is linear with time. Functioning of a TAC unit is schematically shown in Figure 2.11. Following a START pulse, if no STOP pulse is received (i.e. no emission photon detected) by the TAC within a predefined time period, called the "TAC range", the capacitor charging is automatically discontinued without recording

the event and the TAC gets reset within a short time span making the unit ready for the next START and STOP pulses. In the present TCSPC instrument the TAC range can be varied from 50 ns to 200 μs. A suitable TAC range is judicially selected for a particular TCSPC measurement depending on the expected fluorescence lifetime of the sample used.

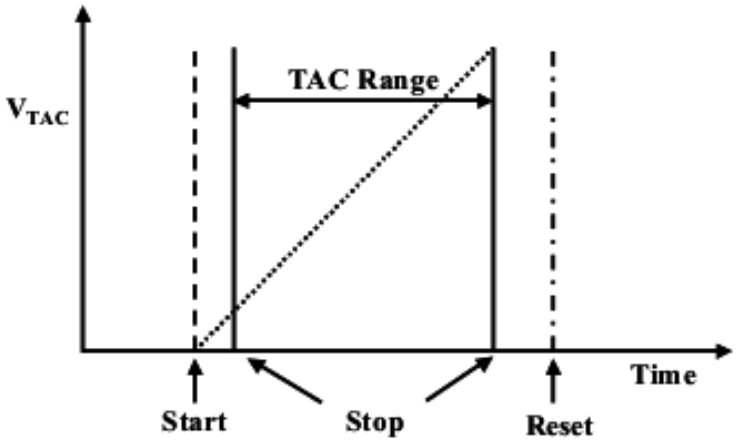

Figure 2.11 Functioning of a TAC unit used in a TCSPC instrument. Start indicates the initiation of the charging process. Stop signal can arrive the TAC unit at any time within the TAC range following the arrival of the start pulse

(e) Multichannel Analyzer (MCA): The MCA used in a TCSPC instrument can be operated either in the Pulse Height Analysis (PHA) mode (for measuring fluorescence decays) or in the Multichannel Scaling (MCS) mode (for measuring time-resolved emission spectra).The data stored in the MCA channels are transferred to a computer for further analysis and processing.

(f) The Start and the stop PMTs: In a typical TCSPC instrument where a nanosecond flash lamp with reasonably low repetition rate (~30 KHz) is normally used for sample excitation, the start and stop PMTs are used to get the respective signals for the TAC unit. In such instruments, an ordinary PMT with medium gain and reasonably low transit time can suitably be used to generate the START signals for the TAC unit, as a part of the light pulse (reasonably high intensity) is directly used to generate the START signal. In these cases, however, a special PMT with high gain and fast response time is required to be used to detect the emission photons from the sample. In TCSPC measurement, the spread in the transit time (the time difference between the emission of a photoelectron and its arrival to the anode) of the PMT has

a pronounced effect on the time resolution achieved by the instrument. As the transit time becomes shorter, the spread of the transit time also becomes shorter, improving the time resolution of the TCSPC measurements. Accordingly, fast PMTs are always preferable for the TCSPC measurements. The important point to be noted, however, that the detected light level for the emission photons from the sample is inherently very low (due to the condition imposed for time correlated single photon detection). Thus to detect the single emission photons effectively, the gain of the STOP PMT should be significantly high. To achieve a high gain for a PMT, one has to increase the number of dynodes for the PMT used. This, however, have a detrimental effect to increase the transit time and consequently the transit time spread, which in turn reduces the time resolution of the TCSPC instrument.

Though in a typical TCSPC instrument, suitable start and stop PMTs are used to carry out the measurements in the present IBH instrument only a single PMT with very high gain and low transit time is used to detect the emission photons from the sample. Thus only photodetector used in the present instrument is a special Hamamatsu PMT, used in combination with a TBX4 module provided by IBH, UK, and is used with a peltier cooling. The detector is having a spectral response from ~300 to 800 nm. In this instrument the measurement is infact made in a reverse mode, that is, the signal from the special PMT is used as a start pulse for the TAC unit and an electrical signal synchronized with the pulsed diode laser or LED is used as the stop pulses. This reverse mode is adopted especially for faster data collection using high repetition rate of the excitation pulses (1 MHz). This reverse mode of detection is essential to avoid unnecessary charging of the TAC unit by the high repetition rate excitation pulses. PC monitor is directly used to display the measured decay curve. Suitable analysis software is used to fit the measured decay curves and thus to obtain the fluorescence lifetime of the samples.

2.2.3.3 Time calibration of the MCA channels in a TCSPC spectrometer

Time calibration of the MCA channels in a TCSPC spectrometer is done by using a number of accurately calibrated delay lines in the path of the STOP pulses.[13,15,17] For this purpose, either the stop or the start signal is bifurcated into two parts, one is fed to the start input of the TAC and the other is routed through the precisely calibrated delay lines and then fed to the stop input of the TAC. As both

START and STOP inputs, of the TAC are originated from the same source, counts are collected only at a single channel of the MCA, determined by the TAC range used for the instrument and the known delay applied at the delay line in the path of the STOP pulse. For different known delays, the counts are thus collected at different channels of the MCA. The MCA data thus obtained are then transferred to a computer and the time calibration is calculated using a suitable analysis program.

2.2.3.4 Analysis of the fluorescence decay curves measured in a TCSPC instrument

As the light pulses used for the sample excitation in a TCSPC spectrometer is having a finite time width and the detection system is also having a finite response time, the experimentally measured fluorescence decay curve, $I(t)$, is effectively a convolution of the true fluorescence decay, $G(t)$, and the time profile of the excitation pulse, $P(t)$. Imagining the excitation pulse to be a combination of large number of δ-pulses, it is possible to express the observed decay, $I(t)$, as the convolution integral of $G(t)$ and $P(t)$ as,[13-16,21-24]

$$I(t) = \int_0^t P(t')G(t-t')dt' \tag{2.10}$$

Experimentally one can obtain both $I(t)$ and $P(t)$. During analysis, a decay function $G(t)$ is first assumed for the sample and this function is convoluted with the observed $P(t)$ according to Equation 2.10 to obtain a calculated curve $Y(t)$, which is then compared with the experimentally observed decay curve $I(t)$.[13-15,22,23] The variables in the function $G(t)$ is iteratively changed until a good comparison (best fit) between the $Y(t)$ and $I(t)$ is obtained. The function $G(t)$ is usually assumed to be a sum of exponentials, such that,

$$G(t) = \sum_i B_i \exp^{\left(\frac{-t}{\tau_i}\right)} \tag{2.11}$$

where, B_i is the pre-exponential factor for the i^{th} component and τ_i is the corresponding fluorescence lifetime. The success of an analysis and accordingly the acceptance of a fit to the observed decay curve is determined from the judgement of the following statistical parameters.

(a) Reduced Chi-square (χ_r^2) values: The reduced chi-square (χ_r^2) is defined as,

$$\chi_r^2 = \frac{\sum_i W_i \{Y(i) - I(i)\}^2}{(n-p)} \tag{2.12}$$

where, $Y(i)$ is the count at the ith channel of the calculated curve, $I(i)$ is the count at the ith channel of the experimentally measured curve, Wi [=1/$I(i)$], is the weighting factor of the counts in the ith channel, n is the number of channels used for the decay to be analysed and p is the number of degrees of freedom in the decay function considered for the analysis (equals to the number of variables in the function $G(t)$. For a good fit, the χ_r^2 value should be very close to unity. Normally a χ_r^2 value between 1.00 to 1.20 is considered to represent a good fit.[13-16,21]

(b) Distribution of weighted residuals: To judge the success of an analysis of a TCSPC data set, the random distribution of the weighted residuals among the data channels is also considered to be important criteria. The weighted residual for the ith channel, r_i, is defined by Equation

$$r_i = \sqrt{W_i}\{Y(i) - I(i)\} \tag{2.13}$$

where, Wi, $Y(i)$ and $I(i)$ are as defined earlier. For a good fit, the weighted residuals should be randomly distributed about the zero line for the whole range of the data channels used in the decay analysis.

(c) Durbin Watson parameter: This parameter was introduced by Durbin and Watson to test for serial correlation in linear regression analysis of econometric data. The defining Equation is

$$DW = \frac{\sum_{i=nL+1}^{nH} (X_i - X_{i-1})^2}{\sum_{i=nL}^{nH} X_i^2} \tag{2.14}$$

Values less than 1.7, 1.75 and 1.8 are indicative for poor fits to single, double, and triple exponential decay models.

2.3 Fluorescence anisotropy measurements

In a homogeneous solution, the ground-state fluorophores are all randomly oriented. When such an isotropic ensemble of chromophores is excited with a polarized

light beam, an anisotropic distribution is generated in the excited state (also in the ground-state which is not considered here) due to the selective excitation of the suitably oriented chromophoric molecules in the solution. Thus, observation and measurement of fluorescence anisotropy is based on the photoselective excitation of fluorophores, which can be better understood in the following manner. Each fluorophore has within its molecular framework a fixed absorption and fixed emission transition dipoles, that have very definite orientations with respect to the molecular axis. The two transition dipoles in a molecule are usually separated from each other by an angle β. Those fluorophores preferentially absorb the excitation photons that have their absorption transition dipoles parallel to the electric field vector parallel to the polarized excitation light. The probability of absorption for a molecule for which its transition dipole is oriented at an angle θ is with respect to the direction of the electric field vector of the polarized light is proportional to $\cos\theta$. Therefore absorption is maximum when $\theta = 0°$ and becomes negligible when θ approaches 90°.[9,13,15,25] Thus, the excited state population obtained following the excitation of the sample by a polarized excitation pulse is not randomly oriented but highly anisotropic in nature. This preferential excitation of molecules creates anisotropy in excited electronic state and this is schematically shown in Figure 2.12. Similarly, an excited molecule emits a photon preferentially with its electric field vector parallel to the emission transition dipole of the molecule. At any other angle θ, the probability of emission is again proportional to $\cos\theta$, where θ is the angle between the electric field vector of the emitted light and the emission transition dipole of the molecule. Thus, due to the selective excitation and emission, the fluorescence obtained following excitation with a polarized light is highly anisotropic in nature.

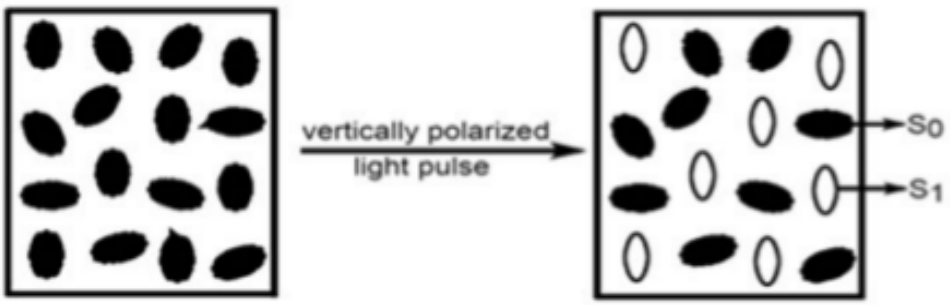

Figure 2.12 Creation of ground-state and excited state anisotropies from an isotropic distribution of molecules

In dilute solution, where depolarization of the excited molecules via energy transfer among chromophoric components is very insignificant, the excited-state anisotropy of the system decays mainly due to the rotational relaxation of the excited species. The anisotropy measurements reveal the average angular displacement of the fluorophore that occurs between the absorption and the subsequent emission process. This angular displacement depends upon the rate and the extent of the rotational diffusion of the excited species during the lifetime of the excited state. As expected the rotational diffusion of a molecule depends upon its size and shape as well as on the viscosity or the rigidity of its local environment. Thus, studies on fluorescence anisotropy have been utilized extensively to explore the local environment of the chromophoric dyes as well as to investigate their interactions with various host molecules or supramolecular systems.

Fluorescence anisotropy can be measured using both steady-state and time-resolved fluorescence spectrometers. In the Steady-state measurement, the sample is illuminated with a continuous beam of plane polarized light, and the intensities of the fluorescence emission are recorded for both parallel and perpendicular polarizations of the emitted light with respect to the vertically polarized excitation light. In the time-resolved anisotropy measurement, the sample is excited with a vertically polarized pulsed excitation light source and the fluorescence decays are collected for both parallel and perpendicular polarizations of the emitted light with respect to the excitation polarization. The general measurement procedure of the fluorescence anisotropy (both steady-state and time-resolved) is illustrated in Figure 2.13. The sample is excited with the vertically polarized light, i.e. the electric vector of the excitation light is oriented along the *z*-axis. The emission from the sample is measured through a polarizer oriented either parallel (||) or perpendicular ($\perp$) with respect to the excitation polarization. When the emission polarizer is oriented parallel to the excitation polarization, the observed intensity is labeled as $I_{\parallel}$. On the other hand, when the emission polarizer is oriented perpendicular to the excitation polarization, the observed intensity is designated as $I_{\perp}$. Since the response of the emission monochromator is not the same for the parallel and perpendicularly polarized light, the measured perpendicular component $I_{\perp}$ is corrected by an appropriate correction factor, known as G-factor, to rectify the polarization bias of the detection setup. Thus, from the measured $I_{\parallel}$ and $I_{\perp}$ values the steady-state anisotropy $(< r >)$ is calculated as,[9,13,15,25]

$$< r >= \frac{I_{\parallel} - GI_{\perp}}{I_{\parallel} + 2GI_{\perp}} \tag{2.15}$$

where, the correction factor G, is obtained independently by keeping the excitation polarization horizontal i.e. along Y- axis and measuring the fluorescence intensities with the emission polarizer oriented vertical (I_{HV}), and horizontal (I_{HH}), respectively where the intensity ratio I_{HV}/I_{HH} gives the measure of the G factor for the measuring emission wavelength. To be mentioned here that the G factor is not a fixed number for an instrument but is strongly dependent on the measuring emission wavelength. As indicated from the Equation 2.15, anisotropy is a dimensionless quantity. Moreover, it is to be noted that the measured anisotropy is independent of the emission intensity of the sample. Similar to steady-state anisotropy, the time resolved fluorescence anisotropy is expressed as

$$< r >= \frac{I_{\parallel} - GI_{\perp}(t)}{I_{\parallel} + 2GI_{\perp}(t)} \tag{2.16}$$

where, $I_{\parallel}$ and $I_{\perp}$ are the two polarized fluorescence decays with emission polarizations parallel and perpendicular to the vertically polarized excitation light.

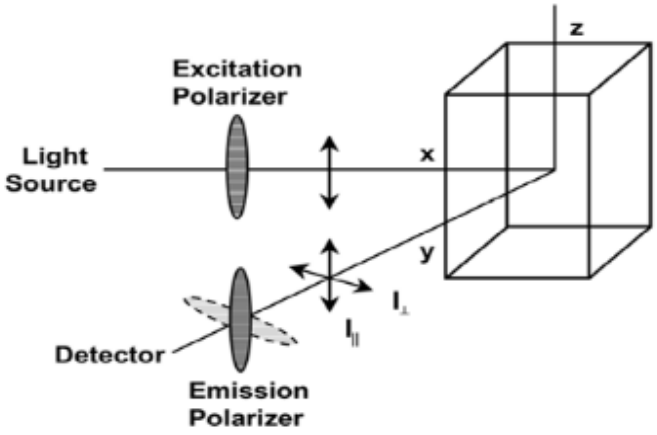

Figure 2.13 Schematic describing measurement of fluorescence anisotropy

There exists a rather simple relationship between the steady-state and the time-resolved anisotropy parameters. The steady-state anisotropy is simply the average of the time-resolved anisotropy, weighted by the intensity decay of the sample. Thus the steady-state anisotropy $< r >$ is given by the average of $r(t)$ weighted by $I(t)$ as, [9,13,15,25]

$$< r >= \frac{\int_0^\infty r(t)I(t)dt}{\int_0^\infty I(t)dt} \tag{2.17}$$

For a fluorophore, which displays a single exponential anisotropy decay with reorientation time τ_r, the function decay can be expressed as

$$r(t) = r_0 \exp^{\left(\frac{-t}{\tau_r}\right)} \tag{2.18}$$

where, r_0 is the initial anisotropy i.e. the anisotropy at $t = 0$ immediately after the δ-excitation pulse. Thus substituting $I(t)$ and $r(t)$ from Equations 2.5 and 2.18 into Equation 2.17 and on integration one can obtain,

$$\langle r \rangle = r_0 \left(\frac{\tau_r}{\tau_r + \tau_f} \right) \tag{2.19}$$

To be mentioned however, this expression is valid only if the intensity and anisotropy decays follow the single exponential functions. In most cases, however, intensity and anisotropy decays are more complex and cannot be fitted by the relations given by equations 2.5 and 2.18. The intensity decay of a fluorophore can follow a biexponential decay law when it is present in different environments (e.g. micelle bound and free dye) and is given by,

$$I(t) = \alpha_1 \exp^{\left(\frac{-t}{\tau f_1}\right)} + \alpha_2 \exp^{\left(\frac{-t}{\tau f_2}\right)} \tag{2.20}$$

where, τ_{f1} and τ_{f2} are the two lifetimes associated with the decay of fluorescence and α_1 and α_2 values are the preexponential factors. A fluorophore usually displays different lifetimes in different environments. Thus, for the same fluorophore in different environments, the value of α_i qualitatively represents the part of the fluorophores present in a particular environment. Similarly for fluorescence anisotropy a biexponential decay may be applicable as,[26-29]

$$r(t) = r_0 \left[\beta_1 \exp^{\left(\frac{-t}{\tau r_1}\right)} + \beta_2 \exp^{\left(\frac{-t}{\tau r_2}\right)} \right] \tag{2.21}$$

In this expression, τ_{r1} and τ_{r2} are the two time constants associated with the two decay component of the measured anisotropy and βi represents the fractional fluorescence arising from each emitting species. More complex intensity and anisotropy decays are also possible and that are usually expressed as the sum of exponentials as,

$$I(t) = \sum_i \alpha_i \exp^{\left(\frac{-t}{\tau_{fi}}\right)} \tag{2.22}$$

$$r(t) = r_0 \left[\sum_i \beta_i \exp^{\left(\frac{-t}{\tau_{ri}}\right)} \right] \tag{2.23}$$

For such complex decays the analysis and interpretation of the results are very difficult and are mainly done with lot of intuitions and modeling of the systems, as well as by gaining additional informations from other supporting measurements.

References:

(1) J. R. Lakowicz, *Principles of Fluorescence Spectroscopy*, Plenum, New York, 1999.

(2) A. Chakrabarty, P. Das, A. Mallick, N. Chattopadhyay, *J. Phys. Chem. B* **2008**, *112*, 3684.

(3) A. Mallick, B. Haldar, N. Chattopadhyay, *J. Phys. Chem. B* **2005**, *108*, 14683.

(4) P. Das, A. Chakrabarty, B. Haldar, A. Mallick, N. Chattopadhyay, *J. Phys. Chem. B* **2007**, *111*, 7401.

(5) A. Mallick, B. Haldar, S. Maiti, S.C Bera, N. Chattopadhyay, *J. Phys. Chem. B* **2005**, *109*, 14675.

(6) M. Shannigrahi, S. Bagchi, *Chem. Phys. Lett.* **2004**, *396*, 367.

(7) R. B. Macgregor, G. Weber, *Nature* **1986**, *319*, 70.

(8) M. Kumbhakar, S. Nath, T. Mukherjee, H. Pal, *J. Chem. Phys.* **2004**, *121*, 6026.

(9) J. B. Birks, *Photo Physics of Aromatic Molecules*, Wiley-Interscience, New York, 1970.

(10) A. Gilbert, J. Baggott, P. J. Wagner, *Essential of Molecular Photochemistry*, Blackwell science Inc.: Cambridge, USA, 1991.

(11) J. R. Lackowicz, *Principles of fluorescence spectroscopy*, 3rd ed., Springer, New York, 2006.

(12) K. K. Rohatgi-Mukherjee, *Fundamentals of Photochemistry*, Wiley Eastern Ltd, India, 1986.

(13) W. Becker, *Advanced time correlated single photon counting technique*, Springer, NewYork, 2005.

(14) J. N. Demas, *Excited state lifetime measurement*, Academic press, New York, 1983.

(15) D. V O'Connor, D. Phillips, *Time Correlatated Single Photon Counting*, Academic, New York, 1984.

(16) W. R. Ware, *Creation and detection of the Excited State*, A. A. Lamola, Ed., Marcel Dekker, New York, 1971, Vol. 1, Part A.

(17) J. Yguerabide, *Meth. Enzymol* **1972**, *26*, 498.

(18) D. A. Gedcke, W. J. McDonald, *Nucl. Instrum. Meth.* **1967**, *55*, 377.

(19) D. A. Gedcke, W. J. McDonald, *Nucl. Instrum. Meth.* **1968**, *58*, 253.

(20) G. R. Haugen, B. W. Wallin, J. E. Lytle, *Rev. Sci. Instrum.* **1972**, *50*, 64.

(21) P. R. Bevington, *Data Reduction and Error Analysis for the Physical Sciences*, McGraw-Hill, New York, 1969.

(22) A. E. McKinnon, A. G. Szabo, D. R Miller, *J. Phys Chem.* **1977**, *81*, 1564.

(23) D. V. O'Connor, W. R. Ware, J. C. Andre, *J. Phys. Chem.* **1979**, *83*, 1333.

(24) W. R.Ware, L. J. Doemeny, T. L. Nemzek, *J. Phys Chem.* **1973**, *77*, 2083.

(25) M. Ito, H. Kume, K. Oba, *IEEE Trans. Nucl. Sci.* **1984**, *31*, 408.

(26) P. K. Singh, M. Kumbhakar, R. Ganguly, V. K. Aswal, H. Pal, S. Nath, *J. Phys.Chem. B* **2010**, *114*, 3818.

(27) P. K. Singh, M. Kumbhakar, H. Pal, S. Nath, *J. Phys. Chem. B* **2008**, *112*, 7771.

(28) P. K.Singh, M. Kumbhakar, H. Pal, S. Nath, *J. Phys. Chem. B* **2009**, *113*, 1353.

(29) P. K. Singh, A. K. Satpati, M. Kumbhakar, H. Pal, S. Nath, *J. Phys. Chem. B* **2008**, *112*, 11447.

Chapter 3

Study of dipole moments of some fluorescent molecules

3.1 Introduction

In recent years, due to fast progress in the field of photophysics and photochemistry, studies of electric dipole moments have gained greater importance. Excitation of a molecule by photon causes a redistribution of charges leading to conformational changes in the excited state. This can result in increase or decrease of dipole moment of the excited state as compared to ground state. The dipole moment of an electronically excited state of a molecule is important property that provides information of the electronic and geometrical structure of the molecule in short-lived state. Knowledge of the excited-state dipole moment of electronically excited molecules is quite useful in designing nonlinear optical materials[1], elucidating the nature of the excited states and in determining the course of photochemical transformation. For a chromophore, the tunability range of the emission energy as a function of polarity of the medium is also determined by excited state dipole moment.[2]

A number of techniques e.g. electronic polarization of fluorescence, electric-dichroism, microwave conductivity and stark splitting[3-6] are available for determination of excited-state dipole moment, but their use is limited because they are considered equipment sensitive and studies have been related to very simple molecules. The solvatochromic method (discussed in detail in chapter 1) is based on the shift of absorption and fluorescence maxima in different solvents of varying polarity. The solvent dependence of absorption and fluorescence maxima is used to determine the excited-state dipole moments of different molecules.

The effect of solvent on the absorption and fluorescence characteristics of organic compounds has been a subject of extensive research[7]. Optical absorption and fluorescence spectroscopic techniques reveal the solute-solvent interactions, which can be characterized from the frequency, shape and the intensity of the spectrum. Spectral shifts result from the general effects of solvents polarity and due to the specific solute solvent interactions such as hydrogen bonding, acid base reactions or charge transfer

interactions. The solvent reorganization around the newly formed excited state of a solute molecule gives rise to the well known Stokes shift.

Theoretical description of solvatochromism is based on the Onsager description of non specific electrostatic solute–solvent interactions and the solvent is described as a dielectric continuum hosting solute molecules into Onsager type cavities. The surrounding solvent molecules get polarized due to the electric dipole moment of the solute molecule. As a result, the solute itself experiences an electric field, the reaction field, which is proportional to the dipole moment of the solute. Several workers have made extensive experimental and theoretical studies on ground state dipole moment (μ_g) and excited state dipole moment (μ_e) using different techniques in variety of organic fluorescent compounds like coumarins[7,8], indoles[9,10], purines[11,12], exalite dyes[13,14], quinazolines[15] etc. Rabahi et. al.[16] recently estimated ground and excited-state dipole moments of coumarin and iminocoumarins from solvatochromic shift and theoretical methods and found higher dipole moment in excited-state than ground- state. Ground and excited state dipole moments of some α-hydroxy phenyl hydrazone derivatives, Sudan dyes, dipolar laser dyes: coumarin 478 (C478), coumarin 519 (C519) and coumarin 523(C523) by using different solvatochromic shift methods were also estimated recently.[17-19] Lalithamba et. al.[20] studied, the absorption and fluorescence emission spectra of (9H-fluoren-9-yl) methyl 1-hydroxypropan-2-ylcarbamate [Fmoc-L-alaninol] in solvents of different polarities. By using solvatochromic shift method, experimental ground and excited states dipole moments were calculated. They observed higher dipole moment of excited state compared to ground state. The fluorescence emission peak undergoes a hypsochromic shift with increase in the polarity of the solvent, through which they confirm $n \rightarrow \pi^*$ transition. Sıdır et. al.[21] estimated ground and excited state dipole moments of Oil Red O (ORO) by using solvatochromic shift methods. Fluorescence spectra show positive solvatochromism whereas absorption spectra do not indicate sensitive behavior to solvent polarity. Excited state dipole moment is found as higher than those of ground state for all of the used methods and it is attributed to more polar excited state of ORO.

Quinine Sulfate (QS) has been the subject of extensive research in the past because of its medical applications as well as its use as fluorescence quantum yield and lifetime standard.[22-26] The photophysical processes in QS and related molecules have

been explored for designing fluorescence optical sensors for halides.[27, 28] On changing pH, various species derived from QS and Quinidine (QD) are: dication (~pH 2), monocation (~pH 7) and neutral molecule (~pH 12).[24, 29]

This chapter discusses the estimation of the ground and excited state dipole moments of Quinine Sulfate monocation (QS^+) and Quinine Sulfate dication (QS^{2+}) using solvatochromic shift method (where values of ground state dipole moment were theoretically calculated). We observed a large change in dipole moment of QS^+ and QS^{2+} in the excited state compared to the ground state. Quinidine monocation (QD^+) and Quinidine dication (QD^{2+}) are diastereomers to QS^+ and QS^{2+} respectively.[30] Since diastereomers are non-equivalent in their physical and chemical properties, the dynamic properties of the diastereomers in different environments become essential for understanding the effects of the conformational change on their chemical reactivities.

3.2 Experimental

Quinine Sulfate and Quinidine were procured from S.D. Fine Mumbai and Sigma Aldrich, respectively, and crystallized several times before using. All the solvents used were of HPLC grade or AR. Absorption spectra were taken with the help of dual beam JASCO V-570 UV/Vis/NIR spectrophotometer and fluorescence spectra were recorded with the help of Shimadzu, RF-5301PC Spectrofluorometer. The data were analyzed using related software. The spectral shifts obtained with different sets of samples were identical in most of the cases and values were within ±1.0 nm. Data were analyzed and were fitted to a straight line using related software. The ground state dipole moment for molecule was calculated by quantum chemical calculations using software Gaussian 03 program. The concentration of Quinine Sulfate and Quinidine in all the solutions prepared in different solvents was 5×10^{-5} M and 10^{-4} M respectively. Density of the Quinidine was estimated by ACD/Chemsketch software. For all spectral measurements, the samples were taken in 1 cm × 1 cm quartz cells.

3.3 Solvatochromic shift and estimation of dipole moment of Quinine Sulfate monocation

The absorption and fluorescence spectra of Quinine Sulfate monocation (QS^+) have been recorded at room temperature in wide range of solvents of different polarities.

The ground-state dipole moment of QS^+ was obtained from quantum mechanical calculations and the excited state dipole moment of QS^+ was estimated from Bakhshiev's and Bilot-Kawski equations by means of solvatochromic shift method. Higher value of dipole moment is observed for excited state as compared to the corresponding ground state value and this is attributed to the more polar excited state.

3.3.1 Results and Discussion

3.3.1.1 Theoretical calculations of ground state dipole moment

The ground state dipole moment (μ_g) of QS^+ was calculated by quantum chemical calculations. Computations were carried out using the Gaussian 03 program. The basis sets at level of theory HF/ 6-31G were used for calculations and corresponding optimized molecular geometry is shown in Figure 3.1.

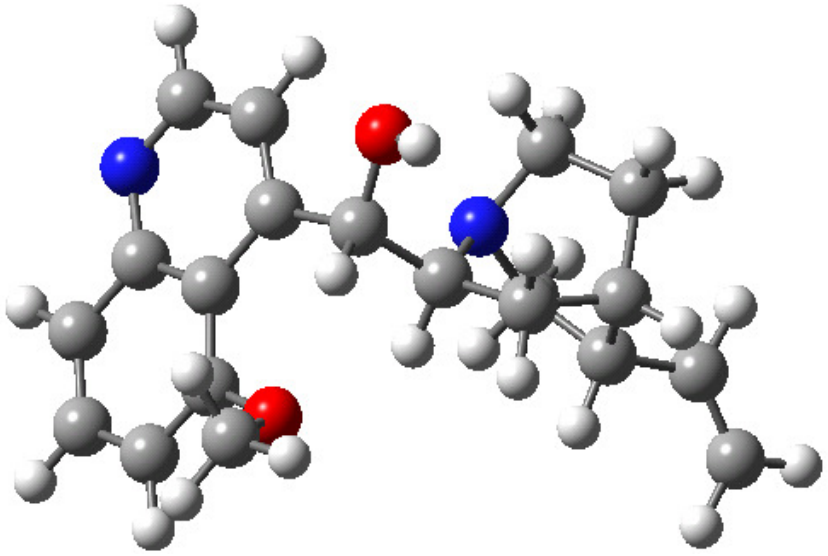

Figure 3.1 Optimized molecular geometries of QS^+ using theory HF/6-31G

3.3.1.2 Steady state measurements

The steady state absorption and fluorescence measurements of QS^+ (molecular structure shown in Figure 3.2) were made in different solvents at room temperature. The absorption spectrum in water and fluorescence spectrum in four different solvents are shown in Figure 3.3. The absorption spectrum shows two bands L_a and L_b at 330 and 280 nm, respectively in all the solvents studied. These two bands correspond to low-lying closely spaced π, π^* states of the main chromophore. The emission spectrum has only a structure-less broad band with maxima around 357 nm in benzene and 390 nm in water

on excitation at 340 nm. The variation of wavenumber of absorption and emission maxima with the solvent polarity function, F_1 (ε, n) are shown in Figure 3.4. The absorption maxima for different solvents studied remains constant with polarity function, whereas the emission maxima shifts towards lower frequencies with the increase in polarity of the solvent. The fluorescence spectrum is more red shifted in the case of water as compared to aprotic and nonpolar solvents. This trend in the fluorescence spectra is a bathochromic shift with increase in polarity[31] and is an indication of π, π^* transition. Solvent polarity functions F_1 (ε, n) and F_2 (ε, n) have been calculated in order to ascertain the ground and excited state dipole moments of the molecule and are given in Table 3.1.

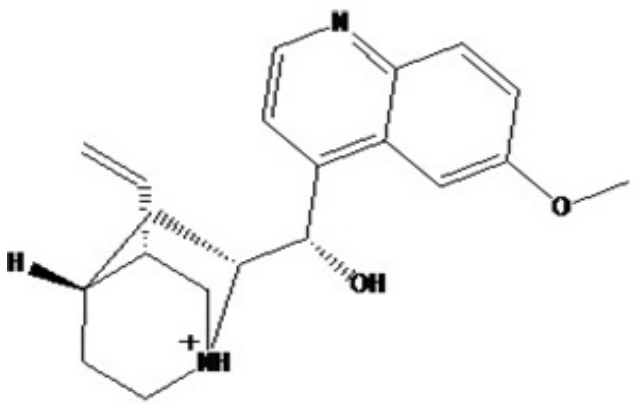

Figure 3.2 Molecular structure of Quinine Sulfate monocation (QS^+)

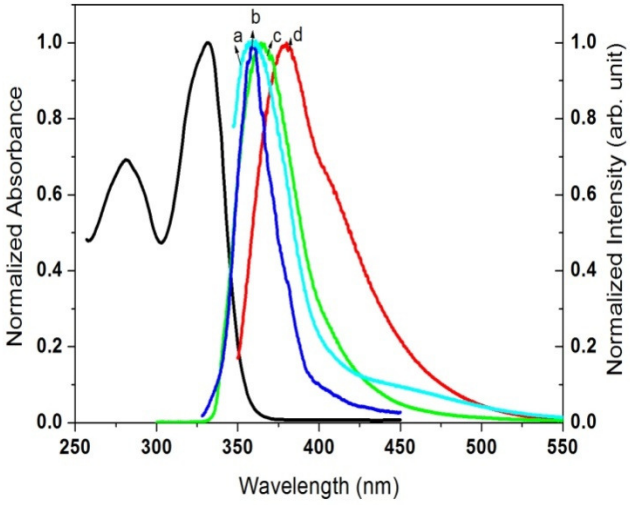

Figure 3.3 Normalized absorption spectrum of QS^+ in water and fluorescence spectra of QS^+ in (a) Benzene (b) Cyclohexane, (c) Dichloromethane and (d) Water

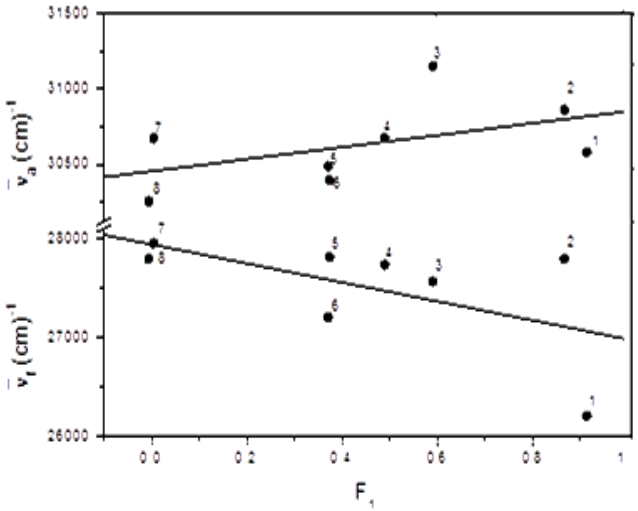

Figure 3.4 Variation of absorption and emission maxima of QS^+ with solvent polarity function. (1) Water, (2) Acetonitrile, (3) Dichloromethane, (4) Ethyl acetate, (5) Chloroform, (6) Diethyl ether, (7) Benzene, (8) Cyclohexane

The spectral shifts $\bar{\nu}_a - \bar{\nu}_f$ versus the solvent polarity function $F_1(\varepsilon, n)$ and $\frac{\bar{\nu}_a + \bar{\nu}_f}{2}$ versus F_2 (ε, n) are shown in Figures 3.5 and 3.6, respectively. The linear behaviour of Stokes shift versus solvent polarity function indicates general solvent effects as a function of dielectric constant and refractive index. Using related software the data fitted to a straight line. By using Bakhshiev's formula (Equation 3.1)[37] and Bilot-Kawski formula (Equation 3.2),[38-40] slopes found to be $S_1 = 1375.86\ cm^{-1}$ and $S_2 = -651.57\ cm^{-1}$ from Figures 3.5 and 3.6, respectively.

$$\bar{\nu}_a - \bar{\nu}_f = S_1 F_1(\varepsilon, n) + \text{const.} \tag{3.1}$$

$$\frac{\bar{\nu}_a + \bar{\nu}_f}{2} = -S_2 F_2(\varepsilon, n) + \text{const.} \tag{3.2}$$

$$\mu_e = \frac{|S_1 + S_2|}{|S_2 - S_1|}\mu_g \tag{3.3}$$

Using software Gaussian 03 we calculated ground state dipole moment for probe QS^+ using level of theory HF/6-31G. The ground -state dipole moment obtained was 4.47 D. From Equation (3.3) we have evaluated the value of μ_e using the above value of μ_g without a need to know the Onsager radius[12,32,33] of the QS^+. The value of μ_e thus obtained is 12.52 D. The change in dipole moment from excited state to ground- state is 8.05 D. All the data related to dipole moment are summarised in Table 3.2. Clearly the

dipole moment in excited state is significantly larger than the dipole moment in the ground state for the probe studied. The dipole moments of a molecule in the ground and excited states are different due to changes in electron densities in these states.

Table 3.1 Different solvent parameters and spectral data of QS^+ in different solvents

Solvent	ε	n	F_1	F_2	$\bar{\nu}_a - \bar{\nu}_f$ (cm^{-1})	$\frac{\bar{\nu}_a + \bar{\nu}_f}{2}$ (cm^{-1})
Water	78.3	1.33	0.9134	0.6815	4367	28393.0
Acetonitrile	37.0	1.32	0.8662	0.6568	3071	29328.5
Dichloromethane	8.9	1.42	0.5903	0.5829	3711	29297.5
Ethylacetate	6.0	1.37	0.4891	0.4979	2943	29203.5
Chloroform	4.8	1.44	0.3701	0.4872	3285	28845.5
Diethylether	4.3	1.35	0.3740	0.4267	2586	29100.0
Benzene	2.27	1.50	0.0036	0.3399	2726	29312.0
Cyclohexane	2.0	1.42	-0.0065	0.2845	2464	29025.0

Table 3.2 Dipole moment of QS^+ molecule in ground and excited states

Theory	S_1(cm^{-1})	S_2(cm^{-1})	μ_g(D)	μ_e(D)	$\Delta\mu$(D)	μ_e/μ_g
HF/6-31G	1375.86	651.57	4.47	12.52	8.05	2.80

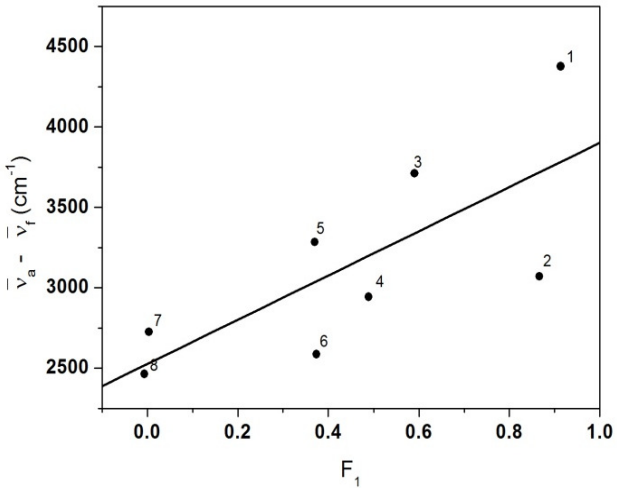

Figure 3.5 Plot for Stokes shift versus solvent polarity function F_1. (1) Water, (2) Acetonitrile, (3) Dichloromethane, (4) Ethyl acetate, (5) Chloroform, (6) Diethyl ether, (7) Benzene, (8) Cyclohexane

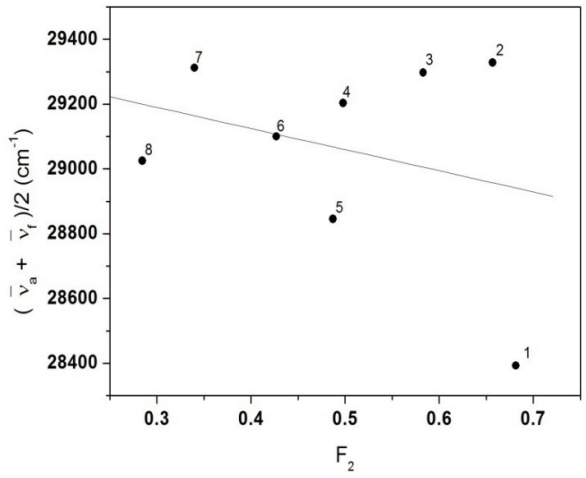

Figure 3.6 Plot for arithmetic average of absorption and fluorescence wavenumbers versus solvent polarity function F_2. (1) Water, (2) Acetonitrile, (3) Dichloromethane, (4) Ethylacetate, (5) Chloroform, (6) Diethyl ether, (7) Benzene, (8) Cyclohexane

3.3.2 Conclusions

We have calculated ground state and exited state dipole moments of QS^+. The μ_g value calculated from quantum chemical calculations is 4.47 D and the estimated excited state dipole moment from the solvatochromic shift method is 12.52 D. This large increase in dipole moment in the excited state of QS^+ is due to the more polar excited state than the ground state. The present study permits one to estimate the value of μ_e from the pre knowledge of μ_g, without the need of knowing the Onsager radius of the molecule, which is often chosen rather arbitrarily and impairs the popularity of solvatochromatic method.

3.4 Ground and excited state dipole moments of Quinine Sulfate dication: Solvatochromic shift of absorption and fluorescence spectra

Electronic absorption and fluorescence spectra of Quinine Sulfate dication (QS^{2+}) have been recorded at room temperature in a wide range of solvents of different polarities. The absorption maximum remains almost unchanged with the increase in solvent polarity, whereas a red shift in fluorescence emission maximum was observed. The ground-state dipole moment of QS^{2+} was obtained from quantum chemical calculations and the first excited singlet state dipole moment of QS^{2+} was obtained from Bakhshiev's and Bilot–Kawski's equations by means of solvatochromic shift method. Very high value of dipole moment is observed for excited state as compared to the corresponding ground state value and this is attributed to the more polar excited state of

QS^{2+}. Compared to the dipole moment of QS^{+}, both the ground and excited state dipole moments of QS^{2+} are lower.

3.4.1 Results and discussion

The structural formula of QS^{2+} is shown in Figure 3.7. In dilute sulphuric acid solutions (1N H_2SO_4), Quinine Sulfate (QS) is present as a di-cationic species, which is quite stable.[34] The nitrogens are adequately bound as the ammonium salt by strong acid of the medium effectively preventing n, π^* and n, σ^* transitions from occurring. The quinoline ring is a main fluorophore responsible for the absorption; methoxy group is very sensitive to the surrounding environment and responsible for anomalous photophysical behavior of QS^{2+}.[29,34-36]

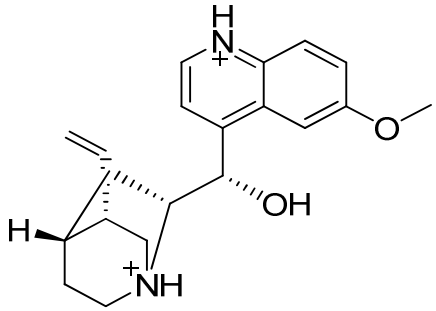

Figure 3.7 Molecular structure of Quinine Sulfate dication (QS^{2+})

3.4.1.1 Theoretical calculations of ground state dipole moment

The ground state dipole moment (μ_g) of QS^{2+} was calculated by quantum chemical calculations. Computations were carried out using the Gaussian 03 program. The basis sets at level of theory B3LYP was used for calculations and corresponding optimized molecular geometry is shown in Figure 3.8.

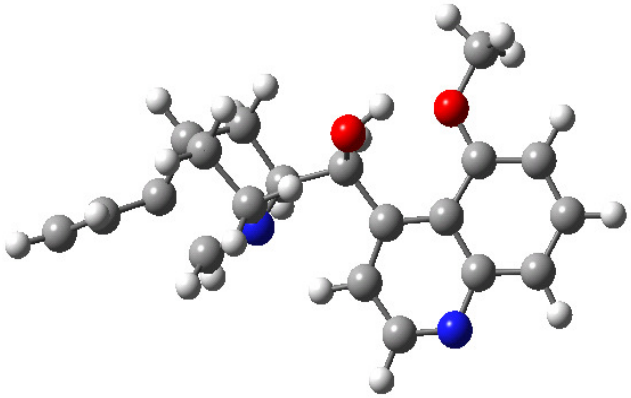

Figure 3.8 Optimized molecular geometry of QS^{2+} using theory B3LYP

3.4.1.2 Steady state measurements

The steady state absorption and fluorescence measurements were made in different solvents of different polarities at room temperature. The absorption spectrum in Dimethylformamide and fluorescence spectrum in three different representative solvents Dimethylformamide, Diethyether (aprotic polar) and Cyclohexane (nonpolar) are shown in Figure 3.9. The absorption spectrum shows two bands L_a and L_b at 346 and 317 nm, respectively in all the solvents studied. These two bands correspond to low-lying closely spaced π, π^* states of the main chromophore. The emission spectrum has only a structure-less broad band in all the solvents studied. The variation of wavenumber of absorption and emission maxima with the solvent polarity function, F_1 (ε, n) are shown in Figure 3.10. The absorption maxima for different solvents studied remains almost constant with polarity function; whereas, the emission maximum shifts toward lower frequencies with the increase in solvent polarity. The fluorescence spectrum is more red shifted in the case of polar aprotic solvents as compared to non polar solvents. This trend in the fluorescence spectra is a bathochromic shift with increase in polarity[31] and is an indication of π, π^* transition. The constant absorption spectrum with solvent polarity implies that the ground state energy distribution is not affected possibly due to less polar nature of the molecule in the ground state. On the other hand, a large red shift of the emission maximum with the solvent polarity indicates greater stabilization of excited state in polar solvents.

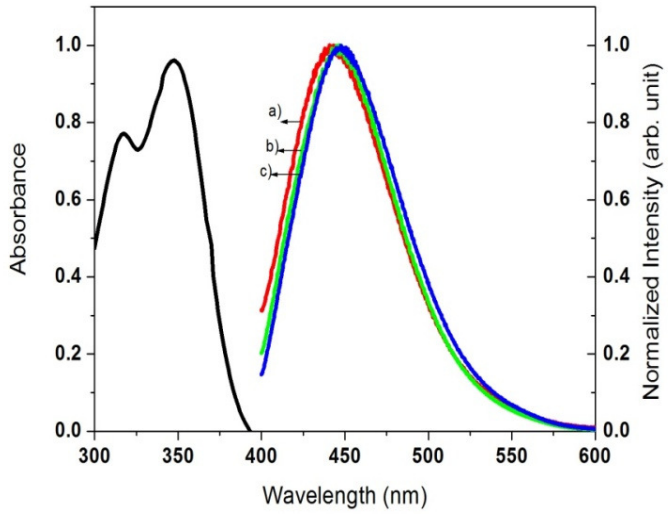

Figure 3.9 Normalized absorption spectra (in Dimethylformamide) and fluorescence spectra of QS^{2+} in (a) Cyclohexane, (b) Diethylether and (c) Dimethylformamide

Solvent polarity functions F_1 (ε, n) and F_2 (ε, n) have been calculated in order to ascertain the ground and excited state dipole moments of the molecule and are given in Table 3.3. The spectral shifts $\bar{\nu}_a - \bar{\nu}_f$ versus the solvent polarity function F_1 (ε, n) and $\frac{\bar{\nu}_a + \bar{\nu}_f}{2}$ versus F_2 (ε, n) are shown in Figure 3.11, and Figure 3.12, respectively.

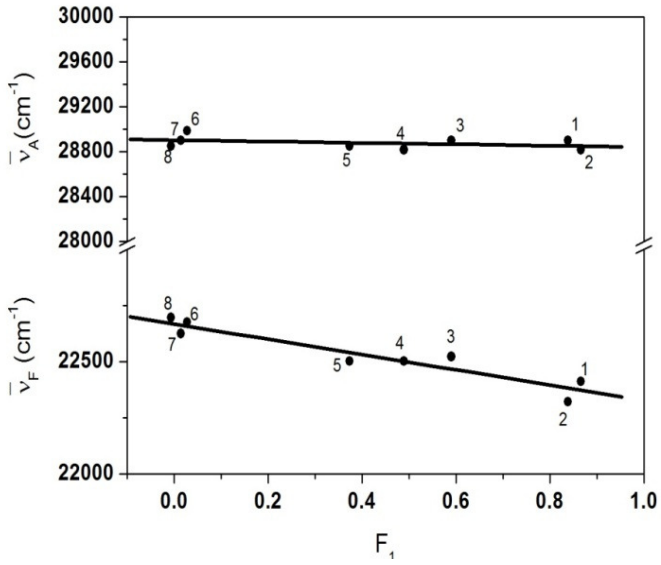

Figure 3.10 Variation of absorption and emission maxima of QS^{2+} with solvent polarity function, (1) Dimethylformamide, (2) Acetonitrile, (3) Dichloromethane, (4) Ethylacetate, (5) Diethylether, (6) o-xylene, (7) Carbontetrachloride, (8) Cyclohexane

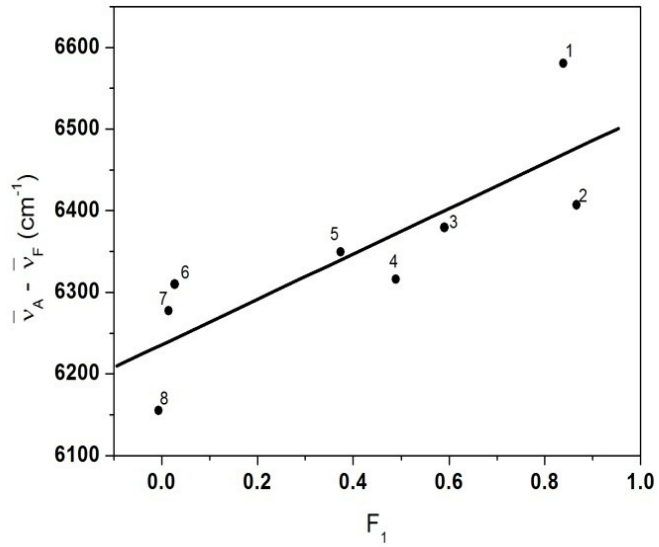

Figure 3.11 Plot for Stokes shift versus solvent polarity function F_1 for QS^{2+} in (1) Dimethylformamide, (2) Acetonitrile, (3) Dichloromethane, (4) Ethylacetate, (5) Diethylether, (6) o-xylene, (7) Carbontetrachloride, (8) Cyclohexane

The linear behaviour of Stokes shift versus solvent polarity function indicates general solvent effects as a function of dielectric constant and refractive index. Related software was used for the data fitted to a straight line. By using Bakhshiev's formula[37] (Equation 3.1) and Bilot-Kawski[38,39] formula (Equation 3.2), Slope values found from Figures 3.11, and 3.12, are given in Table 3.4. Using software Gaussian 03 we calculated ground state dipole moment for probe QS^{2+} using level of theory B3LYP. The ground-state dipole moment thus obtained was 3.2 D. From equation (3.3) we have evaluated the value of μ_e using the above value of μ_g without a need to know the Onsager radius,[12,32,33] of the QS^{2+}. The value of μ_e obtained is very different compared to the ground state dipole moment, the value of μ_e thus obtained is 11.84 D. All the data related to dipole moment are summarized in Table 3.4. Clearly the dipole moment in excited state is significantly larger than the dipole moment in the ground state of the probe molecule QS^{2+}. The dipole moments of a molecule in the ground and excited states are different due to changes in electron densities in these states. The excited state dipole moment value is higher than ground state indicating more polar excited state as compared to ground state. The invariance of absorption spectra with the solvent polarity and continuous variation of emission spectra suggests that the excited state is more sensitive to solvent polarity than the ground state and the change in fluorescence peak position with solvent polarity is responsible for the observed Stokes shift in QS^{2+}.

Table 3.3 Different solvent parameters and spectral data of QS^{2+} in different solvents

Solvent	ε	n	F_1	F_2	$\bar{\nu}_a - \bar{\nu}_f$ (cm^{-1})	$\frac{\bar{\nu}_a + \bar{\nu}_f}{2}$ (cm^{-1})
Dimethylformamide	38	1.43	0.8387	0.7114	6580.3	25611.6
Acetonitrile	37	1.33	0.8662	0.6568	6406.9	25615.0
Dichloromethane	8.9	1.42	0.5903	0.5830	6379.2	25601.6
Ehylacetate	6.0	1.37	0.4891	0.4979	6316.1	25660.4
Diethylether	4.3	1.35	0.3738	0.4269	6349.4	25677.0
o –Xylene	2.4	1.51	0.0277	0.3547	6309.8	25830.6
Carbontetrachloride	2.2	1.46	0.0144	0.3193	6277.3	25763.1
Cyclohexane	2.0	1.42	-0.0065	0.2845	6155.2	25774.0

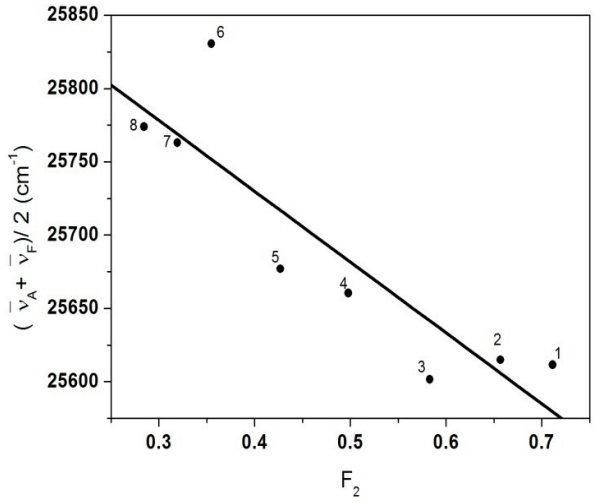

Figure 3.12 Plot for arithmetic average of absorption and fluorescence wavenumbers versus solvent polarity function F_2 for QS^{2+} in (1) Dimethylformamide, (2) Acetonitrile, (3) Dichloromethane, (4) Ethylacetate, (5) Diethylether, (6) o-xylene, (7) Carbontetrachloride, (8) Cyclohexane

Table 3.4 Dipole moment data of QS^{2+} in ground and excited states

Theory Level	$S_1(cm^{-1})$	$S_2(cm^{-1})$	μ_g (D)	μ_e (D)	$\Delta\mu$ (D)	μ_e / μ_g
B3LYP /6-31g(d)	278.09	483.04	3.2	11.84	8.64	3.7

Equations (3.1) and (3.2) are valid for $\tau_r << \tau_f$ [40], where, τ_r is the solvent relaxation time and τ_f is the fluorescence lifetime of the molecule. For most of the solvent molecules, the τ_r value ranges from 10^{-12} s to 10^{-10} s at room temperature. The measured lifetime of QS^{2+} in water at room temperature is ~20 ns and the solvent relaxation time is ~10 ns [34], which is of the order of fluorescence lifetime. So we believe that the dipole moment values, particularly excited state dipole moment can get affected in polar protic solvents due to the slower solvent relaxation resulting in un-relaxed excited state from where the fluorescence process takes place. The short range specific solute–solvent interactions such as hydrogen bonding, the tendency of polar solvent molecules to form aggregates of two or more molecules are not taken into account in the Bilot-Kawski theories. So it is important to select appropriate solvents which should possess moderate electric permittivity and fast excited state solvent relaxation process. As only aprotic and nonpolar solvents lead the correct value of dipole moment in order to eliminate the effect of specific solute-solvent interactions, so we have calculated the dipole moment using only aprotic polar and nonpolar solvents.

Moreover, in these aprotic solvents, the solvent relaxation process is faster than that in protic solvents.[41]

In QS^+, the reported values of ground and excited state dipole moments are, 4.47 D and 12.52 D, respectively.[42] So compared to QS^+, the dipole moments of QS^{2+} are slightly different, both, the ground and excited state dipole moments observed here in QS^{2+} are little less than that in QS^+. Such a small difference in dipole moment could be simply due to the protonation of QS^+ resulting in redistribution of charges both in ground and excited states of QS^{2+}.

3.4.2 Conclusions

The ground state dipole moment value, μ_g calculated for QS^{2+} from quantum chemical calculations is 3.2 D and the estimated excited state dipole moment from the solvatochromic shift method is 11.84 D. This large increase in dipole moment in the excited state of QS^{2+} is due to the more polar excited state than the ground state. The present study permits one to estimate the value of μ_e from the pre knowledge of μ_g, without the need of knowing the Onsager radius of the molecule, which is often chosen rather arbitrarily and impairs the popularity of solvatochromic method. The large variation of the dipole moment value between the ground state and excited state suggests that the fluorescence originates from highly polar excited state. In the excited state it is likely that the charge separation increases, resulting in a large dipole moment than in the ground state.

3.5 Estimation of ground and excited state dipole moments of Quinidine monocation and Quinidine dication: Experimental and numerical methods

Absorption and fluorescence spectra of Quinidine monocation (QD^+) and Quinidine dication (QD^{2+}) have been measured at room temperature in solvents of different polarities. Ground and excited state electric dipole moments are determined experimentally using solvatochromic shift method based on bulk solvent properties. Numerical calculations are also performed using B3LYP/6-31G(D) level of theory for ground state and CIS/6-31G(D) level of theory for first excited singlet state. From both experimental and numerical studies it has been observed that dipole moment values of excited states (μ_e) are higher than corresponding ground state value (μ_g), of QD^+ and QD^{2+}, which is attributed to the higher polarity of excited states of QD^+ and QD^{2+} molecules.

3.5.1 Results and Discussion

3.5.1.1 Numerical calculations

Density functional theory (DFT)[43,44] is emerging out rapidly as a computationally cost-effective general procedure for studying physical properties of molecules. Several research groups are actively involved in systematic comparisons of DFT theories with experiment and also with Hartree Fock (HF) and Møller-Plesset perturbation (MP2) treatments.[45] In our study, geometry optimizations were performed at B3LYP/6-31G(D)[46-48] level of theory for ground states of QD^+ and QD^{2+} and dipole moment values (μ_g) were determined. Frequencies are simultaneously checked while optimizing the geometry (until there is no imaginary frequency in the optimized geometry indicating true energy minima). The basis set employed here is 6-31G (D) which is widely used in studies of moderately large organic molecules. (This basis set has polarization functions on nonhydrogen atoms.) First excited singlet state dipole moment (μ_e) of QD^+ and QD^{2+} were computed by single point calculations (preceded by geometry optimization at ground state at B3LYP/6-31G(D) level at CIS/6-31G(D))[49] level of theory. The Self Consistent Field (SCF) density is used for ground state whereas Configuration Interaction (CI) One-particle and CI density are used for excited state calculations. All calculations were carried out in gas phase using Gaussian 03 suite of program. The optimized structures are given in Fig 3.13.

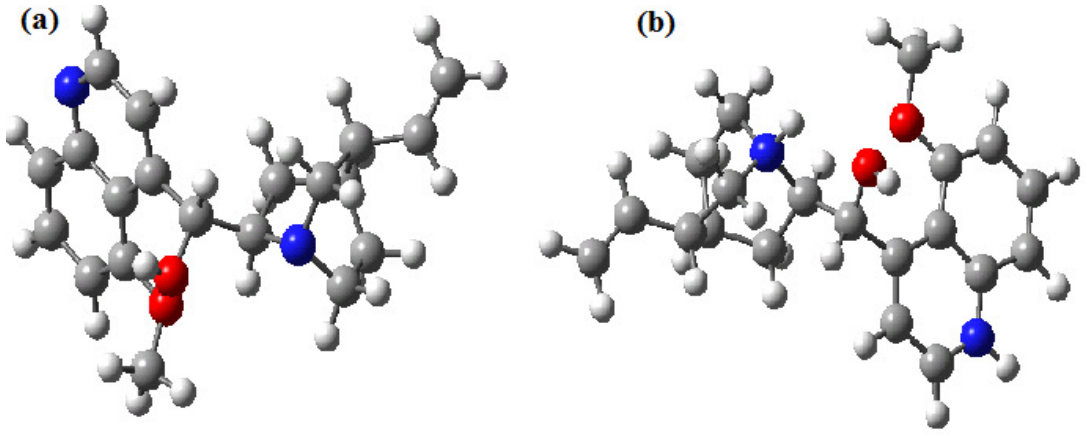

Figure 3.13 Optimised Geometry at B3LYP/6-31G(D) level of (A) Quinidine monocation (QD^+) (B) Quinidine dication (QD^{2+}) in Gas Phase

3.5.1.2 Steady state measurements

The structural formula of QD^+ and QD^{2+} is shown in Figure 3.14. In dilute sulphuric acid solutions (1 N H_2SO_4), Quinidine (QD) is present as a dicationic species, which is quite stable.[36] The nitrogens are adequately bound as the ammonium salt by strong acid of the medium effectively preventing n, π* and n, σ* transitions from occurring. The quinoline ring is a main fluorophore responsible for the absorption; methoxy group is very sensitive to the surrounding environment and responsible for anomalous photophysical behavior of QD^+ and QD^{2+}.[29,34-36] The steady state absorption and fluorescence measurements were made in different solvents of different polarities at room temperature. The absorption spectrum in Cyclohexane and fluorescence spectrum in two different representative solvents Dichloromethane (aprotic polar) and Cyclohexane (nonpolar) are shown in Figure 3.15(A) for QD^+ and Figure 3.15(B) for QD^{2+}.

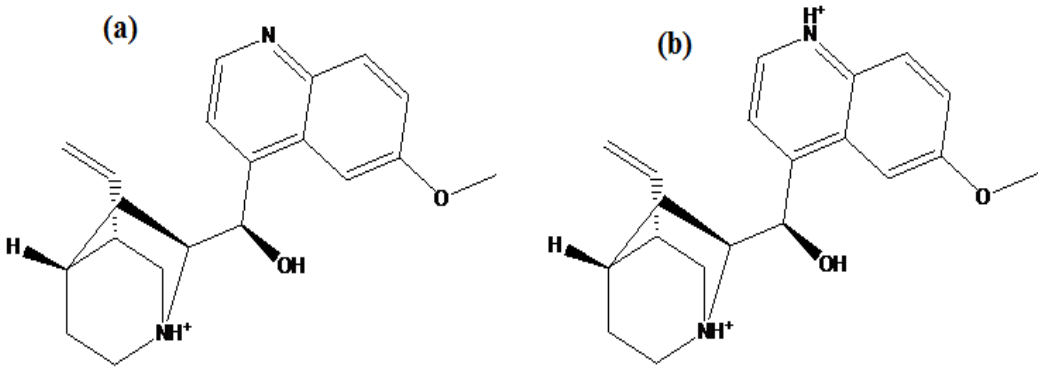

Figure 3.14 Molecular structure of A) Quinidine monocation (QD^+) and B) Quinidine dication (QD^{2+})

Absorption maximum of Quinidine monocation (QD^+) in different solvents was obtained around 334 nm with ±1 nm experimental error and of Quinidine dication (QD^{2+}) absorption peak for all solvents was obtained at 346±1 nm experimental error and emission maximum shifts towards lower frequencies with increase in polarity of the solvent as shown in Figure 3.15(A) and (B) respectively for QD^+ and QD^{2+}. The emission spectrum has only a structure-less broad band in all the solvents studied.

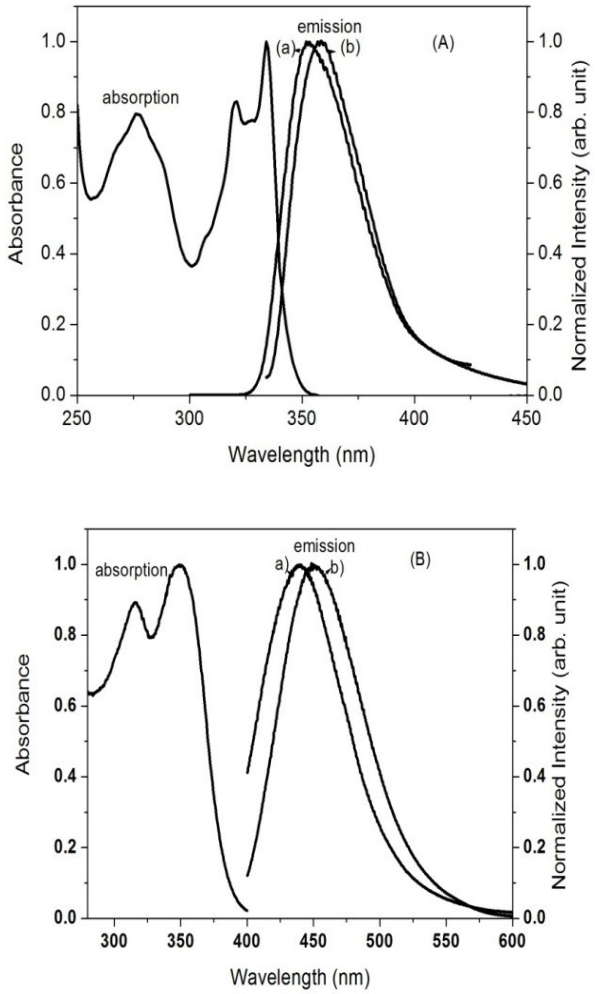

Figure 3.15 Normalized absorption spectrum (in Cyclohexane) and fluorescence spectra in (a) Cyclohexane (b) Dichloromethane. (A) for QD^{+} (B) QD^{2+} respectively

Table 3.5 Different solvent parameters and spectral data of QD^{+} in different solvents

Solvent	ε	n	F_1	F_2	$\bar{\nu}_a - \bar{\nu}_f$ (cm^{-1})	$\frac{\bar{\nu}_a + \bar{\nu}_f}{2}$ (cm^{-1})
Dimethylformamide	38	1.43	0.8387	0.7114	1960.0	28960.0
Dichloromethane	8.9	1.42	0.5903	0.5830	2143.8	28958.1
Ehylacetate	6.0	1.37	0.4891	0.4979	1771.0	29054.5
Chloroform	4.8	1.45	0.5903	0.4872	2115.8	28882.1
Diethylether	4.3	1.35	0.3738	0.4269	1861.0	29099.5
o –Xylene	2.4	1.50	0.0277	0.3547	1850.0	29015.0
Carbontetrachloride	2.2	1.46	0.0144	0.3193	1906.8	28808.6
Cyclohexane	2.0	1.42	-0.0065	0.2845	1530.9	29174.0

The absorption maxima for different solvents studied remains almost constant with polarity function, whereas the emission maximum shifts toward lower frequencies with the increase in solvent polarity. The fluorescence spectrum is more red shifted in the case of polar aprotic solvents as compared to non-polar solvents. This trend in the fluorescence spectra is a bathochromic shift with increase in polarity[31] and is an indication of π, π* transition. The constant absorption spectrum with solvent polarity implies that the ground state energy distribution is not affected possibly due to lesser polar nature of the molecule in the ground state. On the other hand, a large red shift of the emission maximum with the solvent polarity indicates greater stabilization of excited state in polar solvents.

Solvent polarity functions F_1 (ε, n) and F_2 (ε, n) have been calculated in order to ascertain the ground and excited state dipole moments of the molecule and are given in Tables 3.5 and 3.6. The spectral shifts $\bar{\nu}_a - \bar{\nu}_f$ versus the solvent polarity function $F_1(\varepsilon, n)$ and $\frac{\bar{\nu}_a + \bar{\nu}_f}{2}$ versus F_2 (ε, n) are shown in Figures 3.16 and 3.17, respectively for QD^+ and QD^{2+}. The linear behaviour of Stokes shift versus solvent polarity function indicates general solvent effects as a function of dielectric constant and refractive index. Related software was used for the data fitted to a straight line. By using Equations (3.1 and 3.2),[37-40] slope values found from Figures 3.16 and 3.17(A) and (B) are given in Table 3.7.

Table 3.6 Different solvent parameters and spectral data of QD^{2+} in different solvents

Solvent	ε	n	F_1	F_2	$\bar{\nu}_a - \bar{\nu}_f$ (cm^{-1})	$\frac{\bar{\nu}_a + \bar{\nu}_f}{2}$ (cm^{-1})
DMF	38	1.43	0.8387	0.7114	6596.2	25520.3
Dichloromethane	8.9	1.42	0.5903	0.5830	6630.0	25586.7
Ehylacetate	6.0	1.37	0.4891	0.4979	6396.9	25619.9
Chloroform	4.8	1.44	0.5903	0.4872	6645.5	25495.7
Diethylether	4.3	1.35	0.3738	0.4269	6500.3	25651.6
Carbontetrachloride	2.2	1.46	0.0144	0.3193	6277.3	25763.1
Cyclohexane	2.0	1.42	-0.0065	0.2845	6111.8	25762.6

$$\mu_g = \frac{S_2 - S_1}{2}\left[\frac{hca_0^{\,3}}{2S_1}\right]^{1/2} \tag{3.4}$$

$$\mu_e = \frac{S_1 + S_2}{2}\left[\frac{hca_0^{\,3}}{2S_1}\right]^{1/2} \tag{3.5}$$

$$a_0 = \left(\frac{3M}{4\pi\delta N}\right)^{1/3} \tag{3.6}$$

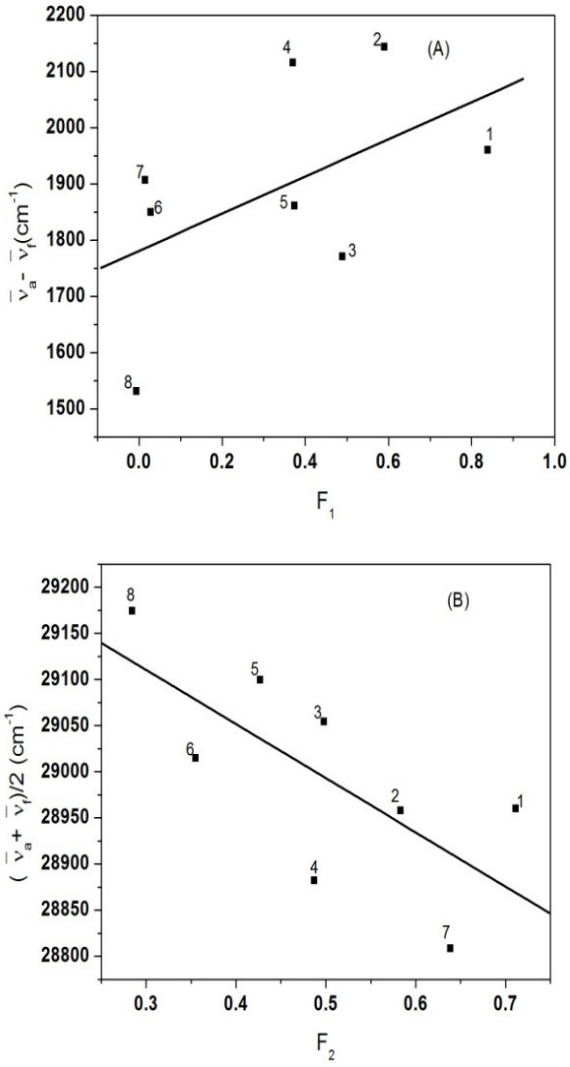

Figure 3.16 (A) Plot for Stokes shift versus solvent polarity function F_1 for QD^+ in (1) Dimethylformamide, (2) Dichloromethane, (3) Ethylacetate, (4) Chloroform, (5) Diethylether, (6) o-xylene, (7) Carbontetrachloride, and (8) Cyclohexane. (B) Plot for arithmetic average of absorption and fluorescence wavenumbers versus solvent polarity function F_2 for QD^+ in (1) Dimethylformamide, (2) Dichloromethane, (3) Ethylacetate, (4) Chloroform, (5) Diethylether, (6) o-xylene, (7) Carbontetrachloride, and (8) Cyclohexane

Further by using Equations (3.4 and 3.5), we have calculated ground and excited-states dipole moment experimentally. Using ACD/ChemSketch software the density of the molecule was found to be 1.21±0.1 g/cm^3. Thus using Eq. (3.6),[50] value of solute cavity radius (a_0) was obtained 4.74 Å.

The value of μ_e obtained is different compared to the ground state dipole moment. All the data related to experimental dipole moments are summarized in Table 3.7. Clearly the dipole moment in excited state is significantly larger than the dipole moment in the ground state of the probe molecules QD^+ and QD^{2+}. The dipole moments of a molecule in the ground and excited states are different due to changes in electron densities in these states. The excited state dipole moment value is higher than ground state indicating more polar excited state as compared to ground state. The invariance of absorption spectra with the solvent polarity and continuous variation of emission spectra suggests that the excited state is more sensitive to solvent polarity than the ground state and the change in fluorescence peak position with solvent polarity is responsible for the observed Stokes shift in QD^+ and QD^{2+}. Theoretical calculations for QD^+ and QD^{2+} also revealed that the excited state dipole moment value is higher than ground state (Table 3.8) due to high polarity of excited state. Molecular dipole moment is an experimental measure of the charge distribution in a molecule. It is difficult to evaluate accurately the global electron distribution in a molecule because it involves all the multipoles. The calculated values of dipole moment based on densities computed by different methods (SCF, CI-one-particle and CI) are usually higher than the values of experimental dipole moments (as observed in earlier theoretical studies as well).[51]

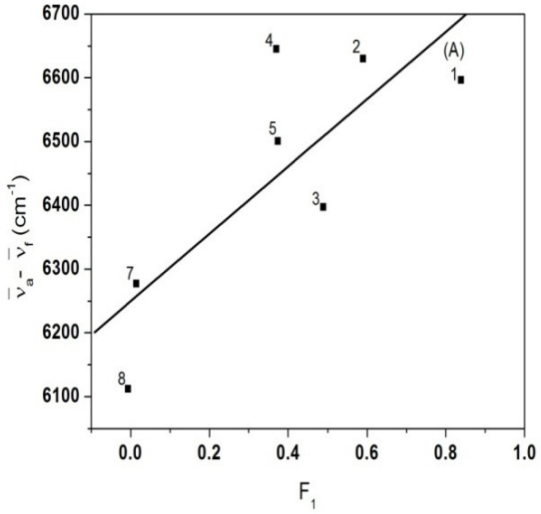

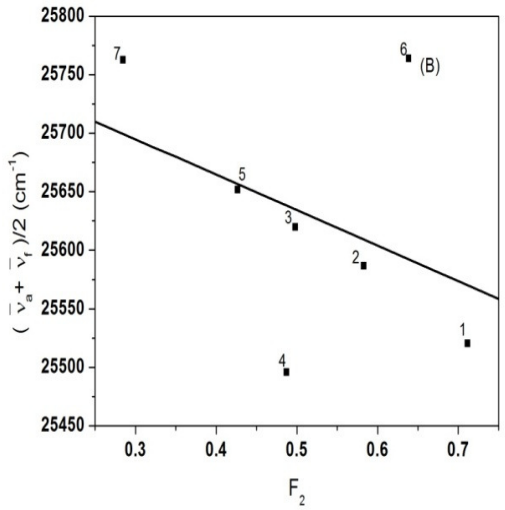

Figure 3.17 (A) Plot for Stokes shift versus solvent polarity function F_1 for QD^{2+} in (1) Dimethylformamide, (2) Dichloromethane, (3) Ethylacetate, (4) Chloroform, (5) Diethylether, (6) Carbontetrachloride, and (7) Cyclohexane. (B) Plot for arithmetic average of absorption and fluorescence wavenumbers versus solvent polarity function F_2 for QD^{2+} in (1) Dimethylformamide, (2) Dichloromethane, (3) Ethylacetate, (4) Chloroform, (5) Diethylether, (6) Carbontetrachloride, and (7) Cyclohexane

Table 3.7 Dipole moment data of QD^+ and QD^{2+} in ground and excited states by experimental method

Molecule	a_0 Å	$S_1(cm^{-1})$	$S_2(cm^{-1})$	μ_g(D)	μ_e(D)	$\Delta\mu$(D)	μ_e / μ_g
QD^+	4.74	330.83	586.04	0.7	2.46	1.76	3.5
QD^{2+}	4.74	528.88	303.00	0.5	1.76	1.26	3.5

One of the limitations of quantum chemical calculations is attributed to the overestimation of uneven electronic distribution in a molecule and thus make it more polar compared to that of the real system. To compute theoretical dipole moments within 0.03 D of the experimental values requires the addition of extensive configuration interaction with a near-HF quality basis.[44] Moreover, all calculations in the present theoretical study were done in gas phase which could not take care of the solute-solvent interactions. A polar solvent polarizes a solute more significantly than a nonpolar solvent and hence it results in a larger charge separation which in turn leads to a higher dipole moment.[45] Even for the simple water molecule, the dipole moment of the gas phase water monomer is 1.85 D. When solvated in bulk water, the dipole moment of an individual water molecule is observed to be enhanced to the much larger value of 2.9 ± 0.6 D.[46]

In the literature there are several examples of variation of dipole moments from the experimental results depending on the quantum chemical method used. In an extensive study,[52] it is found that the DFT, Restricted Hartree Fock (RHF) and MP2 predicted formamide dipole moments are essentially stable using the basis set 6-31G(D). It should be stressed that the RHF values are better than the MP2 ones but worse than the corresponding DFT results. It is observed that dipole moment value in 6-31G basis set is maximum for several systems.[53] Therefore it is concluded that "maximum polarity is observed in this basis set." In another study,[54] the equilibrium dipole moments have been calculated at the HF, MP2, Coupled Cluster Single Double (CCSD) and CCSD(T) levels. All electrons are correlated in the aug-cc-pVxZ basis sets with x = D, T, Q. Augmented basis sets have been used to ensure a flexible description of the outer-valence region.

Table 3.8 Dipole moment data of QD^+ and QD^{2+} in ground and excited states by Theoretical method

Molecule	μ_g (D)[a]	μ_e(D)[b]	μ_e(D)[c]	$\Delta\mu$ (D)[d]	$\Delta\mu$ (D)[e]
QD^+	3.58	5.02	4.58	1.44	1.00
QD^{2+}	5.55	8.41	7.33	2.86	1.78

[a] Ground State Dipole Moment at B3LYP/6-31G(D) (**SCF**) level of theory; density used for ground state is mentioned in bold in parentheses.

[b] First Singlet Excited State Dipole Moment; geometries optimized at B3lyp/6-31G(D) followed by single point calculations at CIS/6-31G(D) (**CI-one-particle**) level of theory, density used for excited state is mentioned in bold in parentheses.

[c] First Singlet Excited State Dipole Moment; geometries optimized at B3LYP/6-31 G(D) followed by single point calculations at CIS/6-31G(D) (**CI**) level of theory, density used for excited state is mentioned in bold in parentheses.

[d] $\Delta\mu$ (D) calculated using[b].

[e] $\Delta\mu$ (D) calculated using[c].

The excellent performance of the CCSD(T) among all methods relies on the fact that the chosen molecules are all dominated by a single configuration. When several configurations are important, the performance of the CCSD(T) model degrades. Thus it is worth mentioning here that the best method to evaluate dipole moment is yet to be explored.

3.5.2 Conclusions

We have estimated and compared dipole moments of the molecules QD^+ and QD^{2+} in the electronic ground and excited states by experimental and numerical methods. We found that both the molecules possess higher dipole moment value in excited state than in the ground state. A comparison of the values indicates that there is no clear-cut preference for any of the methods as far as numerical values are concerned. Theoretically obtained values of excited state dipole moment are also higher than the values of ground state dipole moment of QD^+ and QD^{2+}. This observation correlated well with the experimental study. Numerically higher theoretical values may be resulting from constrained use of basis set and quantum chemical methods due to limited computational facility. Solvation effect should also be incorporated to attain higher level of accuracy. A systematic theoretical study may be performed in future to investigate the proper reason behind the numerical differences between experimental and theoretical data, though both of them vouched for high polarity of excited state (resulting in higher values of dipole moment for excited state compared to that of ground state).

References:

(1) D. S. Chemla, J. Zyss, *Non-linear Optical Properties of Organic Molecules and Crystals*, Academic Press, New York, 1987.

(2) S. Kumar, V. C. Rao, R. C. Rastogi, *Spectrochim. Acta Part A* **2001**, *57*, 41.

(3) A. Kawski, J. F. Rabek (Eds.), *Progress in Photochemistry and Photophysics*, vol. 5, CRC Press, Boca Raton, 1992, pp. 1–47.

(4) W. Liptay, E. C. Lim (Eds.), *Excited States*, vol. 1, Academic Press, New York, 1974.

(5) J. Czekella, *Z. Elektrochem*. **1960**, *64*, 1221.

(6) J. Czekella, *Chimica* **1961**, *15*, 26.

(7) U. S. Raikar, C. G. Renuka, Y. F. Nadaf, B. G. Mulimani, A. M. Karguppikar, M. K. Soudagar, *Spectrochim. Acta Part A* **2006**, *65*, 673.

(8) R. Giri, M. M. Bajaj, *Current Science* **1992**, *62*, 522.

(9) C. Parkanyi, S. R. Oruganti, A. O. Abdelhamid, L. V. Szentpaly, B. Ngom, J. J. Aaron, *J. Mol. Struct.* **1986**, *135*, 105.

(10) N. Sharma, K. Sapan, R.C. Rastogi, *Spectrochim. Acta Part A* **2007**, *66*,171.

(11) J. J. Aaron, M. D. Gaye, C. Parkanyi, N. S. Cho, L. Von Szentpaly, *J. Mol. Struct.* **1987**, *156*, 119.

(12) C. Parkanyi, C. Boniface, J. J. Aaron, M. b. MacNair, M. Dakkouri, *Coll. Czech. Chem. Comm.* **2002**, *67*, 1109.

(13) S. R. Inamdar, Y. F. Nadaf, B. G. Mulimani, *J. Mol. Struct.* **2004**, *678*, 177.

(14) Y. F. Nadaf, B. G. Mulimani, M. Gopal, S. R. Inamdur, *J. Mol. Struct.* **1987**, *156*,119.

(15) J. J. Aaron, A. Times, M. D. Gaye, C. Parkanyi, C. Boniface, T. W. N. Bieze, *Spectrochim. Acta Part A* **1991**, *47*, 419.

(16) A. Rabahi, M. Makhloufi-Chebli, S. M. Hamdi, A. M.S. Silva, D. Kheffache , B. Boutemeur-Kheddis, M. Hamdi, *J. Mol. Liq.* **2014**, *195*, 240.

(17) I. Sıdır, Y. G. Sıdır, F. Demiray, H. Berber, *J. Mol. Liq.* **2014**, *197*, 386.

(18) M. S. Zakerhamidi, S. G. Sorkhabi , A. N. Shamkhali, *Spectrochim. Acta Part A* **2014**, *127*, 340.

(19) S. K. Patil, M. N. Wari, C. Y. Panicker, S. R. Inamdar, *Spectrochim. Acta Part A* **2014**, *123*, 117.

(20) H. S. Lalithamba , S. R. Manohara , B. Siddlingeshwar , Shivakumaraiah, *J. Mol. Liq.* **2014**, *198*, 94.

(21) I. Sıdır, Y. G. Sıdır, *Spectrochim. Acta Part A* **2015**, *135*, 560.

(22) W. H. Melhuish, *J. Phys. Chem*. **1960**, *62*, 762.

(23) D. W. Moss, *Clin. Chim. Acta* **1960**, *5*, 283.

(24) S. G. Schulman, R. M. Threatte, A. C. Capomacchia, W. L. Poul, *J. Pharm. Sci.* **1974**, *63*, 876.

(25) A. Gafni, R. P. Detoma, R. E. Manrow, L. Barnad, *Biophys. J.* **1977**, *17*, 155.

(26) V. I. Stenberg, E. F. Travecedo, *J. Org. Chem.* **1970**, *35*, 4131.

(27) C. J. Rocha, M. H. Gehlen, R. D. Silva, P. M. Donate*, J. Photochem. Photobiol. A: Chem.* **1999**, *123*, 129.

(28) G. D. Geddes, *Meas. Sc. and Tech.* **2001**, *12*, 53.

(29) D. Pant, H. B. Tripathi, D. D. Pant, *J. Lumin.* **1992**, *51*, 223.

(30) N. W. Wu, J. H. Perng, *J. Chin. Chem. Soc.* **2005**, *52*, 915.

(31) N. Tewari, N. K. Joshi, R. Rautela, R. Gahlaut, H.C. Joshi, S. Pant, *J. Mol. Liq.* **2011**, *160*,150.

(32) S. R. Inamdar, Y. F. Nadaf, B. G. Mulimani, *J. Mol. Struct*. **2003**, *624*, 47.

(33) J. Thipperudrappa, D. S. Biradar, S. R. Manohara, S. M. Hanagodimath, S. R. Inamadar, R.J. Manekutla, *Spectrochim. Acta Part A* **2008**, *69*,991.

(34) D. Pant, U. C. Tripathi, G. C. Joshi, H. B. Tripathi, D. D. Pant, *J. Photochem. Photobiol. A: Chem.* **1990**, *51*, 313.

(35) D. Pant, H. B. Tripathi, D. D. Pant, *J. Photochem. Photobiol. A: Chem.* **1991**, *56*, 207.

(36) D. Pant, H.B. Tripathi, D.D. Pant, *J. Lumin*. **1991**, *50*, 249.

(37) N. G. Bakhshiev, *Opti. Spektrosk.* **1964**, *16*, 821.

(38) L. Bilot, A. Kawski, *Z. Naturforsch*. **1962**, *17a*, 621.

(39) L. Bilot, A. Kawski, *Z. Naturforsch.* **1963**, *18a*, 256.

(40) A. Kawski, B. Kuklinski, P. Bojarski, *Chem. Phys.* **2009**, *359*, 58.

(41) G. A. Kenney-Wallace, G. E. Hall, L. A. Hunt, K. Sarantidis, *J. Phys. Chem.* **1980**, *84*, 1145.

(42) S. Joshi, D. D. Pant, *J. Mol. Liq.* **2012**, *166*, 49.

(43) P. Hohenberg, W. Kohn, *Phys. Rev. B* **1964**, *136*, 864.

(44) R. G. Parr, W. Yang, *Density-Functional Theory of Atoms and Molecules, Oxford University Press*, New York, 1989.

(45) J. Baldenebro-López, J. Castorena-González, N. Flores-Holguín, J. Almaral-Sánchez, D.Glossman-Mitnik, *Inter. J. Mol. Sci.* **2012**, *13*, 4418.

(46) A. D. Becke, *J. Chem. Phys.* **1993**, *98*, 5648.

(47) A. D. Becke, *Phys. Rev. A* **1988**, *38*, 3098.

(48) C. Lee, W. Yang, R. G. Parr, *Phys. Rev. B* **1988**, *37*,785.

(49) J. B. Foresman, M. Head-Gordon, J. A. Pople, M.J. Frisch, *J. Phys. Chem.* **1992**, *96*, 135.

(50) P. Suppan, *Chem. Phys. Lett.* **1983**, *94*, 272.

(51) B. Siddlingeshwar, S.M. Hanagodimath, E.M. Kirilova, G.K. Kirilov, *J. Quan. Spect. and Rad. Trans.* **2011**, *112*, 448.

(52) T. Kupkaa, I. P. Gerothanassis, I. N. Demetropoulos, *J. Mol. Struct.* **2000**, *531*, 143.

(53) M. Monajjemi, Z. Eslamifar, S. M. Shoaei, F. Mollaamin, *Afri. J. Micro-biol. Res.* **2012**, *6*, 2338

(54) K. L. Bak, J. Gauss, T. Helgaker, P. Jørgensen, J. Olsen, *Chem. Phys. Lett.* **2000**, *319*, 563.

Chapter 4

Steady state and time-resolved fluorescence spectroscopy of Quinine Sulfate dication in ionic and neutral micelles: Effect of micellar charge on photophysics

4.1 Introduction

The sensitivity and versatility of fluorescence has made it an exceptionally effective tool for a wide range of studies. Fluorescence spectroscopies are especially effective for studies of photophysical and photochemical processes. As we introduce these fluorophores into confined environments, understanding the effect of confinement on their basic photophysics becomes critical. Normal or reverse micelles are a topic of recent investigations due to their unusual physicochemical properties and immense technological applications.[1-4]The nano-micro and macro structural organization of micelles have profound effect on the spectral properties of the molecules. By comparison of spectral properties in micelles with similar data in homogeneous solvents, one learns about the molecular details of micellar structure and effect of confinement on the photophysical process in molecules.[5-11]

Fluorescence spectroscopy is a sensitive technique where one can utilize the environment sensitivity of a molecular probe situated in the micelle. The environment sensitivity can be quantified by the Stokes shift, measured from the difference in emission and absorption maxima, emission wavelength dependence of excitation spectrum and excitation wavelength dependence of the fluorescence spectrum. So it is interesting to study the photophysical properties of environment sensitive molecular probes in molecularly organized assemblies.

The notable progression of supramolecular photophysics and photochemistry over the past decade has resulted, in part, from the advancement in understanding of the host-guest interactions.[12-14] The nature and the structure of the host-guest complexes are of fundamental concern in molecular recognition and are of increasing significance in the applications of supramolecular systems. The nature of the binding forces, the geometry of the intermolecular complexes, and the intermolecular dynamics are the central issues for their applications in synthetic,[15] analytical,[16] and pharmaceutical chemistry.[17]

Complex molecular systems are important in Chemistry, Physics and Biology and therefore a study of their structure, dynamics and function is interesting and necessary. Supramolecular assemblies and ordered molecular aggregates are complex systems formed by the principle of self-assembly involving non-covalent intermolecular forces. Molecular aggregates are clusters that are intermediate between simple molecules and solids. The size of these complex systems may vary from a few nanometers (e.g. folding polymers, micelles) to several micrometers and longer (e.g. thin films and wires, membranes). Study of such molecular assemblies is important because they are potential candidates for biomimetic and optoelectronic molecular devices.

QS is a classical example of a highly fluorescent molecule having anomalous photophysical properties. The photophysical properties of Quinine Sulfate dication (QS^{2+}) (Quinine Sulfate in1N H_2SO_4 solution of water) have been studied extensively in the past[18-40] and are found very sensitive to the surrounding solvent environments as has already seen in chapter three. The Edge Excitation Red Shift (EERS), observed in Quinine and related compounds is very sensitive to polarity, viscosity and the temperature of the surrounding environments.[34]

In this chapter we discusses the effect of nature of charge of surfactants on to the magnitude of EERS, fluorescence lifetimes and rotation time of QS^{2+} and compare these measurements with the previously reported[35-38] photophysics of QS^{2+} in different bulk environments. The molecular fluorescence from QS^{2+} is well suited to furnish information regarding surfactant based systems due to inherent remarkable environment sensitive nature of this molecule. This gives information about the local properties of microenvironments of micelles and interaction of QS^{2+} with differently charged interior of the cationic, anionic and neutral micelles. Photophysics of environment sensitive probe QS^{2+} is found to be significantly modulated in micellar media compared to the aqueous bulk phase. This study provides a detailed picture of dynamics and location of QS^{2+} in micelles by a variety of spectral parameters like fluorescence peak position as a function of excitation wavelength, excitation spectrum, fluorescence decay times, rate constants for radiative and nonradiative relaxation and temporal anisotropy decay of fluorescence.

4.2 Experimental

Quinine Sulfate (QS) was purchased from S.D. Fine Mumbai and used as received. All the solvents were either of spectroscopic grade or were checked for their purity. All the samples of Quinine Sulfate dication (QS^{2+}) were prepared by dissolving the appropriate concentration of QS in 1 N H_2SO_4 containing Milli Q water. The final concentration of QS^{2+} in all the systems studied was 10^{-4} M. The surfactant, Cetyltrimethyl ammonium bromide (CTAB) was purchased from Merck, Sodium dodecylsulfate (SDS) and Triton X-100 (TX-100) surfactants were purchased from SISCO. All surfactants were used as received. The concentrations of surfactants in the solutions prepared were well above the Critical Micellar Concentration (CMC). The CTAB (CMC = 1.0 mM), SDS (CMC = 8 mM), and TX-100 (CMC = 0.2 mM) concentrations in the solutions were 10^{-2} M, 10^{-1} M, and 10^{-2} M, respectively.

4.3 Results and discussions

4.3.1 Steady state absorption and fluorescence measurements

The molecular structure of QS^{2+} is shown in chapter 3 (Figure 3.7) and the structure of different surfactants are shown in Figure 4.1. In dilute sulphuric acid solutions (1 N H_2SO_4), Quinine Sulfate is present as a dicationic species, which is quite stable.[30] The nitrogens are adequately bound as the ammonium salt by strong acid of the medium effectively preventing *n*, π* and *n*, σ* transitions from occurring. The quinoline ring is a main fluorophore responsible for the absorption; methoxy group is very sensitive to the surrounding environment and responsible for anomalous photophysical behavior of QS^{2+}.[29-33]The vinyl group which absorbs around 180 nm, is not considered an active chromophoric group in the near UV–visible region. The absorption and the emission spectra of QS^{2+} are shown in Figure 4.2. The absorption spectrum shows two bands L_a and L_b at 348 and 318 nm, respectively, and is in agreement with the reported peak positions.[31-33] These two bands correspond to low-lying closely spaced π, π* states of the main chromophore. The emission spectrum has only a structure-less broad band with maxima around 447 nm on excitation at 355 nm.

4.3.2 Excitation spectrum measurements

Figure 4.2 shows the absorption and excitation spectra of QS^{2+} in bulk water and in different micellar systems. It is observed that the position of absorption bands does not change appreciably with the presence of surfactant in the bulk water solution of QS^{2+},whereas the corresponding molar absorption coefficient (ε) values of the solute molecule change slightly particularly in SDS surfactant system. In SDS, the absorbance is higher compared to the absorbance in bulk water, CTAB and TX-100 solutions. Excitation spectrum in different micellar systems are also shown in Figure 4.3 along with absorption in the same micelle in order to compare and contrast with the respective absorption spectrum in different micelles. It is observed that the excitation spectrum of QS^{2+} in all the micellar solutions studied fails to coincide with the red edge of the absorption band. There is a red shift in the excitation spectrum at the red edge for all the surfactant solutions studied compared to the absorption spectrum. The early literature on the studies of Quinine has also shown that the excitation spectrum of Quinine does not match the absorption spectrum.[21] The red shift in the excitation spectrum at the red edge indicates the distribution of QS^{2+} molecules in different surfactant solutions.

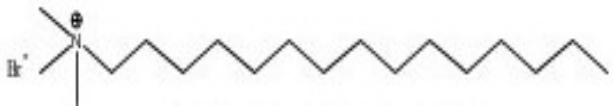

a) CTAB

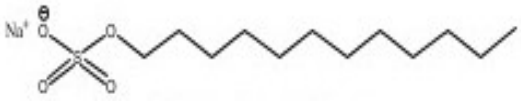

b) SDS

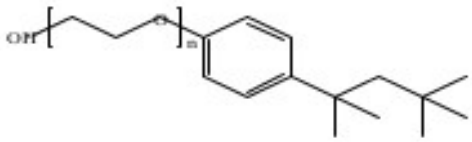

n= Approx. 9.5

c) TX-100

Figure 4.1 Structure of CTAB, SDS and TX-100 molecules

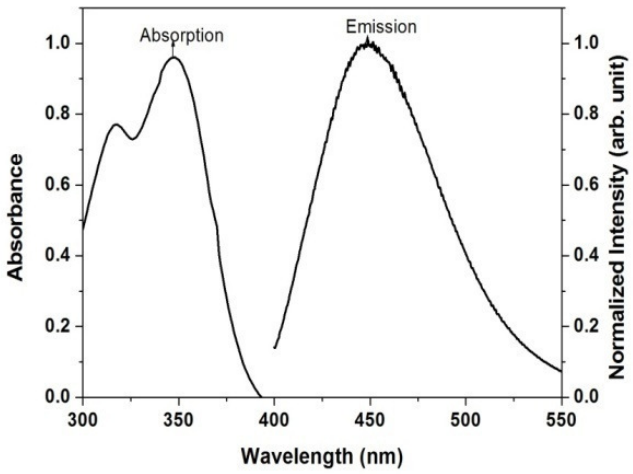

Figure 4.2 Absorption and emission spectrum of QS^{2+} in bulk water, excited by 355 nm

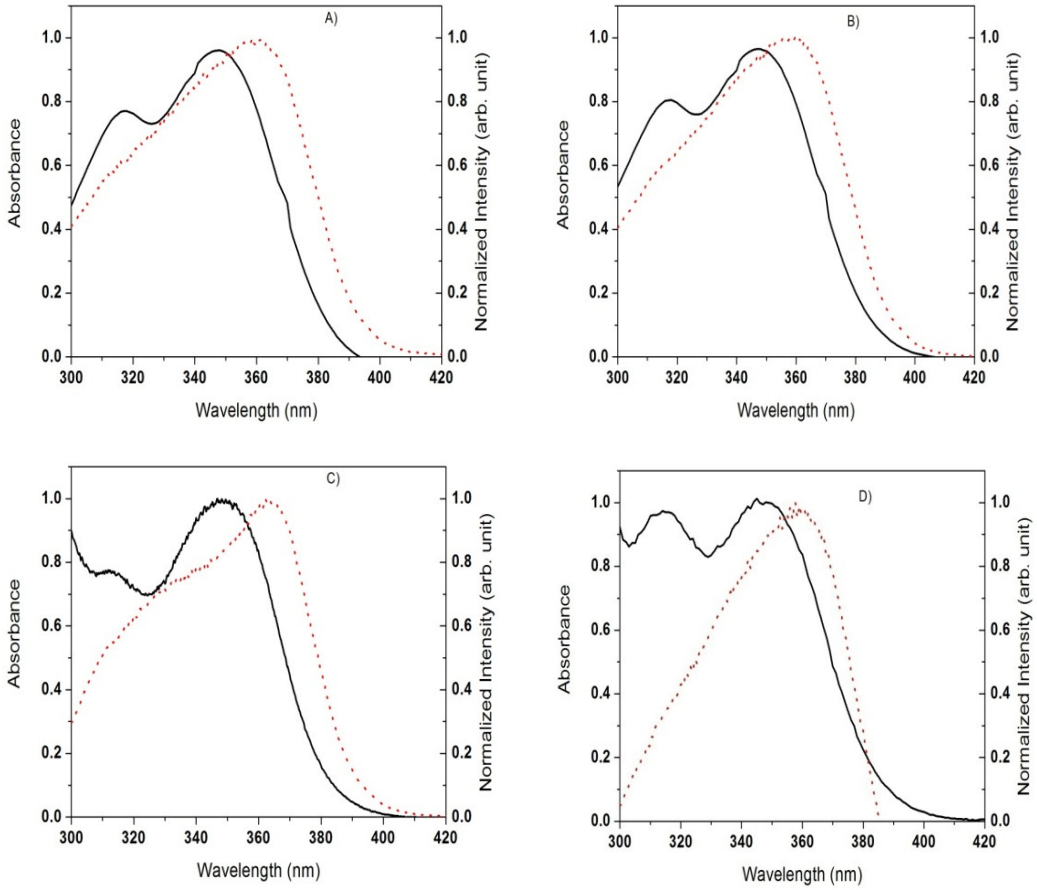

Figure 4.3 Absorption (solid line) and excitation (dotted line) spectra of QS^{2+} in bulk water and in different micellar systems, (A) bulk water (B) CTAB, (C) SDS and (D) TX-100. The excitation spectra were monitored by setting emission wavelength at 450 nm

4.3.3 Edge excitation red shift (EERS) measurements

On shorter wavelength excitation (SWE = 355 nm), the emission maxima does not change with the change in micellar system, whereas on red edge excitation (REE = 415 nm), there is about 5 nm blue shift in the emission maximum for the anionic SDS surfactant compared to the maxima in bulk water. For CTAB and TX-100 surfactants the shift is only of 2 nm. On SWE, the emission maximum is observed at 447 in bulk water solution of QS^{2+} and remains at the same position irrespective of the surfactant molecules present in the solutions studied. However, on REE, the emission spectrum shifts towards the higher frequencies particularly in SDS compared to water solution. The full width at half maximum (FWHM) of the emission spectrum is smaller on REE for each of the solutions studied if compared with the FWHM observed on SWE. The fluorescence spectrum of QS^{2+} in TX-100 solution is narrowest among the spectrums studied. All the steady state data are summarized in Table 4.1.

When excited at the red edge of the first absorption band the emission maximum of QS^{2+} shifts towards the lower frequency side for all the solutions studied (Figure 4.4). This shift in emission spectrum on excitation at the red edge of the first absorption spectrum is known as Edge Excitation Red Shift (EERS) as shown in the normalized emission spectra of QS^{2+} in bulk water (Figure 4.4(a)) and for different surfactant systems, CTAB, SDS and TX-100 in Figure 4.4(b)-(d), respectively. The magnitude of EERS is expressed as the difference in wavenumber (cm^{-1}) between the emission maximum obtained on 355 nm excitation and 415 nm excitation. The magnitude of EERS in bulk water solution is 679 cm^{-1} and is in agreement with the reported values.[29,30] The magnitude of EERS in SDS systems is smaller compared to that in CTAB, TX-100 and bulk water systems. The EERS values as obtained for QS^{2+} in bulk water and different surfactant systems are given in Table 4.1.

Table 4.1 Spectroscopic data for QS^{2+} in bulk water and in different surfactant systems

Medium	Absorption maxima (nm)		Emission maxima (nm)		FWHM (cm^{-1})	EERS (cm^{-1})	
	L_A	L_B	λ_{ex} = 355	λ_{ex}= 415	λ_{ex} = 355	λ_{ex} = 415	
Water	348	317	447	461	3644	3461	679
CTAB	348	318	445	458	3680	3610	638
SDS	347	315	447	455	3633	3502	374
TX-100	347	316	447	458	2970	2492	537

The EERS in QS^{2+} in different environments has been studied extensively in the past and different explanations have been provided by different researchers. Chen[22] found red shift in emission spectrum of QS^{2+} on excitation at red edge of absorption band and suggested that it arises due to two close lying states. Fletcher [23] interpreted this effect as being due to the molecules existing in atleast two different conformers each with its own electronic transition based on solvent relaxation modes. It is generally found that solvent bonding to chromophore restricts the position of auxochrome, which exists at least in two average conformers. Itoh and Azumi[25] gave an explanation that on excitation at the red edge of the absorption band only certain configurations are excited, resulting into red shifted emission which lacks some high frequency components compared to that due to short wavelength excitation. For QS^{2+} and related molecules in the polar fluid medium, we have reported[30-35] from the temperature dependence of fluorescence characteristics that around 160 K a rapid charge transfer from methoxy group to the quinoline ring takes place, whereas at ambient temperature the solvent relaxation process takes place. The observation of EERS in QS^{2+} has also been assigned to solvent relaxation process around the solute molecule. Solvent relaxation refers to the process by which a solvent reorganizes in response to changes in a solute or reacting system. For measurements of solvation dynamics one uses a solute probe molecule which undergoes a large change of dipole moment in the excited state. When such a probe molecule is in the ground state, the solvent dipoles remain randomly arranged around it and are in equilibrium with the solute. However, upon electronic excitation, a sudden change in the dipole moment of the molecule occurs, whereas the solvent dipole configuration remains the same as in the ground state. Immediately after excitation, solute-solvent are not in equilibrium and the energy of the system is high. Subsequent to excitation, the solvent dipoles start reorienting in order to accommodate the change in the excited state dipole moment of the solute and continue to reorient until equilibrium is restored. During this process, there is a continuous loss of energy in the excited state and the energy of the solute dipole decreases; consequently, the fluorescence maximum gradually shifts towards lower energy with time. This is known as time dependent fluorescence Stokes shift. Evidently, at the blue edge of the emission spectrum, the fluorescence originates from the un-solvated solute and decay is observed in the fluorescent transient. Whereas, at the red edge of the spectrum, the fluorescence is from the solvated solute and a rise in the fluorescent transient is observed. The reorganization energy results from the creation of a transient solute dipole (by an exciting photon) in a solvent atmosphere. This induces

a reorganization of the polar solvent molecules about the dipole in a manner that stabilizes the energy of the system. The energy term so involved may be called the reorganization energy.

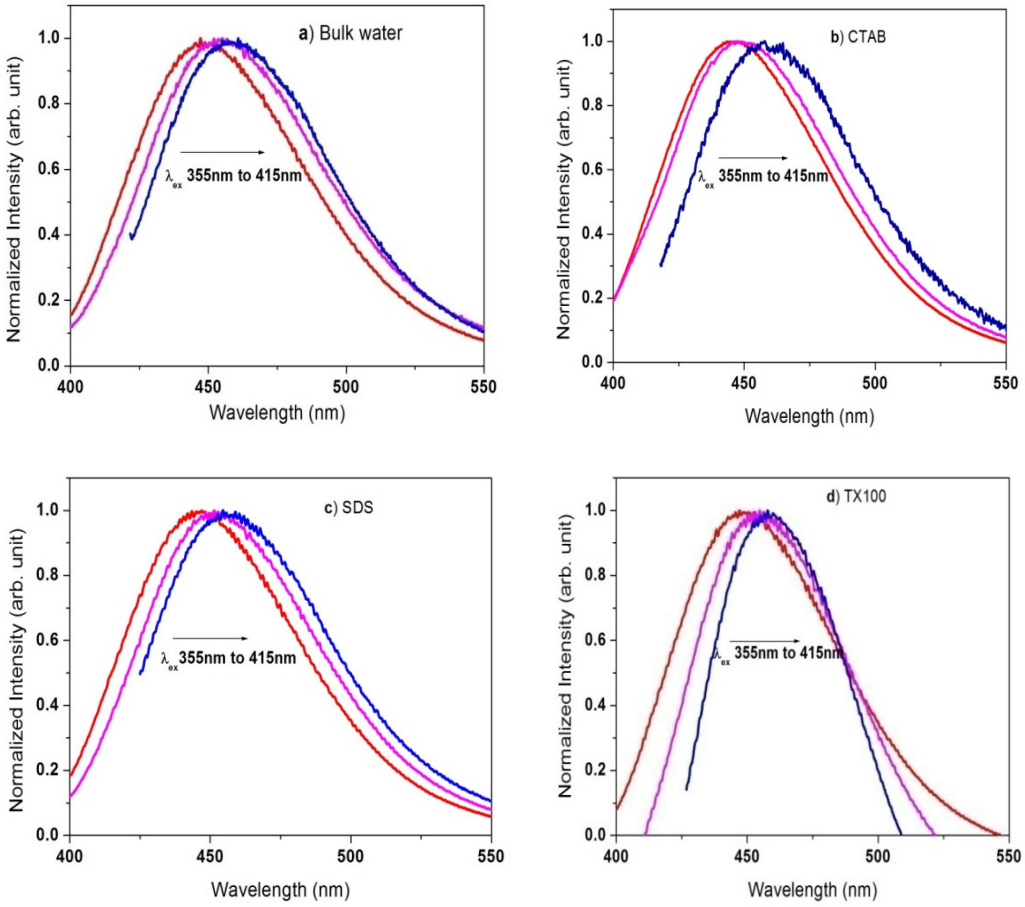

Figure 4.4 Excitation wavelength dependence of fluorescence spectra of QS^{2+} in bulk water and in different micellar systems, (a) bulk water (b) CTAB, (c) SDS and (d) TX-100

For QS^{2+} in surfactant systems, on SWE, the emission maximum is observed at the same location as in polar fluid medium. However, on REE, the spectral maximum is about 5 nm blue shifted for SDS surfactant compared to that with other surfactant solutions and bulk water solution studied. This results in a decrease in the magnitude of EERS for QS^{2+} in SDS surfactant. We attribute this observed decrease in the magnitude of EERS to the decrease in the rate of solvent relaxation in the presence of SDS surfactant in the solution. Water, being a highly polar hydrogen-bonding solvent, could bring about significant stabilization of the electronic state of the polar probe as opposed to the less polar environment inside the surfactant aggregates. The decrease in EERS suggests that QS^{2+} is localized in a restricted inhomogeneous environment of micelles and most probably at the

interface of water and surfactant as the interfacial region is the preferred site for solubilization, even for hydrophobic molecules. This region offers considerable restriction to the reorientational motion of the solvent dipoles around the excited state QS^{2+}. Further, in a heterogeneous system of surfactants, the solute molecule may be distributed over a variety of locations ranging from polar region to relatively low polar region at the interface of water/surfactant and non-polar region far from the interface. As QS^{2+} is highly solvatochromic molecule, the fluorescence spectra depends on the polarity of the medium. So for QS^{2+} in surfactant systems, it is possible to excite the molecule selectively at different locations which results in EERS in fluorescence spectra.

The location of QS^{2+} molecules in the surfactant solutions can be understood considering the nature of charge of surfactant molecules. The SDS anion has an opposite charge to that of QS^{2+} molecules, so its interaction with QS^{2+} is strong, owing to attractive electrostatic forces. As a consequence, QS^{2+} molecules are localized in a restricted inhomogeneous interfacial environment of water/surfactant. In the case of cationic CTAB, the electrostatic repulsive force is operative, resulting to a decrease in the energy of interaction between QS^{2+} and CTAB. In neutral TX-100, as there is no electrostatic force, major portion of the QS^{2+} molecules are in bulk water and the photophysics of QS^{2+} in this solution show the bulk like behavior, except a decrease in FWHM of the emission spectrum compared to FWHM of bulk water fluorescence spectrum.

Interestingly, the EERS in CTAB and TX-100 is found to be $638\ cm^{-1}$ and $537\ cm^{-1}$ respectively, which is similar to the EERS of QS^{2+} in aqueous bulk solution, $679\ cm^{-1}$. This observation suggests that QS^{2+} is not in the restricted interfacial environment in CTAB and does not bind to neutral micelles. The lack of specific and strong electrostatic interaction between the QS^{2+} molecules and the head groups of the neutral surfactant results the penetration of interfacial water inside the micelle. Such water molecules will be experiencing less restricted motion in the micellar environment giving rise to larger EERS in CTAB and in TX-100 compared to SDS surfactant solution.

The EERS in the fluorescence spectrum on REE is due to the slow rate of solvent relaxation around the excited molecule and is a function of motional restriction experienced by the solvent molecules around the fluorophore. This effect is generally observed in polar and viscous solutions, where the solvent relaxation time is of the order of or longer than the fluorescence lifetime of a probe molecule. The magnitude of EERS

can be used as a probe to investigate the mobility parameter around the excited fluorophores. Thus from the observed magnitude of EERS in the present study, we conclude the mobility of water molecules around the QS^{2+} molecules in SDS surfactants is much restricted compared to the mobility in CTAB or TX-100, or bulk water.

4.3.4 Fluorescence lifetime measurements

The fluorescence lifetime of a fluorophore in micellar solutions is very sensitive to the local environment around the probe and helps to understand the different interactions between the probe molecule and the micelle, the location of the probe in micelles and the local viscosity and polarity of the microenvironment.[38-47] Differential degrees of solvent motion around the fluorophore or partitioning of the fluorophore in distinct regions of a confined environment of micelles gives rise to different fluorescence lifetime components.

Figure 4.5 shows the fluorescence decay curve of QS^{2+} in CTAB. Clearly, the fit of the decay curve to the single exponential function gives very high χ^2 and standard deviation values, however, the double exponential fit gives reduced χ^2 and uniformly distributed residuals. The decay curve of QS^{2+} in TX-100 also fits with biexponential function whereas the decay curve of QS^{2+} in SDS micellar solution fits with triexponential function. The fitted fluorescence decay data of QS^{2+} in water and different micellar solutions of various charge types are given in Table 4.2. As can be seen from the Table 4.2 that the fluorescence lifetime in bulk water solution is biexponential at 520 nm emission wavelength, with mean fluorescence lifetime of 21.12 ns, in agreement with the previous literature.[30] The fluorescence decays of QS^{2+} are biexponential at 520 nm emission wavelength in CTAB and TX-100 micellar solutions also and triple exponential in SDS micellar solutions. It is clear from Figure 4.6 that the decay of QS^{2+} in anionic SDS is slower than that in bulk water and cationic and neutral micelles. The two lifetime components observed in TX-100 are slower than that in CTAB micelles. Figure 4.7 shows the fluorescence decay curve of QS^{2+} in bulk aqueous solution and three different micellar environments at longer emission wavelength (520 nm). We observe that there is increase in lifetime in SDS micellar system, compared to bulk at same emission wavelength. In TX-100 solution, the lifetime remains almost same as in bulk solution and in CTAB solution there is increase in lifetime with increase in emission wavelength when compared to shorter wavelength of emission. The fluorescence lifetimes are much

shorter in CTAB solution compared to that in bulk water solution. This decrease of lifetime is simply due to the quenching of fluorescence in CTAB solutions.

The observed multiexponential behavior in micellar solutions may indicate the presence of either more than one species, which may or may not be kinetically coupled in the ground or the excited state, or a single species having more than one type of environment.

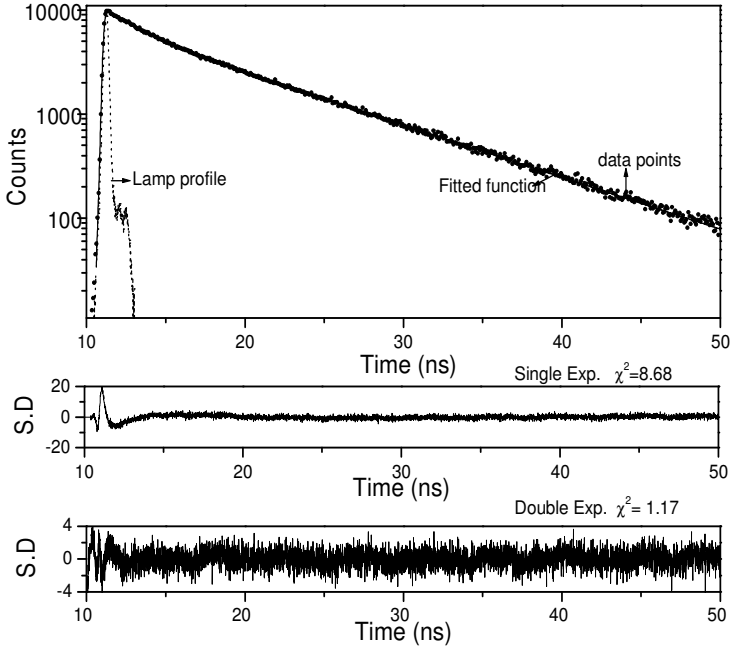

Figure 4.5 Fluorescence decay curve of QS^{2+} in CTAB micelles fitted to a double exponential function (λ_{ex} = 375 nm, λ_{em} = 390 nm). S.D (standard deviation) correspond to the distribution of residuals for single and double exponential fits, respectively

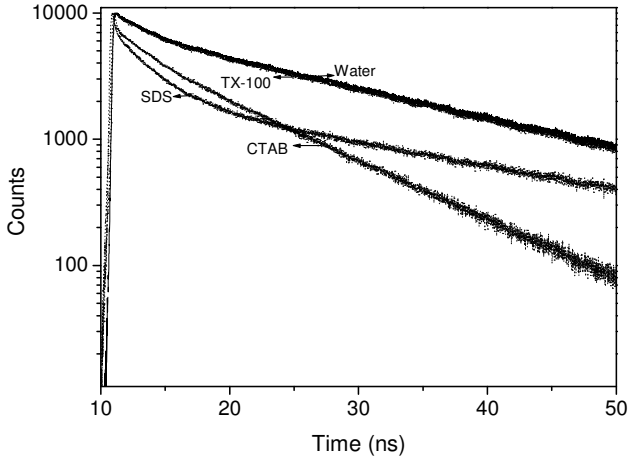

Figure 4.6 Fluorescence decay curve of QS^{2+} in water, CTAB, SDS and TX-100 micelles (λ_{ex} = 375 nm, λ_{em} = 390 nm)

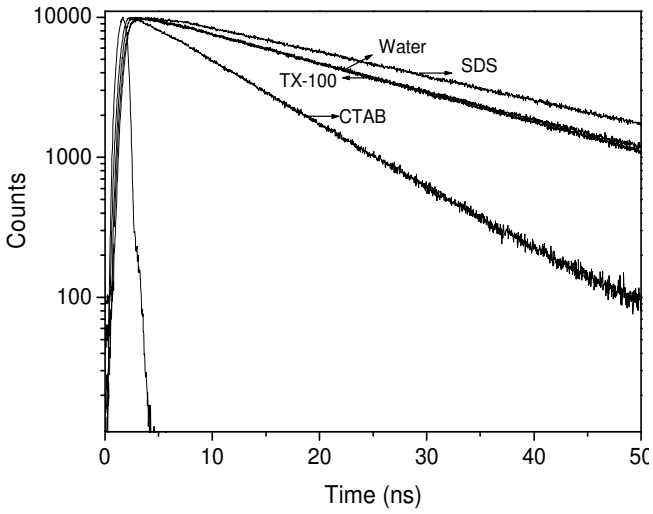

Figure 4.7 Fluorescence decay curve of QS^{2+} in water, CTAB, SDS and TX-100 micelles (λ_{ex} = 375 nm, λ_{em} = 520 nm)

The mean fluorescence lifetimes are also shown in Table 4.2. The mean fluorescence lifetimes in micelles of different surface charges are different, indicating that the local environment experienced by the QS^{2+} is different in different micelles. Interestingly, QS^{2+} in TX-100 shows mean lifetime of 20 ns, which is similar to the mean lifetime value obtained in bulk water.

Table 4.2 Time resolved fluorescence decay parameters of QS^{2+} in bulk water and micellar media

Solution	λ_{em}	τ_1 (ns)	α_1	τ_2 (ns)	α_2	τ_3 (ns)	α_3	$\chi 2$	$\langle\bar{\tau}\rangle$ (ns)
0.5M H_2SO_4									
	390	2.05	0.009	18.25	0.018	-	-	1.19	17.38
	520	1.28	-0.006	20.89	0.032	-	-	1.16	21.12
CTAB									
	390	2.03	0.013	8.38	0.023	-	-	1.17	7.53
	520	1.32	-0.004	8.63	0.031	-	-	1.09	8.78
SDS									
	390	2.77	0.013	0.174	0.026	22.52	0.005	1.12	17.22
	520	2.29	-0.006	0.110	-0.022	24.87	0.029	1.15	25.40
TX-100									
	390	1.74	0.008	18.02	0.017	-	-	1.14	17.31
	520	1.60	-0.005	20.73	0.030	-	-	1.12	20.99

This further shows that TX-100 does not bind with QS^{2+} and is in agreement with the conclusions drawn already from steady state data of QS^{2+}. The most drastic reduction in the mean fluorescence lifetime is observed in the case of QS^{2+} in CTAB micelles with

a mean lifetime of 8.46 ns. The shortening of fluorescence lifetime could be due to the quenching of QS^{2+} in CTAB, resulting from the presence of bromide ions causing the decrease in lifetime of QS^{2+} in CTAB. Further, an increase in the polarity of the environment is known to reduce the lifetime of QS^{2+} owing to fast deactivating process in polar environments. The observed three different fluorescence decay components for QS^{2+} in SDS micelles could be due to three different locations of QS^{2+} in micelles, including the non polar core, Stern layer and a layer near the Stern layer.

So we can conclude that QS^{2+} remains unaffected by the solubilization in TX-100, showing the presence of the probe in the aqueous medium i.e. in palisade layer. The higher value of decay time in SDS compared to TX-100, shows higher solubilization of the probe in the Stern layer of SDS compared to that in TX-100 due to strong interactions of QS^{2+} in SDS. The fluorescence lifetime data suggest that the probe is located in three different locations in SDS, near to bulk water region in CTAB and in bulk water region in TX-100. These lifetime data are consistent with the spectral properties mentioned above.

The values of radiative (k_r) and non-radiative (k_{nr}) rate constants were calculated from the observed fluorescence quantum yield (ϕ) and average lifetimes $\langle\bar{\tau}\rangle$ using the relations and the parameters are tabulated in Table 4.3 and average lifetimes $\langle\bar{\tau}\rangle$ for biexponential and triple exponential decays of fluorescence were calculated from the decay times and preexponential factors using the Equation 1.34 (Chapter 1).

$$k_r = \frac{\phi}{\langle\tau\rangle} \tag{4.1}$$

$$k_{nr} = \frac{(1-\phi)}{\langle\tau\rangle} \tag{4.2}$$

The fluorescence quantum yield values calculated (using QS^{2+} in bulk water as a standard) from the area of total fluorescence emission over the whole spectral range are increased in SDS and TX-100 micellar solutions and decreased in CTAB micelles, compared to bulk water solution. However, the radiative decay rates calculated in all the micelles studied in present study and in bulk water are almost same. The non-radiative rate constant (k_{nr}) in SDS micelles is smaller than that in bulk water and in other micellar solutions. A significant increase in nonradiative rate is observed in CTAB micelles.

The substantial increase of quantum yield in micellar solutions and decrease (k_{nr}), particularly in SDS solution can be assigned to the restricted motion of the probe molecule in the micellar solutions. The appreciable difference of the corresponding parameters in the SDS micelles and pure water rule out the possibility of location of QS^{2+} molecules around the bulk phase and suggest that most of the QS^{2+} molecules in SDS micelles are localized in micellar–water interface.

Table 4.3 Fluorescence quantum yield (ϕ), mean fluorescence decay time $\langle\bar{\tau}\rangle$, and radiative (k_r) and non-radiative (k_{nr}) decay constants of QS^{2+} in bulk water and different micellar media

Medium	ϕ	$\langle\bar{\tau}\rangle$ (ns)	(k_r) (10^8 s^{-1})	(k_{nr}) (10^8 s^{-1})
Water	0.55	20.35	0.27	0.22
SDS	0.67	23.69	0.28	0.14
CTAB	0.24	8.46	0.28	0.89
TX-100	0.58	19.87	0.29	0.21

4.2.5 Fluorescence quenching measurements

The fluorescence quenching data are taken with an intention to see the degree of accessibility of the fluorophore in different surfactant media toward the quencher and to confirm the location of the fluorescence moiety in the micellar environment.[45] Potassium chloride was used to quench the fluorescence of Quinine Sulfate dication (QS^{2+}) in homogeneous aqueous solution and in microheterogeneous environment formed by surfactants. The absorption spectrum for QS^{2+} in water as well as different micellar environments shows two bands, 318 nm and 348 nm, corresponding to L_b and L_a bands, respectively. The peak positions as well as absorbance of QS^{2+} remains constant as we change/ increase the concentration of Cl^- ions from 0 mM to 35 mM for all the micellar as well as bulk solutions studied. This clearly indicates that absorption spectrum is not sensitive to Cl^- ions and rules out the possibility of any complex formation in the ground state.

The fluorescence spectrum of QS^{2+} in aqueous solution for all micellar medium studied exhibits a broad band around 446 nm and was found to be very sensitive to the addition of Cl^- ions. The Cl^- ions quench the fluorescence of QS^{2+} significantly. Figure 4.8 shows the fluorescence spectra of QS^{2+} in bulk water and in different micellar

systems. It can be seen that the intensity of emission is reduced successively with the increase in Cl^- ion concentration in all the solutions studied. The reduction in fluorescence intensity of QS^{2+} for CTAB and TX-100, is almost the same as in bulk water. However, the reduction in fluorescence intensity in SDS micellar solutions is less than that in bulk water (discussed in detail in chapter 5). The full width at half maximum of the fluorescence spectrum of QS^{2+} remains the same in all the solutions studied and no new fluorescence band was observed with the increase in Cl^- concentration, which discards the possibility of any exciplex formation.

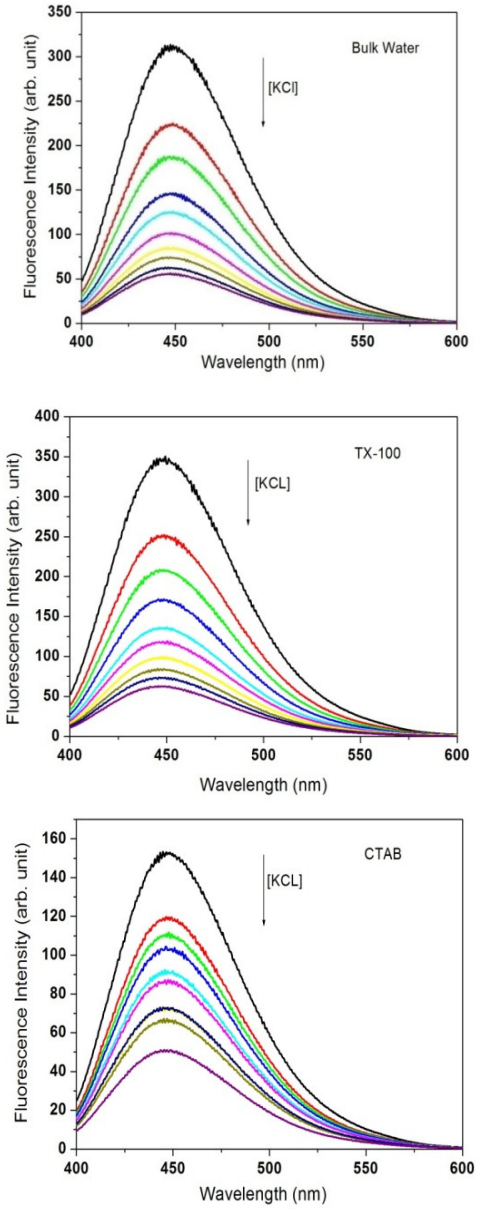

Figure 4.8 Fluorescence emission spectra of QS^{2+} in bulk solution and in different micellar systems with increasing concentration of KCl from 0 to 35 mM, excited at 350 nm

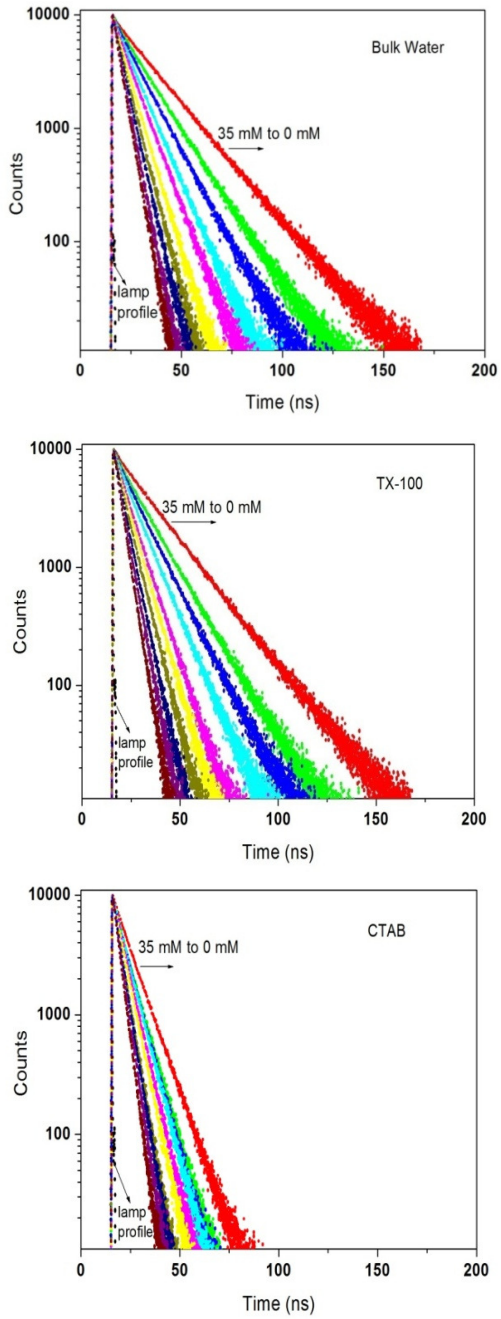

Figure 4.9 The fluorescence decay curve of QS^{2+} in bulk water and in different micellar systems with increasing Cl^- concentration, λ_{em} = 450 nm and excited at 375 nm (The micellar concentrations for CTAB and TX-100 were 10 mM)

The fluorescence decay curves of QS^{2+} in bulk water and in different micellar solutions are shown in Figure 4.9. The fluorescence decay of QS^{2+} in homogenous aqueous solution shows single exponential nature at 450 nm emission wavelength with decay time of 19.92 ns in KCl free aqueous solution and is in agreement with the reported values.[48] It can be seen (Figure 4.9) that the decay time of QS^{2+} in aqueous

solution decreases successively with increasing concentration of KCl from 0 mM to 35 mM from 19.92 to 4.06 ns, respectively.

However, decay time remains single exponential throughout the range of KCl concentration studied. These observations are in agreement with the reported results of quenching of QS^{2+} in bulk solutions.[48] However, when the decay of QS^{2+} is studied in microheterogeneous environment of CTAB micelles, the fluorescence decay remains single exponential at 450 nm for all concentration of KCl, but the fluorescence lifetimes reduce with the increase in Cl^- ion concentrations. For TX-100, the fluorescence decay behaviour in the presence of Cl^- ions remains almost same as in bulk water solution.

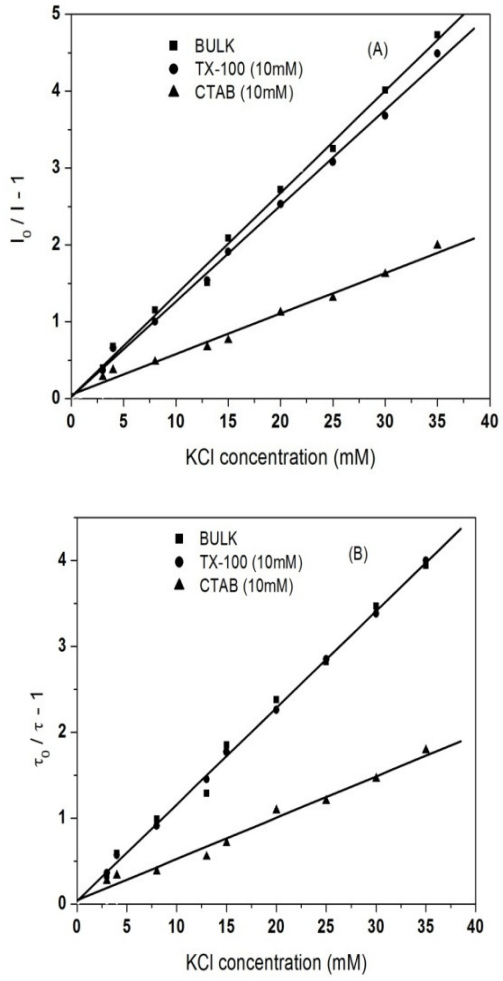

Figure 4.10 Stern-Volmer plots for QS^{2+} in bulk water solution and in different micellar systems with varying KCl concentration, (A) from fluorescence intensity measurements, (B) from fluorescence lifetime measurements. (The surfactant concentrations were above than their CMC concentrations)

Effect of ionic strength on the dynamic quenching of QS^{2+} by KCl in bulk aqueous has been studied earlier by Rocha[48] and it was observed that QS^{2+} molecules are very sensitive to the presence of Cl^- ions in aqueous solutions. The value of quenching constant obtained for QS^{2+} fluorescence in the present study is 132 M^{-1} and this value is in good agreement with the reported value.

The Stern-Volmer (S-V) quenching constant (K_{SV}) and quenching rate constant (K_q) of the system are evaluated using fluorescence intensity and lifetime data from the slopes of linear relationship of Stern-Volmer plots shown in Figure 4.10 using equations 1.35 and 1.36 (chapter 1). All the values, thus obtained are summarized in Table 4.4.

In the presence of CTAB micelles the quenching by Cl^- ions is more significant compared with that in TX-100 and bulk water solutions. This we believe is due to electrostatic attraction of chloride to the cationic micellar headgroups of CTAB, making the quencher concentration higher at the interface. In neutral TX-100, as there is no electrostatic force, major portion of the QS^{2+} molecules are in bulk water and the S-V quenching constant and quenching rate constant are almost same as of QS^{2+} in bulk aqueous solution.

Table 4.4 The S-V quenching constant (K_{sv}) and quenching rate constant (K_q) in bulk water and micellar media

Medium	K_{sv} M^{-1}		K_q M^{-1} S^{-1} (using steady state K_{sv} and Lifetime at λ_{em}= 450 nm)
	Steady state	Lifetime	
Water	132	113	6.62×10^9
CTAB (10mM)	52	48	5.77×10^9
TX-100 (10mM)	125	113	6.33×10^9

4.2.6 Time-resolved fluorescence anisotropy measurements

The fluorescence anisotropy measurement of a probe molecule has been established to be a most powerful and sensitive technique to elucidate information about the complex micro heterogeneous environment.[43-47] In order to obtain the location and mobility of QS^{2+} molecule in micellar systems, time resolved anisotropy measurements were performed. Rotational relaxation of a probe molecule in micellar assembly is determined using time resolved anisotropy measurements.

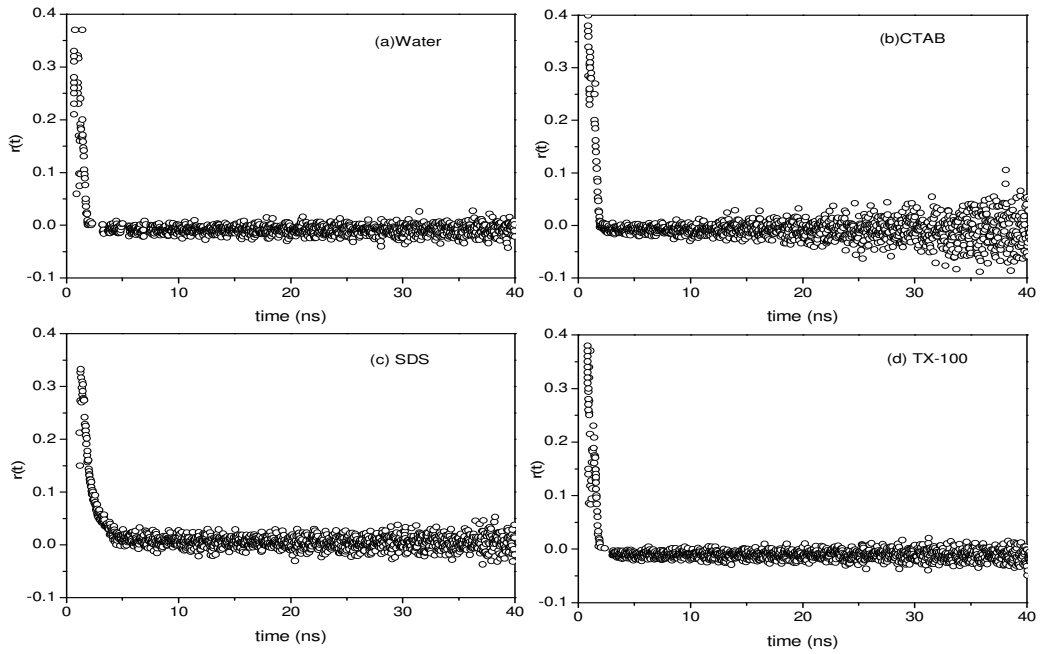

Figure 4.11 Time resolved fluorescence anisotropy decay profiles for QS^{2+} in water, CTAB, SDS and TX-100 micellar solutions, (λ_{ex} = 375 nm, λ_{em} = 450 nm)

Figure 4.11 shows the temporal anisotropy decay of QS^{2+} in water and in different micellar solutions and the anisotropy decay parameters are summarized in Table 4.5. The anisotropy decay of QS^{2+} in bulk water fits well to a single exponential decay function with rotational time of 314 ps. In CTAB and TX-100 micelles also single exponential decay fit of temporal anisotropy decays curves are observed and this reveals that the fluorescence depolarization is due to the rotational dynamics of a single fluorophore species encapsulated in micelles. In contrast, the anisotropy decay measured for QS^{2+} in SDS micellar solution requires a biexponential decay function for an acceptable fit. The functional form of the biexponential anisotropy decay $r(t)$ in micelles can be represented as

$$r(t) = r_0\left[\alpha_1 \exp^{\left(\frac{-t}{\tau_{\text{fast}}}\right)} + \alpha_1 \exp^{\left(\frac{-t}{\tau_{\text{slow}}}\right)}\right] \tag{4.3}$$

where, r_0 is the limiting anisotropy that describes the inherent depolarization of a given molecule, τ_1 and τ_2 are the two reorientation times of the probe and α_1 and α_2 are the corresponding relative amplitudes. The average rotational time for QS^{2+} in SDS solution is longer than that in the bulk water. In CTAB and TX-100 micellar solutions, the

anisotropy decays are faster than in SDS micelles. This is due to the fact that QS^{2+} being of cationic nature should be relatively distant from the positively charged micellar surface of CTAB. Due to the hydrophobic interactions, QS^{2+} remains partly in the Stern layer of CTAB micelles with a major portion in bulk water. The single exponential fit of anisotropy decays in CTAB and TX-100 micellar solutions reveal that the QS^{2+} molecules are free in the intermicellar water. The enhancement in the rotational relaxation time in SDS micellar media compared to pure aqueous media reflect that the fluorophore resides in a motionally restricted environment of micelles.

The observation of biexponential anisotropy decay for QS^{2+} in SDS micellar solutions could be due to several different reasons. One of the possibilities could be that the probe resides in two different solubilization sites in the micelles itself having largely different microenvironments. The viscous microenvironment for the probe in the micellar Stern layer can be another reason for the observed biexponential anisotropy decay. Another common interpretation for the biexponential decay invokes hindered rotational motions of the probe molecule in the micelles. The probe solubilized in the micelles follows a biexponential behavior as suggested by two step and wobbling in cone model.[49-52] The amplitude of the wobble component determines how much the fluorophore rotates in the conical volume and the associated time component corresponds to the rate that the fluorophore samples different configurations within the cone.

According to the two step and wobbling in a cone model, the molecule undergoes slow lateral diffusion on the micelle surface and also a fast wobbling motion in the micelle that is coupled to the rotation of the micelle as a whole. The experimentally measured τ_1 and τ_2 are used to calculate the time constants for lateral diffusion τ_L, wobbling motion τ_w and overall rotation of the micelle τ_M by the relations

$$\frac{1}{\tau_1} = \frac{1}{\tau_w} + \frac{1}{\tau_2} \tag{4.4}$$

$$\frac{1}{\tau_2} = \frac{1}{\tau_L} + \frac{1}{\tau_M} \tag{4.5}$$

The overall rotation of the micelles can be estimated from the Stokes-Einstein-Debye Equation[51]

$$\tau_M = \frac{4\pi\eta r_h^3}{3kT} \tag{4.6}$$

where, r_h is the hydorodynamic radius of the micelle, η is the viscosity of the medium, k and T are the Boltzmann constant and absolute temperature, respectively. For SDS micelle, the radius along which the probe moves is taken from ref.[52]. Thus the rotational time constant for micellar tumbling obtained using equation 4.6 comes out to be 8.3 ns, which is much longer than the slowest rotational time constant observed here in the present study for QS^{2+} in SDS micellar solution. This suggests that the observed 1.3 ns rotational time constant for SDS represents the lateral diffusion time constant of the QS^{2+} molecules. In order to have an idea about the spatial restriction and location of the probe molecules in SDS solution, we have calculated the generalized order parameter (S) using the following equation[51]

$$S^2 = \alpha_2 \tag{4.7}$$

and the value of S calculated to be 0.65 which is very high and strongly suggest that the QS^{2+} molecules reside in restricted environments of SDS and most probably localized at the SDS micelle-water interface. This result is supported by observed less EERS and less nonradiative decay rate in SDS micellar solution compared to CTAB and TX-100 solutions. In the case of interaction of QS^{2+} with SDS, the close interaction of positively charged QS^{2+} with the negatively charged head group results in poor water penetration in micellar interior. This results in relatively nonpolar environment around the probe in SDS micelles, leading to a reduction in EERS and increase in fluorescence lifetime.

Table 4.5 Time resolved decay parameters of fluorescence anisotropy of QS^{2+} in bulk water and micellar media

Environment	r_0	τ_1(ps)	α_1	τ_2(ps)	α_2	$\langle\bar{\tau}\rangle$ (ps)
Water	0.38	314	1	-	-	314
CTAB	0.40	324	1	-	-	324
SDS	0.34	468	0.58	1304	0.42	1016
TX-100	0.39	296	1	-	-	296

Our steady state, time-resolved fluorescence lifetime and fluorescence anisotropy results clearly show that QS^{2+} molecules are localized in the interfacial region of SDS micelles and water, owing to electrostatic attraction between them, whereas QS^{2+} does not bind to the interface of CTAB due to electrostatic repulsion. In bulk water solution the EERS is rationalized by the fact that the excitation of the solute is accompanied by a large change in dipole moment and the solvent reorientation time is not fast enough to bring the molecule in the relaxed state during the lifetime of the excited state. In SDS surfactant system due to heterogeneous restricted motion of solvent molecules the solvent relaxation process of accommodating the change in dipole moment of excited molecule further slows down which results in a decrease in net magnitude of EERS and increase in fluorescence lifetime compared to that in CTAB, TX-100 and bulk water solutions.

The fluorescence probe that preferentially locates itself inside the micellar Stern layer is quite often used to monitor the variations in microenvironments of the Stern layer. In this study we have successfully utilized the steady state and time resolved fluorescence techniques to probe the microenvironment of micelles of different charges of the head groups and their effect on the photophysics of QS^{2+} molecules. We are able to demonstrate that the spectral properties of QS^{2+} are very sensitive to immediate environment in which it resides in micellar solutions and it is inferred from the our results that QS^{2+} can be used as an efficient probe molecule for the surface and interface studies.

4.4 Conclusions

The fluorescence properties of QS^{2+} are remarkably modulated in micelles compared with the bulk phase. The observed EERS in emission maximum of QS^{2+} in bulk water and surfactant systems is due to the solvent relaxation process around the excited solute molecule. The decrease in the magnitude of EERS in anionic SDS surfactant systems is due to the decrease in solvent relaxation rate as a consequence of restricted motion of the water molecules around the QS^{2+} in interfacial region, where its mobility is considerably reduced. The microenvironment around the probe molecules bound to surfactants can be conveniently monitored using the EERS measurements. The magnitude of EERS can be used as a probe to determine the microenvironmental and restrictive motion of solvent molecules around the probe molecule in surfactants. In the case of CTAB, QS^{2+} molecules are more in bulk type water consequently solvation is much faster.

Modulated photophysics of QS^{2+} in micellar systems compared to aqueous media has been demonstrated using steady state and time-resolved studies. The location of the probe molecule in micellar systems is ascertained by a variety of spectral parameters such as EERS, average fluorescence decay time, radiative and non radiative rate constants, and rotational relaxation time. All experimental results suggest that the QS^{2+} molecule resides at micellar–water interface. However, the penetration towards the micellar core in nonionic surfactant is more important, relative to ionic surfactant. Further the rotational mobility of QS^{2+} in these micelles is found to be dependent on the surface charge of micelles. The longest rotational correlation time is observed for anionic SDS micelles and is attributed to the lateral diffusion of QS^{2+} molecules. In summary, the micellar surface charge can modulate the conformation and dynamics of QS^{2+} probe molecule. These results are relevant to understand the role of surface charge of membranes in the interaction of membranes with the membranes. This type of study can be extended to biologically important heterogeneous systems like membranes, enzymes, peptides and proteins to understand the aggregation behavior and structure of the microenvironments using QS^{2+} as a fluorescent probe molecule and particularly to understand the role of surface charge of membranes in interaction of peptides with membranes. This study provides excited state dynamical behavior of QS^{2+} molecules in different micelles of different surface charges and adds knowledge about the understanding of microstructure of surfaces and interfaces.

References:

(1) P. Alexandridis, B. Lindman, *Amphiphilic Block Copolymers: Self-Assembly and Applications*, Elsevier, Amsterdam, 2000.

(2) R. Savic, B.L. Luo, A. Eisenberg, D. Maysinger, *Sci.* **2003**, *300*, 615.

(3) A. J. Massey, A.M. Winnik, I. Manners, H.Z.V. Chan, M.J. Ostermann, R. Enchel-maier, P. J. Spatz, M. Moller, *J. Am. Chem. Soc.* **2001**, *123*, 3147.

(4) F. T. Jaramillo, H. S. Baeck, R. B. Cuenya, W. E. McFarland, *J. Am. Chem. Soc.* **2003**, *125*, 7148.

(5) R. J. Cardinal, P. Mukherjee, *J. Phys. Chem.* **1978**, *82*, 1614.

(6) Y. K. Law, *J. Photochem. Photobiol*. **1981**, *33*, 799.

(7) G. D. Hall, *J. Chem. Soc. Faraday Trans. 2* **1981**, *77*, 1973.

(8) P. Bilski, F. C. Chignell, *J. Photochem. Photobiol. A: Chem.* **1994**, *77*, 49.

(9) R. E. Riter, E. P. Undiks, N.E. Levinger, *J. Am. Chem. Soc.* **1998**, *120*, 6062.

(10) D. Pant, N. E. Levinger, *Langmuir* **2000**, *16*, 10123.

(11) D. Pant, R. E. Riter, N. E. Levinger, *J. Chem. Phys.* **1998**, *109*, 9995.

(12) V. Balzani, L. DeCola, *Supramolecular Chemistry*; Eds. Kluwer Academic Publishers: Dordrecht, Netherlands, 1992.

(13) M. Komiyama, H. Shigekawa, J. L. Atwood, J. E. D. Davies, D. D. MacNicol, F. Vögtle, Eds. Pergamon, New York, 1996,Vol. 3, pp 401.

(14) J. H. Schneider, H. Durr, *Frontiers in Supramolecular Chemistry and Photochemistry*, Eds.VCH: Weinheim, 1992.

(15) M. L Bender, M. Komiyama, *Cyclodextrin Chemistry*, Eds. Springer Verlag: Berlin, 1978.

(16) J. Szejtli, T. Osa, *Comprehensive Supramolecular Chemistry*, Eds. Elsevier: NewYork, 1996, Vol. 3.

(17) M. E. Davis, M. E. Brewester, *Nature* **2004**, *3*, 1023.

(18) W. H. Melhuish, *J. Phys. Chem.* **1960**, *64*, 762.

(19) D.W. Moss, *Clin. Chim. Acta* **1960**, *5*, 283.

(20) A. Gafni, R. P. Detoma, R. E. Manrow, L. Barnad, *Biophys. J.* **1977**, *17*, 155.

(21) V. I. Stenberg, E. F. Travecedo, *J. Org. Chem.* **1970**, *35*, 4131.

(22) R. F. Chen, *Anal. Biochem.* **1967**, *19*, 374.

(23) A. N. Fletcher, *J. Phys. Chem.* **1968**, *72*, 2742.

(24) A. P. Demchenko, *J. Lumin.* **2002**, *17*, 19.

(25) K. Itoh, T. Azumi, *Chem. Phys. Lett.* **1973**, *22*, 395.

(26) D. V. O'Connor, S. R. Meech, D. Phillips, *Chem. Phys. Lett.* **1982**, *88*, 22.

(27) D. A. Barrow, B. R. Lentz, *Chem. Phys. Lett.* **1984**, *104*, 161.

(28) S. R. Meech, D. Phillips, *J. Photochem.* **1983**, *23*, 193.

(29) P. Gangola, N.B. Joshi, D.D. Pant, *Chem. Phys. Lett.* **1977**, *51*, 144.

(30) D. Pant, U.C. Tripathi, G. C. Joshi, H. B. Tripathi, D. D. Pant, *J. Photochem. Photobiol. A: Chem.* **1990**, *51*, 313.

(31) D. Pant, H. B. Tripathi, D. D. Pant, *J. Photochem. Photobiol. A: Chem.* **1991**, *56*, 207.

(32) D. Pant, H. B. Tripathi, D. D. Pant, *J. Lumin.* **1991**, *50*, 249.

(33) D. Pant, H. B. Tripathi, D. D. Pant, *J. Lumin.* **1992**, *51*, 223.

(34) S. Pant, H.B. Tripathi, D.D. Pant, *J. Photochem. Photobiol. A: Chem.* **1995**, *85*, 33.

(35) H. C. Joshi, A. Upadhyay, H. Mishra, H. B. Tripathi, D. D. Pant, *J. Photochem. Photobiol. A: Chem.* **1999**, *122*, 185.

(36) H. C. Joshi, H. Mishra, H. B. Tripathi, T. C. Pant, *J. Lumin.* **2000**, *90*, 17.

(37) H. Mishra, D. Pant, T. C. Pant, H. B. Tripathi, *J. Photochem. Photobiol. A: Chem.* **2006**, *177*, 197.

(38) J. R. Lakowicz, *Principles of Fluorescence Spectroscopy*, Second edition, Plenum, New York, 1999.

(39) P. Bhattacharya, S. Chakravorti, *J. Photochem. Photobiol. A: Chem.* **2013**, *263*, 8.

(40) P. Bhattacharya, S. Chakravorti, *Chem. Phys. Lett.* **2013**, *571*, 71.

(41) A. Sarkar, N. Kedia, P. Purkayastha, S. Bagchi, *Chem. Phys. Lett.* **2014**, *592*, 138.

(42) B. K. Paul, N. Guchhait, *J. Mol. Liq.* **2014**, *199*, 309.

(43) E. R. Macedo, L. D. Boni, L. Misoguti, C. R. Mendonca, H.P. de Oliveira, *Colloids Surf. A: Physicochem. Eng. Aspects* **2011**, *392*, 76.

(44) Y. Tej Varma, S. Joshi, D. D. Pant, *Spectrochim. Acta Part A* **2014** (in press).

(45) S. Dhar, D. K. Rana, S. C. Bhattacharya, *Colloids Surf. A: Physicochem. Eng. Aspects* **2012**, *402*, 117.

(46) A. Sarkar, N. Kedia, P. Purkayastha, S. Bagchi, *J. Lumin*. **2011**, *131*, 1731.

(47) P. Banerjee, S. Pramanik, A. Sarkar, S. C. Bhattacharya, *J. Phys. Chem. B* **2008**, *112*, 7211.

(48) C. J. Rocha, M. H. Gehlen, R. D. Silva, P. M. Donate*, J. Photochem. Photobiol. A: Chem* **1999**, *123*, 129.

(49) G. Lipari, A. Szabo, *Biophys. J.* **1980**, *30*, 489.

(50) C. C. Wang, R. J. Peeora, *Chem. Phys*. **1980**, *72*, 5333.

(51) E. L. Quitevis, A. H. Marcus, M. D. Fayer, *J. Phys. Chem.* **1993**, *97*, 5762.

(52) N. C. Maiti, M. M. G. Krishna, P. J. Britto, N. J. Periasamy, *J. Phys. Chem. B* **1997**, *101*, 11051.

Chapter 5

Steady state and time-resolved fluorescence spectroscopy of Quinine Sulfate dication bound to Sodium dodecylsulfate micelles: Fluorescent complex formation

5.1 Introduction

Dye-surfactant interactions are essential in a variety of dyeing processes as well as in understanding excited state relaxation processes in photobiology, photochemistry and photosensitization.[1-3] Surfactants are principally used as wetting, dispersing, and leveling agents for improving dyeing processes by increasing the solubility, stabilizing the dispersed state, and promoting a uniform distribution of dye in a textile. Therefore, studies of dye-surfactant interactions provide applicable information for industrial applications.[4,5] Dye-surfactant associations are interesting for their complex nature.[6-8] These associations depend particularly on the chemical structures of the compounds.[9,10]

Surfactant assemblies are well known for tuning the electronic spectra of solution of dyes and various chromophores.[11,12] The positions of the absorption bands of the dyes are sensitive to medium effects; therefore they can be used as solvatochromatic micropolarity reporter molecules. The nature of interactions involved in aqueous ionic dyes and oppositely charged ionic surfactants adds to our understanding of the combined electrostatic and hydrophobic[13] interactions encountered in the various biological as well as physicochemical systems.[14,15] The spectral changes of the ionic dyes in presence of oppositely charged surfactants below their Critical Micelle Concentration (CMC) have been attributed to various interactions viz., formation of dye surfactant salts,[16,17] ion pairs,[18-21] dye-rich induced micelles,[22] self-assembly of the dye-surfactant complexes,[23,24] change in the chromophore microenvironment.[25,26] Such manifestations of interactions between ionic dyes with oppositely charged surfactants pertain to combined columbic and hydrophobic interactions taking place in biological systems.

This chapter describes the effect of concentration of anionic surfactant on to the photophysics of cationic molecule and observed an interesting behavior of fluorescence

of QS^{2+} at different concentrations of Sodium dodecylsulfate (SDS). At premicellar concentrations of SDS, the ion–pairs have been formed between the QS^{2+} molecules and monomers of surfactant and are highly fluorescent even at room temperature. On the other hand, at postmicellar concentrations, the QS^{2+} molecules are in monomeric form and bind strongly with the micelles. The steady state absorption, fluorescence, steady state and time-resolved fluorescence aniosotropy, fluorescence lifetimes and fluorescence quenching measurements and the polarity, viscosity, refractive index of microenvironment of SDS around the probe molecule reveal that the probe molecule resides at the water-micelle interface. This study demonstrates that QS^{2+} molecule has the potential to serve as a sensitive probe for studying the microenvironments in chemical, micellar and biological systems.

5.2 Experimental

Quinine Sulfate (QS) was purchased from Alfa Aesar and used as received. All the solvents were either of spectroscopic grade or were checked for their purity. All the samples of Quinine Sulfate dication (QS^{2+}) were prepared by dissolving the appropriate concentration of QS in 1N H_2SO_4 containing Milli Q water. The final concentration of QS^{2+} in all the systems studied was 10^{-4} M. The surfactant, Sodium dodecylsulfate (SDS) was purchased from SISCO and was used as received. Absorption spectra were taken with the help of dual beam JASCO V-570 UV/Vis/NIR spectrophotometer and fluorescence and excitation spectra were recorded with the help of Shimadzu, RF-5301PC Spectrofluorometer. The data were analyzed using related software. The spectral shifts obtained with different sets of samples were identical in most of the cases and values were within ±1.0 nm.

The fluorescence lifetimes were measured from time resolved intensity decays by the method of Time Correlated Single Photon Counting (TCSPC) technique. The light source used was picoseconds diode laser (Nano LED) at 372 nm and 300 nm (Horiba Jobin Yvon, USA). The typical response time of this laser system was 70 ps. The fluorescence decays were deconvoluted using the Datastation software for acquisition and IBH DAS6 for data analysis. The signals were collected at the magic angle (54.7^0).

5.3 Results and discussions

5.3.1 Absorption and fluorescence spectral properties

The visible absorption spectra of mixed solution of a fixed concentration of QS^{2+} at 10^{-4} M for different concentrations of SDS ranging from 4×10^{-4} M to 1×10^{-2} M in aqueous media at 298 K are illustrated in Figure 5.1. The absorption spectrum in aqueous bulk water shows two bands L_a and L_b at 348 and 318 nm, respectively. These two bands correspond to low-lying closely spaced π, π^* states of the main chromophore.

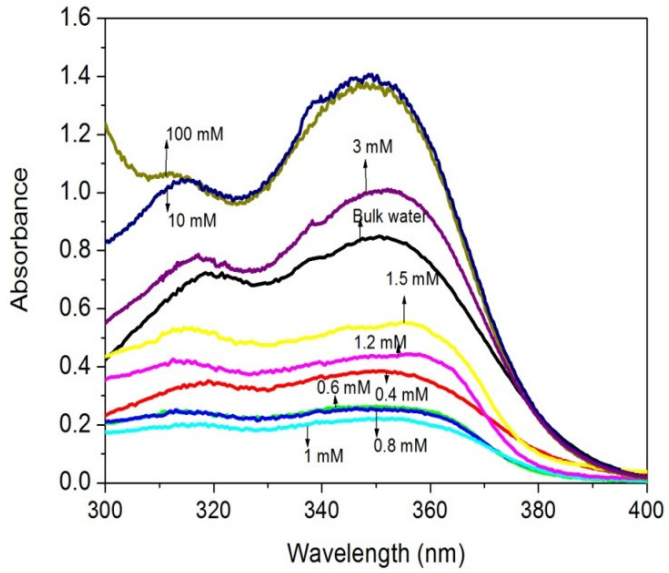

Figure 5.1 Absorption spectra of QS^{2+} in bulk water and in different micellar concentrations of SDS surfactant

It is observed that the position of absorption bands does not change appreciably with the concentration of surfactant in the solution of QS^{2+}; however, the corresponding molar absorption coefficient (ε) values of L_a and L_b bands of the solute molecule change with the concentration of SDS. At lower concentrations of SDS, the overall absorbance of QS^{2+} decreases with the increase in concentration of SDS surfactant compared to the absorbance of QS^{2+} in bulk water; however, with further increase in surfactant concentration the absorbance value increases. Moreover, at lower concentrations of SDS, it is interesting to note that the absorbance corresponding to the L_a band becomes relatively stronger than L_b with the increase of surfactant concentration; however, at higher concentrations of SDS, the overall absorbance increases with the increase in concentration and the relative absorbance of L_a and L_b correspond to the relative

intensities of L_a and L_b in bulk water. The absorption data clearly suggest that the environment around the probe molecules in aqueous surfactant solutions is different from bulk water solution.

Clearly, at lower concentrations of SDS, the decrease in absorbance with the increase in concentration indicates that the probe molecules are not in free monomeric form, instead associated with the surfactant molecules to form a complex between dye and surfactant monomers and this has been observed for many other different probe-surfactant systems.[27-31] The complex formation of probe molecule and surfactant is a consequence of electrostatic interactions. The increase in absorbance with the increase in surfactant concentration is due to the incorporation of solute molecules to micelles. As more dye molecules are incorporated to micelles the absorbance value increases and reaches a limiting value and becomes almost constant for concentrations above 10 mM of SDS. In 10 mM SDS concentration, the solubilization of QS^{2+} in the micelles is practically completed and further addition of SDS failed to bring any spectral change.

Figure 5.2 illustrates the fluorescence spectra of QS^{2+} at fixed concentration in aqueous solution for different concentrations of SDS surfactant. In bulk water solution of QS^{2+}, the emission spectrum has only a structure-less broad band with maximum around 447 nm on excitation at 355 nm. On introducing a small amount of SDS (concentration 4×10^{-4} M) in QS^{2+} aqueous solution, the fluorescence intensity decreases with the appearance of an extra fluorescence band around 380 nm. On further increase in concentration, the intensity corresponding to the band around 450 nm decreases; whereas, the intensity corresponding to the band around 380 nm increases. The appearance of an extra fluorescence band around 380 nm could be simply due to the change in acid–base properties in the excited state due to the deprotonation of QS^{2+} in the presence of SDS surfactant molecules. In the past, using steady state and time resolved fluorescence techniques we have done a detailed study on to the protonation and deprotonation of QS as a function of pH of the solution and it was observed that the probe molecule exists in doubly protonated form around pH 2 with fluorescence peak value around 450 nm, in mono-cationic form at pH 7 with fluorescence peak around 390 nm and neutral form at pH 11 with peak around 385 nm.[32-35]

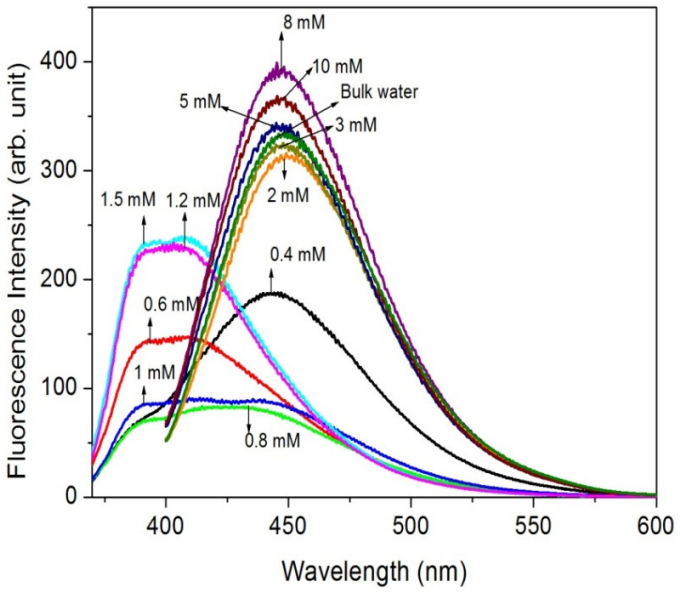

Figure 5.2 Fluorescence spectrum of QS^{2+} in bulk water and in different concentrations of SDS, excited at 355 nm

At high concentrations of SDS, above 2 mM, the fluorescence intensity increases with the increase in concentration and the spectrum shows only one structure less band which corresponds to the fluorescence band of QS^{2+} in bulk water. On further increase in surfactant concentration, above 3 mM, the fluorescence intensity becomes even more pronounced compared to the intensity of QS^{2+} in bulk water.

The observation of only one fluorescence band of QS^{2+} around 450 nm (corresponding to the dicationic form of Quinine Sulfate) for the higher concentrations of SDS rules out the possibility of deprotonation of QS^{2+} in the presence of SDS molecules. Consequently, observation of dual fluorescence, decrease in fluorescence intensity and blue shift of the overall fluorescence at lower concentrations of SDS are not due to the deprotonation of QS^{2+}, but are the indications of association of QS^{2+} with free SDS molecules in such a way that their exposure to water is minimized and hence sense a less polar environment. We attribute the new observed fluorescence band at lower concentrations of SDS to the fluorescent complex formation between the probe molecules and monomers of surfactant.

At higher concentrations of SDS, only one highly fluorescent band is observed and the characteristic fluorescence band corresponding to ion pair complex formation

disappears. This clearly indicates that the dye surfactant complex is unstable and this complex does not exist at higher concentrations of SDS. At higher concentrations of SDS, the surfactant molecules tend to aggregate to form micelles. The increase in absorbance and fluorescence intensities with the increase in surfactant concentration above 0.8 mM is due to the incorporation of QS^{2+} molecules to the aggregates of surfactants. The observance of increase in fluorescence intensity, disappearance of second fluorescence band and the red shift of the spectrum are attributed to the formation of micelles in the higher concentrations of the surfactant.

As the fluorescence intensity of water soluble QS^{2+} changes with the change in concentration of SDS, this observation is used to determine the Critical Micellar Concentration (CMC) of SDS, from the fluorescence intensity data of QS^{2+} at fluorescence maxima, excited at 355 nm at different concentrations of SDS. The ratio of fluorescence intensities of QS^{2+} in the absence and presence of surfactant vs. concentration of surfactant plot is shown in Figure 5.3. The resulting sharp break points correspond to the CMC value. Clearly, there are two break points, the first point is at around 0.8 mM and the second one is at 2 mM. These break points are well below the reported normal CMC value (8 mM) in aqueous solutions. There are already several reports[36-38] in the literature about the observation of multiple CMC values of SDS. We assign the first break point around 0.8 mM to association of SDS with QS^{2+} and formation of probe-surfactant ion pair complex. The second break point around 2 mM can be assigned to the premicellar aggregation of SDS in aqueous solution. In the present study, the observation of low CMC could be simply due to the acidic nature of the solution. There are several reports in literature[39-41] about the decrease in CMC with the decrease in pH of the solution. The CMC of SDS in HCl aqueous solution at pH 2 has been reported about 2 mM which is much lower than that in pure water because of the effect of ionic strength of the solution.[38] Further, it has been observed that SDS interacts with labelled poly-acrylic acid in solution of pH 3 to form a polymer/SDS complex with a CMC value lower than the normal CMC of SDS in bulk water.[40] The surfactant concentration required to induce binding to the polymer has been referred to as the Critical Aggregation Concentration (CAC), which is generally lower than the CMC in polymer-free solution.[41]

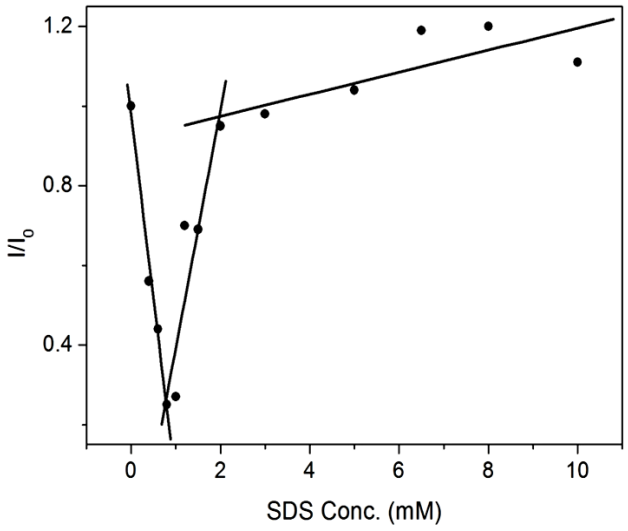

Figure 5.3 The ratio of fluorescence intensities of QS^{2+} in the absence (I_0) and presence (I) of SDS surfactant as a function of SDS surfactant concentration

5.3.2 Probe-surfactant association and binding constant

In the premicellar region, where the QS^{2+} when interacts with oppositely charged surfactants have been attributed to the formation of an ion-pair complex. This behaviour clearly suggests the formation of probe-surfactant complex through an intermediate species, similar observations were made by Gawandi et. al.[30,31] They studied interaction of cationic dye with anionic surfactant and they concluded that absorption spectra are sensitive to SDS environment which have been attributed to the formation of ion-pair complex. They calculated the equilibrium association constant of cresyl violet dye with anionic surfactants using absorption data in the region of low surfactant concentration and binding constant using data above CMC and they reported the association K_A and binding constant, K_B of cresyl violet dye with SDS surfactant as 2.6×10^5 and 0.8×10^5 ($dm^3\ mol^{-1}$), respectively.

We calculated the equilibrium association constant of QS^{2+} with anionic SDS surfactants using absorption data in the region of low surfactant concentration and the association constant K_A value obtained is 4.4×10^3 $dm^3\ mol^{-1}$ and is given in Table 5.1.

In the present study, the absorbance data in the region of low surfactant concentration were used to compute[31] the equilibrium constant (K_A) for the association of QS^{2+} with the SDS anionic surfactant. Thus if the molar absorption coefficients of the

free and complex dye at a given wavelength are ε_{aq} and ε_c, respectively, the observed absorbance (A) is given by

$$A = \varepsilon_{aq}(1 - f_c)[C]_T l + \varepsilon_c f_c [C]_T l \tag{5.1}$$

where, l is the optical path length and f_c is the fraction of the probe present as the complex and is given by

$$f_c = \frac{1}{\left\{1 + \frac{1}{K_A([S]_T - f_c[C]_T)}\right\}} \tag{5.2}$$

where, $[C]_T$ and $[S]_T$ are the total probe and surfactant concentrations, respectively. In these experiments $[C]_T$ was kept constant at 10^{-4}M whereas $[S]_T$ was varied from 4×10^{-4} M to 10^{-3} M. Substituting f_c in Equation (5.1), the observed absorbance can be shown to be related to surfactant concentration as given in Equation 1.51 and using this equation we have calculated association constant as discussed in chapter 1.

As f_c is not known, an appropriate plot can be constructed using $[S]_T$ instead of $\{[S]_T - f_c[C]_T\}$ with $f_c = 0$, and approximate value of K_A so computed can be used to get f_c for each surfactant concentration ($[C]_T$ kept constant) from Equation (5.3), which is quadratic Equation inf_c (derived from Equation 5.2):

$$K_A[C]_T f_c^2 + \{-K_A[S]_T + K_A[C]_T + 1\} f_c + K_A[S]_T = 0 \tag{5.3}$$

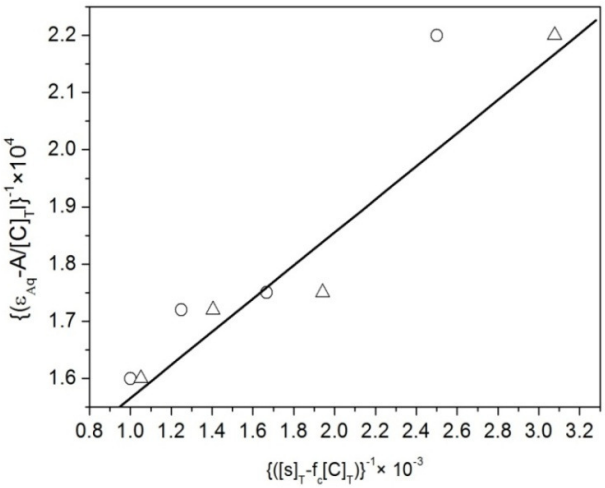

Figure 5.4 Plot of (i) $\{\varepsilon_{aq} - A/[C]_T l\}^{-1}$ vs $\{([S]_T)\}^{-1}$ (…o) (ii) $\{\varepsilon_{aq} - A/[C]_T l\}^{-1}$ vs $\{([S]_T - f_c[C]_T)\}^{-1}$ (…Δ)

Out of the two values of f_c obtained from the above quadratic equation, only the root having a value <1 is to be taken as f_c is a fraction. A more accurate plot is now constructed using these f_c values and this successive approximation procedure is repeated until K_A and f_c become invariant (Figure 5.4). The association constant, K_A thus obtained is 4.4×10^3 dm^3 mol^{-1} and is given in Table 5.1. The extinction coefficient of the complex, (ε_c) determined from the intercept of Figure 5.4 is also shown in Table 5.1.

For calculating probe–micelle binding constant we considered absorption of QS^{2+} in surfactants having concentrations above 2 mM. The binding constant, K_B can be shown related[37] to the measured absorbance of the probe (Equation 1.52), as already discussed in chapter 1.

As f_m is not known, an initial plot was drawn with $f_m = 0$ .The approximate value of K_B obtained was used to get the value of f_m for each micelle concentration from Equation (5.4), which is quadratic in f_m,

$$K_B[C]_T f_m^2 + \{-K_B[M]_T + K_B[C]_T + 1\} f_m + K_B[M]_T = 0 \qquad (5.4)$$

where, f_m is the fraction of the probe ($[C]_T$, kept constant at 10^{-4} M) in the micellar form and $[M]_T$ is the total micelle concentration given by Equation 1.53 already discussed in chapter 1. Out of the two values of f_m obtained from the above quadratic equation, only root having a value <1 is to be taken as f_m is a fraction. A more accurate plot is now constructed using these f_m values and this successive approximation procedure is repeated until K_B and f_m become invariant (Figure 5.5). The K_B value thus obtained is 2.4×10^6 dm^3 mol^{-1} and is given in Table 5.1. The extinction coefficient of the micellized probe, (ε_m) determined from the intercept of Figure 5.5 is also shown in Table 5.1.

Table 5.1 Association and binding constants of QS^{2+}-Micelle interactions

Surfactant	K_A(L/mole)	K_B(L/mole)	ε_c(L/mole-cm)	ε_m(L/mole-cm)
SDS	4.4×10^3	2.4×10^6	4.63×10^2	1.16×10^4

ε_c and ε_m are extinction coefficient of complex and micellized probe respectively.

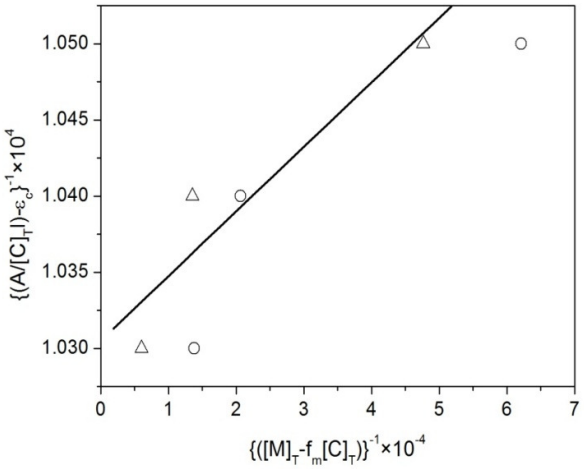

Figure 5.5 Plot of (i) $\{(A/[C]_T l)-\varepsilon_c\}^{-1}$ vs $\{([M]_T)\}^{-1}$ (o) (ii) $\{(A/[C]_T l)-\varepsilon_c\}^{-1}$ vs $([M]_T - f_m[C]_T)\}^{-1}$ (Δ)

In the present study, the high value of the binding constant between the probe and the micelle can be used to determine the amount of free and bound probe concentrations using the following relation[39]

$$[P]_0 = \frac{[P]_T}{(1 + K[M])} \tag{5.5}$$

where, $[P]_0$ and $[P]_T$ are concentrations of free and total probe, respectively. $[M]$ is the micellar concentration, and K is the binding constant, respectively. We found that almost all the QS^{2+} molecules bound with the micelles and this strong binding of QS^{2+} with the SDS clearly indicates that QS^{2+} molecule can be used as an efficient probe molecule to characterize micellar environments.

5.3.3 Microenvironment around the fluorophore

Determination of the polarity in the immediate vicinity of the fluorophore provides valuable information about the location of the probe in micellar environments. Fluorescent probes serve important roles in determining the microscopic polarity, viscosity and refractive index of the biological and biomimicking environments.[42,43] These parameters around a probe in biomimetic environments can be estimated by comparison of spectral properties of fluorophore in the environment with those of probe in pure solvents of known polarities.[42-48] The polarity of homogeneous and microheterogeneous media cannot be exactly same, however a relative estimate of such environment is made through such measurements.

Khumbhakar et. al.[49] determined the micropolarity around coumarin 153 in TX-100 and they suggested that the fluorophore resides in the core region of micelle. From the absorption and fluorescence spectra of probe in different solvents, we calculated the corresponding Stoke's shifts and the relevant data and plots are given in Table 5.2 and Figure 5.6 respectively.

The QS^{2+} molecules dissolved in surfactant SDS solution are in new kind of solvent environment having very different polarity, viscosity and refractive index and E_T (30) than that of water. As the values of E_T (30) and dielectric constant are lower than that of water and refractive index is larger than that of water, we conclude that the probe QS^{2+} resides in interfacial region of the micelle.

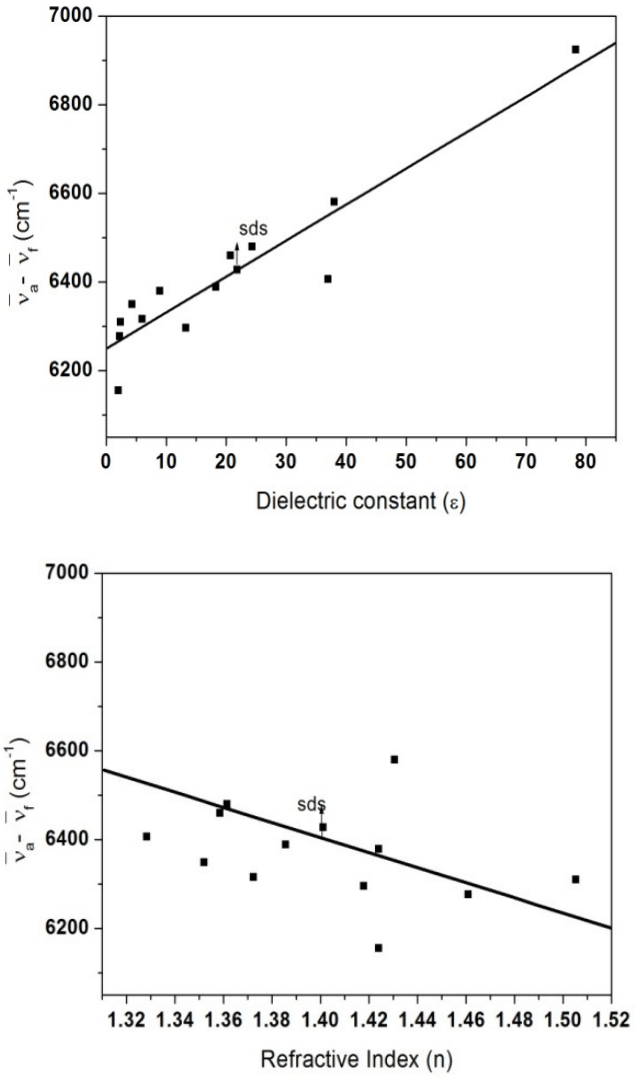

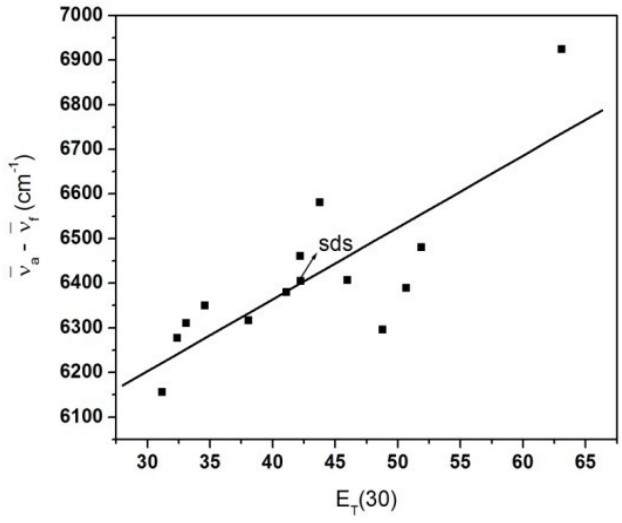

Figure 5.6 Stokes shift vs. solvent dielectric constant, refractive index and E_T (30) respectively

Table 5.2 Different solvent parameters and spectral data of QS^{2+} in different solvents

Solvent	ε	n	$E_T(30)$	$\bar{v}_a - \bar{v}_f$ (cm^{-1})
Water	78.3	1.3300	63.1	6924.0
Dimethylformamide	38	1.4305	43.8	6580.3
Acetonitrile	37	1.3284	46.0	6406.9
Methanol	32.6	1.3284	55.4	6437.0
Ethanol	24.3	1.3614	51.9	6480.2
Acetone	20.7	1.3586	42.2	6460.0
Isopropanol	18.3	1.3856	50.7	6389.0
Hexanol	13.3	1.4178	48.8	6295.9
Dichloromethane	8.9	1.4241	41.1	6379.2
Ethylacetate	6	1.3724	38.1	6316.0
Diethylether	4.3	1.3520	34.6	6349.4
O- Xylene	2.4	1.5054	33.1	6309.8
Carbontetrachloride	2.2	1.4610	32.4	6277.3
Cyclohexane	2	1.4240	31.2	6155.2
SDS	21.83[a]	1.4011[a]	42.25[a]	6427.4[a]

a: These values estimated from our study.

5.3.4 EERS measurements

The EERS of QS^{2+} in bulk water is shown in Figure 5.7(A). The magnitude of EERS expressed as the difference in wavenumber (cm^{-1}) between the emission maximum obtained on 340 nm excitation and 400 nm excitation in bulk water solution is 679 cm^{-1} and is in agreement with the reported values.[32,50] Figure 5.7(B) shows the excitation wavelength dependence of fluorescence spectra of 0.4 mM concentration of SDS in QS^{2+} solution. At lower wavelengths of excitation (340 nm), the spectrum shows the fluorescence bands, one around 380 nm corresponding to complex formation and other around 420 nm, corresponding to QS^{2+} in bulk water solution. The magnitude of EERS increases remarkably in 0.4 mM concentration of SDS compared to that in bulk water system. Unlike bulk water system, a sudden shift in the emission maximum is observed on excitation around 400 nm and only one band is observed around 460 nm. The magnitude of EERS in 0.4 mM concentration of SDS is very large compared to the bulk water. The EERS calculated as the difference in wavenumber between the emission maximum obtained on excitations at 340 nm and 400 nm is around 2500 cm^{-1}. On further increase in concentration, a decrease is observed in the EERS. The excitation wavelength dependence of emission spectra of 10 mM of SDS is shown in Figure 5.7(C). The magnitude of EERS, calculated for concentrations 10 mM and above of SDS, is less when compared to that in bulk water solution of QS^{2+}.

The EERS in QS^{2+} in different environments has been studied extensively in the past and different explanations have been provided by different researchers. Chen[51] found red shift in emission spectrum of QS^{2+} on excitation at red edge of absorption band and suggested that it arises due to two close lying states. Fletcher [52] interpreted this effect as being due to the molecules existing in at least two different conformers each with its own electronic transition based on solvent relaxation modes. It is generally found that solvent bonding to chromophore restricts the position of auxochrome, which exists at least in two average conformers. Itoh and Azumi[53] gave an explanation that on excitation at the red edge of the absorption band only certain configurations are excited, resulting into red shifted emission which lacks some high frequency components compared to that due to short wavelength excitation.

We attribute this observed decrease in the magnitude of EERS to the decrease in the rate of solvent relaxation in the presence of SDS surfactant in the solution.

Water, being a highly polar hydrogen bonding solvent, could bring about significant stabilization of the electronic state of the polar probe as opposed to the less polar environment inside the surfactant aggregates. The decrease in EERS suggests that QS^{2+} is localized in a restricted inhomogeneous environment of micelles and most probably at the interface of water and surfactant, as the interfacial region is the preferred site for solubilization, even for hydrophobic molecules. This region offers considerable restriction to the reorientational motion of the solvent dipoles around the excited state QS^{2+}. Further, in a heterogeneous system of surfactants, the solute molecule may be distributed over a variety of locations ranging from polar region to relatively low polar region at the interface of water/surfactant and non-polar region far from the interface. As QS^{2+} is highly solvatochromic molecule, the fluorescence spectra depends on the polarity of the medium. So for QS^{2+} in surfactant systems it is possible to excite the molecule selectively at different locations which results in EERS in fluorescence spectra.

In bulk water solution the EERS is rationalized by the fact that the excitation of the solute is accompanied by a large change in dipole moment and the solvent reorientation time is not fast enough to bring the molecule in the relaxed state during the lifetime of the excited state. In SDS surfactant system due to heterogeneous restricted motion of solvent molecules the solvent relaxation process of accommodating the change in dipole moment of excited molecule further slows down which results in a decrease in net magnitude of EERS compared bulk water solutions. The location of QS^{2+} molecules in the surfactant solutions can be understood considering the nature of charge of surfactant molecules. The SDS anion has an opposite charge to that of QS^{2+} molecules, so its interaction with QS^{2+} is strong, owing to attractive electrostatic forces. As a consequence, QS^{2+} molecules are localized in a restricted inhomogeneous interfacial environment of water/surfactant.

The EERS in the fluorescence spectrum on REE is due to the slow rate of solvent relaxation around the excited molecule and is a function of motional restriction experienced by the solvent molecules around the fluorophore. This effect is generally observed in polar and viscous solutions, where the solvent relaxation time is of the order of or longer than the fluorescence lifetime of a probe molecule.

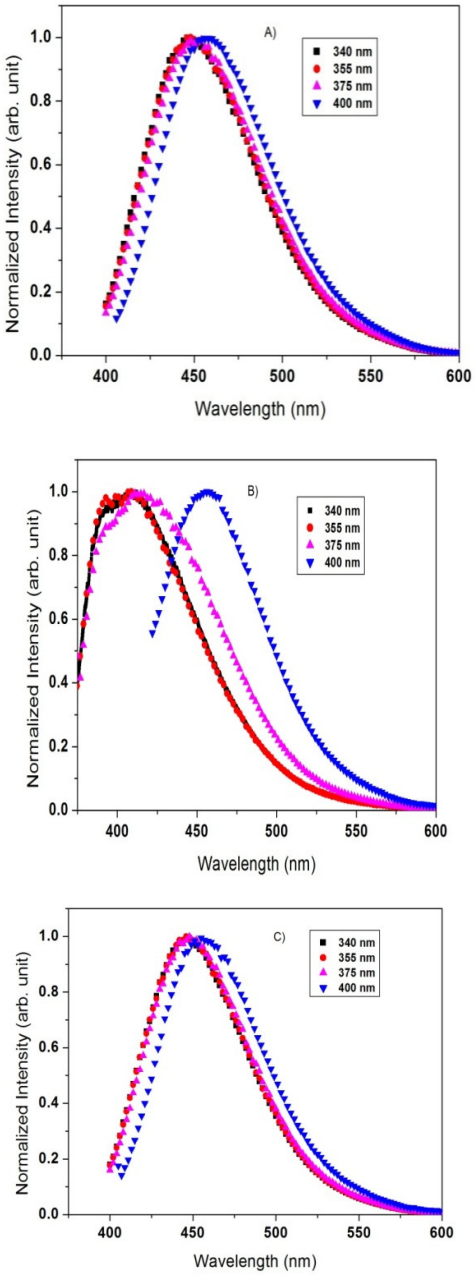

Figure 5.7 Excitation wavelength dependence of fluorescence spectra of QS^{2+} (10^{-4} M) in bulk water and in different micellar concentrations of SDS, (A) bulk water (B) 0.4 mM SDS and (C) 10 mM SDS

We have studied the solvation dynamics of Brij-30/cyclohexane reverse micelles, TX-100/cyclohexane reverse micelles, AOT reverse micelles, TGE/H_2O mixtures for different water concentrations at the surfaces of semiconducting nanoparticles.[54-58] The solvent relaxation rate inside the non-ionic reverse micelles were substantially reduced compared to the solvation dynamics of bulk water. The overall solvent relaxation process of water inside TX-100 reverse micelles was slower than the dynamics inside the Brij-30

or AOT reverse micelles. The dynamics of water inside the Brij-30 reverse micelles were relatively faster than dynamics of AOT reverse micelles at the same hydration level. The measured solvent relaxation process was significantly slower for TGE/H_2O mixtures compared to those for bulk water.

5.3.5 Fluorescence lifetime measurements

The fluorescence lifetime of a fluorophore in micellar solutions is very sensitive to the local environment around the probe and helps to understand the different interactions between the probe molecule and the micelle, the location of the probe in micelles, the local viscosity and polarity of the microenvironment.[59] Differential degrees of solvent motion around the fluorophore or partitioning of the fluorophore in distinct regions of a confined environment of micelles gives rise to different fluorescence lifetime components.

We have noticed the effect of varying the SDS surfactant concentration on fluorescence lifetime of QS^{2+} and Figure 5.8 shows the average lifetime of QS^{2+} for three different emission wavelengths as a function of concentrations of SDS. As we keep on increasing the surfactant concentration there is increase in average lifetime and this increase in lifetime is observed upto 8 mM concentration of SDS, after this concentration, on further increase in surfactant concentration the lifetime remains almost constant for all the three emission wavelengths studied. The mean fluorescence lifetime were calculated using Equation 1.34 (chapter 1) and are shown in Table 5.3. The fluorescence decays of QS^{2+} are triexponential at lower wavelengths of emission of QS^{2+} in SDS micellar solutions for all the concentrations of SDS studied. At higher concentrations of SDS, the fluorescence decays are biexponential for longer wavelengths of emission of QS^{2+}. The observed three fluorescence decay components for QS^{2+} in SDS micelles could be due to different conformers of QS^{2+} in SDS solutions. The increase in average lifetime at higher concentrations of SDS can be explained by the incorporation of QS^{2+} in premicellar and micellar aggregates of SDS. The higher value of decay time in SDS at the higher wavelengths of emission compared to bulk water, shows higher solubilisation of the probe in the Stern layer of SDS. The appreciable difference of the corresponding parameters in the SDS micelles and pure water rules out the possibility of location of QS^{2+} molecules around the bulk phase and suggest that most of the QS^{2+} molecules in SDS micelles are localized in micelle-water interface.

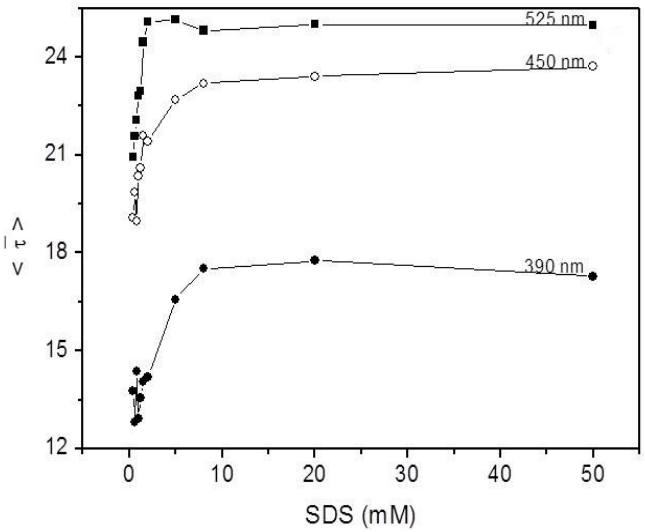

Figure 5.8 Variation of average lifetime of QS^{2+} with concentration of SDS, at three different emission wavelengths, excited at 300 nm

Table 5.3 Fluorescence quantum yield (ϕ), mean fluorescence decay time $\langle\bar{\tau}\rangle$ (λ_{em} = 450 nm) and radiative (k_r) and non-radiative (k_{nr}) decay constants of QS^{2+} in micellar media by varying the surfactant concentration

SDS Conc. (mM)	ϕ	$\langle\bar{\tau}\rangle$ (ns)	(k_r) (10^8 s^{-1})	(k_{nr}) (10^8 s^{-1})
0	0.55	19.92	0.27	0.23
0.4	0.82	19.08	0.43	0.10
0.6	0.82	19.85	0.41	0.10
0.8	0.63	18.96	0.33	0.20
1	0.83	20.34	0.41	0.10
1.5	0.66	21.60	0.31	0.16
2	0.57	21.41	0.27	0.20
5	0.64	22.70	0.28	0.16
8	0.70	23.20	0.30	0.13
20	0.57	23.41	0.24	0.18
50	0.57	23.70	0.24	0.18
100	0.57	23.69	0.24	0.18

As shown in Figure 5.8, the average fluorescence lifetime values of the probe in micellar media at lower concentrations of SDS are shorter than that in water at the lower wavelengths of emission, whereas the lifetime values are longer at longer wavelengths of emission. Both, at longer and shorter wavelengths of emission there is an increase in average lifetime with the increase in concentration of SDS. The fluorescence quantum yield calculated from the area of total fluorescence emission over the whole spectral range shows an increase in quantum yield in micellar solution for lower concentrations of SDS compared to the quantum yield in bulk water solution. The values of radiative (k_r) and non-radiative (k_{nr}) rate constants were calculated from the observed fluorescence quantum yield (ϕ), and average lifetimes $\langle\bar{\tau}\rangle$ using the Equations 4.1 and 4.2 (chapter 4) and corresponding values are given in Table 5.3. The increase in radiative rate particularly at lower concentrations of SDS is due to the fluorescent ion–pair complex formation. These ion-pairs are not stable at higher concentrations of SDS and surfactant molecules aggregate to form the micelles and consequently there is a decrease in radiative rate of QS^{2+} at higher concentrations of SDS.

5.3.6 Fluorescence quenching measurements

Quenching measurement can reveal the accessibility of fluorophores to the quencher.[60,61] Potassium chloride was used to quench the fluorescence of Quinine Sulfate dication (QS^{2+}) in homogeneous aqueous solution and in microheterogeneous environment formed by surfactant (SDS).We have calculated the quenching constant of QS^{2+} in bulk water (discussed in detail in chapter 4) and in the presence of SDS micellar solution. The absorption spectra for QS^{2+} in water as well as different micellar environments shows two bands, 348 nm and 318 nm, corresponding to L_a and L_b bands, respectively. The peak position as well as absorbance remains constant as we change/ increase the concentration of Cl^- ions from 0 mM to 35 mM for SDS micellar solution as well as bulk solutions studied. This clearly indicates that absorption spectrum is not sensitive to Cl^- ions and rules out the possibility of any complex formation in the ground state.

The fluorescence spectrum of QS^{2+} in micellar solution of SDS exhibits a broad band around 446 nm and is found to be very sensitive to addition of Cl^- ions and quench the fluorescence of QS^{2+}. Figure 5.9 shows the fluorescence spectra of QS^{2+} in SDS micellar solution. However, the reduction in fluorescence intensity in SDS micellar solutions is less than that in bulk water. The fluorescence decay curves of QS^{2+} is studied in microheterogeneous environment of SDS micelles, it can be seen from Figure 5.10 that fluorescence decay becomes biexponential at 450 nm emission wavelength for all concentrations of KCl studied from 0 to 35 mM and we observed that there is less reduction in lifetime as we increase the concentration of Cl^- ions, compared to bulk water. We found that the Stern-Volmer quenching constant (using Equation 1.35 discussed in chapter 1) decreased drastically from 132 M^{-1} in bulk water to 18 M^{-1} in SDS solution. The appreciable difference of the quenching constant in SDS micelles and pure water rules out the possibility of location of QS^{2+} molecules around the bulk phase of micelles and suggest that most of the QS^{2+} molecules in SDS micelles are localized in micellar-water interface. The surfactant dependence of the Stern-Volmer constant has been attributed to the location of the probe in the micellar environment. The fact that QS^{2+} molecules are less accessible to the quencher may be simply due to the strong interactions that occur between cationic QS^{2+} and anionic micelles attracting QS^{2+}molecules at the micelle-water interface, thus reducing and protecting its accessibility to the chloride quencher.

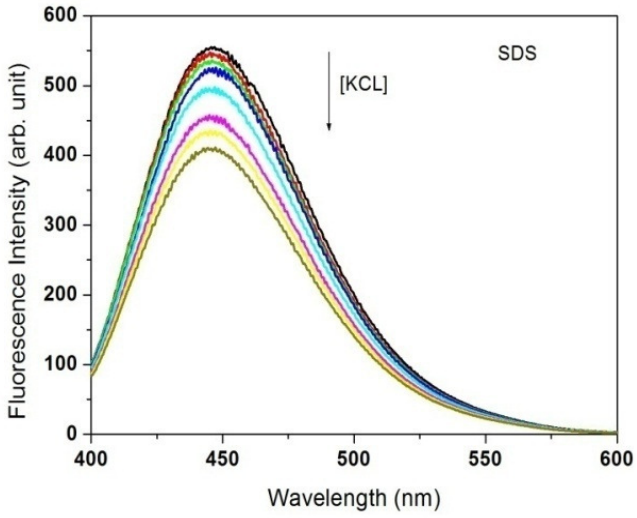

Figure 5.9 Fluorescence emission spectra of QS^{2+} in SDS micellar solution with increasing concentration of KCl from 0 to 35 mM, excited at 350 nm

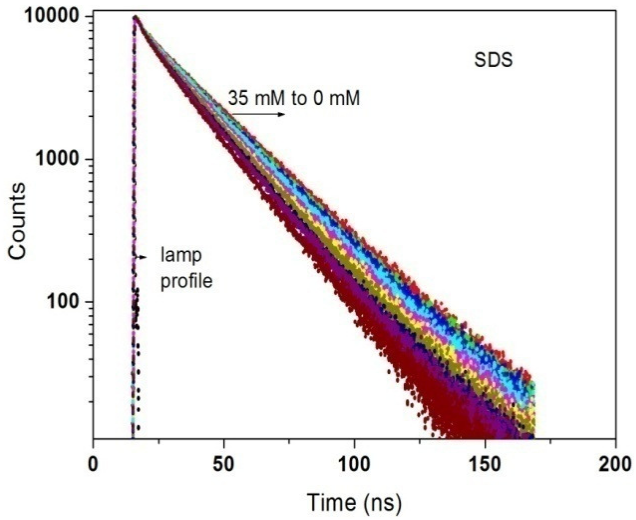

Figure 5.10 The fluorescence decay curve of QS^{2+} in SDS micellar solution with increasing Cl^- concentration, λ_{em} = 450 nm and λ_{ex} = 375 nm (The micellar concentrations for SDS = 50 mM)

5.3.7 Time-resolved fluorescence anisotropy measurements

Figure 5.11 shows the temporal anisotropy decay of QS^{2+} in water and in SDS micellar solution. As already discussed in chapter 4, the anisotropy decay of QS^{2+} in bulk water fits well to a single exponential decay function with rotational time of 314 ps. Whereas, the anisotropy decay measured for QS^{2+} in SDS micellar solution require a biexponential decay function for an acceptable fit. The functional form of the biexponential anisotropy decay r(t) in micelles can be represented as equation 4.3 (chapter 4). The average rotational time for QS^{2+} in SDS solution is longer than in the bulk water. The enhancement in the rotational relaxation time in SDS micellar media compared to pure aqueous media reflect that the fluorophore resides in a motionally restricted environment of micelles.

The observed large EERS and multiexponential decay of fluorescence for QS^{2+} at lower concentrations of SDS can be explained in terms of distribution of different conformers of different energies in the ground state. The EERS and multiexponential decay can arise when an inhomogeneous distribution of the molecules that differ in their solvation sites and in their energies exist in the ground state. This in homogeneity can originate from the difference in the interaction energies between the solvent molecules and the solute probe molecules. Selective excitation of the energetically different species will emit at different energies resulting in EERS and different fluorescence lifetime

components. In the present case, the electrostatic interaction between the anionic surfactant and cationic QS^{2+} is expected to dominate other interactions and probably plays the most important role in creating a distribution of energetically different molecular species in the ground state that allows their photoselection. Moreover, the solvent relaxation time of QS^{2+} is of the order of nanoseconds and is of the order of fluorescence lifetime. So un-relaxed fluorescence gives rise to the excitation wavelength dependent emission behaviour observed in the case of QS^{2+} molecules even in the case of bulk water solution. In the surfactant solutions, particularly at the low concentrations of surfactant, ion pairs of different energies exist in the solution which are highly fluorescent, so at lower wavelength of excitation all the ion pairs having different energies get excited giving the fluorescence corresponding to ion pairs and the bulk molecules in the solution. However on higher wavelength excitation, only the species having lower energies get excited and the fluorescence corresponding to the bulk species is observed. Thus the photoselection of the species by the excitation photons results in a continuous shift of the fluorescence spectrum resulting in a large magnitude of EERS. This model also explains the observed large FWHM at lower wavelength excitation compared to the FWHM at higher wavelength excitation.

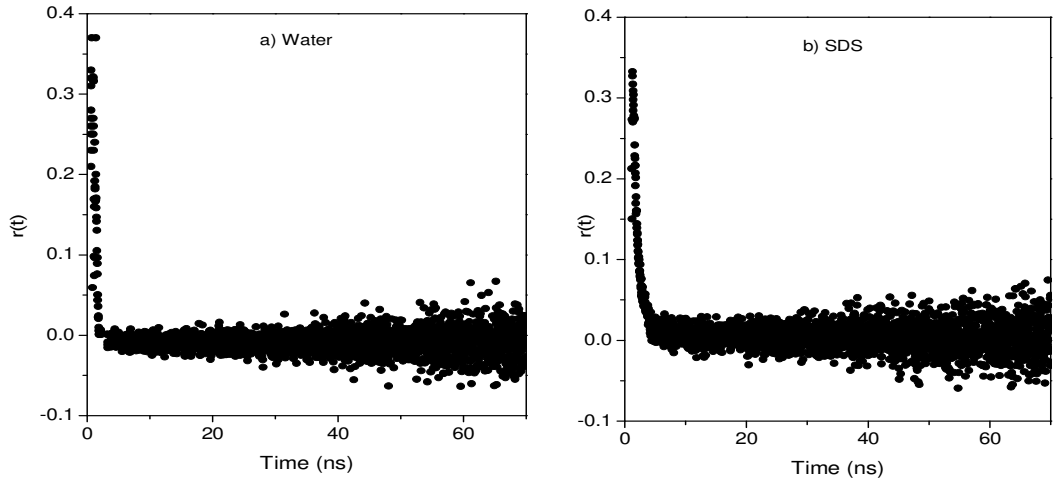

Figure 5.11 Time resolved fluorescence anisotropy decay profiles for QS^{2+} in bulk water and SDS micellar solution, (λ_{ex} = 375 nm, λ_{em} = 450 nm)

5.4 Conclusions

The location of QS^{2+} probe in SDS micellar solution has been ascertained by a variety of parameters such as dielectric constant, E_T (30), viscosity, absorption, emission, anisotropy, lifetimes and quenching constant etc. All these studies indicate that the probe

molecule binds strongly with the micelles and resides at the water-micelle interface in the SDS solutions. This study provides significant insight into the behaviour of the probe inside the micelles and its variation with change in surfactant concentration and modulated photophysics of QS^{2+} has been observed here in micellar environments compared to the photophysics of QS^{2+} in homogeneous environments.[32-35]

The decrease in absorbance and in fluorescence intensity, observation of a new fluorescent band around 380 nm at lower concentrations of SDS in aqueous solution of QS^{2+} are attributed to the fluorescent complex formation between the monomers of surfactant and QS^{2+} molecule surfactant. The complex formed in present system studied are highly fluorescent which are in general non fluorescent as observed for other systems studied in the past.[27-31] These fluorescent complexes are not stable and at higher concentrations of SDS, they dissociate to aggregate and to form the micelles. At higher concentrations of SDS, the decrease in the magnitude of EERS is due to the decrease in solvent relaxation rate as a consequence of restricted motion of the water molecules around the QS^{2+} in interfacial region, where its mobility is considerably reduced. At lower concentrations of SDS, the observed large magnitude of EERS is due to the presence of energetically different ion pairs in the ground state of QS^{2+}.

From the data of solvent effect on QS^{2+}, it is evident that the microenvironment around the probe molecule in SDS micelles is less polar and highly viscous than that of water and these observations are in agreement with other probe–micellar systems studied.[42-49] The time-resolved fluorescence decay analyses suggest distribution of different conformers of QS^{2+} of different energies in SDS micellar solution. The fluorescence anisotropy and quenching measurements reveal that the QS^{2+} molecules are in restricted environment.

This study clearly demonstrates that the photophysics of QS^{2+} is very sensitive to the local environment of the probe in SDS micelles. The remarkable sensitivity of QS^{2+} molecules to microstructures of surfaces and interfaces will attract attention to use this molecule as a probe to investigate the microstructure of different micelles and reverse micelles to understand its interactions with relevant biological media.

References:

(1) M. Purkait, S. DasGupta, S. De, *Sep. Purif. Tech.* **2004**, *37*, 81.

(2) M. Purkait, S. DasGupta, S. De, *J. Colloid Interface Sci.* **2004**, *270*, 496.

(3) P. Bilski, R. Holt, C. Chignell, *J. Photochem. Photobiol. A: Chem.* **1997**, *110* 67.

(4) A. R. Tehrani Bagha, H. Bahrami, B. Movassagh, M. Arami, F.M.Menger, *Dyes and Pigments* **2007**, *72*, 331.

(5) E. Kartal, H. Akbas, *Dyes and Pigments* **2005**, *65*, 191.

(6) A. K. Mandal, M. K. Pal, *Spectrochim. Acta Part A:* **1999**, *55*, 1347.

(7) R. Dutta, S. Bhat, *Bull. Chem. Soc. Jpn.* **1993**, *66*, 2457.

(8) M. Sarkar, S. Poddar, *J.Colloid Interface Sci.* **2000**, *221*, 181.

(9) M. J. Minch, S. S. Shah, *J. Org. Chem.* **1979**, *44*, 3252.

(10) S. Moulik, S. Ghosh, A. Das, *Colloid Poly. Sci.* **1979**, *257*, 645.

(11) A. Chakraborty, A. Mallick, V. Halder, P. Purkayastha, P. Das, N. Chattopadhyay, *Langmuir* **2007**, *23*, 4842.

(12) K. M. Chena, L. H. Lin, C. F. Wang, M. C. Hwang, *Colloids Surf. A: Physicochem. Eng. Aspects* **2010**, *356*, 46.

(13) L. Ramosa, M. Sch'onhoff, Y. Luana, H. M'ohwald, G. Brezesinski, *Colloids Surf. A: Physicochem. Eng. Aspects* **2007**, *303*, 79.

(14) T. M. Rana, *Nature Rev. Mol. Cell Biol*. **2007**, *8*, 23.

(15) M. R. Watry, T. L. Tarbuck, G. L. Richmond, *J. Phys. Chem. B* **2003**, *107*, 512.

(16) P. Mukherjee, K. J. Mysels, *J. Amer. Chem. Soc.* **1955**, *77*, 2937.

(17) G. V. Scott, *Anal. Chem.* **1968**, *40*, 768.

(18) B. Gohain, P. M. Saikia, S. Sarma, S. N. Bhat, R. K. Dutta*, Phys. Chem. Chem. Phys.* **2002**, *4*, 2617.

(19) M. R. Alavijeh, S. Javadian, H. Gharibi, M. Moradi, A. R. T. Baghab, A. A. Shahir, *Colloids Surf. A: Physicochem. Eng. Aspects* **2011**, *380*, 119.

(20) A. A. Shahir, S. Javadian, B. B. M. Razavizadeh, H. Gharibi, *J. Phys. Chem. B* **2011**, *115*, 14435.

(21) R. L. Reeves, S. A. Harkaway, in: K.L. Mittal (Ed.), *Micellization, Solubilization and Microemulsions*, vol.2, Plenum, New York, 1977.

(22) K. K. Karukstis, D. A. Savin, C. T. Loftus, N. D. D' Angelo, *J. Colloid Interface Sci.* **1998**, *203*, 157.

(23) Y. Guan, M. Antoniette, F. J. C. Faul, *Langmuir* **2002**, *18*, 5939.

(24) M. E. Diaz Gracia, A. San-Medel, *Talanta* **1986**, *33*, 255.

(25) R. K. Dutta, S. N. Bhat, *Bull. Chem. Soc. Jpn.* **1993**, *66*, 2457.

(26) M. Hojo, T. Ueda, T. Inoue, M. Ike, *J. Phys. Chem. B* **2007**, *111*, 1759.

(27) P. Mukherjee. K. J Mysels, *J. Am. Chem. Soc.* **1955**, *77*, 2937.

(28) J. Hevesi., Z. Rozsa , *Acta Phys. Chem.* **1971**, *17*,127.

(29) W. U. Malik , P. Chand, *J. Electroanal. Chem. Interfacial Electrochem.* **1972**, *40*, 385

(30) S. N. Guha, P. N. Moorthy , K. N. Rao, *Proc Indain Acad. Sci (Chem. Sci.)* **1982**, *91*,73.

(31) V. B. Gawandi, S. N. Guha, K. I. Piyadarsini, H. Mohan, *J Colloid Interface Sci.* **2001**, *242*, 220.

(32) D. Pant, U.C. Tripathi, G.C. Joshi, H.B. Tripathi, D.D. Pant, *J. Photochem. Photobiol. A: Chem.* **1990**, *51*, 313.

(33) D. Pant, H.B. Tripathi, D.D. Pant, *J. Photochem. Photobiol. A: Chem.* **1991**, *56*, 207.

(34) D. Pant, H.B. Tripathi, D.D. Pant, *J. Lumin.* **1991**, *51*, 249

(35) D. Pant, H.B. Tripathi, D.D. Pant, *J. Lumin.* **1992**, *51*, 223.

(36) A. Mallick, B. Haldar, S. Maiti, N. Chattopadhyay, *J. Colloid Interface Sci.* **2004**, *278*, 215

(37) M. Almgren, F. Grieser, J. K. Thomas., *J. Am. Chem. Soc.***1979**, *101*, 279.

(38) A. F. Tarek, E. L. Safaa, EL-Din, Z. Naglaa, *J. Lumin*. **2006**, *121*, 431

(39) Y. Qiao, S. Zhang, O. Lin, L. Deng, A. Dong, *J. Phys. Chem. B* **2007**, *111*, 11134.

(40) M. Thongngam, D. J. McClements, *Langmuir* **2005**, *21*,79.

(41) H. Maeda, S. Muroi, R. Kakehashi, *J. Phys. Chem.* **1997**, *101*,7378.

(42) A. Chakrabarty, P. Das, A. Mallick, N. Chattopadhyay, *J. Phys. Chem. B* **2008**, *112*, 3684.

(43) J. R. Lakowicz, *Principles of Fluorescence Spectroscopy*, Plenum, New York, 1999.

(44) A. Mallick, B. Haldar, N. Chattopadhyay, *J. Phys. Chem. B* **2005**, *108*, 14683.

(45) P. Das, A. Chakrabarty, B. Haldar, A. Mallick, N. Chattopadhyay, *J. Phys. Chem. B* **2007**, *111*, 7401.

(46) A. Mallick, B. Haldar, S. Maiti, S. C. Bera, N. Chattopadhyay*, J. Phys. Chem. B* **2005**, *109*, 14675.

(47) M. Shannigrahi, S. Bagchi, *Chem. Phys. Lett.* **2004**, *396*, 367.

(48) R. B. Macgregor, G. Weber, *Nature* **1986**, *319*, 70.

(49) M. Kumbhakar, S. Nath, T. Mukherjee, H. Pal, *J. Chem. Phys.* **2004**, *121*, 6026.

(50) H. C. Joshi, A. Upadhyay, H. Mishra, H. B. Tripathi, D. D. Pant, *J. Photochem. Photobiol.* A: Chem. **1999**, *122*, 185.

(51) R. F. Chen, *Anal. Biochem.* **1967**, *19*, 374.

(52) A. N. Fletcher, *J. Phys. Chem.* **1968**, *72*, 2742.

(53) K. Itoh, T. Azumi, *Chem. Phys. Lett.* **1973**, *22*, 395.

(54) D. Pant, N. E. Levinger, *Langmuir* **2000**, *16*, 10123.

(55) D. Pant, R. E. Riter, N. E. Levinger, *J. Chem. Phys.* **1998**, *109*, 9995.

(56) D. Pant, N. E. Levinger, *Chem. Phys. Lett.* **1998**, *292*, 200.

(57) D. Pant, N. E. Levinger, *J. Phys. Chem. B* **1999**, *103*, 7846.

(58) D. Pant, H. H. Girault, *Phys. Chem. Chem. Phys*. **2005**, *7*, 3457.

(59) A. Mahata, D. Sarkar, D. Bose, D. Ghosh, P. Das, N. Chattopadhyay, *J. Colloid Interface Sci.* **2009**, *335*, 234.

(60) D. K. Ranaa, S. Rakshit, S. Dhar, S. C. Bhattacharyaa, *J. Photochem. Photobiol. A: Chem.* **2013**, *270*, 67.

(61) Maria E. Pacheco, L. Bruzzone, *J. Lumin*. **2012**, *132*, 2730.

Chapter 6

Interaction of Quinine Sulfate with anionic micelles of Sodium dodecylsulfate: A time-resolved fluorescence study at different pH

6.1 Introduction

The study of photophysics and photochemistry of probe molecules at various surfaces and interfaces have been drawing the attention of the scientific community due to their vital role in many biological and natural processes.[1-3] Above a certain concentration, called Critical Micellar Concentration (CMC), surfactants in aqueous media form stable micelles of different shapes and sizes. These micelles having sizes in nanometer range may modulate the excited state relaxation processes of molecules due to their location with respect to the micelle-water interface. At the interface of self-organized assemblies, both the viscosity and static polarity of the medium differ considerably from those in bulk water and confinement imposes considerable restraints on the movement of reactants.[4,5]

Among many reactions one such reaction namely Excited State Proton Transfer (ESPT) is well known and one of the most fundamental phenomenon consist of a reversible adiabatic transfer of a proton. Recently, proton transfer attracts progressive interest to the researchers due to its key role in a variety of biological and chemical processes.[6,7] Excited state protonation and proton transfer reactions have been a subject of intense interest due to their potential applications in a variety of systems, such as fluorescent anion sensors and proton lasers.[8] The importance of ESPT phenomenon crops up even today given the promising roles of various ESIPT molecules in a vast range of applications, such as development of photostabilizers,[9,10] proton transfer lasers,[11-13] and white-light emitting diode.[14]

Proton transfer plays a vital role in fuel cell operation and in many enzymatic reactions.[15,16] Detailed studies of intermolecular Excited State Proton Transfer (ESPT) in confined media have increased dramatically for understanding the basic proton transfer dynamics.[17-20] Studies of different excited-state photoacids provide several pathways of excited state proton transfer reaction and roles of environment on proton transfer

dynamics.[17-21] Douhal et. al. demonstrated on the utilization of intermolecular ESPT chromophores to study the protein conformations and binding site polarity.[22]

ESPT investigations have been carried out on various molecules in microheterogeneous media formed by micelles, reverse micelles etc.[23-28] For instance, it was observed that the ESPT reaction in 2-(2'- pyridyl) benzimidazole is enhanced in the presence of Sodium dodecylsulfate (SDS) micelles, which was attributed to the increased local acidity at the micelle-water interface. [29] Arghya et. al.[30] observed that microhetrogenous media formed by SDS micelles enhance the ESPT reaction.

Hazara et. al.[31] reported the Photophysics and proton transfer dynamics of an eminent anticancer drug, Ellipticine (EPT) inside a biocompatible Octyl-β-D-Glucoside (OBG) micellar medium using steady state and time-resolved fluorescence spectroscopic techniques. EPT exists as protonated form in aqueous solution of pH 7. They observed that when EPT molecules are encapsulated in OBG micelles, protonated form is converted to neutral form in the ground state due to the hydrophobic effect of the micellar environment. Steady state fluorescence results indicated that both neutral and protonated forms of EPT exists in the excited state, even though neutral molecules are selectively excited, and it is attributing to the conversion of protonated to neutral form of EPT by Excited State Proton Transfer (ESPT) process. This kind of proton transfer dynamics is not observed in other conventional micelles, such as, SDS, TX-100 and CTAB, when studied with EPT. They assigned ESPT dynamics phenomenon to the combined effects of local dielectric constant felt by EPT and local proton concentration at the OBG micellar surface.

It is somewhat surprising in view of the usefulness of fluorescence studies to find that relatively few studies have been made in confined environments. Present chapter discusses the effect of microheterogeneous environment of SDS micelles on the photophysics of QS molecule at different pH and compared them. On changing pH, various species derived from QS are: dication (~pH 2), monocation (~pH 7) and neutral molecule (~pH 12).[32,33] We observed that photophysics of QS well known antimalarial agent, changes, when it is encapsulated inside one of the well studied anionic micelle, namely, SDS micelle. We have chosen SDS because it is well characterized micelle using various techniques.

The photophysical and /or photochemical properties of QS have been shown to be strongly dependent on the nature of the environment. Interestingly when we studied interaction of SDS with QS at different pH, it has been observed that the cationic form of Quinine Sulfate (at pH 2) forms a fluorescent ion-pair complex with the surfactant molecules at lower concentrations of surfactant, however, for higher concentrations of SDS, the probe molecule binds strongly with the micelles and resides at the water-micelle interface. At pH 7, QS is singly protonated in bulk aqueous solution and at lower concentrations of SDS aggregation between probe and surfactant molecules has been observed. Whereas, at higher concentrations of SDS at pH 7, an additional fluorescence peak corresponding to dicationic form of QS appears and this has been attributed to double protonation of the QS molecule. Different photophysical properties of QS studied at pH 7 show substantial changes in the presence of SDS micelles compared to that in the bulk water solution. At pH 12, an increase in fluorescence intensity and lifetimes has been observed and this is attributed to increase in radiative rate due to incorporation of QS at the micelle-water interface.

6.2 Experimental

Quinine Sulfate (QS) and Sodium dodecylsulfate (SDS) were purchased from Alfa Aesar and used as received. All the solvents were either of spectroscopic grade or were checked for their purity. All the samples of QS were prepared by dissolving the appropriate concentration of QS in Milli Q water. The final concentration of QS in all the systems studied was 10^{-4} M. NaOH and H_2SO_4 were used for the adjustment of pH of the solutions and were procured from Merck. Absorption spectra were taken using dual beam Thermo Evolution 201 UV/Vis/NIR spectrophotometer and fluorescence spectra were recorded using Shimadzu, RF-5301PC Spectrofluorometer. The data were analyzed using related software. The spectral shifts obtained with different sets of samples were identical in most of the cases and values were within ±1.0 nm. The fluorescence lifetimes were measured from time resolved intensity decays by the method of Time Correlated Single Photon Counting (TCSPC) technique. The light source used was picoseconds diode laser (Nano LED) at 300 nm (Horiba Jobin Yvon, USA).

6.3 Results and discussions

6.3.1 Steady state absorption and emission spectra

The molecular structures of various species derived from QS are shown in Figure 6.1. In order to demonstrate the effect of acidic and basic micellar environment, on to the photophysics of QS, steady state measurements are done at different pH of the surfactant solutions. The quinoline ring is a main fluorophore responsible for the absorption; methoxy group is very sensitive to the surrounding environment and responsible for photophysical behavior of QS.[33-38] The absorption spectrum of QS at pH 2 is distinctly different from that at pH 7 and pH 12. The absorption spectrum in aqueous bulk water at pH 2 shows two bands L_a and L_b at 348 and 318 nm, respectively, while at pH 7 and pH 12 the two bands L_a and L_b are at 330 and 280 nm, respectively. These band positions are in agreement with the reported absorption bands of QS in bulk water at different pH values.[33] These two bands correspond to low-lying closely spaced π, π^* states of the main chromophore.

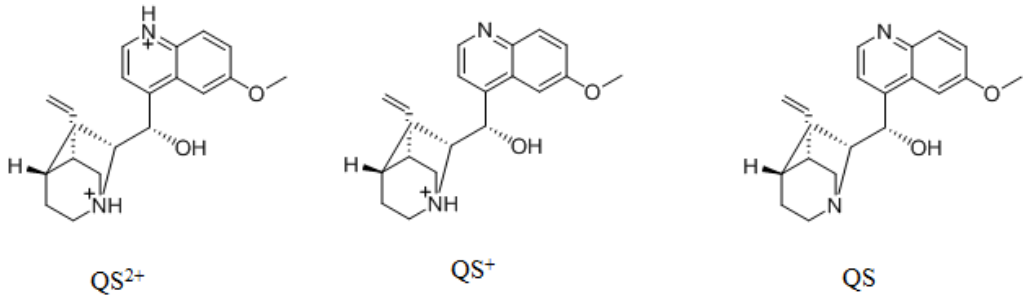

QS^{2+} QS^{+} QS

Figure 6.1 Structure of QS molecule various species at different pH dication (QS^{2+} ~pH 2), monocation (QS^{+} ~pH 7) and neutral molecule (QS ~pH 12)

The visible absorption spectra of fixed concentration of QS (10^{-4} M) in SDS surfactant for different concentrations ranging from 4×10^{-4} M to 5×10^{-2} M in aqueous media at 298 K at pH 2, pH 7 and pH 12 are illustrated in Figure 6.2(a), (b) and (c), respectively. At pH 2, for lower concentrations of SDS, the overall absorbance of QS decreases with the increase in concentration of SDS compared to the absorbance of QS in bulk water; however, with further increase in surfactant concentration the absorbance value increases. Whereas at pH 7, with the increase in concentration of SDS in bulk aqueous solution of QS, reduction in absorbance is observed upto 4 mM concentration of SDS. Further increase in concentration of SDS increases absorbance and the absorption peak corresponding to 330 nm becomes

structured. Further, a red shift of about 4 nm is observed for all the concentrations above CMC of SDS studied and absorbance value becomes almost equal to that observed for bulk water. At pH 12, the absorbance remains almost constant as we increase the concentration of SDS and this indicates that the absorption spectrum is not sensitive to the increase in SDS concentration at this pH.

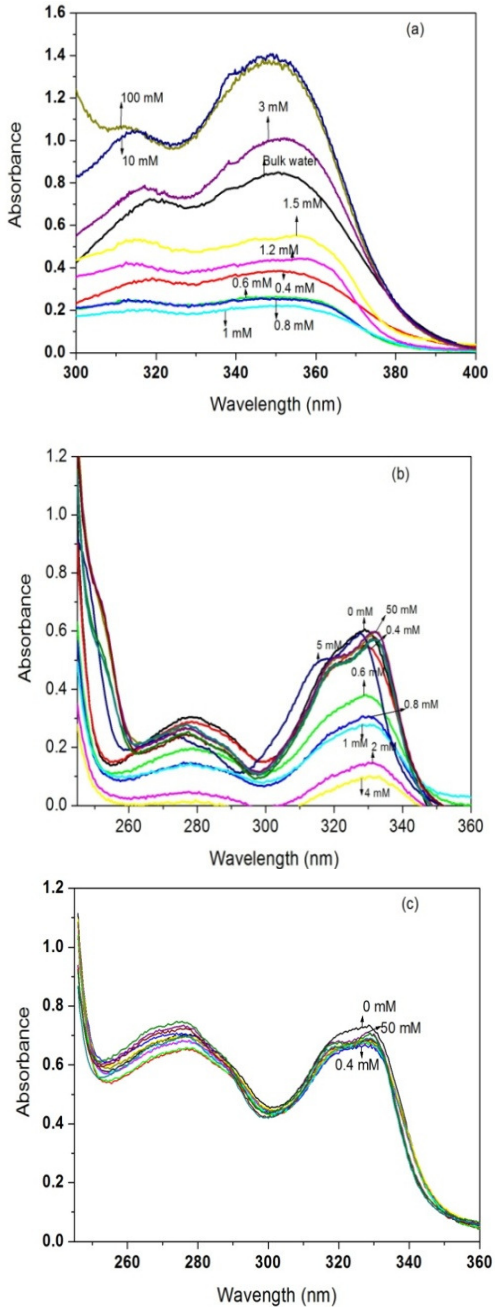

Figure 6.2 Absorption spectra of QS in bulk water and different micellar concentrations of SDS surfactant (a) at pH 2 (b) at pH 7 and (c) at pH 12

Figure 6.3(a) illustrates room temperature emission spectra of QS at fixed concentration in aqueous solution at pH 2 for different concentrations of SDS surfactant. In bulk water solution of QS, the emission spectrum has only a structure-less broad band with maximum around 447 nm on excitation at 355 nm. Initially, with gradual addition of SDS surfactant to an aqueous solution of fluorophore, one can see from spectra that for lower concentrations of SDS, the fluorescence intensity decreases with the appearance of an extra fluorescence band around 380 nm. On further increase in concentration, the intensity corresponding to the band around 450 nm decreases; whereas, the intensity corresponding to the band around 380 nm increases. At high concentrations of SDS, above 2 mM, the fluorescence intensity increases with the increase in concentration and the spectrum shows only one structure less band which corresponds to the fluorescence band of QS in acidic media in the presence of SDS molecules and in chapter 5, we have attributed this, new observed fluorescence band at lower concentrations of SDS to the fluorescent complex formation between the probe molecule and monomers of surfactant.[39] This complex does not exist at higher concentrations of SDS. At pH 7, in bulk water solution of QS, the emission spectrum has only one structure-less band with maximum around 390 nm as shown in Figure 6.3(b). This band corresponds to monocation form of QS.[33] On introducing a small amount of SDS (concentration 4×10^{-4} M) in QS aqueous solution at pH 7, the fluorescence intensity decreases upto 4 mM concentration of SDS and a shoulder appears as we move to higher concentration of SDS at 5 mM. A clear Stoke's shifted emission band around 452 nm appears for SDS concentrations around 5 mM and above. This 452 nm emission band that appears at concentrations around CMC of the surfactant is same as the emission band of the QS molecule at pH 2 in the absence of surfactant. Therefore, this cationic band of QS observed in the presence of SDS may be attributed to double protonation of the molecule at pH 7.

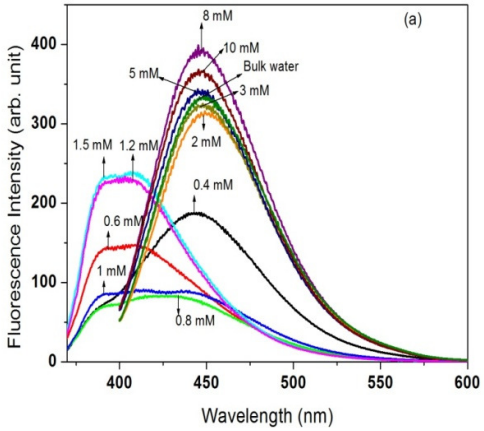

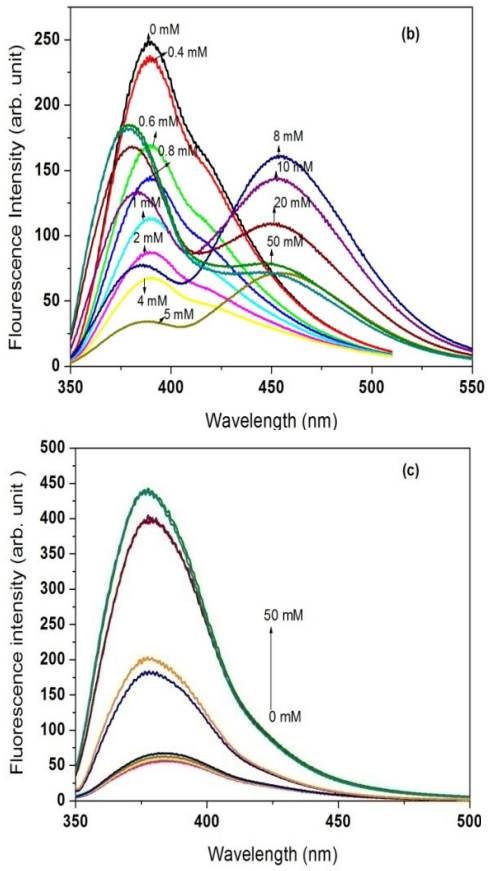

Figure 6.3 Fluorescence spectrum of QS in bulk water and in different concentrations of SDS, excited at (a) λ_{ex} = 355 nm at pH 2, (b) λ_{ex} = 330 nm at pH 7 and (c) λ_{ex} = 330 nm at pH 12

It is interesting to note that the observed cationic fluorescence band (around 452 nm) of QS at pH 7, first increases in intensity on increasing the concentration of the surfactant upto its CMC value and then starts decreasing in intensity as more surfactant is added above CMC. For higher concentrations of SDS, the peak corresponding to monocation form (around 390 nm) becomes more intense and a blue shift has been observed as shown in Figure 6.3(b). If micelle formation was involved in the appearance of the cationic band (around 452 nm), then the fluorescence intensity of this band would have increased continuously with the increase in SDS concentration. So the observed decrease in the fluorescence intensity of the 452 nm band above CMC rules out involvement of micelles in the formation of the band. Appearance of the dicationic peak around 450 nm could simply be due to double protonation of the QS molecule. Further, this could be explained in terms of lowering of local pH at the micelle-water interface as the concentration of protons at a negatively charged micellar surface is higher than that

in bulk aqueous phase. Figure 6.4 clearly shows that by introducing SDS, in the aqueous solution of QS, the pK_A value get reduced to 5.6 from the reported value of 9.7 in bulk water.[33] So this leads to lower value of local pH at the surface of SDS micelles. The observed decrease in local pH of QS solution in the presence of SDS at pH 7, is an indication of the further protonation of the molecule. It is possible that the strong electrostatic interaction between the QS molecules and surfactant ions at the interface provide the way for the second protonation of the molecule. Mukherjee et. al.[29] has observed similar kind of effect when studied 2PBI (2-(2'-pyridyl) benzimidazole) at micelle-water interface. They observed that ESPT, which occurs to a rather small extent at pH 7, has been found to be enhanced remarkably at the interface of SDS micelles and water. They explained it in the light of change of pK_A and a more acidic local pH in the micelle-water interface. As we can see from Figure 6.3(b) that once micelle formation is complete at higher SDS concentrations, the peak corresponding to monocation form get intense with the blue shift of the position compared to bulk emission. This could be due to incorporation of QS probe molecules inside micelle so experiencing less polar environment and hence blue shift. We have discussed earlier in chapter 5 that QS molecules form closely packed ion-pairs with SDS at concentrations lower than CMC and these ion-pair break down as the micelles are formed above CMC of the surfactant.[39] Thus the close packing of micelles above CMC is paving way for the protonation of the molecule. Whereas, at pH 12, this molecule is in neutral form, it can be seen from Figure 6.3(c) that the emission spectrum is broad and unstructured with a maximum around 386 nm. The fluorescence intensity remains almost constant upto 2 mM concentration of SDS, on further gradual addition of SDS concentration, increase in fluorescence intensity is observed and a few nanometer blue shift is also observed. This indicates, after 2 mM concentration of SDS, the probe bound to the micellar surface leading to decrease in the rate of radiationless process caused by decrease in the polarity and/or hydrogen bonding capacity and a decrease in the free motion of probe on the micellar surface.

The change in fluorescence maximum and intensity with the addition of surfactant can be attributed to the passage of QS molecules from highly polar aqueous medium to a relatively non-polar micellar environment. In the present study, as the fluorescence intensity of water soluble QS changes with the change in concentration of SDS, this observation is used to determine the CMC of SDS, from the fluorescence

intensity data at different concentrations of SDS. The ratio of fluorescence intensities of QS in the absence and presence of surfactant vs concentration of surfactant are shown in Figure 6.5(a), (b) and (c) at pH 2, pH 7 and pH 12, respectively. The resulting sharp break points in intensity of fluorescence of probe molecule correspond to the CMC value of the surfactant. Clearly, there are two break points for pH 2 and pH 7 solutions. At pH 2, first point is around 0.8 mM and second one is around 2 mM. At pH 7, the first break point is around 4.4 mM and the second one is at 8 mM. Thus we get two CMC values at these two pH values and has been observed by other researchers also in other systems.[40] The lower CMC could be attributed to the aggregation of probe-surfactant and second higher one is assigned to some phase transformation corresponding to a change in micelle size/or shape. Whereas, at pH 12 (Figure 6.5(c)) there is only one break point that is around 8 mM, which corresponds to the normal CMC of SDS.[41]

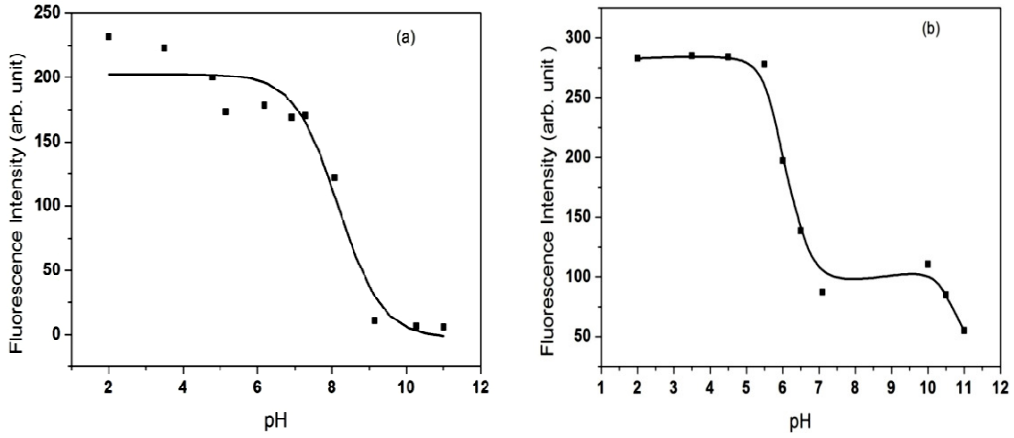

Figure 6.4 Plot of fluorescence intensity of QS vs pH of the solution, (a) bulk water, (b) 10 mM SDS micelle

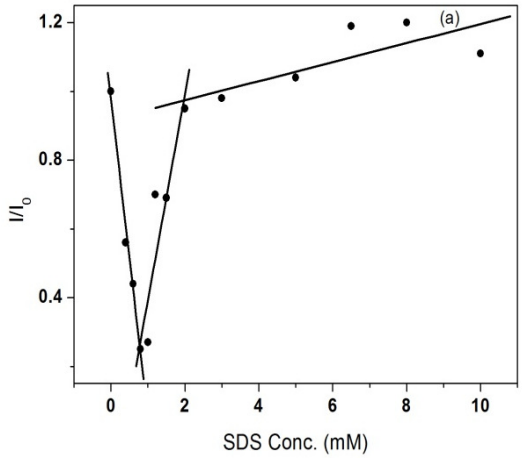

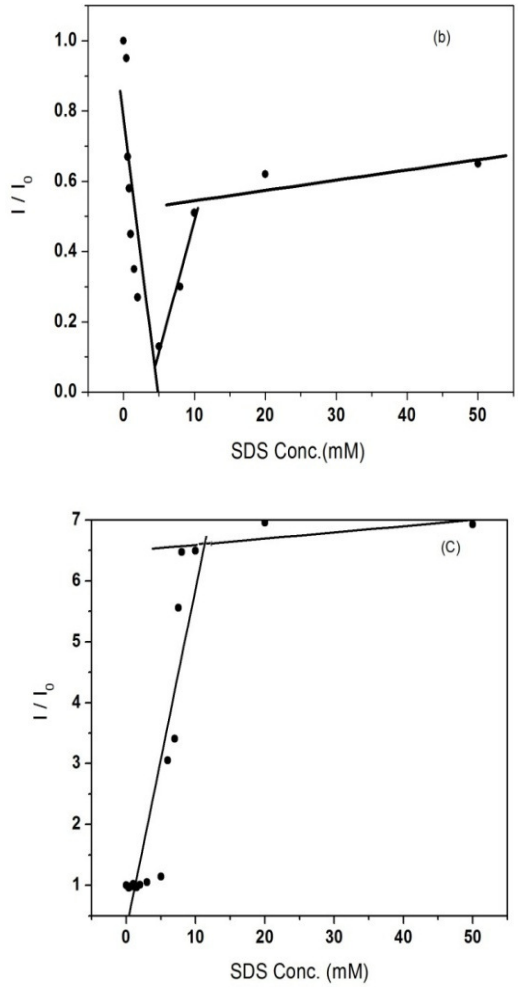

Figure 6.5 The ratio of fluorescence intensities of QS in the absence (I_0) and presence (I) of SDS surfactant as a function of SDS surfactant concentration, (a) pH 2, (b) pH 7 and (c) pH 12

6.3.2 Polarity of the micellar microenvironment and probable location of the fluorophore

Micelles are generally characterized by three distinct regions: a non-polar core formed by the hydrocarbon tails of the surfactant, a compact stern layer having the headgroups, and a relatively wider and diffuse Gouy-Chapman layer that encompasses majority of the counter ions. Depending on the nature of the probe and the micelle, a probe molecule may bind either to the non-polar core of micelles or to the micelle-water interface. From the absorption and fluorescence spectra of probe in different solvents, we calculated the corresponding Stoke's shift and the relevant data are given in Table 6.1 and corresponding plots are shown in Figure 6.6.

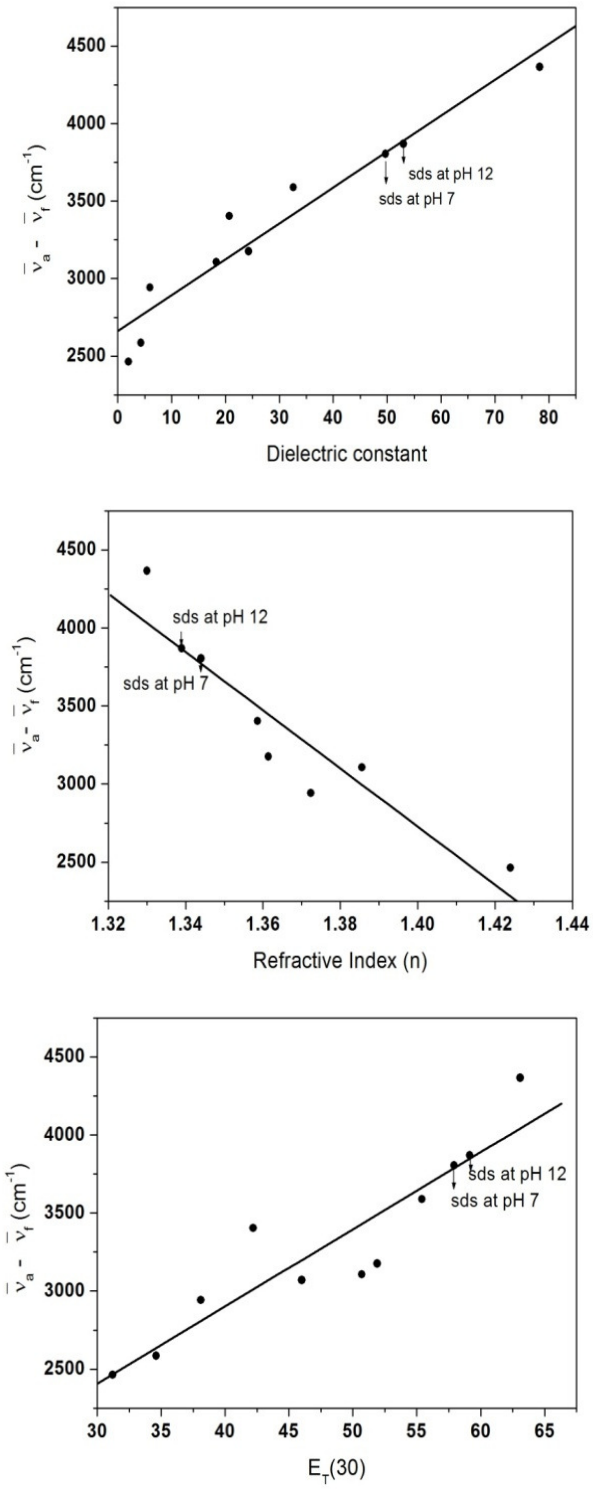

Figure 6.6 Stokes shift of QS vs. solvent dielectric constant, refractive index and $E_T(30)$ respectively

The QS molecules at pH 2, pH 7 and pH 12 dissolved in surfactant SDS solutions are in new kind of solvent environment having very different polarity, refractive index and $E_T(30)$ than that of water. As the values of $E_T(30)$ and dielectric constant in SDS micelles are lower than that of bulk water and refractive index is larger than that of water, we conclude that the probe QS resides in interfacial region of the micelle.

Table 6.1 Different solvent parameters and spectral data of QS in different solvents

Solvent	ε	n	$E_T(30)$	$\bar{\nu}_a - \bar{\nu}_f$ (cm^{-1})
Water	78.3	1.3300	63.1	4367.0
Acetonitrile	37	1.3284	46.0	3071.0
Methanol	32.6	1.3284	55.4	3589.0
Ethanol	24.3	1.3614	51.9	3177.0
Acetone	20.7	1.3586	42.2	3404.0
Isopropanol	18.3	1.3856	50.7	3107.0
Dichloromethane	8.9	1.4241	41.1	3711.0
Ehylacetate	6.0	1.3724	38.1	2943.0
Diethylether	4.3	1.3520	34.6	2568.0
Cyclohexane	2.0	1.4240	31.2	2464.0
SDS (at pH 2)	21.8[a]	1.4011[a]	42.25[a]	6427.4[a]
SDS (at pH 7)	51.2[b]	1.3440[b]	57.92[b]	3804.7[b]
SDS (at pH 12)	55.6[b]	1.3390[b]	59.15[b]	3869.9[b]

a: Taken from paper.[36]

b: These values estimated from our study.

6.3.3 Steady state fluorescence and fluorescence anisotropy correlation

Steady state anisotropy (r) plays very important role in biochemical and biophysical research owning to their ability to produce valuable information about environments in immediate vicinity of the fluorophore. An increase in the rigidity of the neighbouring environment of a fluorophore results in increase in fluorescence anisotropy. Thus study of fluorescence anisotropy provides information about probable location of the probe in microheterogeneous environments.[42] Fluorescence anisotropy (r) measurements were also performed since this parameter serves as a sensitive indicator for monitoring fluorophore binding to motionally constrained regions of biological

membrane[43]. The value of *r* is expected to be very low in fluid solution where the fluorophore can freely rotate, and high for rigid environment. The variation of steady state fluorescence intensity and steady state anisotropy as a function of SDS concentration are given Figure 6.7. In the present study, the steady state fluorescence anisotropy of QS calculated using Equation 1.38 (chapter 1). In SDS solutions at premicellar concentrations due to complex formation or premicellar aggregation there is decrease in anisotropy or remains constant and same is observed for fluorescence intensity for all the values of pH studied. However, around CMC and for higher concentrations of SDS (concentrations larger than CMC of surfactant), the anisotropy and fluorescence values increases and become constant for all values of pH studied. The increase in anisotropy value with the increase in pH of the surfactant solution indicates that the motional restriction of the molecules increases with the increase in pH of the solution.

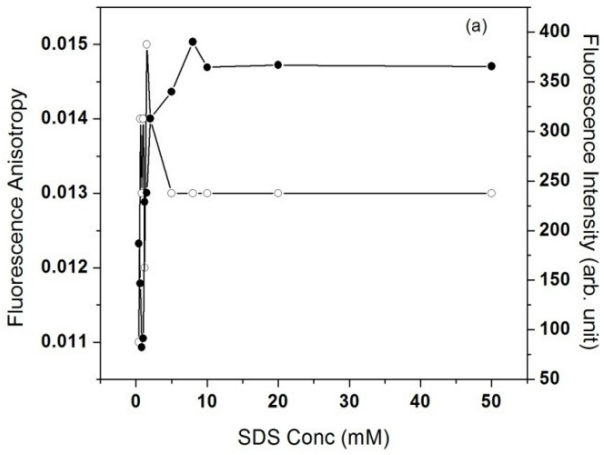

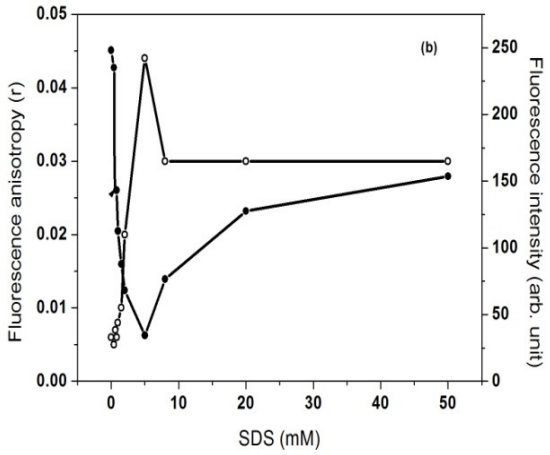

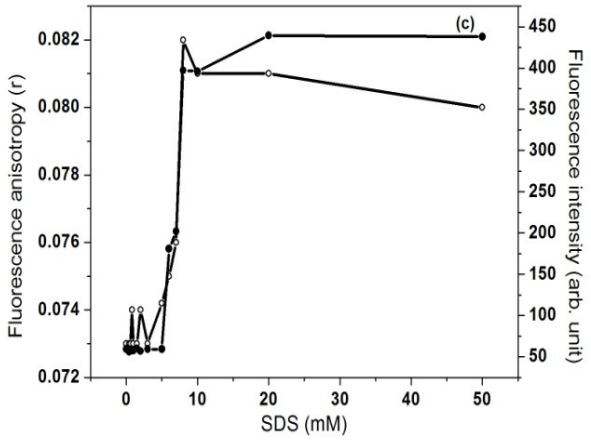

Figure 6.7 Variation of steady state fluorescence anisotropy (open circle) and intensity (closed circle) respectively of QS with increasing concentration of SDS. (a) at pH 2, λ_{em} = 450 nm (b) at pH 7, λ_{em} = 390 nm and (c) at pH 12, λ_{em} = 390 nm

6.3.4 Fluorescence lifetime measurements

The fluorescence lifetime is a useful parameter to get ideas about local environment around a fluorophore because of its sensitivity to excited state interactions. Fluorescence lifetime serves as an excellent indicator to discuss the location of probe in a multicomponent environment.[44] Differential degree of solvent relaxation around the fluorophore in distinct regions of a confined environment give rise to differences in fluorescence lifetime of the fluorophore. So photophysical response of QS at pH 2, pH 7 and pH 12 in micellar microenvironment formed by SDS is compared with aqueous bulk media.

As shown in Figure 6.8(a), (b) and (c), we have noticed the effect of varying the SDS surfactant concentration on fluorescence lifetime of QS at different pH values at pH 2, pH 7 and pH 12, respectively. The average fluorescence lifetime value of the probe in micellar media at lower concentrations of SDS is shorter than that in water, at lower wavelengths of emission. Both, at longer and shorter wavelengths of emission, there is an increase in average lifetime with the increase in concentration of SDS. The mean fluorescence lifetime were calculated using the Equation 1.34 (chapter 1) and are summarized in Table 6.2.

As can be seen from Table 6.2 at pH 7, the fluorescence decay of QS is triexponential at lower wavelengths of emission of QS in SDS micellar solutions for all the concentrations of SDS studied. At longer emission wavelengths fluorescence decay is biexponential and the lifetime observed here at pH 2 are same as observed for dicationic form of QS at higher

concentrations of SDS, which we have already discussed in chapter 5. The observation of increase of fluorescence lifetime with the wavelength of emission and the observation of negative component for longer wavelengths of emission of QS are salient features of solvent relaxation process.[34] The increase in average lifetime at higher concentrations of SDS can be explained by the incorporation of QS^{2+} in premicellar and micellar aggregates of SDS. At pH 12, the fluorescence lifetime is very less when compared with the lifetimes measured at pH 2 and pH 7. The average fluorescence lifetime of QS increases as we increase concentration of SDS at pH 12. The fluorescence decays of QS are triexponential at all wavelengths of emission of QS in SDS micellar solutions for all the concentrations of SDS studied and are summarized in Table 6.2. The mean fluorescence lifetimes of QS in surfactant solutions is significantly different from bulk solutions.

Table 6.2 Fluorescence lifetime data of QS for different concentrations of SDS, excited at 300 nm wavelength

SDS (mM)	λ_{em}	τ_1 (ns)	α_1	τ_2 (ns)	α_2	τ_3 (ns)	α_3	$\chi 2$	$\langle\bar{\tau}\rangle$ (ns)
pH 2									
0	390	2.05	0.009	18.25	0.018	-	-	1.19	17.38
	540	1.28	-0.006	20.89	0.032	-	-	1.16	21.12
0.6	390	0.28	0.009	2.46	0.005	17.38	0.002	1.13	12.80
	540	0.53	-0.002	2.23	-0.001	21.19	0.008	1.13	21.58
8	390	0.29	0.030	2.80	0.021	22.80	0.008	1.03	17.51
	540	1.99	-0.008	24.38	0.034	-	-	1.05	24.81
50	390	0.31	0.039	2.87	0.021	23.76	0.007	1.06	17.29
	540	1.97	-0.009	25.21	0.035	-	-	1.05	25.68
pH 7									
0	330	1.37	0.029	3.73	0.016	-	-	1.19	2.79
	430	5.03	0.029	14.34	0.006	-	-	1.14	8.48
0.6	330	0.12	0.130	1.25	0.025	3.56	0.012	1.19	2.15
	430	4.72	0.030	14.11	0.005	-	-	1.15	7.84
8	330	0.27	0.065	1.30	0.023	5.49	0.001	1.21	1.39
	450	6.35	0.005	17.38	0.025	-	-	1.10	16.62
	525	0.38	-0.032	18.04	0.033	23.42	-0.002	1.17	17.97
50	330	0.17	0.027	1.94	0.022	3.08	0.016	1.03	2.44
	450	4.23	0.007	23.79	0.024	-	-	1.00	22.83
	525	1.93	-0.005	24.58	0.027	-	-	1.00	24.91

pH 12									
0	330	0.18	0.039	1.43	0.001	-	-	1.16	0.39
	430	0.28	0.028	2.63	0.0005	-	-	1.18	0.62
0.6	330	0.06	0.089	0.29	0.008	1.77	0.0005	1.01	0.30
	430	0.12	0.038	0.47	0.007	3.28	0.0003	1.11	0.60
8	330	0.22	0.006	0.74	0.012	2.25	0.0008	0.98	0.86
	430	1.03	0.009	3.72	0.003	17.67	0.0003	1.08	5.62
50	330	0.08	0.011	1.94	0.013	2.26	0.0008	0.97	0.89
	430	1.07	0.008	3.76	0.003	19.00	0.0004	1.05	7.14

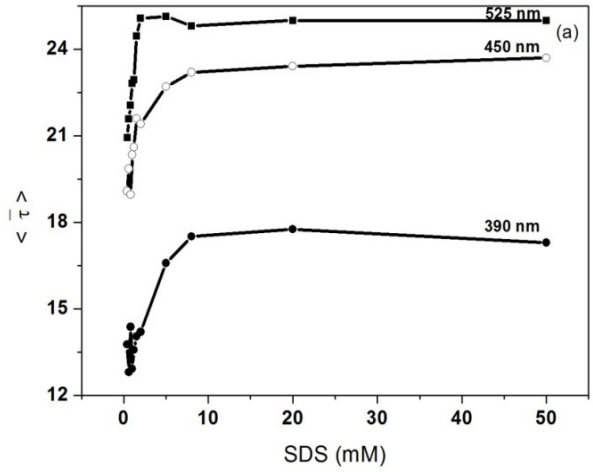

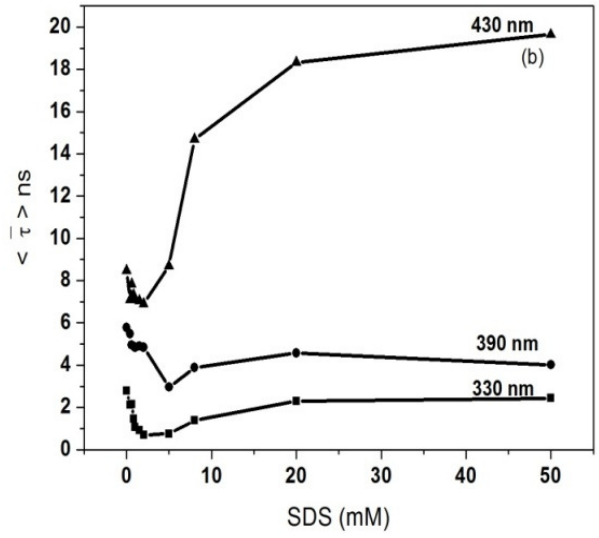

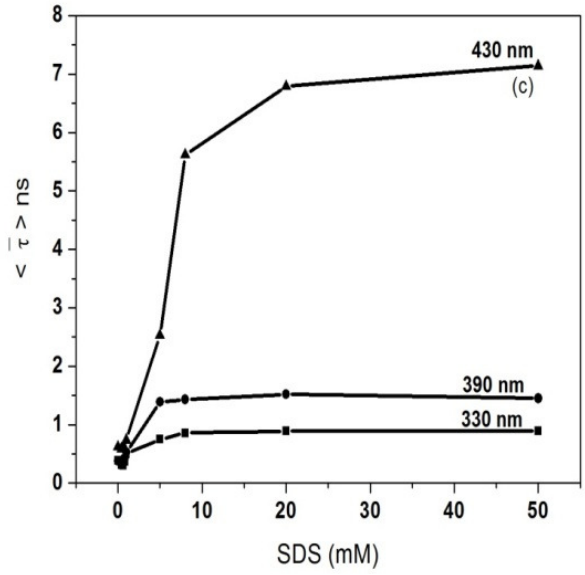

Figure 6.8 Variation of average lifetime of QS with concentration of SDS, at three different emission wavelengths, excited at 300 nm, (a) at pH 2, (b) pH 7 and (c) pH 12

The appreciable difference of the corresponding parameters of fluorescence decay at different pH, studied in bulk aqueous solution and in SDS micelles, indicate that the local environment experienced by QS molecules is different in surfactant solutions at different pH and rules out the possibility of location of QS molecules around the bulk phase. This observation suggests that most of the QS molecules in SDS micelles are localized in micelle-water interface.

At pH 2 the fluorescence quantum yield calculated from the area of total fluorescence emission over the whole spectral range shows an increase in quantum yield in micellar solution for lower concentrations of SDS compared to the quantum yield in bulk water solution, which we have already discussed in chapter 5.[39] At pH 7, minor increase has been observed in quantum yield in micellar solution for lower concentrations of SDS compared to the quantum yield in bulk water solution. For the concentrations around CMC and above it is almost same as for bulk solution. The values of radiative (k_r) and non-radiative (k_{nr}) rate constants are calculated from the observed fluorescence Quantum yield (ϕ), and average lifetimes $\langle\bar{\tau}\rangle$ using the Equations 4.1 and 4.2 respectively (discussed in chapter 4) and the corresponding values are given in Table 6.3. At pH 12, as we increase the concentration of SDS, quantum yield increases due to the increase in fluorescence intensity of QS in the micellar medium at higher concentration of SDS. This could be due to association of the probe in less polar site

within the micelle as compared to aqueous phase and also fluorescence yield may be due to decrease in non-radiative relaxation in the confined cavity and the corresponding values are given in Table 6.3.

It can be noted that the observed triple exponential decay at lower wavelengths of emission of QS at pH 7 is in conformity with the proton transfer in the excited state and subsequent formation of dication. The longer lived (τ_2) component of decay can be attributed to the proton transfer state and shorter lived (τ_1) component to the original locally excited state which gives rise to the ESPT state. The (τ_3) component is due to the decay of emission of the dicationic form of the probe molecule. At pH 12, as already discussed earlier, both, the fluorescence intensity as well as average lifetime increases considerably for concentrations of SDS around and above the CMC of SDS. As there is no significant change in absorbance with the increase in SDS concentration, this increase in intensity and lifetime can be attributed to increased radiative rate of QS due to its incorporation at the micelle-water interface.

Table 6.3 Fluorescence Quantum yield (ϕ), mean fluorescence decay time $\langle\bar{\tau}\rangle$ (λ_{em} = 390 nm), and radiative (κ_r) and non-radiative (κ_{nr}) decay constants of QS in micellar media by varying the surfactant concentration

	pH 7				pH 12			
SDS Conc. (mM)	ϕ	$\langle\tau\rangle$ (ns)	κ_r (10^8 s^{-1})	κ_{nr} (10^8 s^{-1})	ϕ	$\langle\tau\rangle$ (ns)	κ_r (10^8 s^{-1})	κ_{nr} (10^8 s^{-1})
0	0.29	5.03	0.06	0.14	0.12	0.38	0.31	2.31
0.4	0.34	5.48	0.06	0.12	0.14	0.37	0.37	2.32
0.6	0.34	4.95	0.07	0.13	0.14	0.39	0.36	2.21
0.8	0.38	4.91	0.08	0.13	0.15	0.42	0.36	2.02
1	0.42	4.85	0.09	0.12	0.15	0.53	0.28	1.60
1.5	0.40	4.91	0.08	0.12	0.15	0.48	0.31	1.77
2	0.43	4.85	0.09	0.12	0.15	0.54	0.28	1.57
5	0.30	2.96	0.04	0.29	0.15	1.39	0.11	0.61
8	0.29	3.88	0.07	0.18	0.74	1.43	0.52	0.18
20	0.30	4.57	0.07	0.15	0.81	1.52	0.53	0.13
50	0.28	4.02	0.07	0.18	0.82	1.45	0.56	0.12

The complex decay kinetics across the emission band of QS studied at different pH is due to the presence of different interconvertible species (dication, monocation and neutral molecules) having different geometries**.** The observation of fluorescence from both the cation and neutral molecule is an indication of a partial establishment of equilibrium in the lowest excited state.

6.3.5 Time –resolved fluorescence anisotropy measurements

The time-resolved decay of the fluorescence anisotropy provides significant insights about the rotational relaxation of the fluorophore in organized assemblies.[45] Therefore, with a view to delve into the microenvironment formed by the SDS micelle, time resolved fluorescence anisotropy of QS at different pH has been recorded. In bulk water the anisotropy decay at pH 2, pH 7 and pH 12 is monoexponential and the observed time constant are 0.3 ns, 0.6 ns and 2.0 ns respectively. All the data related to anisotropy decay measurements are summarized in Table 6.4.

Table 6.4 Time resolved decay parameters of fluorescence anisotropy of QS at different pH in bulk water and micellar media

Environment	λ_{em} (nm)	τ_1 (ns)	α_1	τ_2 (ns)	α_2	$\langle\bar{\tau}\rangle$ (ns)
Water (pH 2)	450	0.3	1	-	-	0.3
SDS (50 mM) (pH 2)	450	0.5	0.58	1.3	0.42	1.0
Water (pH 7)	390	0.6	1	-	-	0.6
SDS (50 mM) (pH 7)	390	1.2	1	-	-	1.2
Water (pH 12)	390	2.0	1	-	-	2.0
SDS (50 mM) (pH 12)	390	5.3	0.30	1.9	0.70	3.0

Figure 6.9 shows the temporal anisotropy decay of QS in water and in SDS micellar solution at different pH. The anisotropy decay of QS bound to SDS micelle is found to be slower for all the three pH values studied compared to that in bulk water. The anisotropy decay of QS in micelles is biexponential at pH 2 and pH 12, whereas, single exponential at pH 7. The larger rotational time at pH 12 in bulk solution compared to pH 2 and pH 7 may be simply due to the increase in viscosity of the solution. Aggregation of QS molecules at pH 12 can be an additional factor for the observed increase in time constant. The observed longer time constants in micellar solutions compared to that in bulk water may be ascribed to the larger volume of rotating species

(probe molecule along with the micelle). The time-resolved anisotropy results reveal that the motional restriction of the QS molecules increases with the increase in pH of the solution. This observation is in agreement with the results obtained using steady state anisotropy measurements.

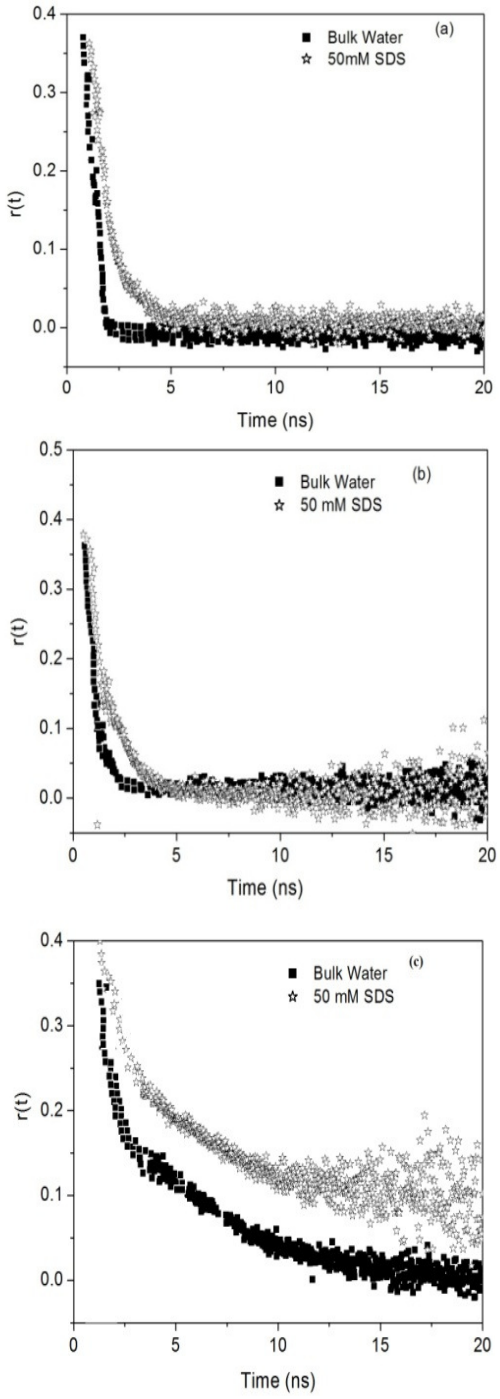

Figure 6.9 Time resolved fluorescence anisotropy decay profiles for QS in bulk water and 50 mM SDS micellar solution, (a) pH 2 (λ_{ex} = 375 nm, λ_{em} = 450 nm) (b) at pH 7 (λ_{ex} = 300 nm, λ_{em} = 390 nm) (c) at pH 12 (λ_{ex} = 300 nm, λ_{em} = 390 nm)

6.4 Conclusions

In this chapter we have investigated the effect of anionic surfactant SDS on photophysics of QS at pH 2, pH 7 and pH 12. The photophysical behaviour of QS is dramatically modified in micelles from that in bulk aqueous phase. At pH 2, the observed new fluorescent band around 380 nm, at lower concentrations of SDS in aqueous solution of QS, is attributed to the fluorescent complex formation between monomers of surfactant.

These fluorescent complexes are not stable and at higher concentrations of SDS, they dissociate to aggregate and to form the micelles. At pH 7, as we increase the concentration of SDS, proton transfer phenomenon is favoured due to change in local pH in the micellar surface region. The results indicate that at pH 7, in the presence of SDS micelles, hydrophobic microenvironment enhances the dication emission and also causes an increase in lifetime of dication emission. The monocationic QS molecules get protonated to form dicationic molecule due to the change in local pH at the micelle-water interface. The SDS micelles, at pH 7, promote the ESPT and consequently lead the formation of dicationic species of QS in the excited state. No ESPT has been observed for the dicationic and neutral forms of QS. Time-resolved studies of QS show very different excited state dynamical properties in premicellar and micellar regions. The information on electrostatic and hydrophobic interactions studied in this chapter may add to our understanding pertaining to biological systems. The shift in fluorescence due to formation of the dication can make it a potential sensor for negatively charged surfaces. The present study have shown that solvent environment sensitive fluorescence of QS can be used as an efficient probe for the study of bio-mimetic medium at varying pH, ranging from pH 1 to pH 12.

References:

(1) J. A. Organero, L. Tormo, M. Sanz, A. Douhal, *J. Inclusion Phenom. Macrocyclic Chem.* **2006**, *56*, 161.

(2) A. Douhal, F. C De Schryver, S. De Feyter and G. Schweitzer, *Femtochemistry in nanocavities in Femtochemistry*, Wiley-VCH Verlag: Weinheim, Germany, 2001.

(3) A. H. Zewail, A. Douhal, D. P. Zhong, *Proc. Natl. Acad. Sci. U.S.A.* **2000**, *97*, 14056.

(4) L. P. Novaki, O. A. El Seoud, *Langmuir* **2000, 16,** 35.

(5) B. L Bales, R. Zana, *J. Phys. Chem. B* **2002**, *106*, 1926.

(6) P. Chou, D. McMorrow, T. J. Aartsma, M. Kasha, *J. Phys. Chem.* **1984**, *88*, 4596

(7) M. Rini, Z. B. Magnes, E. Pines, J. T. E. Nibbering, *Science* **2003,** *301*, 349.

(8) G. Mathias, Marx, *Proc. Natl. Acad. Sci. U.S.A.* **2007,** *104*, 6980.

(9) J. Catalan, F. Fabero, M. S. Guijarro, R. M. Claramunt, M. D. Santa Maria, M. C. Foces-Foces, F. H. Cano, J. Elguero, R. Sastre, *J. Am. Chem. Soc*. **1990**, *112*, 747.

(10) D. Kuila, G. Kwakovszky, M. A. Murphy, R. Vicare, M. H. Rood, K. A. Fritch, J. R. Fritch, *Chem. Mater.* **1999**, *11*, 109.

(11) B. M. Uzhinov , S. I. Druzhinin, *Russ. Chem. Rev.* **1998**, *67*, 123.

(12) R. M. Tarkka, X. Zhang, S. A. Jenekhe, *J. Am. Chem. Soc.* **1996**, *118*, 9438.

(13) P. T. Chou, M. L. Martinez, J. H. Clements, *J. Phys. Chem.***1993**, *97*, 2618.

(14) K. T. Kamtekar, A. P. Monkman, M. R. Bryce, *Adv. Mater.* **2010**, *22*, 572.

(15) D. K. Kreuer, *Chem. Mater.* **1996**, *8*, 610.

(16) M. Ruitenberg, A. Kannt, E. Bamberg, K. Fendler, H. Michel, *Nature* **2002**, *417*, 99.

(17) D. B. Spry, A. Goun, K. Glusac, D. E. Moilanen, M. D. Fayer, *J. Am. Chem. Soc.* **2007**, *129*,8122.

(18) K. J. Tielrooij, M. J. Cox, H. J. Bakker, *Chem. Phys. Chem.* **2009**,*10*, 245.

(19) T. Mondal, A. K. Das, D. K. Sasmal, K. Bhattacharyya, *J. Phys. Chem. B* **2010**,*114*, 13136.

(20) S. S. Mojumdar, T. Mondal, A. K. Das, S. Dey, K. Bhattacharyya, *J. Chem. Phys.* **2010**, *132*, 194505.

(21) T. H. Tran-Thi, T. Gustavsson, C. Prayer, S. Pommeret, J.T. Hynes, *Chem. Phys. Lett.* **2000**, *329*, 421.

(22) N. A. Carmona, B. Cohen, J. A. Organero, A. Douhal*, J. Photochem. Photobiol. A: Chem.* **2012**, *234*, 3.

(23) H. P. Soroka, R. Simkovitch, A. Kosloff, S. Shomer, A. Pevzner, O. Tzang, R. Tirosh, F. Patolsky, D. Huppert, *J. Phys. Chem. C* **2013**, *117*, 25786.

(24) J. Kuchlyan, D. Banik, N. Kundu, S. Ghosh, C. Banerjee, N. Sarkar, *J. Phys. Chem. B* **2014**, *118*, 3401.

(25) S. D. Choudhury, H. Pal, *J. Phys. Chem. B* **2009**, *113*, 6736.

(26) C. Banerjee, C. Ghatak, S. Mandal, S. Ghosh, J. Kuchlyan, N. Sarkar, *J. Phys. Chem. B* **2013**, *117*, 6906.

(27) R. Rai, S. Pandey, *Langmuir* **2014**, *30*, 10156.

(28) N. Amdursky, R. Simkovitch, D. Huppert, *J. Phys. Chem. B* **2014**, *118*, 13859.

(29) T. K. Mukherjee, P. Ahuja, A. L. Konar , A. Datta, *J. Phys. Chem. B* **2005**, *109*, 12567.

(30) D. Arghya, G. N. Patwari, *J. Chem. Sci.* **2011**, *123*, 909.

(31) K. Gavvala, R. K. Koninti, A. Sengupta, P. Hazra, *Phys. Chem. Chem. Phys.* **2014**, *16*, 14953.

(32) S. G. Schulman, R.M. Threatte, A. C. Capomacchia, W.L. Poul, *J. Pharm. Sci.* **1974**, *63*, 876.

(33) D. Pant, H. B. Tripathi, D. D. Pant, *J. Lumin.* **1992**, *51*, 223.

(34) D. Pant, U. C. Tripathi, G. C. Joshi, H. B. Tripathi, D. D. Pant, *J. Photochem. Photobiol. A: Chem.* **1990**, *51*, 313.

(35) D. Pant, H. B. Tripathi, D. D. Pant, *J. Photochem. Photobiol. A: Chem.* **1991**, *56*, 207.

(36) D. Pant, H. B. Tripathi, D. D. Pant, *J. Lumin.* **1991**, *50*, 249.

(37) S. Pant, H. B. Tripathi, D. D. Pant, *J. Photochem. Photobiol. A: Chem.* **1995**, *85*, 33.

(38) H. C. Joshi, A. Upadhyay, H. Mishra, H. B. Tripathi, D. D. Pant, *J. Photochem. Photobiol. A: Chem.* **1999**, *122*, 185.

(39) S. Joshi, D. D. Pant, *J. Lumin.* **2014**, *145*, 224.

(40) A. Acevedoa, P. Takhistov , C. Pinzón de la Rosaa, V. Florián, *Carbohydrate Poly.* **2014**, *102*, 74.

(41) R. Ranganathan, M. Peric, B. L. Bales, *J. Phys. Chem. B* **1998**, *108*, 8436.

(42) A. Mahata, D. Sarkar, D. Bose, D. Ghosh, P. Das, N. Chattopadhyay, *J. Colloid Interface Sci.* **2009**, *335*, 234.

(43) R. Saxenaa, S. Shrivastavaa, S. Haldar, A. S. Klymchenko, A. Chattopadhyaya, *Chem. Phys. Lipids* **2014**, *183*, 1.

(44) P. Banerjee, S. Pramanik, A. Sarkar, S. C. Bhattacharya, *J. Phys. Chem. B* **2008**, *112*, 7211.

(45) V.G. Rao, C. Ghatak, R. Pramanik, S. Sarkar, N. Sarkar, *Chem. Phys. Lett.* **2010**, *499*, 89.

Conclusions

General Conclusions

Ground and excited state dipole moments of fluorescent molecules such as Quinine Sulfate monocation (QS^+), Quinine Sulfate dication (QS^{2+}), Quinidine monocation (QD^+) and Quinidine dication (QD^{2+}), have been estimated using solvatochromic shift method and quantum mechanical calculations. We observed that these solute probe molecules undergo a large change of dipole moment in the excited state. Here we also studied the photophysics of QS in micellar environment and found that micellar surface charge can modulate the conformation and dynamics of QS probe molecule. These results are relevant to understand the role of surface charge of membranes in the interaction of membranes with the membranes. The present work can be extended to biologically important heterogeneous systems like membranes, enzymes, peptides and proteins to understand the aggregation behavior and structure of the microenvironments using QS as a fluorescent probe molecule and particularly to understand the role of surface charge of membranes in interaction of peptides with membranes. This study provides excited state dynamical behavior of QS molecules in different micelles of different surface charges and adds knowledge about the understanding of microstructure of surfaces and interfaces.

Specific Conclusions

The thesis entitled "**Photophysics of Fluorescent Molecules in Micellar Systems**" is divided in six chapters. A brief overview of these chapters is presented below.

The first chapter of the thesis presents the basic aspects of photophysical and photochemical processes involving excited chromophoric molecules. This chapter also describes the general aspects of micelles used as the confined medium in the present study. The systems that have been chosen for the investigation in the present study are described in this chapter.

The second chapter deals with the methods used in the present research work. Different instrumental techniques used in the present study to carry out different

photophysical and photochemical measurements have been described briefly in this chapter. Working principle of the Time Correlated Pingle photon Counting (TCSPC) spectrometer has been discussed in this chapter with some greater detail. Basic principles of the other instrumental techniques used in the present study, e.g. absorption spectrophotometry, steady-state spectrofluorimetry have also been described briefly in this chapter.

The third chapter discusses about the estimation of dipole moment in ground and excited states of fluorescent molecules such as Quinine Sulfate monocation (QS^+), Quinine Sulfate dication (QS^{2+}), Quinidine monocation (QD^+) and Quinidine dication (QD^{2+}), using solvatochromic shift method and quantum mechanical calculations. The spectroscopic techniques utilized in this chapter are UV-Visible absorption spectroscopy and fluorescence emission spectroscopy. We have calculated ground and exited state dipole moments of different these fluorescent molecules and observed higher dipole moment in excited state. Higher dipole moment in excited state is attributed to the more polar excited state.

The four chapter presents the results that show the effects of micellar surface charge on the photophysics of a QS^{2+} in cationic, Cetyltrimethylammonium bromide (CTAB), anionic, Sodium dodecylsulphate (SDS) and neutral, Triton X-100 (TX-100) surfactants at concentrations above the Critical Micelle Concentrations (CMC) in aqueous phase. Results have been explained on the basis of electrostatic interaction between positively charged probe (QS^{2+}) and charge that different surfactant headgroups contain. We have observed that QS^{2+} molecule has the extraordinary capability to sense the surrounding environment which make it very efficient for surface and interface studies and can also be used as a probe to investigate the mobility of solvent molecules around the excited molecules.

The fluorescence properties of QS^{2+} are remarkably modulated in micelles compared with the bulk phase. The observed EERS in emission maximum of QS^{2+} in bulk water and surfactant systems is due to the solvent relaxation process around the excited solute molecule. The decrease in the magnitude of EERS in anionic SDS surfactant systems is due to the decrease in solvent relaxation rate as a consequence of restricted motion of the water molecules around the QS^{2+} in interfacial region, where its mobility is considerably reduced. The microenvironment around the probe molecules

bound to surfactants can be conveniently monitored using the EERS measurements. The magnitude of EERS can be used as a probe to determine the microenvironmental and restrictive motion of solvent molecules around the probe molecule in surfactants. In the case of CTAB, QS^{2+} molecules are more in bulk type water consequently solvation is much faster.

Modulated photophysics of QS^{2+} in micellar systems compared to aqueous media has been demonstrated using steady state and time-resolved studies. The location of the probe molecule in micellar systems is ascertained by a variety of spectral parameters such as EERS, average fluorescence decay time, radiative and non radiative rate constants, and rotational relaxation time. All experimental results suggest that the QS^{2+} molecule resides at micellar–water interface. Further the rotational mobility of QS^{2+} in these micelles is found to be dependent on the surface charge of micelles. The longest rotational correlation time is observed for anionic SDS micelles and is attributed to the lateral diffusion of QS^{2+} molecules. In summary, the micellar surface charge can modulate the conformation and dynamics of QS^{2+} probe molecule. This study provides excited state dynamical behavior of QS^{2+} molecules in different micelles of different surface charges and adds knowledge about the understanding of microstructure of surfaces and interfaces.

In chapter 5 we have discussed about photophysical characterization of QS^{2+} in normal micelles formed by anionic surfactant Sodium dodecylsulphate (SDS). It has been studied at different premicellar, micellar and postmicellar concentrations in aqueous phase using steady state, time-resolved fluorescence and fluorescence anisotropy techniques. The QS^{2+}- SDS binding constant and association constants were determined by monitoring the changes in the absorption and steady-state fluorescence. We observed here that at lower concentrations of SDS in aqueous solution of QS^{2+}, there is fluorescent complex formation between monomers of surfactant and QS^{2+} molecules. The complex formed was highly fluorescent which in general are non fluorescent. These fluorescent complexes are not stable and at higher concentrations of SDS, they dissociate to aggregate and to form the micelles. At higher concentrations of SDS, the decrease in the magnitude of EERS is due to the decrease in solvent relaxation rate as a consequence of restricted motion of the water molecules around the QS^{2+} in interfacial region, where its mobility is considerably reduced. At lower concentrations of SDS, the observed large

magnitude of EERS is due to the presence of energetically different ion pairs in the ground state of QS^{2+}. The time-resolved fluorescence and anisotropy measurements were also carried out to support the steady-state measurements.

The location of QS^{2+} probe in SDS micellar solution has been ascertained by a variety of parameters such as dielectric constant, E_T (30), viscosity, absorption, emission, anisotropy, lifetimes and quenching constant etc. All these studies indicate that the probe molecule binds strongly with the micelles and resides at the water-micelle interface in the SDS solutions. This study provides significant insight into the behaviour of the probe inside the micelles and its variation with change in surfactant concentration. Modulated photophysics of QS^{2+} has been observed here in micellar environments compared to the photophysics of QS^{2+} in homogeneous environments.

From the data of solvent effect on QS^{2+}, it is evident that the microenvironment around the probe molecule in SDS micelles is less polar and highly viscous than that of water and these observations are in agreement with other probe–micellar systems studied. The time-resolved fluorescence decay analysis suggests distribution of different conformers of QS^{2+} of different energies in SDS micellar solution. The fluorescence anisotropy and quenching measurements reveal that the QS^{2+} molecules are in restricted environment.

This study clearly demonstrates that the photophysics of QS^{2+} is very sensitive to the local environment of the probe in SDS micelles. The remarkable sensitivity of QS^{2+} molecules to microstructures of surfaces and interfaces will attract attention to use this molecule as a probe to investigate the microstructure of different micelles and reverse micelles to understand its interactions with relevant biological media.

In chapter 6 we have discussed the effect of anionic surfactant SDS on photophysics of QS at pH 2, pH 7 and pH 12. The photophysical behaviour of QS is dramatically modified in micelles from that in bulk aqueous phase. At pH 2, there is decrease in absorbance and fluorescence intensity. Observation of a new fluorescent band around 380 nm at lower concentrations of SDS in aqueous solution of QS is attributed to the fluorescent complex formation between monomers of surfactant. These fluorescent complexes are not stable and at higher concentrations of SDS, they dissociate to aggregate and to form the micelles. At pH 7, as we increase the concentration of SDS,

proton transfer phenomenon is favoured due to change in local pH in the micellar surface region. The results indicate that at pH 7 in presence of SDS micelles, hydrophobic microenvironment enhances the dication emission and also causes an increase in lifetime of dication emission. The anionic surfactant SDS, around CMC of the surfactant, protonates the monocationic QS molecules to form dicationic molecules due to the change in local pH at the micelle-water interface. The SDS micelles, at pH 7, promote the ESPT and consequently lead the formation of dicationic species of QS in the excited state. No ESPT has been observed for the dicationic and neutral forms of QS. Time-resolved studies show different excited state dynamics in premicellar and micellar regions. Further, the effect of variation of pH of the micellar solution provides support to our conclusion about the location of QS molecules at the micelle-water interface. Information on such an interaction may add to our understanding of the combined electrostatic and hydrophobic interaction, pertaining to biological systems. The shift in fluorescence due to formation of the dication can make it a potential sensor for negatively charged surfaces. The present study have shown that solvent environment sensitive fluorescence of QS can be used as an efficient probe for the study of bio-mimetic medium at varying pH, ranging from pH 1 to pH 12.

Future scope of the work

In the present study, the photophysics of fluorescent molecules has been studied in bulk and restricted environments formed by normal micelles of ionic and non ionic surfactants. The probe molecules studied are Quinine Sulfate (QS) and Quinidine (QD). QS is highly fluorescent, have unique photophysical properties and very sensitive to surrounding environment in bulk solutions and is used as a fluorescence quantum yield standard.

Solvatochromic behaviour of QS and QD has been studied and reported in different solvents of different polarities at room temperature. Ground and excited state dipole moments of these molecules have been determined using solvatochromic method and quantum chemical calculations. Knowledge of dipole moment is useful in designing nonlinear optical materials and also can be useful in optimizing the efficiency and performance of laser dyes.

The effect of micellar charge on photophysics of QS has been discussed in this thesis. The micellar surface charge modulates the conformation and dynamics of QS probe molecule. These results are relevant to understand the role of surface charge of membranes in the interaction of membranes with the membranes. The present work can be extended to biologically important heterogeneous systems like membranes, enzymes, peptides and proteins to understand the aggregation behavior and structure of the microenvironments using QS as a fluorescent probe molecule and particularly to understand the role of surface charge of membranes in interaction of peptides with membranes.

This type of study can be extended to different fluorescent molecules in order to find a most suitable probe molecule sensitive to the microstructures of micelles and reverse micelles. Further, this study can be done in AOT reverse miceller environment to understand the effect of confinement on to the photophysical and photochemical processes. In micellar systems the relaxation processes will be controlled by the energy barrier, electron transfer distance, and relative orientation of the donar and acceptor molecules. Additionally, these processes are highly sensitive to the surrounding electronic environment. Hence, the nature of micellar interface

will likely present interesting effects on different excited state relaxation processes. The restrictive environment of the micelle will fix the relative orientation and geometry of the conformers in the molecules, therefore these processes are not anticipated to be diffusion limited. In addition to these studies, one can also examine the effect of the counterion in reverse micellar systems. Further, these studies can be extended to different carbon chain lengths of surfactants in order to understand the modulation in photophysical processes of molecules in micellar systems.

List of publications

From thesis work

Published in peer reviewed international journals:

1. S. Joshi, D. D. Pant, Interaction of Quinine Sulfate with anionic micelles of Sodium dodecylsulfate: A time-resolved fluorescence study at different pH. *Spectrochim. Acta Part A:* **2015**, *148*, 49-59**.**

2. S. Joshi, D. D. Pant, Steady state and time-resolved fluorescence spectroscopy of Quinine Sulfate dication bound to Sodium dodecylsulfate micelles: Fluorescent complex formation. *J. Lumin.* **2014**, *145*, 224-231.

3. S. Joshi, Y. Tej Varma, D. D. Pant, Steady state and time-resolved fluorescence spectroscopy of Quinine Sulfate dication in ionic and neutral micelles: Effect of micellar charge on photophysics. *Colloids and Surfaces A: Physicochem. Eng. Aspects* **2013**, *425*, 59-67.

4. S. Joshi, R. Bhattacharjee, Y. Tej Varma, D. D. Pant, Estimation of ground and excited state dipole moments of Quinidine and Quinidine dication: Experimental and numerical methods. *J. Mol. Liq.* **2013**, *179*, 88-93.

5. S. Joshi, D. D. Pant, Ground and Excited State Dipole Moments of Quinine Sulfate Dication: Solvatochromic Shift of Absorption and Fluorescence Spectra. *J. Mol. Liq.* **2012**, *172*, 125 - 129.

6. S. Joshi, D. D. Pant, Solvatochromic shift and estimation of dipole moment of Quinine Sulfate. *J. Mol. Liq.* **2012**, *166*, 49 – 52.

Publications other than Thesis work

Published in peer reviewed international journals:

1. S. Joshi, S. Kumari, R. Bhattacharjee, R. Sakhuja and D. D. Pant, Estimation of ground and excited-state dipole moments of synthesized coumarin derivative, (S)-(1-((7-hydroxy-2-oxo-2H-chromen-4-yl)methyl)-1H-1,2,3-triazol-4-yl)methyl 2-(((9H-fluoren-9-yl)methoxy)cabonylamino)-3-phenylpropanoate from a solvatochromic shift and theoretical methods. *J. Mol. Liq*. **2015** (Revised Manuscript).

2. R. Sharma, S. Joshi, D. D. Pant, Solvent effect on absorption and fluorescence spectra of Cinchonine and Cinchonidine dications: Estimation of ground and excited state dipole moments by experimental and numerical studies. *J. Mol. Liq*. **2015**, *206*, 159-164.

3. S. Kumari, S. Joshi, A. Shakoor, S. S. Panda, D. D. Pant, R. Sakhuja, Synthesis, absorption and fluorescence studies of coumaryl labelled amino acids/dipeptides linked via triazole ring. *Aust. J. Chem.* ***2015*** (in press).

4. Y. Tej Varma, S. Joshi, D. D. Pant, Effect of nanosize micelles of ionic and neutral surfactants on the photophysics of protonated 6-methoxyquinoline: Time resolved fluorescence study. *Spectrochim. Acta Part A:* **2015**, *138*, 818-826.

5. S. Joshi, S. Kumari, R. Bhattacharjee, R. Sakhuja and D. D. Pant, Estimation of ground and excited state dipole moments of synthesized coumarin derivative [*N*-(2-oxo-2*H*-chromen-4-yl)imino]triphenyl-phosphorane. *J. Mol. Liq.* **2014**, *200*, 115-119.

6. Y. Tej Varma, S. Joshi, D. D. Pant, Solvatochromatic shift of absorption and fluorescence spectra of 6-methoxyquinoline: Estimation of ground and excited state dipole moments. *J. Mol. Liq.* **2013**, *179*, 7–11.

7. D. D. Pant, S. Joshi, H. H. Girault, Surface second harmonic generation from coumarin 343 dye-attached TiO_2 nanoparticles at liquid - liquid interface. *J. Nanoparticle Research* **2011**, *13*, 7057 - 7064.

Papers published in National/International Conference proceedings:

1. S. Joshi, Y. Tej Varma, D. D. Pant, Dynamic Fluorescence Quenching of Quinine Sulfate dication by Chloride Ion in Ionic and Neutral Micellar Environments, 58th DAE Solid State Physics Symposium December 17-21, 2013, Thapar University, Patiala, *AIP Conf. Proc.* **2014**, *1591*, 848-850.

2. S. Joshi, D. D. Pant, Solvatochromic study of Quinidine: Determination of ground and excited state dipole moments, International Conference on Recent Trends in Applied Physics and Material Science, Feb 01-02, 2013, Govt. Colleage of Engineering and Technology, Bikaner, *AIP Conf. Proc.* ***2013****, 1536, 797-798.*

3. S. Joshi, D. D. Pant, Solvent effects on the absorption and fluorescence spectra of Quinine Sulfate: Estimation of ground and excited-state dipole moments, 56th DAE Solid State Physics Symposium December 19-23, 2011, SRM University, Tamil Nadu, *AIP Conf. Proc*. ***2012*** , *1447*, 201-202.

4. S. Joshi, D. D. Pant Photophysics of Quinine Sulfate dication in micellar environments, National conference on condensed matter physics, Feb. 24-25, 2012, Birla Institute of Technology and Science, Pilani, Rajasthan, India, *Inter. J. Phys. Math. Sci*. (online) **2012**, *2*, 70-77.

5. S. Joshi and D. D. Pant, Solvatochromic shift and estimation of dipole moment of Quinine Sulfate dication, Conference Proceedings of 'World Academy of Science , Engineering and Technology (WASET)', Spain, **2012**, *6*, 425-429.

Brief biography of the Candidate

SUNITA JOSHI obtained her M.Sc. (hons. Physics) in 2009, from Birla Institute of Technology & Science, Pilani. She joined Birla Institute of Technology & Science, Pilani in the year 2011, to pursue her Doctor of Philosophy (Ph.D.). Till date, she has published 12 papers in peer-reviewed international journals and has published 5 papers in international/ national conference proceedings. At present, she is Senior Research Fellow in CSIR-SRF scheme. She has presented her research work in several national and international conferences.

Brief biography of the Supervisor

Dr. D. D. Pant is an Associate Professor and head, Department of Physics, Birla Institute of Technology & Science (BITS) Pilani, Pilani Campus, Rajasthan. He obtained his M.Sc. degree in physics with specialization in Electronics in 1986, from Kumaun University, Nainital, India and obtained his Ph.D. in Physics (Spectroscopy) from Photophysics Laboratory, Nainital, India. The title of his Ph.D. thesis was "Excited State Relaxation Studies: Solvation Dynamics and charge transfer complexes". After completing his Ph.D, he has been directly selected through UPSC, New Delhi as a Central Government's scientific staff and joined National Testing Laboratory, Ghaziabad, India. Subsequently he moved to U.S.A. He was Postdoctoral Research Associate at Texas Tech University, Lubbock, Texas, USA, Colorado State University, Fort Collins, USA and University of Notre Dame, USA. In 2000, he was a visiting scientist at TIFR, Mumbai, India. From July 2001-December 2002, he joined Department of Physics, BITS, Pilani, India as a lecturer. From 2003 to 2005, he was senior research scientist at Swiss Federal Institute of Technology, Lausanne (EPFL), Switzerland. He joined again, Department of Physics, BITS, Pilani, India in 2006 as Assistant Professor. He became Associate Professor in 2013 and head of the department in 2014. His research interests include time-resolved fluorescence spectroscopy of dye molecules at the surfaces of nanoparticles and inside the micelles, reverse micelles. Linear and non-linear optical properties of molecules at the surfaces of nanoparticles and at the liquid-liquid interface. Photophysical studies of fluorescent molecules in micellar and nanoparticle systems. Study on solvation dynamics and rotational relaxation of molecules in different micellar systems. At present, he is handling two major research projects financially supported by UGC and DST, New Delhi. As a result of his research accomplishment, he has published number of research articles in international journals. He is having more than 600 citations of his research papers. He is also reviewer of a number of many reputed national and international journals. Currently, Dr. D. D. Pant is guiding three Ph.D. students.